The Dissertation Committee for Joung Eun Yoo certifies that this is the approved version of the following dissertation:

Understanding the Processing-Structure-Property Relationships of Water-Dispersible, Conductive Polyaniline

Committee:

Isaac C. Sanchez, Supervisor

Yueh-Lin Loo

Donald R. Paul

Keith J. Stevenson

Christine E. Schmidt

Venkat Ganesan

Understanding the Processing-Structure-Property Relationships of Water-Dispersible, Conductive Polyaniline

by

Joung Eun Yoo, B.S.; M.S.

Dissertation

Presented to the Faculty of the Graduate School of

The University of Texas at Austin

in Partial Fulfillment

of the Requirements

for the Degree of

Doctor of Philosophy

The University of Texas at Austin

May, 2009

Dedication

To God,

And to my family.

Acknowledgements

I am first ever grateful to God, the Creator and the Guardian, and to whom I owe my very existence. God was a major source of strength when I worked on my thesis research. I would like to thank the almighty God for his grace.

I would like to express my deep appreciation and gratitude to the following people for helping me complete this thesis. My most earnest acknowledgement must go to my advisor, Prof. Yueh-Lin (Lynn) Loo, who has been instrumental in ensuring my academic, professional, financial, and moral well being ever since. I could not have imagined having a better advisor for my PhD. During the five years of my PhD, I have seen in her an excellent advisor who can bring the best out from her students, an outstanding researcher who can constructively criticize research, and a nice human being who is honest, fair and helpful to others. Thank you for always supporting me.

I am also extremely grateful for the support and friendship of my group members. Working with all the members has been one of the highlights of my time during PhD. A special thanks to Dr. Kwang Seok Lee and Jacob Tarver for having the patience to answer all of my questions regarding polyaniline, Dr. Tracy Bucholz for answering all of my chemistry questions, and proving me with polymers whenever I needed them, Dr. Enrique Gomez for fruitful discussion about solar cell fabrication and characterization, and Drs. Kimberly Dickey, Dmitry Krapchetov, Kyle Guice, Chang Su Kim, Jongbok

Kim, and Wei Tang, Stephanie Lee, Keith Gallow, Nathalie Pinkerton, and He Wang for being inspiring colleagues.

I would like to acknowledge our many collaborators: Jennifer Cross and Dr. Matthew Espe for their help and discussion with solid-state NMR studies, Dr. Suyong Jung for the temperature-dependent conductivity measurements, Drs. William Krekelberg and Thomas Truskett for their help and discussion with polyaniline particle studies, Dr. Yangming Sun for his help and guidance with XPS studies, and Kimberly Baldwin for her pK_a measurements.

I thank Drs. Issac Sanchez, Donald Paul, Keith Stevenson, Christine Schmidt, and Venkat Ganesan for providing feedback for my research as my doctorate committee members.

I am forever grateful to my family in Korea whose unconditional love and support have always helped me persevere through my studies in the United States.

Finally, I acknowledge the following funding agencies: the DuPont Young Professor Grant, the Beckman Foundation, the Keck Foundation, the NSF (DMR-0753148), and the Welch Foundation.

Understanding the Processing-Structure-Property Relationships of Water-Dispersible, Conductive Polyaniline

Publication No._____

Joung Eun Yoo, Ph.D.

The University of Texas at Austin, 2009

Supervisor: Isaac C. Sanchez

Polyaniline (PANI), when doped with small-molecule acids, is an attractive candidate for organic and polymer electronics because of its high electrical conductivity. Its utility as functional components in electrical devices, however, has been severely restricted because such PANI has limited processibility stemming from its limited solubility in common solvents. To overcome this barrier, we have developed water dispersible PANI that is template polymerized in the presence of a polymer acid, poly(2-acrylamido-2-methyl-1-propanesulfonic acid), or PAAMPSA. The polymer acid serves two roles: it acts as a dopant to render PANI conductive and excess water soluble pendant groups provide dispersibility of PANI in aqueous media. While the introduction of polymer acids renders the conducting polymer processible, such gain in processibility is often accompanied by a significant reduction in conductivity. As such, PANI that is doped with polymer acids has only seen limited utility in organic electronics. Given the

promise of conducting polymers in organic electronics in general, this thesis focuses on the elucidation of processing-structure-property relationships of PANI-PAAMPSA with the aim of ultimately improving the electrical conductivity of polymer acid-doped PANI.

By controlling the molecular weight and molecular weight distribution of the polymer acid template, we have improved the conductivity of PANI-PAAMPSA from 0.4 to 2.5 S/cm. The conductivity increases with decreasing molecular weight of PAAMPSA, and it further increases with narrowing the molecular weight distribution of PAAMPSA. Strong correlations between the structure and the conductivity of PANI-PAAMPSA are observed. In particular, the crystallinity of PANI increases with increasing the conductivity of PANI-PAAMPSA. Given that the crystallinity qualifies the molecular order in PANI-PAAMPSA, we observe a linear correlation between molecular order and macroscopic charge transport in PANI-PAAMPSA.

PANI-PAAMPSA forms electrostatically stabilized sub-micron particles during polymerization due to strong ionic interactions between the sulfonic acid groups of PAAMPSA and aniline. When cast as films, the connectivity of these particles must play an important role in macroscopic conduction. The size and size distribution of PANI-PAAMPSA particles is strongly influenced by the molecular characteristics of polymer acid template. Templating the synthesis of PANI-PAAMPSA with a higher molecular weight PAAMPSA results in larger particles, and templating with a PAAMPSA having a larger molecular weight distribution results in a large size distribution in the particles. Because conduction in PANI-PAAMPSA films is governed by how these particles pack, the macroscopic conductivity of PANI-PAAMPSA films increases with increasing particle density, that is reducible from the molecular

characteristics of PAAMPSA. Moreover, PANI-PAAMPSA particles are structurally and chemically inhomogeneous. The conductive portions of the polymer preferentially segregate to the particle surface. Conduction in these materials is therefore mediated by the particle surface and conductivity thus scales superlinearly with particle surface area per unit film volume.

We further have improved the electrical conductivity of PANI-PAAMPSA by more than two orders of magnitude via post-processing solvent annealing with dichloroacetic acid (DCA). Since DCA is a good plasticizer for PAAMPSA and its pK_a is lower than that of PAAMPSA (pK_as of DCA and PAAMPSA are 1.21 and 2.41, respectively, at room temperature), DCA can effectively moderate the ionic interactions between PANI and PAAMPSA, thereby relaxing the sub-micron particulate structure arrested during polymerization. PANI-PAAMPSA can thus rearrange from a "compact coil" to an "extended chain" conformation upon exposure to DCA. Efficient charge transport is thus enabled through such "extended chain" PANI-PAAMPSA structure. DCA-treated PANI-PAAMPSA exhibits an average conductivity of 48 S/cm. The DCA treatment is not only specific to PANI-PAAMPSA. This treatment can also enhance the conductivity of commercially-available poly(ethylene dioxythiophene) that is doped with poly(styrene sulfonic acid), or PEDOT-PSS. Specifically, DCA-treated PEDOT-PSS exhibits a conductivity of 600 S/cm; this conductivity is the highest among polymer acid-doped conducting polymers reported so far.

PANI-PAAMPSA can effectively function as anodes in organic solar cells (OSCs) whose active layer is a blend of poly(3-hexylthiophene), P3HT, and [6,6]-phenyl-C61-butyric acid methyl ester (PCBM). Specifically, the OSCs with PANI-PAAMPSA

anodes exhibit an average short circuit current density of 1.95 mA/cm^2, open circuit voltage of 0.52 V, fill factor of 0.38, and efficiency of 0.39 %. The use of DCA-treated PANI-PAAMPSA as anodes increases device performance (i.e., short circuit current density and thereby efficiency) of OSCs by approximately two and a half fold. The OSCs with DCA-treated PANI-PAAMPSA anodes exhibit short circuit current density and efficiency as high as 4.95 mA/cm^2 and 0.97 %, respectively.

We demonstrated several factors that govern the electrical conductivity of polymer acid-doped conducting polymers. Design rules, such as those illustrated in this study, can enable the development of conducting polymers that is not only easily processible from aqueous dispersions, but also sufficiently conductive for electronic applications, and should bring us closer to the realization of low-cost organic and polymeric electronics.

Table of Contents

List of Tables

List of Figures

Chapter 1: Introduction

CONDUCTING POLYMER

Until about 60 years ago, all carbon-based polymers were regarded as insulators. Polymers were therefore only utilized as inactive packaging or insulating materials in electronic applications. This very narrow perspective on the utility of polymers in the electronics industry has rapidly changed since the discovery of conducting polymers.[1-3]

The study of conducting polymers has emerged as a prosperous field in organic electronics following breakthroughs by Alan Heeger, Alan MacDiarmid, and Hideki Shirakawa in the late 1970s.[1-3] They were awarded the Nobel Prize in Chemistry in 2000 for the discovery of a conducting polymer, namely iodine vapor doped polyacetylene, as well as for the subsequent development and investigation of new conducting polymer systems.[1-3] Their work was the first to explore the mechanisms and physical origins of electrical conduction in this novel class of materials.[4]

Much success was accompanied by the discovery that polyacetylene films could be oxidatively "doped" with gaseous iodine to induce metal-like conductivities.[4] In Figure 1.1, the conductivities of conducting polymers are compared with those of common conducting materials.[5] "Doping" refers to the process in which a conjugated polymer is transformed to its conducting form, usually by chemical oxidation or reduction. The different doping processes of conducting polymers are detailed in the next section. Iodine vapor doping produces free radicals along the conjugated backbone of polyacetylene; it is the delocalization of these free radicals that gives rise to electrical

conductivity.[6] This phenomenon, however, is not stable under ambient conditions because the free radicals can be easily quenched by oxygen.[6] The conductivity of iodine-doped polyacetylene therefore reverts to that of its initial insulating form upon exposure to air. This environmental instability has limited the utility of polyacetylene in practical applications.[6] Subsequently, much research has been directed towards the development of materials that are conductive, yet chemically stable at ambient conditions.

Of the many interesting conducting polymers, such as polypyrrole and poly(p-phenylene vinylene), poly(3,4-ethylenedioxythiophene) (PEDOT) and polyaniline (PANI) have attracted the most attention.[7, 8] The chemical structures for these conducting polymers are shown in Figure 1.2. These conducting polymers are environmentally stable; however, the extent of conjugation along the polymer backbone often renders these materials insoluble in common solvents. In order to overcome the intractability of conducting polymers, numerous alkyl and alkoxy derivatives, as well as those containing other substituents have been developed.[9, 10] Of particular interest has been the use of water-soluble polyelectrolytes to promote water-dispersibility in conducting polymers. In PEDOT, for example, delocalized radicals are generated by an oxidizing agent, and they are subsequently stabilized via ionic interactions between the charged polymer and the spent dopant.[11] Polyelectrolytes, such as poly(styrene sulfonic acid) (PSS), have been introduced as charge-balancing counter ions to the dopants.[12, 13] PEDOT-PSS has been commercially available as an aqueous dispersion since the early 1990s.[14] With such improvements to their environmental stability and solubility,

conducting polymers continue to be promising candidates for electronic device applications.[15, 16]

The conductivities of conducting polymers (10^{-5} – 10^{-1} S/cm) remain, however, several orders of magnitude lower than those of metals, such as gold and silver (10^{5} – 10^{6} S/cm). Despite their lower conductivities, conducting polymers are attractive candidates for use in electronic devices that do not require high power. The most exciting developments involve the use of conducting polymers in organic light-emitting diodes (OLEDs). OLEDs are already used as active components in thin-panel televisions and other electronic displays due to their low power consumption compared to the inorganic LEDs.[17] Considerable progress in the use of conducting polymers has been also made in the development of organic thin-film transistors (OTFTs) and organic solar cells (OSCs) with aims of reducing cost and increasing ease in processing.[18, 19] Additionally, batteries containing conducting polymer have demonstrated longer life times and higher discharge capacities compared to traditional lead-acid or nickel-cadmium batteries.[20] These batteries can generally be used in calculators, watches, and other products that only require a low power output.[20] Since the conductivities of conducting polymers can depend on their environment, the use of these materials in sensors and indicators is also interesting.[15, 21] In these applications, the conductivity of polymer tags would change when the material is exposed to certain temperatures, gases, or other chemicals.[21] Conducting polymers allow smart windows to change color and transparency with bias.[22] Conducting polymers also show excellent selectivity so they can be used in gas separation membranes or controlled release medicine systems.[23, 24] In short, conducting

polymers are very promising candidates in many applications that do not require high current output.

ELECTRICAL CONDUCTIVITY OF CONDUCTING POLYMERS

1) Band Theory

The free electron model is useful for explaining electrical conduction in metals. This model assumes that the valence electrons of the metal are free to move through the volume of the metal leading to electrical conduction. This free electron model does not apply to the discussion of conduction in semiconductors and insulators.

The energy difference between the valence and conduction bands, known as the energy gap or band gap, is strongly dependent on materials. Metals do not have a band gap; their valence and conduction bands overlap significantly. Semiconductors have band gaps less than 2.5 eV. Insulators have band gaps higher than 2.5 eV.[25] Figure 1.3 shows the band diagrams for metals, semiconductors, and insulators. For metals, the valence and conduction bands overlap so the electrons can move freely along the energy bands. For an insulator, the valence band is completely filled with electrons while the conduction band is empty. In order to achieve conductivity, the highest energy electrons in the valence band need to gain sufficient energy to overcome the band gap in order to reach the empty orbitals of conduction band. If the band gap is small enough, thermal excitation can provide sufficient energy to excite the electrons into the conduction band. In fact, semiconductors are insulators at low temperature, at which thermal energy alone cannot promote electrons into the conduction band. At room temperature, however, thermal excitation of electrons from the valence band to conduction band results in

electrical conductivity. This phenomenon is a thermally activated process, so the electrical conductivity increases with temperature in semiconducting materials. The excited electrons in conduction band and holes in valence band become charge carriers and contribute to the macroscopic conduction when an external bias is applied.

2) Doping Types in Conducting Polymers

There are two main types of doping processes for converting a conducting polymer from its insulating form to its semiconductor or conducting forms.

Conducting polymers have π-conjugated backbone that can be oxidized or reduced by chemical or electrochemical reactions. This process changes the number of electrons associated with the polymer backbone, and further produces charges along the backbone. These charges are stabilized by counter ions of the dopant. P-type redox doping occurs when electrons are removed from the backbone of the conducting polymer (oxidation). This process produces holes along the backbone, which are balanced by negative counter ions. In contrast, n-type redox doping occurs when the polymer backbone is reduced, or when electrons are added to the conducting polymer. These negative charges are then balanced by positive counter ions.

Conducting polymers can also be made conductive by an entirely different doping process, involving the use of a protonic acid. In this case, the number of protons, rather than electrons, changes along the conducting polymer backbone. Proton acid doping is used extensively to convert PANI from its neutral state to its conductive form; a nine to ten orders of magnitude increase in conductivity is observed as a consequence.[26]

POLYANILINE (PANI)

The first synthesis of polyaniline (PANI), involving the electrochemical oxidation of aniline in sulfuric acid, was reported in 1862 by H. Letheby.[27] Due to the incomprehension of polymers at the time, however, PANI was not examined in any detail before the 1960s. In 1968, N. de Serille et al. reported that the conductivity of PANI originates from proton doping of the stable half-oxidized and half-reduced form.[28] PANI was then subjected to intense structural, physical, and electrical characterization. A wave of interest was generated by A. Heeger, A. MacDiarmid, and H. Shirakawa's work on the physical mechanisms behind hole transport in these materials.[1-3] Unlike other conducting polymers, delocalization of radicals along PANI occurs via protonation by an acid, rather than by oxidation. This unique doping mechanism provides unprecedented environmental stability to PANI.[26]

PANI can exist in various distinct oxidation states.[29] The chromic and electrical properties of PANI are dependent on the oxidation states.[29] Figure 1.4 shows the oxidation states of PANI. The fully reduced state is referred to as leucoemeraldine base (LB) (Figure 1.4 (a)). The half-oxidized and half-reduced form is known as emeraldine base (EB) (Figure 1.4 (b)), while the fully oxidized form is known as pernigraniline base (PB) (Figure 1.4 (c)).[29, 30] While none of these base forms are electrically conductive, conductive PANI can be obtained by converting EB to emeraldine salt (ES) (Figure 1.4 (d)) through proton acid doping. The LB, EB, PB, and ES are yellow, blue, violet, and green, respectively.[26] The doping process starts with EB, which contains equal moles of reduced (benzenoid) and oxidized (quinoid) units, as shown in Figure 1.4 (b). Exposure to an acid protonates the imine nitrogens in EB. As a result, the EB is converted into ES,

as shown in Figure 1.4 (d). In ES, the charges are delocalized along the PANI backbone resulting in charge transport through PANI.[26, 31, 32] PANI ES typically exhibits a conductivity ranging from 10^{-5} to 10^{2} S/cm, whereas PANI EB exhibits a conductivity of 10^{-10} S/cm.

The electrical conductivity of PANI can be enhanced dramatically by secondary doping.[33, 34] During secondary doping, a solvent is introduced to induce structural rearrangement of PANI.[33] It has been reported that PANI undergoes a compact coil to expanded chain conformational change, which results in a further increase in the electrical conductivity. Secondary doping effects have been observed when spun-cast films of camphor sulfonic acid (CSA)-doped PANI are exposed to m-cresol, resulting in an increase in conductivities from 0.2 S/cm to 300 S/cm. This enhanced conductivity is maintained after the complete evaporation of m-cresol. After exposure of PANI-CSA to m-cresol, the crystallinity of PANI increases significantly.[33] UV-vis-NIR spectrum of m-cresol treated PANI-CSA also shows a dramatic increase in the intensity of the peak in NIR region.[35] These observations suggest a straightening of PANI chains, ultimately resulting in an increase in conductivity by increasing electron delocalization along the PANI backbone.

In the early years, PANI was doped with small molecule acids, such as hydrochloric acid. The major problem with these systems is their insolubility in any common solvents, which severely limits processibility of the final material. This insolubility arises from stronger inter-chain interactions between conjugated moieties, compared to van der Waals interactions or hydrogen bonding that typically exists in non-conjugated polymer systems.[36] Since the melting temperature of PANI is higher than its

degradation temperature, melt processing of PANI is also not feasible. Moreover, these small molecule acid dopants are volatile; their eventual vaporization leading to the de-doping of PANI drastically limits the utility of small molecule acid-doped PANI.

In the early 1990s, solution-processible PANI was successfully demonstrated by using functionalized protonic acids, such as camphor sulfonic acid (CSA) and dodecylbenzene sulfonic acid (DBSA), as dopants.[37] These surfactant-like acids have an acid head group that can protonate PANI and a long alkyl tail at end that can impart solubility to the doped PANI complex in non-polar or weakly polar organic solvents.[37] The final conductive PANI is thus processible from organic solvents.

More recently, aqueous dispersions of conductive PANI have been demonstrated through the synthesis of aniline in the presence of polymer acid templates.[38] In this process, PANI is protonated by the acid pendant groups in the polymer acid template. Excess acid groups in the polymer acid render the final PANI-polymer acid complex water-dispersible.[13] Moreover, compared to small-molecule acids, polymer acids are not volatile, so the use of polymer acids for doping PANI greatly increases the chemical stability and preserves the electrical conductivity of the final material.[39] Subsequently, much research has been carried out to characterize PANI that are either chemically-,[39-41] electrochemically-,[42, 43] or enzymatically-[44, 45] synthesized on polymer acid templates. The polymer acids that have been used as dopants include poly(styrene sulfonic acid),[46] poly(2-acrylamido-2-methyl-1-propanesulfonic acid),[47] poly(ethylenesulfonic acid),[48] poly(thiophenylenesulfonic acid),[49] etc.

Although useful for enhancing the processibility of PANI systems, polymer acid template synthesized PANI has struggled to achieve conductivities comparable to those

of small molecule acid-doped PANI. The conductivities of polymer acid-doped PANI systems are generally between 10^{-5} and 10^{-1} S/cm.[47, 50-53] Such PANI systems have therefore only seen limited utility in organic electronics.[54, 55] Moreover, the understanding of processing-structure-property relationships of polymer acid-doped PANI has not been elucidated. Such understanding is very important before applications involving PANI can be realized.

This thesis focuses on the investigation of the processing-structure-property relationships of a water-dispersible polymer acid-doped PANI system. The polymer acid of interest is poly(2-acrylamido-2-methyl-1-propanesulfonic acid), or PAAMPSA. Because it is a strong acid, aniline polymerization is thus carried out between pH 1 and 2.[56, 57] Polymerization of aniline at such acidic conditions results in a linear and defect-free PANI that contains para-substituted aniline units.[45, 58] Additionally, the amide groups in PAAMPSA (see chemical structure in Figure 1.5) can provide additional hydrogen bonding opportunities, which further enhances the water dispersibility of the final material.[54] To synthesize PANI-PAAMPSA, PAAMPSA is first dispersed in water. Aniline is then added and polymerized along the polymer acid template. As increasingly more sulfonic acid groups participate in doping of PANI during the polymerization, PAAMPSA becomes decreasingly hydrophilic. As s result, PANI-PAAMPSA forms sub-micron size colloidal particles that are electrostatically stabilized by the strong ionic interactions between the sulfonic acid groups of PAAMPSA and the PANI backbone.[38]

The resulting PANI-PAAMPSA exhibits the highest conductivity (0.4 - 2.4 S/cm) among PANI that are chemically-synthesized with polymer acids (typically 10^{-5} - 10^{-2}

S/cm),[40, 59, 60] and are slightly higher than those of enzymatically-synthesized PANI (typically 10^{-2} - 10^{-1} S/cm).[39, 44, 61] The highest conductivity previously reported is 0.15 S/cm for PANI that was enzymatically-synthesized with a PSS template.[58]

We improved the electrical conductivity of PANI-PAAMPSA by controlling the molecular characteristics of polymer acid template. We also investigated the mechanism of macroscopic conduction in PANI-PAAMPSA film. To further improve the conductivity of PANI-PAAMPSA, we explored secondary doping of cast films with dichloroacetic acid (DCA). The conductivity of PANI-PAAMPSA is improved by more than two orders of magnitude with DCA treatment.

THESIS OVERVIEW

The field of conducting polymers has come a long way since the initial discovery that polymers can be electrically conductive. The electrical and optical properties of conducting polymers have led to many studies for their exciting applications, such as organic electronics, sensors, conductive coatings, etc.[52, 62-65] However, conducting polymers have been only used in special fields that do not require high power outputs due to their inherently low conductivities compared to metals. The conductivities of polymer acid-doped conducting polymer systems are yet lower than those of small molecule acid-doped systems. The physics governing the conduction mechanism of polymer acid doped-conducting polymers is also poorly understood. Given the promise of broad applications of polymer acid doped-conducting polymers in organic electronics, it is important that we understand the factors that govern the electrical properties of such systems. The aim of this dissertation is therefore to establish the origins of electrical behavior of polymer acid-doped conducting polymer system, specifically PANI-PAAMPSA.

Chapter 2 describes the synthesis of the polymer acid template, PAAMPSA, via both conventional free-radical polymerization (CFRP) and atom transfer radical polymerization (ATRP). CFRP-derived PAAMPSA has a broad molecular weight distribution that is described by the most probable distribution, while ATRP-derived PAAMPSA has a significantly narrower molecular weight distribution. The template synthesis of PANI-PAAMPSA is provided as well. This chapter also provides brief descriptions of experimental techniques used in our research.

Chapter 3 details the effects of PAAMPSA molecular weight and Chapter 4 details those of PAAMPSA molecular weight distribution on the conductivity of PANI-PAAMPSA. Strong correlations between the conductivity and the structure of PANI-PAAMPSA are observed in both chapters. In particular, we show that conductivity increases with increasing crystallinity of PANI. The crystallinity of PANI qualifies the molecular order in PANI-PAAMPSA; increase in molecular order enhances charge transport in PANI-PAAMPSA films.

Chapter 5 describes the mechanism of macroscopic conduction in PANI-PAAMPSA film. When cast as films, the interconnected PANI-PAAMPSA particles govern charge transport. This phenomenon can be quantified by examining the particle density per unit volume of the cast film. Specifically, higher particle density enhances inter-particle charge transport, leading to higher conductivity of the cast-PANI-PAAMPSA film.

Chapter 6 reports the mechanism of PANI-PAAMPSA conductivity improvement with DCA treatment. We expand this technique for improving the conductivity of other polymer acid-doped conducting polymers, including PANI-PSS and PEDOT-PSS. Additionally, we demonstrate that the performances of organic solar cells (OSCs) can be improved two and a half fold by using DCA-treated conducting polymer anodes as opposed to using untreated conducting polymer anodes.

Chapter 7 summarizes the major achievements of our research and provides suggestions for future work.

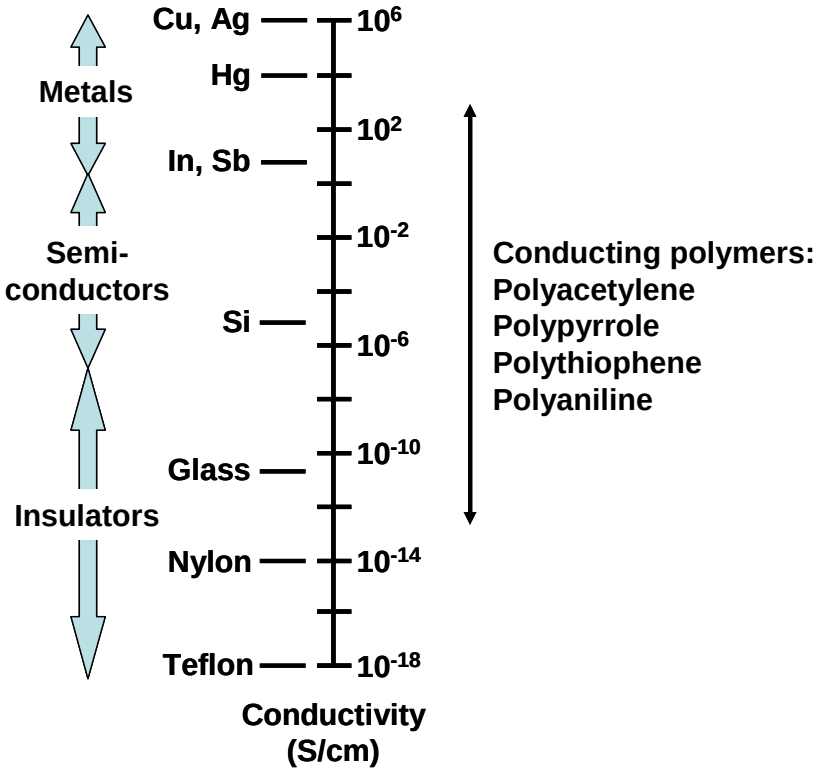

Figure 1.1. Electrical conductivities of common materials.[5]

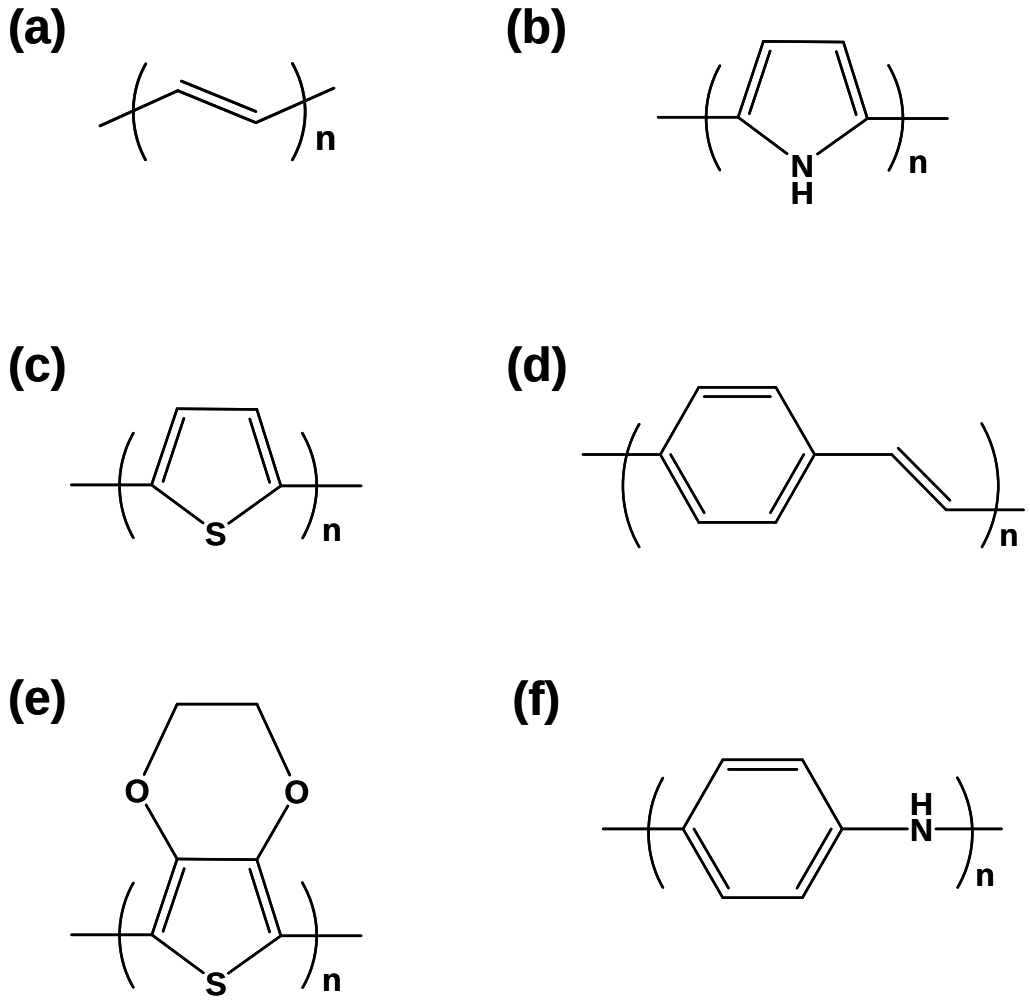

Figure 1.2. Chemical structures of conducting polymers: (a) polyacetylene, (b) polypyrrole, (c) polythiophene, (d) polyphenylene vinylene, (e) poly(3,4-ethylenedioxythiophene), and (f) polyaniline. n represents the number of repeat units.

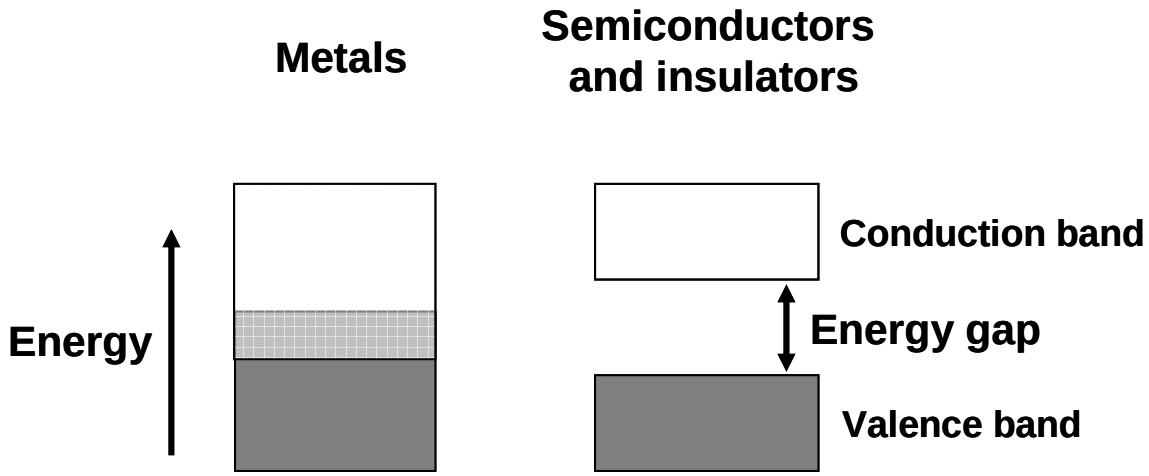

Figure 1.3. Band diagrams of metals, insulators, and semiconductors. Dark areas represent filled energy states. Semiconductors have band gaps that are smaller than 2.5 eV while insulators have band gaps that are greater than 2.5 eV.

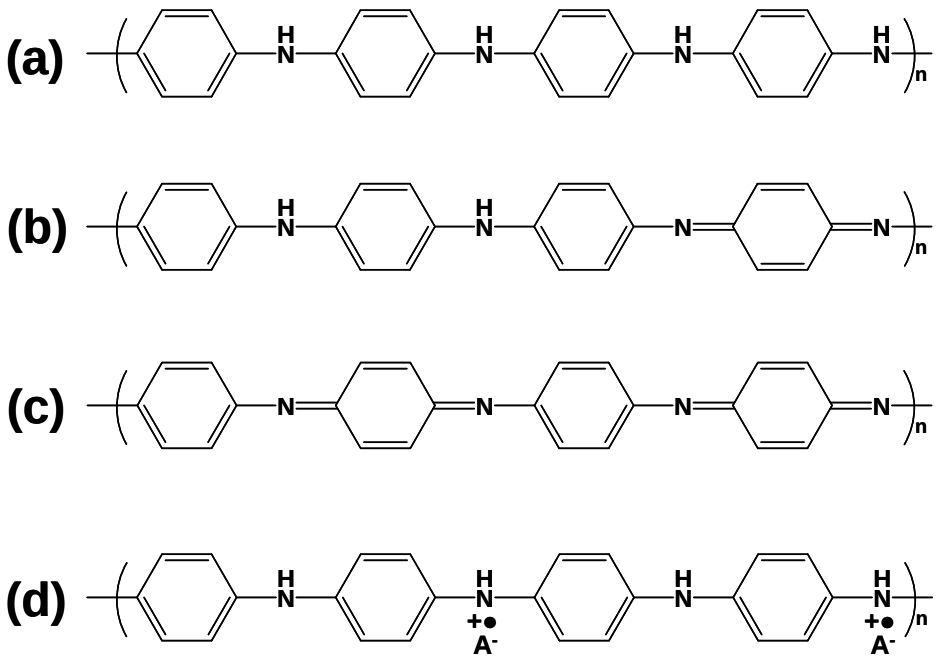

Figure 1.4. The oxidation states of PANI: (a) leucoemeraldine base (LB), (b) emeraldine base (EB), (c) pernigraniline base (PB), and (d) emeraldine salt (ES). A^- in (d) represents the counter ion of the acid dopant. n represents the number of repeat units.

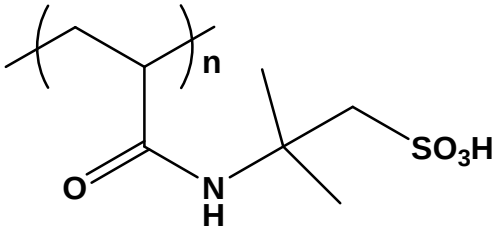

Figure 1.5. The chemical structure of PAAMPSA. n represents the number of repeat units.

REFERENCES

1. A. J. Heeger, *Rev. Mod. Phys.*, 2001, **73**, 681.
2. A. G. MacDiarmid, *Rev. Mod. Phys.*, 2001, **73**, 701.
3. H. Shirakawa, *Rev. Mod. Phys.*, 2001, **73**, 713.
4. C. K. Chiang, C. R. Fincher, Jr., Y. W. Park, A. J. Heeger, H. Shirakawa, E. J. Louis, S. C. Gau and A. G. MacDiarmid, *Phys. Rev. Lett.*, 1977, **39**, 1098.
5. Electrical conductivity, **http://en.wikipedia.org/wiki/Electrical_conductivity**.
6. C. K. Chiang, Y. W. Park and A. J. Heeger, *J. Chem. Phys*, 1978, **69**, 5098.
7. A. J. Epstein and Y. Yang, *MRS Bull.*, 1997, **22**, 13.
8. T. A. Skotheim, R. L. Elsenbaumer and J. R. Reynolds, *Handbook of conducting polymers*, Marcel Dekker, New York, 1998.
9. M. Leclerc and K. Faid, *Adv. Mater.*, 1997, **9**, 1087.
10. R. D. McCullough, *Adv. Mater.*, 1998, **10**, 93.
11. L. B. Groenendaal, F. Jonas, D. Freitag, H. Pielartzik and J. R. Reynolds, *Adv. Mater.*, 2000, **12**, 481.
12. E.-C. Chang, M.-Y. Hua and S.-A. Chen, *J. Polym. Res.*, 1998, **5**, 249.
13. M. Angelopoulos, N. Patel, J. M. Shaw, N. C. Labianca and S. A. Rishton, *J. Vac. Sci. Technol., B: Microelectron. Nanometer Struct.*, 1993, **11**, 2794.
14. Bayer AG, Eur. Patent, 440957, 1991.
15. J. Janata and M. Josowicz, *Nature*, 2003, **2**, 19.
16. P. Zarras, N. Anderson, C. Webber, D. J. Irvin, J. A. Irvin, A. Guenthner and J. D. Stenger-Smith, *Radiat. Phys. Chem.*, 2003, **68**, 387.

17. Engadget, *The Sony Drive XEL-1 OLED TV: 1,000,000:1 contrast starting December 1st, October 1 2007, retrieved on October 1 2007*.

18. H. Hoppe and N. S. Sariciftci, *J. Mater. Res.*, 2004, **19**, 1924.

19. G. Horowitz, *Organic Field-Effect Transistors*, CRC Press, New York, 2007.

20. M.-K. Song, W. I. Jung and R. H. -W., *Molecular crystals and liquid crystals science and technology*, 1998, **316**, 337.

21. J.-S. Huh, H. R. Hwang, J. G. Roh, D. D. Lee and J.-O. Lim, *Mat. Res. Soc. Symp. Proc.*, 2002, **698**, EE 3.2.1.

22. J.-C. Lassegues and D. Rodriguez, *Proc. SPIE*, 1992, **1728**, 241.

23. M. Gerard, A. Chaubey and B. D. Malhotra, *Biosens. Bioelectron.*, 2002, **17**, 345.

24. Y. M. Lee, S. Y. Ha, Y. K. Lee, D. H. Suh and S. Y. Hong, *Ind. Eng. Chem. Res.*, 1999, **38**, 1917.

25. *Principles of electronic materials and devices*, McGraw-Hill, Boston, 2006.

26. A. G. MacDiarmid and A. J. Epstein, *Faraday Discuss. Chem. Soc.*, 1989, **88**, 317.

27. H. Letheby, *J. Am. Chem. Soc.*, 1862, **15**, 161.

28. R. d. Surville, M. Jozefowicz, L. T. Yu, J. Perichon and R. Buvet, *Electrochim. Acta*, 1968, **13**, 1451.

29. J. C. Chiang and A. G. MacDiarmid, *Synth. Met.*, 1986, **13**, 193.

30. A. G. MacDiarmid, *Angew. Chem. Int. Ed. Engl.*, 2001, **40**, 2581.

31. P. McManus, S. C. Yang and R. J. Cushman, *J. Chem. Soc. Commun.*, 1985, **1**, 1556.

32. G. Wnek, *Synth. Met.*, 1986, **15**, 213.

33. A. G. MacDiarmid and A. J. Epstein, *Synth. Met.*, 1994, **65**, 103.

34. A. G. MacDiarmid and A. J. Epstein, *Synth. Met.*, 1995, **69**, 85.

35. Y. Min, Y. Xia, A. G. MacDiarmid and A. J. Epstein, *Synth. Met.*, 1995, **69**, 159.

36. A. J. Heeger, *Angew. Chem., Int. Ed.*, 2001, **40**, 2591.

37. Y. Cao, P. Smith and A. J. Heeger, *Synth. Met.*, 1992, **48**, 91.

38. L. Sun, S. C. Yang and J.-M. Liu, *Polym. Prepr.*, 1992, **33**, 379.

39. B.-C. Ku, S.-H. Lee, W. Liu, J. Kumar, F. F. Bruno and L. A. Samuelson, *Mat. Res. Soc. Sym. Proc.*, 2002, **708**, BB10.12.1.

40. S.-A. Chen and H.-T. Lee, *Macromolecules*, 1995, **28**, 2858.

41. R. Nagarajan, S. Tripathy, J. Kumar, F. F. Bruno and L. Samuelson, *Macromolecules*, 2000, **33**, 9542.

42. G. Li, M. Josowiez and J. Janata, *Electrochem. Solid-State Lett.*, 2002, **5**, D5.

43. P. N. Bartlett, P. R. Birkin, M. A. Ghanem and C.-S. Toh, *J. Mater. Chem.*, 2001, **11**, 849.

44. F. F. Bruno, R. Nagarajan, S. Roy, J. Kumar, S. Tripathy and L. Samuelson, *Mat. Res. Soc. Symp. Proc.*, 2001, **660**, JJ8.6.1.

45. W. Liu, J. Kumar, S. Tripathy, K. J. Senecal and L. Samuelson, *J. Am. Chem. Soc.*, 1999, **121**, 71.

46. K. Shannon and J. E. Fernandez, *J. Chem. Soc. Chem. Commun.*, 1994, **1**, 643.

47. J. E. Yoo, J. L. Cross, T. L. Bucholz, K. S. Lee, M. P. Espe and Y.-L. Loo, *J. Mater. Chem.*, 2007, **17**, 1268.

48. J. H. Hwang and S. C. Yang, *Synth. Met.*, 1989, **29**, E271.

49. K. Miyatake, J.-S. Cho, S. Takeoka and E. Tsuchida, *Macromol. Chem. Phys.* , 1999, **200**, 2597.

50. S. K. Sahoo, R. Nagarajan, S. Chakraborty, L. A. Samuelson, J. Kumar and A. L. Cholli, *J. Macromol. Sci., Part A: Pure Appl. Chem.*, 2002, **A39**, 1223.

51. S. K. Sahoo, R. Nagarajan, L. Samuelson, J. Kumar, A. L. Cholli and S. K. Tripathy, *J. Macromol. Sci., Part A: Pure Appl. Chem.*, 2001, **A38**, 1315.

52. D. R. Smith, M. A. Moy, A. R. Dolan and T. D. Wood, *Analyst*, 2006, **131**, 547.

53. J. E. Yoo, T. L. Bucholz, S. Jung and Y.-L. Loo, *J. Mater. Chem.*, 2008, **18**, 3129.

54. K. S. Lee, G. B. Blanchet, F. Gao and Y.-L. Loo, *Appl. Phys. Lett.*, 2005, **86**, 074102.

55. K. S. Lee, T. J. Smith, K. C. Dickey, J. E. Yoo, K. J. Stevenson and Y.-L. Loo, *Adv. Func. Mater.*, 2006, **16**, 2409.

56. S. Beuermann, M. Buback, P. Hesse, T. Junkers and I. Lacik, *Macromolecules*, 2006, **39**, 509.

57. S. R. Gooda and M. B. Huglin, *J. Polym. Sci., Part A: Polym. Chem.*, 1992, **30**, 1549.

58. L. A. Samuelson, A. Anagnostopoulos, K. S. Alva, J. Kumar and S. K. Tripathy, *Macromolecules*, 1998, **31**, 4376.

59. H. S. Moon and J. K. Park, *J. Polym. Sci., Part A: Polym. Chem.*, 1998, **36**, 1431.

60. H. S. Moon and J. K. Park, *Synth. Met.*, 1998, **92**, 223.

61. S. K. Sahoo, R. Nagarajan, S. Roy, L. A. Samuelson, J. Kumar and A. L. Cholli, *Macromolecules*, 2004, **37**, 4130.

62. T. Akai, T. Abe, T. Shimomura and K. Ito, *Jpn. J. Appl. Phys.*, 2001, **40**, L1327.

63. P. N. Bartlett and P. R. Birkin, *Synth. Met.*, 1993, **61**, 15.

64. R. V. Belosludov, A. A. Farajian, Y. Kikuchi, H. Mizuseki and Y. Kawazoe, *Comput. Mater. Sci.*, 2006, **36**, 130.

65. Y. Niu, *Polym. Compos.*, 2006, **27**, 627.

Chapter 2: Experimental Techniques

This chapter provides an overview of the synthetic, experimental, and analytical details of our work. First, we present the synthesis of poly(2-acrylamido-2-methyl-1-propanesulfonic acid), PAAMPSA, using two different polymerization techniques, conventional free-radical polymerization (CFRP) and atom transfer radical polymerization (ATRP). These polymerization techniques were used to make polymer acids having different molecular weights. These polymer acids were subsequently used as templates to make polyaniline (PANI). Following is thus the description of the template synthesis of PANI on PAAMPSA. We subsequently discuss the analytical techniques used to characterize our materials. Finally, we describe the fabrication and characterization of organic solar cells (OSCs) with PANI-PAAMPSA anodes. Details associated with data analysis are also described.

Synthesis of PAAMPSA by CFRP

CFRP is the most widely used method of chain polymerization because it allows the polymerization of a wide variety of monomers with different chemical functionalities.[1] This reaction is divided into three steps: initiation, propagation, and termination. The initiation step involves the formation of free radicals from an initiator, and the initial addition of a monomer to the free radicals. The propagation step involves the growth of the polymer chain by sequential addition of monomer to the free-radical active sites. In the termination step, growth of the polymer chain is terminated either by

coupling or disproportionation. Both termination processes involve two polymer radicals. During coupling, two polymer radicals annihilate to result in a polymer chain whose length is the sum of the two original polymer chains. Disproportionation occurs when the proton that is located on the α carbon transfers to a radical center that is on another chain.[2] This process results in a polymer chain with a saturated chain end and the other with an unsaturated chain end. Disproportionation is generally more common than coupling during free-radical polymerization.[2]

Two main aspects of CFRP affect the molecular weight distribution of the resulting polymer. First, the rate of initiation is usually much slower than that of propagation.[2] Second, the rate of termination is comparable to that of initiation.[3] As such, polymer chain growth is initiated and terminated throughout the polymerization. Assuming that termination occurs via disproportionation, CFRP-derived polymers thus have molecular weight distributions represented by the most probable distribution.[2] The polydispersities (PDIs) of these polymers can be expressed by equation (2.1).[2]

$$PDI = \frac{M_w}{M_n} = 1 + p \qquad (2.1)$$

where M_w is the weight-average molecular weight of the polymer, M_n is the number-average molecular weight of the polymer, and p is the fraction of monomer units that has reacted. The PDIs of the CFRP-derived polymers thus approach 2 at high conversions.[1]

To synthesize PAAMPSA, CFRP of AAMPSA (Aldrich, 99%) was carried out in deionized water (DI water). Potassium persulfate (Aldrich, 99+%) was used as the

initiator. We varied the molar ratio of monomer to initiator to obtain PAAMPSA having different molecular weights. We refer to the different PAAMPSA templates as PAAMPSA-X, where X refers to the poly(ethylene oxide)-, PEO-, equivalent number-average molecular weight of the polymer, in kg/mol. To synthesize PAAMPSA-45, for example, a monomer and initiator molar ratio of 1:0.4 (15 g and 7.83 g, respectively) was dissolved in 100 mL of DI water. Monomer to initiator molar ratios of 1:0.2, 1:0.1, and 1:0.02 were used to synthesize PAAMPSA-83, PAAMPSA-106, and PAAMPSA-255, respectively. The total concentration of monomer and initiator in the aqueous solution was fixed at 1.0 mol/L for all polymerizations. The polymerizations were carried out at 75 °C for 5 h, after which the reaction media were precipitated into tetrahydrofuran (THF) to recover PAAMPSA. The polymer acid was then dried in the vacuum oven at 55°C overnight. We also used a commercially-available PAAMPSA (Scientific Polymer Products Inc., 10.3 wt% in water, reported M_w = 800 kg/mol) for our study. This polymer was precipitated in THF and then dried in a vacuum oven at 55 °C before use. The PEO-equivalent number-average molecular weight of this polymer is 724 kg/mol so we refer to this polymer as PAAMPSA-724 in our study for consistency. The PDIs of these PAAMPSA, as probed by gel permeation chromatography (GPC), range between 1.43 and 1.64. These PDIs are lower than those expected of CFRP-derived polymers likely due to selective fractionation during polymer clean-up. Table 2.1 lists the molecular weight and molecular weight distribution of the PAAMPSA templates used in this study.

Synthesis of PAAMPSA by ATRP

Unlike CFRP, ATRP, a controlled free-radical polymerization technique, enables the synthesis of polymers with narrow molecular weight distributions.[4] The key feature of ATRP is the use of metal-ligand complexes to establish an equilibrium between the dormant and active states of polymer radicals during the reaction. This process effectively reduces the termination reactions during polymerization. This phenomenon is described by Equation (2.2).

$$P_n - X + L_n M^{+z} \xleftrightarrow{\rightarrow} P_n^{\bullet} + L_n M^{+(z+1)} X \qquad (2.2)$$

In this reaction scheme, P_n-X is the dormant polymer chain that is capped with a halogen atom, X. L_nM^{+z} is the metal-ligand complex. This metal-ligand complex typically consists of a copper halide (usually $Cu^{I}Cl$ or $Cu^{I}Br$) complexed with an amine-containing ligand. The metal core in the metal-ligand complex is oxidized with the extraction of the halogen atom to create a polymer radical (P_n•). During the radical activation step, Cu^{I} is oxidized to Cu^{II}, and then is returned to its original state during deactivation step.

The removal of the halogen atom from the dormant polymer chain end creates a free radical at the end of a polymer chain, which enables chain extension. The metal-ligand complex then reassociates with the free radical on the end of polymer chain and restores the halogen atom to the chain end. The key to ATRP lies in the equilibrium of this process, represented by the relative magnitude of the arrows in the reaction scheme.

The equilibrium of this reaction favors the dormant species heavily so the radical concentration is kept low throughout the polymerization. The probability of termination reactions is thus greatly reduced as a consequence. As the termination rate tends to zero, ATRP approaches living polymerization so all the polymer chains are of a uniform length. The molecular weight distributions of the resulting polymers thus approach 1.

Dr. Tracy L. Bucholz, a former graduate student in our group, synthesized PAAMPSA by ATRP to obtain polymers with narrow molecular weight distributions. Unlike in CFRP, AAMPSA cannot be directly polymerized by ATRP because the sulfonic acid group in AAMPSA can protonate the coordinating amine ligand.[2] The sodium salt form of the monomer (AAMPSA-Na; supplied by Lubrizol) was used instead. For AAMPSA-Na polymerization, a 1:1 v/v solution of DI water and dimethyl formamide (DMF; Aldrich 98%) was used as the solvent. The concentration of AAMPSA-Na used was 1 M. We used $Cu^{I}Cl$ (Aldrich, 98%) and $Cu^{II}Cl_2$ (Aldrich, 98%) as the catalyst, tris(2-dimethylaminoethyl)amine (Me_6TREN; supplied by Dr. Chris Bielawski in the Chemistry Department at the University of Texas at Austin) as the coordinating ligand, and ethyl 2-bromoisobutyrate (EBiB; Aldrich, 98%) as the initiator. We synthesized a series of PAAMPSA-Na templates with varying molecular weights ranging from 30 to 287 kg/mol by varying the monomer to initiator molar ratio. We refer to the resulting polymers, after converting back to its acid form, as aPAAMPSA-Y, where Y refers to the PEO-equivalent number-average molecular weight of the polymer in kg/mol. To synthesize aPAAMPSA-30, -67, and -117, a $Cu^{I}Cl$: $Cu^{II}Cl_2$: initiator molar ratio of 1 : 1 : 1 was used and the Me_6TREN to initiator molar ratio was kept at 2 : 1. Specifically, we first dissolved $Cu^{I}Cl$ (0.1486 g, 1.5 mmol), $Cu^{II}Cl_2$ (0.2016 g, 1.5

mmol), EBiB (0.20 mL, 1.5 mmol), and AAMPSA-Na solution (50% by weight in water; 57 mL, 150 mmol) in a mixture of DI water (40 mL) and DMF (75 mL). The solution was stirred and degassed with N_2 for 30 minutes. Me_6TREN (0.76 mL, 3 mmol) was then injected into the flask using a gas-tight syringe to start the reaction. The reaction was terminated at different time points to obtain aPAAMPSA-Na of different molecular weights. For the synthesis of aPAAMPSA-150, we increased the $Cu^{I}Cl$: $Cu^{II}Cl_2$: initiator molar ratio to 2 : 2 : 1 to further suppress termination reactions during polymerization. During the polymerization of aPAAMPSA-287, we added even more $Cu^{II}Cl_2$, but also used a bifunctional initiator, dimethyl 2,6-dibromoheptanedioate (Aldrich, 98%), instead of EBiB. Typically, a bifunctional initiator produces polymers with higher molecular weight and narrower molecular weight distribution compared to a monofunctional initiator.[3] The resulting $Cu^{I}Cl$: $Cu^{II}Cl_2$: initiator ratio was thus to 2 : 4 : 0.5 for this polymerization. In all polymerizations, Me_6TREN was maintained at a 1 : 1 molar ratio with the total copper content. The polymerization was carried out at room temperature, after which the reaction mixture was exposed to air and diluted with DI water to terminate the reaction. The reaction mixture was then placed in dialysis bag (nominal molecular weight cutoff 6000-8000 g/mol) and dialyzed against DI water to remove unreacted aAAMPSA-Na and DMF. After dialysis, the mixture was concentrated and precipitated into THF to collect aPAAMPSA-Na. The THF supernatant was decanted, and the precipitate was rinsed with THF twice more. The aPAAMPSA-Na precipitate was then dried in a vacuum oven at 30 °C overnight. To convert aPAAMPSA-Na to its acidic form, the purified polymer was redissolved in DI water and passed through a column containing a strong acid ion exchange resin

(Amberlyst® 15 (dry), Acros Organics). The ion exchange resin was rinsed with DI water until the water ran clear prior to use. The conversion to acid was confirmed by pH measurements by comparing against that of commercially-available PAAMPSA-724 (100% sulfonic acid groups). The pH of PAAMPSA-724 at 0.12 M sulfonic acid groups is 1.5. We therefore measured the pH of our aPAAMPSA solutions at 0.12 M sulfonic acid groups to verify the complete conversion of aPAAMPSA-Na to aPAAMPSA. The measured pHs of aPAAMPSA samples were all 1.5. Furthermore, aPAAMPSA eluted at the same time as aPAAMPSA-Na with no significant peak broadening during GPC analysis, indicating that the acid conversion did not affect the molecular weight or molecular weight distribution of the polymer. Given that the termination reactions are suppressed during ATRP, the molecular weight distribution of aPAAMPSA is much narrower compared to that of CFRP-derived PAAMPSA having a comparable molecular weight. The PDIs of aPAAMPSA range between 1.16 and 1.28. Figure 2.1 contains the GPC traces of aPAAMPSA-30 (PDI = 1.16) and PAAMPSA-45 (PDI = 1.43) for comparison. The GPC trace of aPAAMPSA-30 is narrower than that of PAAMPSA-45, indicating a narrower molecular weight distribution. The peaks at longer elution times ($\geq$ 40 min) are due to solvents. Table 2.1 contains the molecular weight and molecular weight distribution of aPAAMPSA obtained from GPC experiments.

To examine the structure of PAAMPSA (and aPAAMPSA), we performed ^{1}H NMR on PAAMPSA (and aPAAMPSA) in deuterated water. Figure 2.2 shows the ^{1}H NMR spectra of (a) aPAAMPSA-30 and (b) PAAMPSA-45. The chemical structure of PAAMPSA (or aPAAMPSA) is also included with the proton contributions appropriately labeled. Peak **A** (δ = 1.3 ppm) corresponds to the protons in the two methyl groups (six

protons per repeat unit). Peak **B** (δ = 1.5 – 1.8 ppm) corresponds to the methylene backbone protons (two protons per repeat unit). Peak **C** (δ = 1.8 – 2.1 ppm) represents the methyne backbone proton (one proton per repeat unit) and peak **D** (δ = 3.0 – 3.5 ppm) corresponds to the protons in the methylene unit adjacent to the sulfonic acid group in PAAMPSA (and aPAAMPSA; two protons per repeat unit). The rest of peaks are associated with protons in solvents; the solvents have been identified in Figure 2.2 for clarity. The most pronounced peak at 4.7 ppm is from water; this peak is observed in the spectra of both PAAMPSA-45 and aPAAMPSA-30. The peaks at 1.7 and 3.6 ppm, as well as those in 2.7 – 2.9 ppm are only observed in the spectrum of aPAAMPSA-30. These peaks are associated with residual THF and DMF, respectively, introduced during the ATRP reaction.

Synthesis of PANI-PAAMPSA

To obtain water-dispersible, electrically-conductive PANI, we template polymerized aniline in the presence of PAAMPSA (or aPAAMPSA).[4, 5] We used PAAMPSA (and aPAAMPSA) of different molecular weights to dope PANI in order to investigate how the molecular characteristics of polymer acid template influence the conductivity of PANI-PAAMPSA (and PANI-aPAAMPSA). Scheme 2.1 summarizes the template synthesis of PANI-PAAMPSA (or PANI-aPAAMPSA). The polymer acid template serves two roles. The sulfonic acid group in PAAMPSA is responsible for doping PANI to produce the electrically conductive form of the PANI. Excess sulfonic

acid groups can impart water dispersibility to the resulting PANI-PAAMPSA (or PANI-aPAAMPSA) complex.

To synthesize PANI-PAAMPSA (or PANI-aPAAMPSA), PAAMPSA (or aPAAMPSA) (5.8g, 0.028 mol) was first dissolved in 375 mL of DI water. Aniline monomer (Fisher Scientific, 99.9%; 2.6g, 0.028 mol) was then added to the PAAMPSA (or aPAAMPSA) solution at 1:1 aniline to acid molar ratio, and stirred at room temperature for 1 h. An oxidizing agent, ammonium peroxydisulfate (Fisher Scientific, 98.2%; 5.8g, 0.025 mol), at 1:0.9 aniline to oxidizing agent molar ratio, was dissolved separately in 25 mL of DI water. The solutions were purged with N_2 for 30 min. The PAAMPSA (or aPAAMPSA)-aniline solution was then cooled in an ice water bath before the ammonium peroxydisulfate solution was added dropwise using a gas-tight syringe at the rate of approximately 1.25 mL/min. The reaction medium was kept at ice water temperature for the first 6 hours of the reaction and was vigorously stirred during the polymerization. The reaction was allowed to proceed overnight to ensure complete conversion. As aniline is polymerized along the PAAMPSA (or aPAAMPSA) backbone, PAAMPSA (or aPAAMPSA) becomes decreasingly hydrophilic. As a result, PANI-PAAMPSA (and PANI-aPAAMPSA) forms sub-micron size colloidal particles that are electrostatically stabilized by the ionic interactions between PANI and PAAMPSA (or aPAAMPSA). These PANI-PAAMPSA (and PANI-aPAAMPSA) particles are characterized in Chapter 5; the size and size distribution of which influence the conductivity of PANI-PAAMPSA (and PANI-aPAAMPSA) dramatically. To recover PANI-PAAMPSA (or PANI-aPAAMPSA), acetone was added slowly to the polymer suspension. The supernatant was decanted and then the rest of the mixture was

filtered to obtain a green powder that is the emeraldine salt form of PANI-PAAMPSA. The samples were then dried in the vacuum oven at 50°C overnight. To cast PANI-PAAMPSA films for further characterization, the green powder was redispersed in DI water at 5 wt% concentration. Because the particles are stabilized by strong ionic interactions, their size and size distribution are maintained after further processing. We denote these materials as PANI-PAAMPSA-X, (or PANI-aPAAMPSA-X) with X being the PEO-equivalent number-average molecular weight of the PAAMPSA (or aPAAMPSA) template, in kg/mol, that was used for the PANI synthesis. For ^{15}N solid-state NMR experiments, we polymerized ^{15}N aniline (Cambridge Isotope Laboratories, Inc., 99.7+%) according to the procedures above to yield ^{15}N PANI-PAAMPSA (or ^{15}N PANI-aPAAMPSA).

To examine the structure-conductivity relationships of PANI-PAAMPSA (and PANI-aPAAMPSA), the monomer acid-doped counterpart, PANI-AAMPSA, was also synthesized with reagents at the same molar ratios and procedures mentioned above. AAMPSA monomer is used to template polymerize aniline instead of PAAMPSA. X-ray diffraction (XRD) and conductivity measurement were subsequently performed on the sample, and the data were compared against those of PANI-PAAMPSA (and PANI-aPAAMPSA).

To investigate the influence of aniline composition on the electrical conductivity of PANI-PAAMPSA, we opted to polymerize aniline at varying aniline to sulfonic acid group molar feed ratios using PAAMPSA-45. To prepare these PANI-PAAMPSA samples, we used the same synthesis procedure as mentioned above, except we varied the aniline to acid molar feed ratio. In this series of PANI-PAAMPSA, the molar feed ratio

of aniline to sulfonic acid group was 1:0.5, 1:1, 1:1.5, 1:2, and 1:3. X-ray photoelectron spectroscopy (XPS) analysis on this series of polymers yielded aniline to sulfonic acid group molar ratios of 1:0.72, 1:0.85, 1:1.05, 1:1.26, and 1:1.91 for the resulting polymers, respectively. Differences between the feed ratios and resulting ratios of aniline to sulfonic acid group arise from the residual unpolymerized aniline monomers that were removed during purification. The experimental details of the XPS study are detailed later in this chapter. We refer to these polymers as PANI-PAAMPSA y:z where y:z is the aniline to sulfonic acid group molar ratio, as determined by XPS.

Deprotonation of PANI-PAAMPSA

To examine the structure of the non-conductive emeraldine base form of PANI (EB), the PAAMPSA (or aPAAMPSA) template was removed from PANI-PAAMPSA (or PANI-aPAAMPSA) samples through the addition of excess ammonium hydroxide. This process begins with preparing a 2 wt% PANI-PAAMPSA or PANI-aPAAMPSA dispersion in DI water. The dispersion was stirred for 5 days. We added 10-, 20-, 30-, 50-, and 80-fold molar excess of ammonium hydroxide to PANI-PAAMPSA-45, -83, -106, -255, and -724 dispersions, respectively, to neutralize PAAMPSA. These dispersions were stirred for 2 days. The PANI-PAAMPSA dispersion was green prior to the addition of ammonium hydroxide. Upon addition of ammonium hydroxide, the dispersion turned blue-black, a distinct color of dedoped PANI. The resulting dedoped PANI consisted of a very fine powder. We thus centrifuged the dispersion for 1 hour at 4500 rpm to recover the solids, which were subsequently washed thoroughly with water

and dried in the vacuum oven at 50°C. We refer to the dedoped materials as PANI-X where X denotes the PEO-equivalent number-average molecular weight of the initial PAAMPSA (or aPAAMPSA) template, in kg/mol, and as PANI y:z where y:z denotes the aniline to sulfonic acid group molar ratio obtained by XPS.

Gel Permeation Chromatography (GPC)

Gel permeation chromatography (GPC) is a size exclusion method to determine the molecular weight and molecular weight distribution of polymers. The injected polymer solutions are separated based on their hydrodynamic volumes (V_h). Species having larger hydrodynamic volumes (thus larger sizes) elute at shorter times.[36] The hydrodynamic volume of the polymer is directly proportional to the logarithm of its molecular weight.[36] The elution volume of a polymer, equivalent to the elution time at a flow rate of 1 mL/min, is thus inversely proportional to the logarithm of its molecular weight.

GPC on PAAMPSA and aPAAMPSA was performed using a Waters 2414 HPLC solvent pump that is attached to four Ultrahydrogel columns (300 x 7.8 mm, Waters Technology Corp.) in series, and a Waters 2414 refractive index detector (Waters Technology Corp.). A 4:1 v:v mixture of 0.1 M aqueous sodium nitrate solution and acetonitrile was used as the eluent (flow rate = 1 mL/min, T = 40°C). The PAAMPSA and aPAAMPSA solutions were prepared at 0.001 wt% polymer in eluent solvent. A series of near-monodispersed poly(ethylene oxide), PEO, standards were used for molecular weight calibration. Figure 2.1 shows the GPC traces for (a) aPAAMPSA-30

and (b) PAAMPSA-45. A slightly longer elution time and narrower peak width are observed in aPAAMPSA-30 compared to PAAMPSA-45, indicating a slightly lower molecular weight and narrower molecular weight distribution of the polymer. Calibration against PEO standards yields a molecular weight of 30 kg/mol and PDI of 1.16 for PANI-aPAAMPSA-30 and a PEO-equivalent number average molecular weight of 45 kg/mol and PDI of 1.43 for PANI-PAAMPSA-45. The molecular weight and molecular weight distribution of PANI-PAAMPSA, PANI-aPAAMPSA, and PANI were not examined by GPC because the polymers do not form homogeneous solutions in any common solvents.

Proton Nuclear Magnetic Resonance (^{1}H NMR) Spectroscopy

^{1}H NMR spectroscopy was used to identify the different proton environments of the polymer samples. The protons that are specific to each polymer can be observed. ^{1}H NMR spectroscopy on PAAMPSA (and aPAAMPSA) and PANI-PAAMPSA (PANI-aPAAMPSA) was performed with a Varian Unity+ 300 MHz spectrometer. The solvent used for our samples was deuterium oxide (D_2O), and 1 wt% of polymer solutions were prepared for the ^{1}H NMR experiments. Figure 2.3 shows the ^{1}H NMR spectra of (a) PAAMPSA-45 and (b) PANI-PAAMPSA-45. The composition determination using these spectra is challenging and is not accurate because of proton exchange with deuterated water.[6] D_2O easily exchanges deuteriums with the labile protons of the sulfonic acid and amide groups in PAAMPSA (or aPAAMPSA), resulting in the absence of these peaks in the NMR spectra of our samples obtained in D_2O. We thus used these

spectra only for chemical identification purposes. The chemical structure of PAAMPSA-45 was clearly identified from its ^{1}H NMR spectrum (Figure 2.2 (b)). In addition to the protons associated with PAAMPSA-45, the protons associated with the benzenoid rings in the PANI backbone (7.3 - 7.5 ppm) can be observed in the NMR spectrum of PANI-PAAMPSA-45 ((b) in the inset of Figure 2.3). The data in the inset were smoothed with an 11-boxcar.

Solid-State Nuclear Magnetic Resonance (Solid-State NMR) Spectroscopy

Typically, delocalization of electrons in conducting polymers causes the paramagnetic broadening in NMR signals.[7] Owing to this broadening, NMR analysis is challenging in conducting polymers. The elimination of delocalized electrons along the polymer backbone can result in higher resolution NMR spectra.[7] We thus examined dedoped conducting polymers to identify their chemical structures by NMR. Given that dedoped PANI does not dissolve in any commercially-available deuterated solvents, we carried out our structural characterization studies via solid-state NMR.

We performed solid-state ^{13}C and ^{15}N NMR (Varian Unityplus-200 spectrometer) in collaboration with Jennifer L. Cross and Prof. Matthew P. Espe in the Chemistry Department at the University of Akron. The solid-state NMR spectra were collected using cross-polarization with a 1 ms cross-polarization time and magic-angle spinning configuration (CP/MAS). ^{13}C chemical shifts were collected with a recycle delay of 2 seconds and referenced with respect to hexamethylbenzene ($\delta\ ^{13}C_{methyl} = 17.3$ ppm). ^{15}N solid-state NMR spectra were collected with a recycle delay of 5 seconds, and ^{15}N

chemical shifts were referenced with respect to ammonium nitrate (δ $^{15}NH_4^+$ = 0 ppm). All samples were packed into 7 mm silicon nitride rotors with Kel-F caps and the samples were spun at 5 kHz.

Figure 2.4 contains the ^{13}C solid-state NMR spectra of (a) PAAMPSA-45, (b) PANI-PAAMPSA-45, and (c) PANI-45. The chemical structures of the polymers are also included with the carbon contributions labeled. In the spectrum of PAAMPSA-45 (Figure 2.4 (a)), peak **a** (δ = 175 ppm) corresponds to the carbon in the amide functionality. Peak **b** (δ = 57 ppm) is due to the carbon in the methylene functionality adjacent to the sulfonic acid groups. Peak **c** (δ = 54 ppm) is assigned to the methylene functionality along the polymer backbone. Peak **d** (δ = 42 ppm) represents the dimethylated carbon next to the amine. Peak **e** (δ = 35 ppm) is associated with the methyne backbone carbon and peak **f** (δ = 28 ppm) corresponds to the pendant methyl carbons. The ^{13}C NMR spectrum of PANI-PAAMPSA-45 (Figure 2.4 (b)) contains a broad bump between 100 and 160 ppm in addition to the peaks associated with PAAMPSA-45. The broad bump is attributed to doped PANI; individual carbon environments are not resolvable because of heterogeneities in the distribution of positive charges along the PANI chains.[8, 9] To resolve this peak associated with PANI, ^{13}C NMR was performed on dedoped PANI-45 (Figure 2.4 (c)). The elimination of charge delocalization along the PANI backbone results in an NMR spectrum whose carbon environments are now individually resolvable. Peak **1** (δ = 158 ppm) in Figure 2.4 (c) is due to the carbon in the 1, 4 positions of the quinoid ring along the backbone. The other quinoid carbons appear at 136 ppm (peak **2**). Peak **3** (δ = 148 ppm) and the peak labeled **4, 5** (δ = 142 ppm) are associated with the carbons in the parapositions of the benzenoid

rings along the PANI backbone. The other carbons on the benzenoid ring show up at slightly different chemical shifts depending on their proximity to the quinoid unit. The strong peak labeled **6, 7** (δ = 123 ppm) is assigned to benzenoid carbons directly attached to the quinoid rings (represented by **6** and **7** on the chemical structure). The benzenoid carbons that are one ring away from the quinoid unit appear at 114 ppm (peak **8**). The assignments for PANI-45 are consistent with those reported previously,[8, 10] and indicate PANI-45 to be linear chains with low defect (such as ortho and meta linkages) densities.

In addition to ^{13}C NMR, ^{15}N NMR is useful for studying PANI due to its sensitivity to the chemical environments of charged and uncharged nitrogens in the polymer backbone. The chemical shifts due to differences between charged and uncharged nitrogens in ^{15}N NMR are large compared to those due to differences between carbon environments detected by ^{13}C NMR. For example, the chemical shift difference between the resonances arising from amine and imine structures is ~ 200 ppm, while the chemical shift difference between the corresponding benzenoid and quinoid species is only ~ 10-20 ppm in ^{13}C NMR. Figure 2.5 shows the ^{15}N solid-state NMR spectrum of PANI-PAAMPSA-724. The broad peak, labeled **I** (δ = 322 ppm), arises from residual unprotonated imine nitrogens. Peak **III** (δ = 115 ppm) is assigned to protonated amines whose charges are delocalized along the PANI-PAAMPSA backbone. While localized protonated amine environments, denoted **II** on the chemical structure in Figure 2.5 (b), have been reported for other polymer acid templated PANI systems,[11-13] we do not observe the presence of such localized amines in any of our samples.

X-ray Photoelectron Spectroscopy (XPS)

To examine the compositions of PANI-PAAMPSA, we performed x-ray photoelectron spectroscopy (XPS). XPS analysis was conducted in collaboration with Dr. Yangming Sun affiliated with the Texas Materials Institute at the University of Texas at Austin with a Physical Electronics ESCA 5700 spectrophotometer equipped with a monochromatic Al Kα X-ray source, a hemispherical electron analyzer and a low energy electron flood gun for charge compensation of insulating samples. Samples were introduced through a preparation chamber before they were transferred into the analysis chamber at $2x10^{-10}$ Torr. High-resolution scans were collected to quantitatively identify specific binding environments of C, O, N, and S for PANI-PAAMPSA and PANI-aPAAMPSA samples. During data analysis, the binding energy of the core level C1s peak was set at 284.5eV to compensate for surface charging effects.[14, 15] Data analysis consisted of fitting and subtracting a linear baseline from each high-resolution elemental spectrum, and then numerically integrating each baseline-subtracted peak. The integrated area was then corrected by the appropriate sensitivity factor[16] for each element. To compare samples, the integrated peak intensities were normalized by the integrated peak intensity of a common reference peak whose composition is believed to be constant throughout.

We performed XPS on PANI-PAAMPSA samples to determine the compositions of the polymers. We varied the takeoff angle, defined as the angle between the sample and the detector, to examine the composition along the depth of the film. Varying the takeoff angle allows us to tune the x-ray penetration depth; the larger the takeoff angle, the deeper the penetration of x-rays into the polymer film. The takeoff angle was varied from 15, 30, 45, 60, to 80°. For this experiment, 5 wt% of PANI-PAAMPSA

dispersions were drop cast on 1 cm by 1cm pieces of silicon wafer. Table 2.2 lists the compositions of C, O, N, and S atoms in PANI-PAAMPSA 1:0.85 at different takeoff angles. The compositions determined at 45, 60, and 80° are nearly constant. We can therefore assume that XPS measurements at larger incident angles reflect the bulk compositions of PANI-PAAMPSA.

Depth profiling with XPS has qualitatively demonstrated that the surface concentration differs from that of the bulk in PANI-PAAMPSA films. To establish a quantitative relationship between concentration and depth of the film, we performed a series of XPS studies that kept the incident angle constant at 45°, but incrementally removed layers from the film. To access greater film depths, an argon ion beam was used to sputter the sample at an ionization energy of 250 eV. After 5 to 10 min sputtering intervals, surface XPS scans were acquired. The sputtering rate was estimated to be approximately 15 nm/min. For this experiment, we spin coated a 5 wt% PANI-PAAMPSA dispersion on a 1 cm by 1cm piece of silicon wafer.

Figure 2.6 contains the (a) nitrogen and (b) sulfur XPS spectra of PANI-PAAMPSA-724 obtained prior to any sputtering. The nitrogen and sulfur spectra were deconvoluted with Gaussian functions using non-linear least squares analysis. During peak fitting in the nitrogen and sulfur regions, the full widths at half the maximum intensity (FWHM) of the peaks and the peak positions were kept constant, with peak intensities being the only floating parameters. Specifically, the nitrogen spectrum was deconvoluted into three components: a peak located at 399.2 eV attributed to the amide groups in PAAMPSA; one centered at 400.4 eV attributed to the protonated nitrogens associated with polarons and bipolarons in PANI-PAAMPSA (denoted N_1^+); and a third

located at 401.3 eV attributed to protonated nitrogens that are ionically associated with the sulfonic acid groups in PAAMPSA (denoted N_2^+).[17, 18] The FWHM of the individual peaks were kept constant at 1.4 eV.[17, 18] The XPS data in the sulfur region was deconvoluted into two doublets with individual peaks at 167.5 and 168.7 eV; and 168.3 and 169.5 eV.[19-21] The doublet at lower binding energy corresponds to sulfurs in the ionized sulfonic acid groups of PAAMPSA ($-SO_3^-$) while that at higher binding energy corresponds to the sulfurs in the sulfonic acid groups of PAAMPSA ($-SO_3H$) that do not participate in the protonation of PANI.[19, 21] The individual peaks within the doublets maintaine a FWHM of 1.0 eV during peak fitting.[19-21]

X-ray Diffraction (XRD)

X-ray diffraction (XRD) is a common technique used to determine the crystal structures of crystalline (or semicrystalline) materials. X-rays primarily interact with electrons in atoms of materials. When x-ray photons collide with electrons, some photons from the incident beam are deflected away from the direction where they originally travel. Diffracted waves from different planes of atoms can interfere with each other and the resultant intensity distribution is strongly modulated by this interaction. If the atoms are arranged in a periodic fashion, as in crystals, the diffracted waves consist of sharp interference maxima peaks. Measuring the diffraction pattern therefore allows to deduce the distribution of atoms in a material. Specifically, the peaks in XRD pattern are directly related to the inter-atomic planar distances with Bragg's Law, shown in Equation (2.3).

$$n\lambda = 2d \sin\theta \qquad (2.3)$$

In this equation, n is the integer representing the order of the diffraction peak, λ is the wavelength of the x-ray, d is the characteristic distance between lattice planes, and 2θ is the scattering angle.[48]

We conducted XRD (Philips Electronic Instruments Model PW 1720) on PANI-PAAMPSA and PANI-aPAAMPSA. Nickel-filtered Cu-Kα radiation from a sealed-tube generator operating at 40 kV and 40mA provided the incident source. Data were obtained from 2θ = 10° to 50° at a scan rate of 0.12 deg/min. We adhered 15 mg of PANI onto a glass slide with a 1cm × 1cm piece of double-sided tape. A blank glass slide was used as background. Figure 2.7 (a) shows the XRD spectrum of PANI-PAAMPSA-45. To calibrate 2θ during these experiments, we added 2.5 wt% sodium chloride (NaCl) (~ 0.4 mg) to PANI-PAAMPSA (or PANI-aPAAMPSA) samples. Figure 2.7 (b) is the XRD pattern of a mixed powder of PANI-PAAMPSA-45 and NaCl. The Bragg reflections of NaCl are identified with arrows (2θ = 31.7° and 45.5°). The Bragg reflections of PANI-PAAMPSA-45 were then shifted against published reflections of NaCl, which are also included in Figure 2.7 (c).[22] Due to a limited number of Bragg reflections and the low crystallinity in the sample, we were not able to determine the exact crystal structure of the polymer.

Ultraviolet-Visible Near-Infra-Red Spectroscopy (UV-vis-NIR)

UV-vis-NIR spectroscopy (Varian Model Cary 5000 and Agilent 8453) was used to examine the electronic structures of PANI-PAAMPSA and PANI-aPAAMPSA. The UV-vis-NIR experiments were performed on PANI-PAAMPSA (or PANI-aPAAMPSA) thin films. To make the films, 5 wt% PANI-PAAMPSA (or PANI-aPAAMPSA) aqueous dispersions were spin-coated at 500 rpm for 1 min on clean glass slides. A clean glass slide was used as background for this experiment. Data were collected in the wavelength range 300-1300 nm at a scan rate of 1 nm/sec with Varian Model Cary 5000 and in the wavelength range 300-1100 nm with Agilent 8453. Figure 2.8 shows the UV-vis-NIR spectrum of PANI-PAAMPSA-724. The peak at 310 nm corresponds to the π-π^* transition of the benzenoid and the peak at 450 nm is attributed to the polaronic shoulder.[23-25] The other broad peak at approximately 800 nm corresponds to the polaron interband transition.[23-25]

Dynamic Light Scattering (DLS)

Dynamic Light Scattering (DLS) gives the size and size distribution of particles in dilute dispersions by measuring the Brownian motion due to their collisions with solvent molecules.[61] The velocity of the Brownian motion is defined by the translational diffusion coefficient (D). The diffusion coefficient is in turn related to the hydrodynamic diameter (D_h) of the particles according to the Stokes-Einstein equation (Equation 2.4), assuming spherical, non-interacting particles.[61]

$$D_h = \frac{kT}{3\pi\eta D} \qquad (2.4)$$

where k is the Boltzmann's constant, T is the absolute temperature, and η is the viscosity of the solution. Because the particles are on the order of wavelength of the incident rasiation, they scatter light. The Brownian motion of the particles thus causes the intensity of the scattered light to fluctuate with time, from which a correlation function of the scattered intensity can be determined as a function of time. We analyzed the correlation function using the CONTIN algorithm with inverse Laplace transformation,[26] in order to determine the size and size distribution of electrostatically stabilized PANI-PAAMPSA and PANI-aPAAMPSA particles that were arrested during aniline polymerization.

For these studies, we prepared a very dilute PANI-PAAMPSA (and PANI-aPAAMPSA) dispersion in an aqueous NaCl solution. Unlike regular polymers, polyelectrolytes involve interchain electrostatic interactions. The overall scattering intensity detected by DLS thus reflects the contributions from different electrostatic interactions in the system. NaCl is thus used to effectively screen the interparticle electrostatic interactions.[27] Samples were prepared at 0.0001 wt% polymer in 0.1 M NaCl aqueous solution at 25 °C. Both polymer and salt concentrations were selected after a series of control experiments. Figure 2.9 (a) shows the hydrodynamic diameter of PANI-PAAMPSA-724 obtained at varying salt concentrations. The hydrodynamic diameter decreases with increasing NaCl concentration up to 10^{-2} M, suggesting that the diameter reflects that of PANI-PAAMPSA aggregates at NaCl concentrations below 10^{-2}

M. These aggregates form due to the interparticle electrostatic interactions. At NaCl concentrations above 10^{-2} M, however, the particle diameter is nearly constant with salt concentration. This observation suggests that we can effectively screen the interparticle electrostatic interactions above 10^{-2}M NaCl concentrations and the diameter measured at high salt concentrations is representative of that of individual particle. Figure 2.9 (b) shows the hydrodynamic diameter of PANI-PAAMPSA-724 particles obtained from DLS experiments on 0.1M NaCl solutions at varying polymer concentrations. Below a polymer concentration of 0.001 wt%, the hydrodynamic diameter is constant, suggesting that this value is representative of individual particle diameter. The hydrodynamic diameter, however, increases above 0.001 wt%, indicating that particle aggregation occurs above 0.001 wt%. We therefore selected 0.0001 wt% PANI-PAAMPSA (and PANI-aPAAMPSA) in 0.1 M NaCl solution for all the DLS experiments during this study.

The DLS Measurements were performed on a Brookhaven Instruments Inc. BI-200SM, equipped with a neodymium-doped yttrium aluminum garnet (Nd:YAG) laser that operates at 532 nm and an ALV 5000 autocorrelator at normal incidence. Each sample dispersion was measured 7 times with 10 scans each time (10 seconds per scan). The variations in the runs were used to determine the standard deviations reported in size and size distribution of PANI-PAAMPSA and PANI-aPAAMPSA particles. Figure 2.10 shows the number-weighted DLS intensity distribution of PANI-PAAMPSA-724. The mean hydrodynamic diameter was determined at the peak position of the intensity distribution, and the particle size distribution was quantified by the full width of the intensity distribution at half the maximum intensity (FWHM).

Transmission Electron Microscope (TEM)

We used a transmission electron microscope (TEM) to directly observe the particles of PANI-PAAMPSA (or PANI-aPAAMPSA). To prepare TEM samples, 50 µL of PANI-PAAMPSA (or PANI-aPAAMPSA) aqueous dispersion that was originally prepared for DLS experiments (0.0001 wt% polymer in 0.1 M NaCl aqueous solution) was drop cast onto carbon-coated 200 mesh copper grids (Electron Microscopy Sciences), and the excess solution was wicked away with a piece of filter paper. A Zeiss 910 operating at 100 keV and 10^{-7} Torr was used to acquire images of PANI-PAAMPSA (or PANI-aPAAMPSA) particles.

ATOMIC FORCE MICROSCOPY (AFM)

The solid-state structures of PANI-PAAMPSA (or PANI-aPAAMPSA) were obtained on a Digital Instrument Nanoscope IIIa. PANI-PAAMPSA (and PANI-aPAAMPSA) films were prepared by spin coating 5 wt% PANI-PAAMPSA (or PANI-aPAAMPSA) aqueous dispersions at 1000 rpm for 1 min on silicon wafers. The topography and root mean square (r.m.s) roughness of PANI-PAAMPSA (or PANI-aPAAMPSA) films were acquired in tapping mode. The r.m.s roughness was quantified using NanoScope software version 7.00b20.

Conductivity Measurements

The electrical conductivities of PANI-PAAMPSA (or PANI-aPAAMPSA) films were measured using the four-probe method,[28] as well as the transmission-line method[29, 30] at the room temperature with an Agilent 4145B Semiconductor Parameter Analyzer. To prepare the samples, we made 5 wt% PANI-PAAMPSA (or PANI-aPAAMPSA) dispersions in water, and stirred them for 10 days. We then drop cast the polymer dispersions onto glass substrates with pre-defined gold electrodes. The films were dried in air for 2 h before conductivity measurements.

Figure 2.11 shows the schematic diagram of our four-probe measurement setup. Four gold electrodes are equally spaced 0.4 cm apart. The resistance (R) of PANI-PAAMPSA (or PANI-aPAAMPSA) films is obtained by normalizing the potential drop across the inner electrodes by the current measured across the two outer electrodes to eliminate contact resistance. The conductivity (σ) is then obtained given the film resistance and the device geometry, as shown in Equation (2.5).

$$\sigma = \frac{L}{RA} = \frac{L}{R \cdot lt} \qquad (2.5)$$

where the cross-sectional area (A) is defined by the gold electrodes; it is the product of the length (l) of gold electrode and the thickness (t) of PANI-PAAMPSA (or PANI-aPAAMPSA) film. The distance, L, is defined between the two inner gold electrodes.

Figure 2.12 contains the schematic diagram of the transmission-line experimental setup. To extract the conductivity using transmission-line method, we first measured

the resistances (R) between pairs of electrodes at predefined distances. To reduce the conductivity errors originated from the film thickness (t), we measured the thickness of the film at each pair of electrode. We then plotted $R \bullet t$ against distance (L) between the electrodes. The distance (L) between two electrodes was varied between 100 and 300 μm. Figure 2.13 shows a representative $R \bullet t$ of PANI-PAAMPSA-724 as a function of the distance between electrodes. The conductivity of the sample is then extracted from the inverse slope of the data normalized by the length (l) of gold electrode; this method also eliminates contact resistance.

We have made multiple films from different batches of aqueous dispersions and different batches of polymerizations for each sample. Both the four-probe method and the transmission-line method yielded comparable conductivities for each sample. Table 2.3 lists the conductivities of PANI-PAAMPSA (and PANI-aPAAMPSA). In each of these methods, the same stencil masks were used to define electrodes so the relative errors from geometrical factors and dimension measurements are zero across all samples. The only measurable error in our experimental setup arises from thickness determination; this error is reflected in the standard deviation of conductivities (Table 2.3). The thickness of each film was measured by a Dektak II profilometer.

We also measured the temperature dependent conductivity in a cryostat from 81 K to 298 K using the four-probe method. For variable temperature measurements, PANI-PAAMPSA (or PANI-aPAAMPSA) aqueous dispersions were drop cast on transparencies to minimize the mechanical stresses due to differences in the thermal expansion coefficients of the substrate and PANI-PAAMPSA (or PANI-aPAAMPSA) on cooling. PANI-PAAMPSA (or PANI-aPAAMPSA) was then encapsulated in an acrylic

resin. The conduction process in PANI can be accounted for in terms of electron hopping with the assistance of proton transfer, for which the presence of water plays an essential role.[31] The conductivity measured under air is thus typically higher than that measured under high vacuum. We thus used an acrylic resin to encapsulate our samples during this experiment, in order to minimize the removal of water under high vacuum. We measured the thickness of PANI-PAAMPSA (or PANI-aPAAMPSA) films before encapsulation.

Organic Solar Cells (OSCs) Fabrication and Chracterization

A solar cell is a device that converts solar energy into electrical energy. In organic solar cells (OSCs), the photoactive layer consists of two organic semiconductors, an electron-donor and an electron-acceptor. The photoactive layer is sandwiched between an anode and a cathode. The process of converting sunlight into electrical current in solar cells is accomplished in four steps. Figure 2.14 shows the schematic of the four steps that are involved during the operation of OSCs. In the first step, tightly bound electron-hole pairs, or excitons, are generated in a photoactive layer when light is absorbed. Generation of excitons can occur in the electron-donor layer or in the electron-acceptor layer, depending on the photoabsorption properties of the respective materials. The generated excitons then diffuse toward the electron-donor and electron-acceptor interface (step 2). The excitons then dissociate; the electrons are transferred to the electron-acceptor and the holes are transferred the electron-donor. The final step involves the transport of the newly generated charge carriers towards their respective electrodes.

Exciton diffusion lengths in polymeric and other disordered materials are generally in the range of a few nanometers to a few tens of nanometers.[32] This limited distance implies that only excitons that are generated within the range of diffusion distance to the electron-donor and electron-acceptor interface can contribute towards photocurrent generation. Excitons that are generated further away from the interface typically recombine before they reach the interface. With this in mind, the bilayer structures of OSCs have been supplanted by bulk-heterojunction type devices (BHJ), in which the active layer consists of nanoscale domains of the electron-donor and electron-acceptor.[33] The BHJ architecture provides a significantly larger interfacial area between the electron-donor and electron-acceptor (Figure 2.15) compared to the bilayer architecture. This structure of BHJ effectively shortens the average distance that excitons have to diffuse before charge separation, and thus enhances photocurrent generation. BHJs have therefore been considered as the more promising device types in OSCs.

In these OSCs, indium thin oxide (ITO) is widely used as anodes because of its high conductivity and excellent optical transmittance. The use of ITO, however, appears to be increasingly problematic due to the limited availability of indium.[34] Additionally, its brittleness limits the overall flexibility of devices on plastic substrates.[35, 36] Several candidates have been reported for replacing ITO, such as other transparent conducting oxides, carbon nanotube films, and conducting polymer films, etc.[37-39] To assess the suitability of PANI-PAAMPSA as a replacement for ITO, we fabricated OSCs with PANI-PAAMPSA anodes. To fabricate BHJ OSCs with PANI-PAAMPSA as device anodes, we started with the deposition of gold grids on bare glass substrates to

reduce device contact resistance. We then spin coated PANI-PAAMPSA aqueous dispersions on the glass substrates with predefined gold grids at 1000 rpm for 1 min. We used a blend of poly(3-hexylthiophene) (P3HT; Merck) and [6,6]-phenyl-C61-butyric acid methyl ester (PCBM; NanoC) for the active layer. P3HT is the electron donor, and PCBM is the electron acceptor. P3HT and PCBM was codissolved in chlorobenzene and the solution was deposited by spin coating directly on PANI-PAAMPSA electrodes at 500 rpm for 1 min. The P3HT and PCBM was kept at 1:0.8 (w/w) in a 2.4 wt% solution. We then deposited 100 nm of aluminum by thermal evaporation through a shadow mask as the cathode. The active area of OSCs is 0.0625 cm^2. We also fabricated reference OSCs with ITO anodes with the same device geometry and dimensions for comparison. All devices were fabricated and tested immediately in air.

To evaluate the device characteristics of these OSCs, we performed current density-voltage (J-V) measurements using a solar cell testing setup (Newport Corporation) equipped with a solar simulator (1.5 AM and 100 mW/cm^2). Figure 2.16 shows the representative J-V characteristics of an OSC with ITO anode under illumination. Several parameters to characterize the devices can be extracted from this figure. The short-circuit current (*Jsc*) is the maximum current through the unbiased device, and the open circuit voltage (*Voc*) is the maximum voltage in the device when no current is flowing. These two values are indicated with (a) and (b), respectively, in Figure 2.16. Between (a) and (b), in the fourth quadrant, the device generates power (current × voltage). At a certain point, the product between current and voltage, and thus the power output, can be maximized ($P_{MAX} = I_{MAX} \times V_{MAX}$). To determine the efficiency (η) of the solar cell, the generated power (P_{OUT}) is compared with incident

power (P_{IN}) due to photo irradiation. The fill factor (*FF*) is the ratio of the actual maximum obtainable power to the theoretical power, so it can be calculated as Equation (2.6).[40]

$$FF = \frac{I_{MAX} V_{MAX}}{I_{SC} V_{OC}} \tag{2.6}$$

With this, the power conversion efficiency can be written as Equation (2.7).[40]

$$\eta = \frac{P_{OUT}}{P_{IN}} = \frac{I_{MAX} V_{MAX}}{P_{IN}} = \frac{FF \cdot I_{SC} \cdot V_{OC}}{P_{IN}} \tag{2.7}$$

Generally, the J-V characteristics of a solar cell device can be described by Equation (2.8).[40]

$$I = I_0 \cdot \left\{ \exp\left(\frac{e}{nkT}(U - IR_S)\right) - 1 \right\} + \frac{U - IR_S}{R_{SH}} - I_{PH} \tag{2.8}$$

where I_0 is the dark current, *e* is the elementary charge, *n* is the diode ideality factor, *U* is the applied voltage, R_S is the series resistance, R_{SH} is the shunt resistance, and I_{PH} is the photocurrent. The corresponding equivalent circuit diagram is shown in Figure 2.17. Typically, the series resistance is attributed to the finite conductivity of the semiconducting material in photoactive layer, the contact resistance between the

semiconductors and the adjacent electrodes, and the resistance associated with electrodes and interconnections. In contrast, the shunt resistance is introduced to consider the loss of photocurrent due to the presence of leakage path ways. The presence of this leakage current could be attributed to pinholes in the active layer and the recombination and trapping of the carriers during their transit through the devices. For high FF, two elements are required: the series resistance should be very low to get a sharp increase in the forward current, and the shunt resistance should be high to limit leakage currents.

In this chapter, we provided an overview of the synthetic details and characterization techniques associated with our work. Water-dispersible, electrically conductive PANI-PAAMPSA will be characterized for its structure-conductivity relationships in Chapters 3 and 4. In Chapter 5, we describe the origin of PANI-PAAMPSA macroscopic conductivity. In Chapter 6, we explore the mechanism of PANI-PAAMPSA conductivity improvement after post-processing solvent annealing. Over the course of these chapters, GPC, ^{1}H solution NMR, ^{13}C and ^{15}N solid-state NMR, XPS, XRD, UV-vis-NIR, DLS, TEM, AFM, and conductivity measurements are used to characterize PANI-PAAMPSA. The fabrication and characterization of OSCs involving PANI-PAAMPSA are also described in Chapter 6.

Table 2.1. Physical Characteristics of PAAMPSA and aPAAMPSA that were used to dope PANI. PAAMPSA was synthesized via CFRP and aPAAMPSA was synthesized via ATRP.

Nomenclature	M_n* (kg/mol)	PDI
PAAMPSA-45	45	1.43
PAAMPSA-83	83	1.53
PAAMPSA-106	106	1.53
PAAMPSA-255	255	1.64
PAAMPSA-724	724	1.64
aPAAMPSA-30	30	1.16
aPAAMPSA-67	67	1.14
aPAAMPSA-117	117	1.20
aPAAMPSA-150	150	1.25
aPAAMPSA-287	287	1.28

* PEO-equivalent M_n, in kg/mol

Table 2.2. XPS results for PANI-PAAMPSA 1:0.85 with varying takeoff angles.

Takeoff angle	Molar ratio of element					$NH : SO_3$ molar ratio
	C (%)	O (%)	N (%)	S (%)	Total (%)	
15	65.31	20.46	10.18	4.05	100	1:0.66
30	66.23	20	9.77	4.00	100	1:0.69
45	64.72	21.4	9.53	4.35	100	1:0.84
60	64.42	21.35	9.78	4.45	100	1:0.83
80	65.39	20.14	9.88	4.59	100	1:0.87

Table 2.3. The conductivities of PANI-PAAMPSA and PANI-aPAAMPSA.

Nomenclature	Conductivity (S/cm)
PANI-PAAMPSA-45	1.09 ± 0.03
PANI-PAAMPSA-83	0.82 ± 0.02
PANI-PAAMPSA-106	0.67 ± 0.01
PANI-PAAMPSA-255	0.55 ± 0.02
PANI-PAAMPSA-724	0.43 ± 0.02
PANI-aPAAMPSA-30	2.39 ± 0.03
PANI-aPAAMPSA-67	1.95 ± 0.11
PANI-aPAAMPSA-117	1.52 ± 0.12
PANI-aPAAMPSA-150	1.32 ± 0.05
PANI-aPAAMPSA-287	1.07 ± 0.03

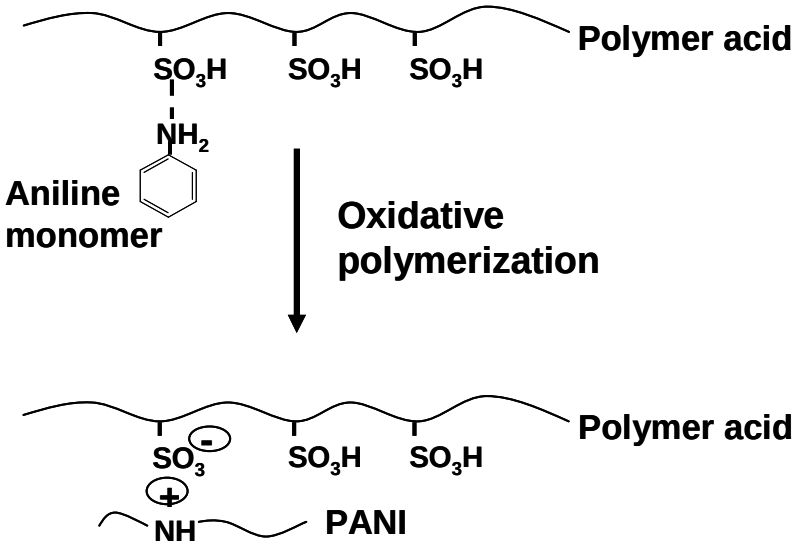

Scheme 2.1. Template synthesis of water-dispersible PANI-PAAMPSA (or PANI-aPAAMPSA). The sulfonic acid group in PAAMPSA dopes PANI; excess sulfonic acid groups impart water-dispersibility to the PANI-PAAMPSA (or PANI-aPAAMPSA) complex.

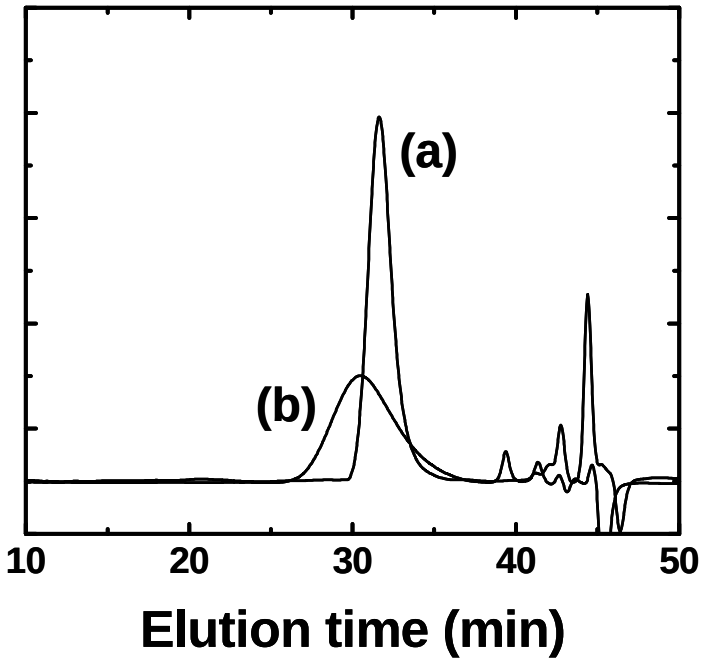

Figure 2.1. The GPC traces of (a) aPAAMPSA-30 (PDI=1.16) and (b) PAAMPSA-45 (PDI=1.43).

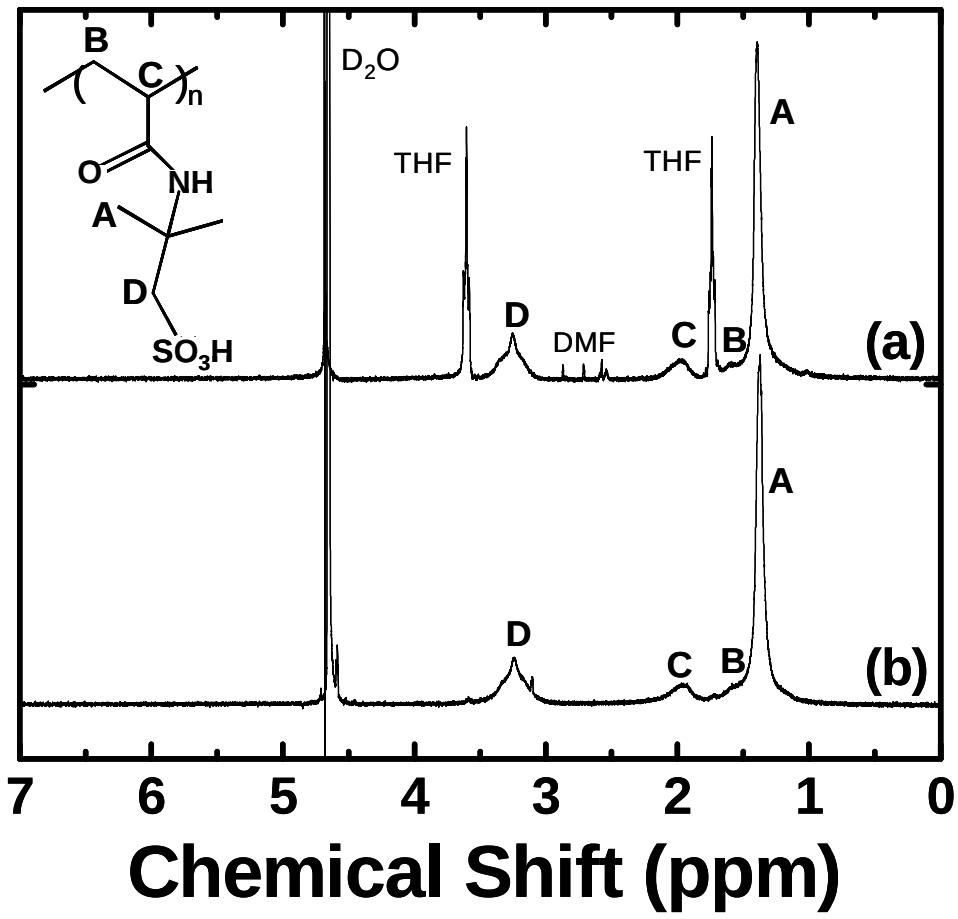

Figure 2.2. ^{1}H NMR spectra of (a) aPAAMPSA-30 and (b) PAAMPSA-45 in deuterium oxide. The proton contributions of the polymers are labeled for clarity. Solvent peaks are also included. The chemical structure of PAAMPSA (or aPAAMPSA) is provided in the inset for reference.

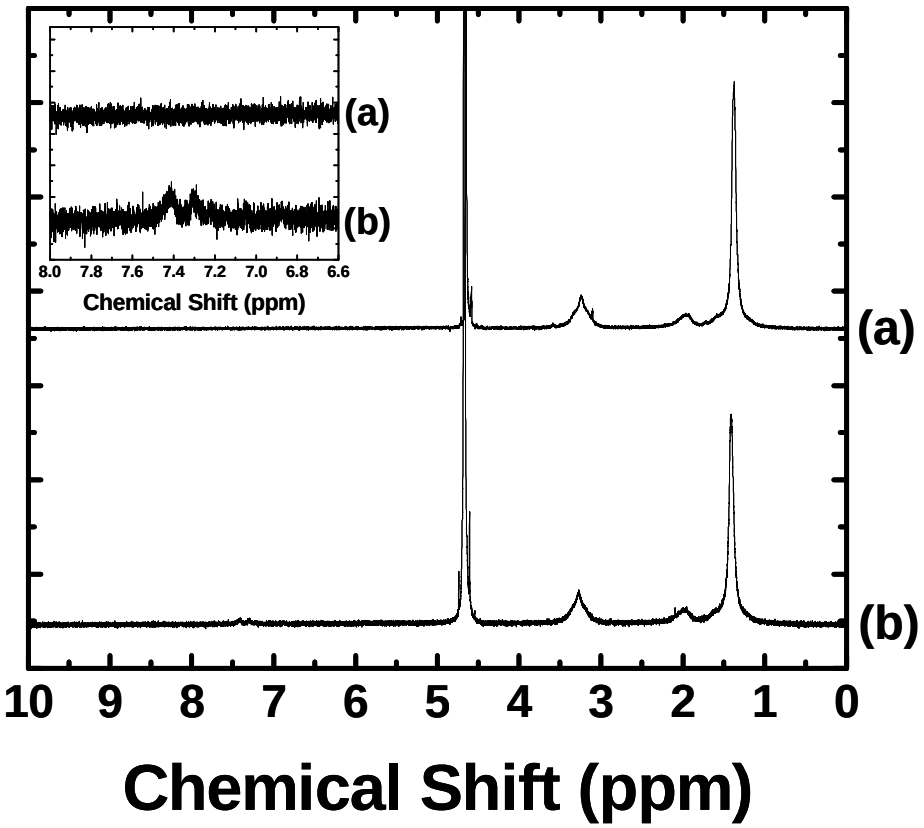

Figure 2.3. ^{1}H NMR spectra of (a) PAAMPSA-45 and (b) PANI-PAAMPSA-45. Inset: magnified ^{1}H NMR spectra of (a) PAAMPSA-45 and (b) PANI-PAAMPSA-45.

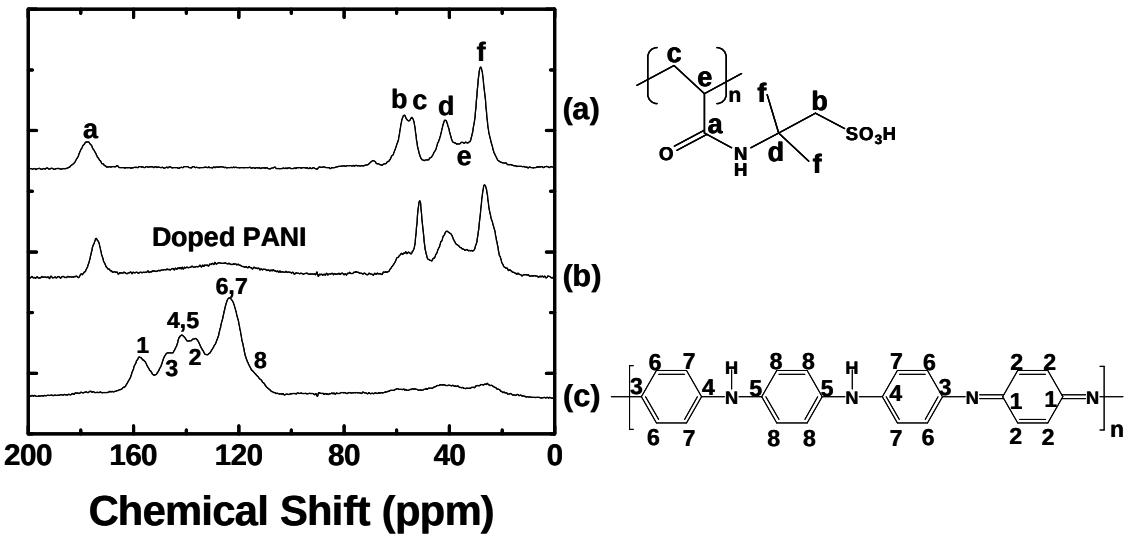

Figure 2.4. ^{13}C solid-state NMR spectra of (a) PAAMPSA-45, (b) PANI-PAAMPSA-45, and (c) PANI-45. The carbon contributions of the polymers are labeled for clarity. The chemical structures of PAAMPSA and dedoped PANI are also included.

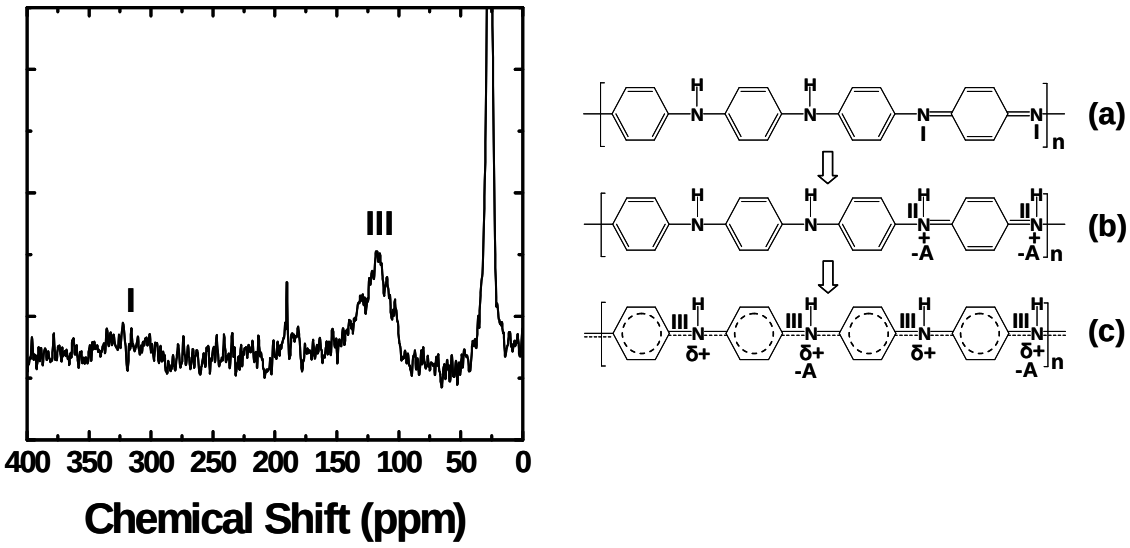

Figure 2.5. ^{15}N solid-state NMR spectrum of PANI-PAAMPSA-724. The nitrogen contributions of the polymer are labeled for clarity. The chemical structures of PANI during chemical doping is also included in (a) – (c) with the nitrogen environments labeled.

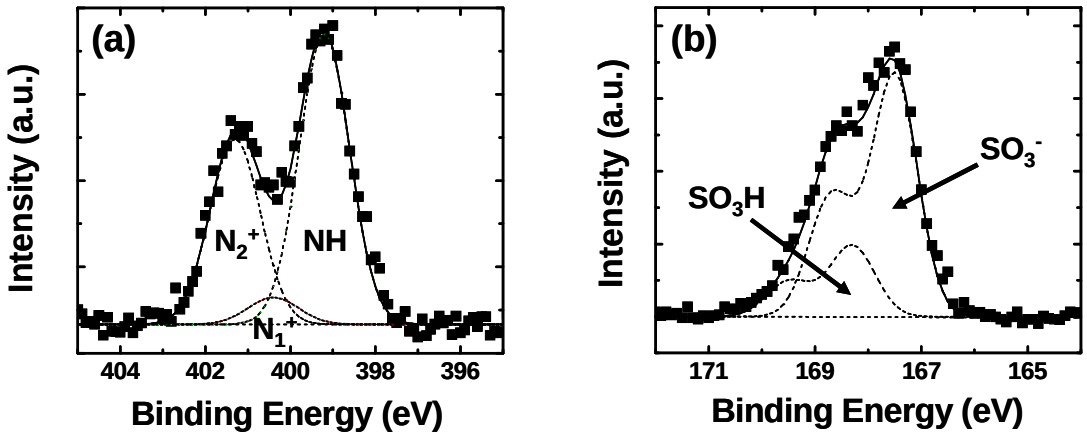

Figure 2.6. XPS spectra of the (a) nitrogen and (b) sulfur regions for as-cast PANI-PAAMPSA-724 with peak deconvolutions.

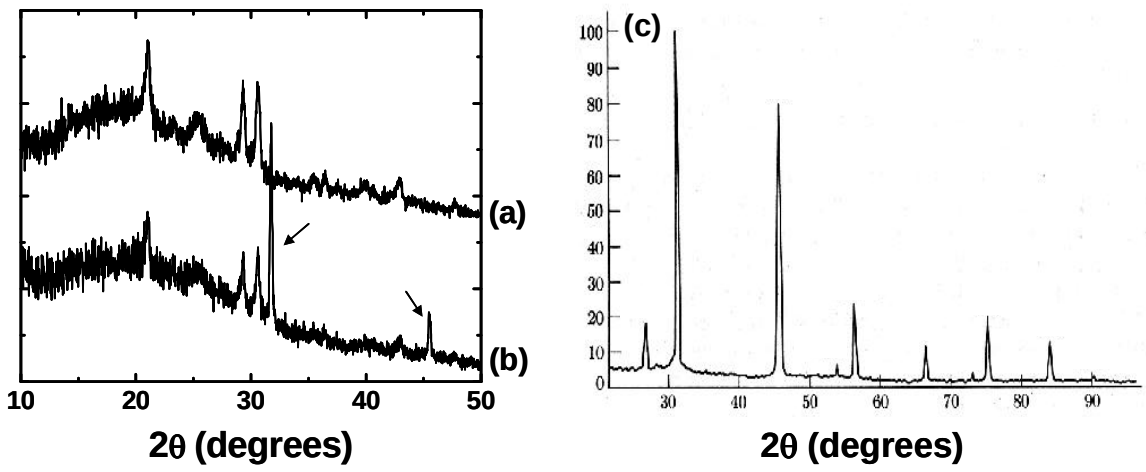

Figure 2.7. XRD spectra of (a) PANI-PAAMPSA-45 and (b) PANI-PAAMPSA-45 with 2.5 wt% NaCl. The Bragg reflections of NaCl are indicated with arrows in (b). (c) XRD spectrum of NaCl.[22]

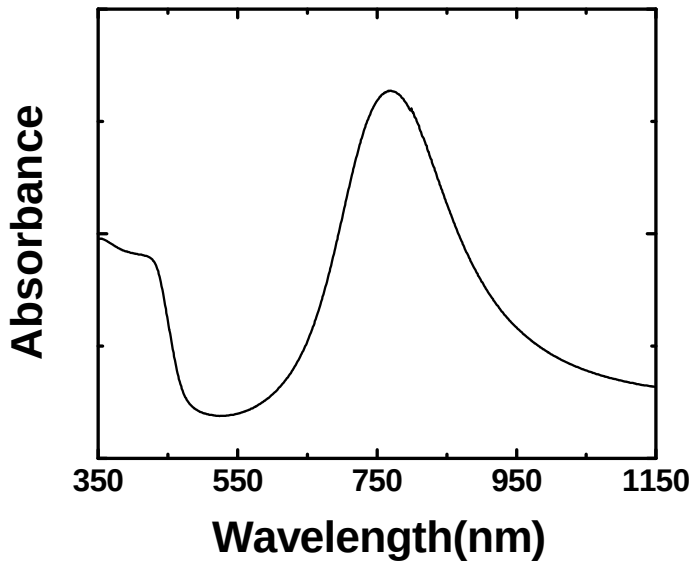

Figure 2.8. UV-vis-NIR spectrum of PANI-PAAMPSA-724.

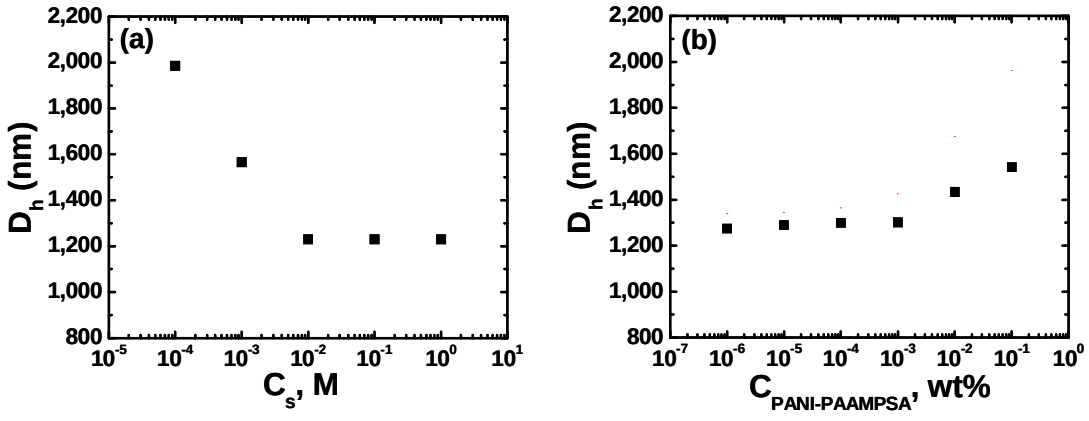

Figure 2.9. The mean hydrodynamic diameter of PANI-PAAMPSA-724 obtained from DLS experiments as a function of (a) salt concentration at a constant polymer concentration of 0.0001 wt%; (b) polymer concentration at a constant salt concentration of 0.1M.

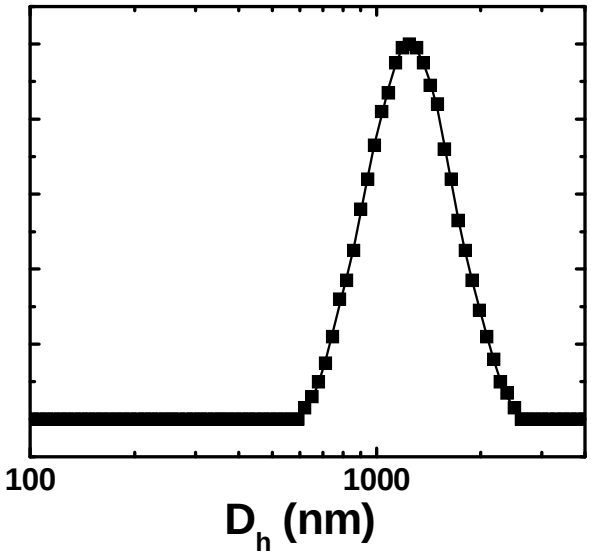

Figure 2.10. Intensity distribution of PANI-PAAMPSA-724 measured by DLS at 0.0001 wt% polymer in 0.1 M NaCl aqueous solution at 25 °C.

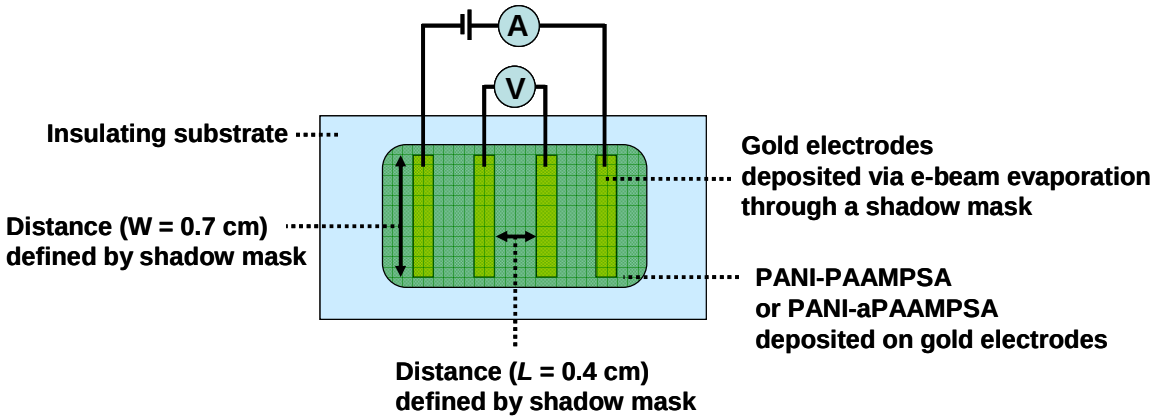

Figure 2.11. Schematic of the four-point probe experimental setup.

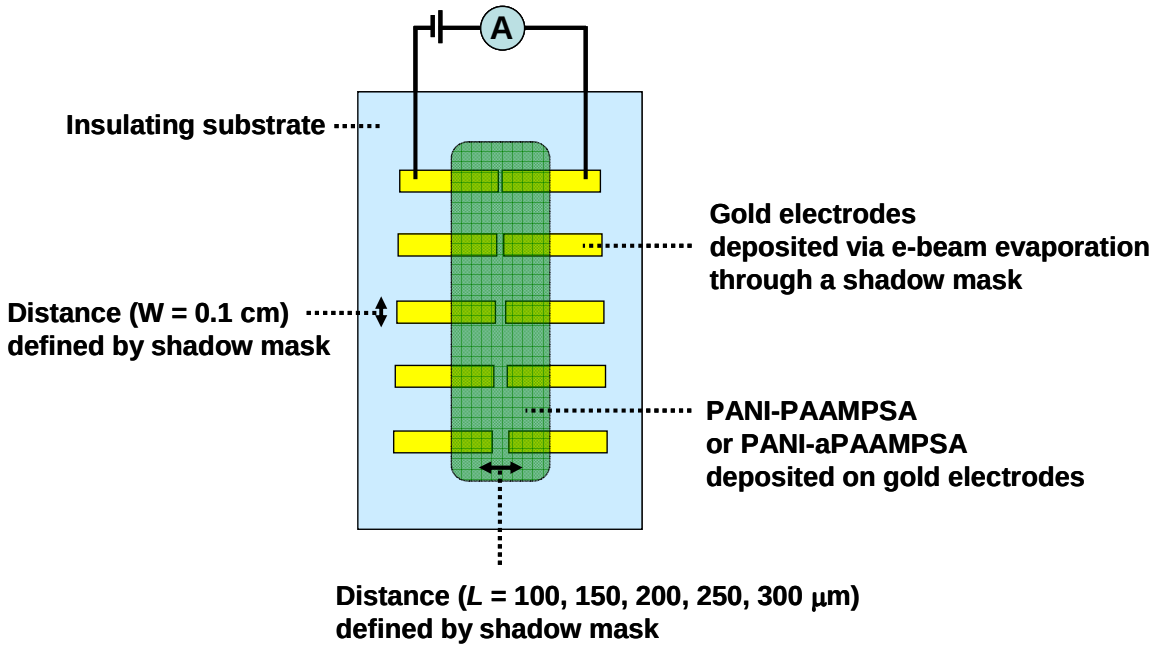

Figure 2.12. Schematic of the transmission-line method experimental setup.

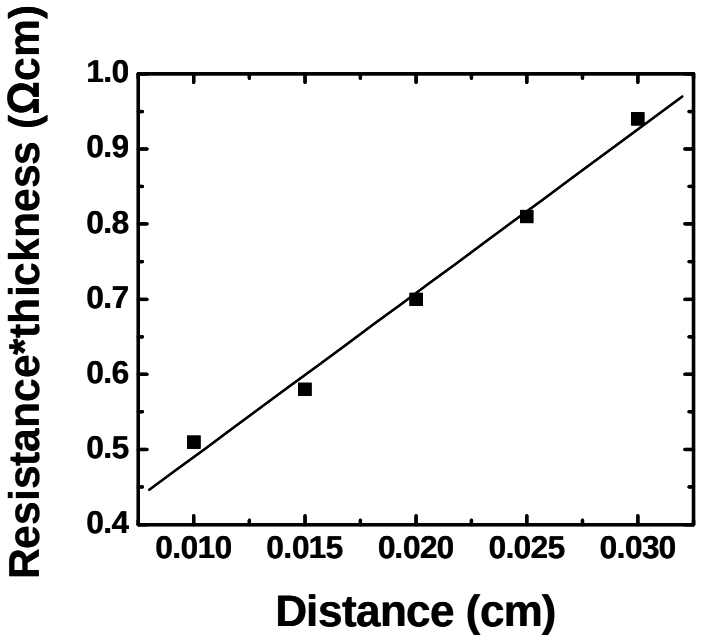

Figure 2.13. Thickness normalized resistance of PANI-PAAMPSA-724 as function of the distance between electrodes. The conductivity is extracted from the inverse of the slop normalized with the width of gold electrode.

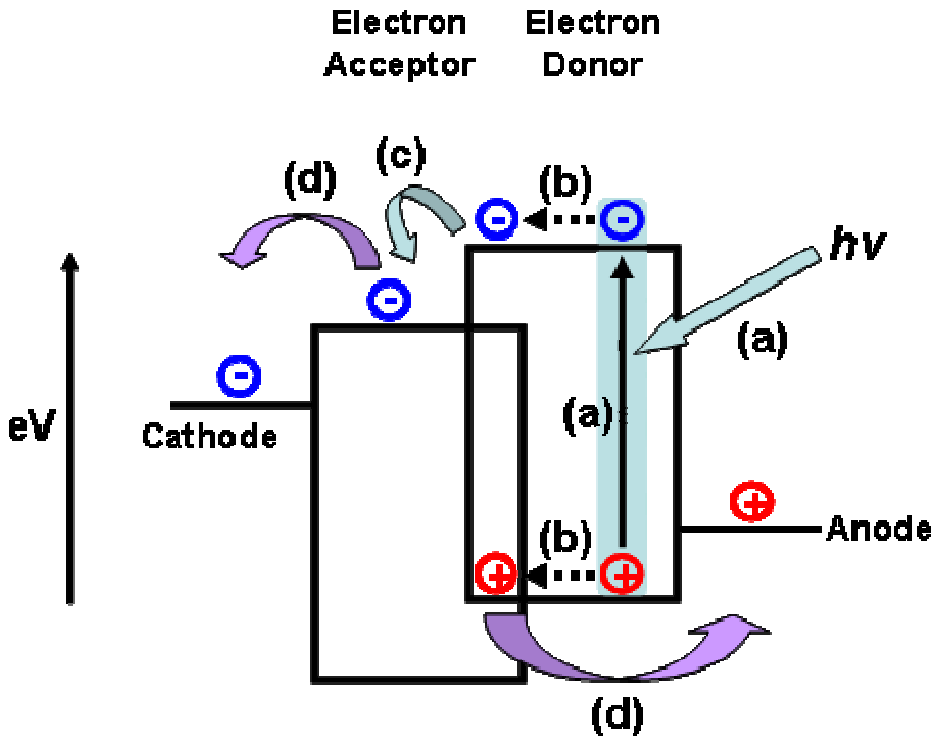

Figure 2.14. Schematic of the four steps that are involved during the operation of an OSC: (a) photoabsorption to generate excitons, (b) exciton diffusion toward the electron-donor and electron-acceptor interface, (c) exciton dissociation (electrons are transferred to the electron-acceptor layer and holes are transferred the electron-donor layer), and (d) charge transport towards the respective electrodes.

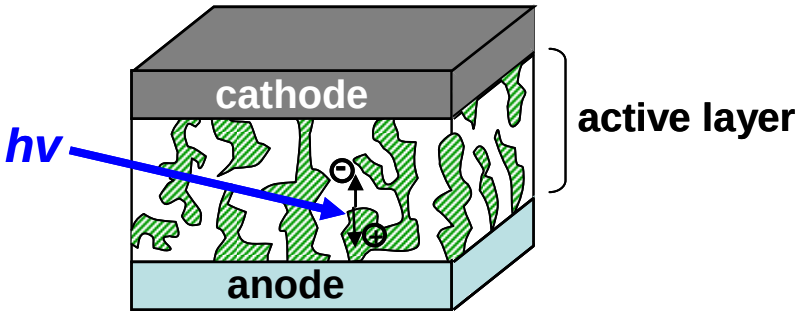

Figure 2.15. Schematic view of a bulk-heterojunction solar cell. The electron-donor is represented by unfilled region and the electron-acceptor is represented by hashed regions.

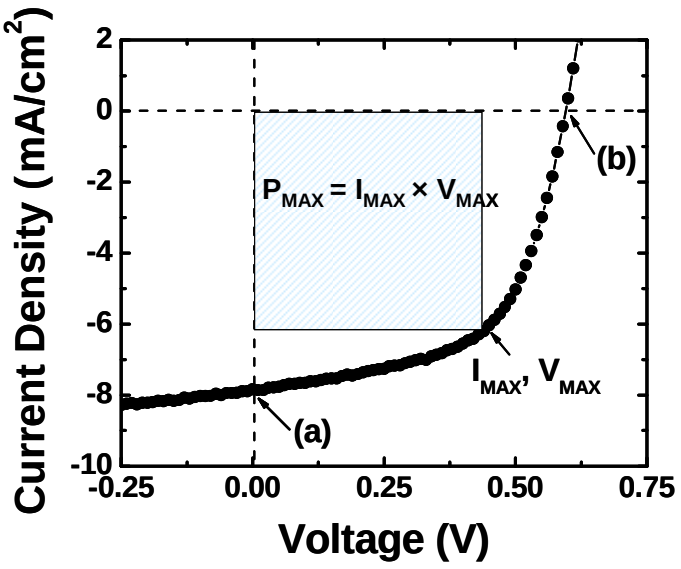

Figure 2.16. Current density-voltage characteristics of an OSC with ITO anode. (a) The short-circuit current and (b) open circuit voltage are included. The device was measured under illumination of AM 1.5 (100 mW/cm^2) with active area of 0.0625 cm^2.

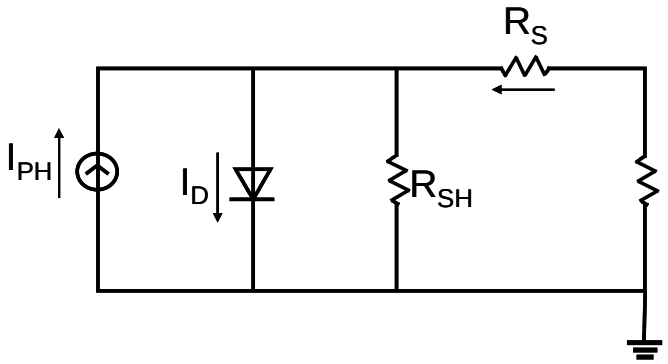

Figure 2.17. The circuit diagram of an idealized solar cell: I_{PH} is the photocurrent, I_D is the diode, R_S is the series resistance, and R_{SH} is the shunt resistance.[40]

REFERENCES

1. R. J. Young and P. A. Lovell, *Introduction to Polymers*, Chapman & Hall, London, 1991.
2. S. Perrier, S. P. Armes, X. S. Wang, F. Malet and D. M. Haddleton, *J. Poly. Sci., Poly. Chem.*, 2001, **39**, 1696.
3. V. M, H. A and W. P, *J. Appl. Polym. Sci.*, 1991, **42**, 629.
4. M. Angelopoulos, N. Patel, J. M. Shaw, N. C.Labianca and S. A. Rishton, *J. Vac. Sci. Technol. B*, 1993, **11**, 2794.
5. L. Sun, H. Liu, R. Clark and S. C. Yang, *Synth. Met.*, 1997, **84**, 67.
6. W. Reusch, NMR spectroscopy, http://www.cem.msu.edu/~reusch/VirtualText/Spectrpy/nmr/nmr1.htm, Accessed October 22, 2006.
7. H. Meng, D. F. Perepichka, M. Bendikov, F. Wudl, G. Z. Pan, W. Yu, W. Dong and S. Brown, *Journal of the American Chemical Society*, 2003, **125**, 15151.
8. S. Kaplan, E. M. Conwell, A. F. Richter and A. G. MacDiarmid, *J. Am. Chem. Soc.*, 1988, **110**, 7647.
9. S. Kaplan, E. M. Conwell, A. F. Richter and A. G. MacDiarmid, *Synth. Met.*, 1989, **29**, 235.
10. S. Kababya, M. Appel, Y. Haba, G. I. Titelman and A. Schmidt, *Macromolecules*, 1999, **32**, 5357.
11. S. K. Sahoo, R. Nagarajan, S. Chakraborty, L. A. Samuelson, J. Kumar and A. L. Cholli, *J. Macromol. Sci., Part A: Pure Appl. Chem.*, 2002, **A39**, 1223.

12. S. K. Sahoo, R. Nagarajan, S. Roy, L. A. Samuelson, J. Kumar and A. L. Cholli, *Macromolecules*, 2004, **37**, 4130.

13. S. K. Sahoo, R. Nagarajan, L. Samuelson, J. Kumar, A. L. Cholli and S. K. Tripathy, *J. Macromol. Sci., Part A: Pure Appl. Chem.*, 2001, **A38**, 1315.

14. H. S. Chan, H. S. Munro, C. Davies and E. T. Kang, *Synth. Met.*, 1988, **22**, 365.

15. P. Snauwaert, R. Lazzaroni, J. Riga and J. J. Verbist, *Synth. Met.*, 1987, **16**, 245.

16. D. A. Shirley, *Phys. Rev. B*, 1972, **5**, 4709.

17. E. T. Kang, K. G. Neoh and K. L. Tan, *Prog. Polym. Sci.*, 1998, **23**, 277.

18. J. Yue and A. J. Epstein, *Macromolecules*, 1991, **24**, 4441.

19. J. Y. Kim, J. H. Jung, D. E. Lee and J. Joo, *Synth. Met.*, 2002, **126**, 311.

20. G. Greczynski, T. Kugler and W. R. Salaneck, *Thin Solid Films*, 1999, **354**, 129.

21. K. Z. Xing, M. Fahlman, X. W. Chen, O. Inganaes and W. R. Salaneck, *Synth. Met.*, 1997, **89**, 161.

22. X-ray Diffraction (XRD), http://www.physics.pdx.edu/~pmoeck/phy381/Topic5a-XRD.pdf.

23. J. M. Ginder and A. J. Epstein, *Phys. Rev. B: Condens. Matter*, 1990, **41**, 10674.

24. P. M. McManus, R. J. Cushman and S. C. Yang, *J. Phys. Chem.*, 1987, **91**, 744.

25. S. Stafstrom, J. L. Bredas, A. J. Epstein, H. S. Woo, D. B. Tanner, W. S. Huang and A. G. MacDiarmid, *Phys. Rev. Lett.*, 1987, **59**, 1464.

26. K. S. Schmitz, *An Introduction to Dynamic Light Scattering by Macromolecules*, Academic Press, New York, 1990.

27. M. Sedlak, *Langmuir*, 1999, **15**, 4045.

28. K. S. Lee, G. B. Blanchet, F. Gao and Y.-L. Loo, *Appl. Phys. Lett.*, 2005, **86**, 074102.

29. S. Luan and G. W. Neudeck, *J. Appl. Phys.*, 1992, **72**, 766.

30. J. Zaumseil, K. W. Baldwin and J. A. Rogers, *J. Appl. Phys.*, 2003, **93**, 6117.

31. J. P. Travers and M. Nechtschein, *Synth. Met.*, 1987, **21**, 135.

32. V. Bulovic and S. R. Forrest, *Chemical Physics Letters*, 1995, **238**, 88.

33. G. Yu, J. Gao, J. C. Hummelen, F. Wudl and A. J. Heeger, *Science*, 1995, **270**, 1789.

34. M. W. Rowell, M. A. Topinka, M. D. McGehee, H.-J. Prall, G. Dennler, N. S. Sariciftci, L. Hu and G. Gruner, *Appl. Phys. Lett.*, 2006, **88**, 233506.

35. A. R. Schlatmann, D. W. Floet, A. Hillberer, F. Garten, P.J.M.Smulders, T. M. Klapwijk and G. Hadziioannou, *Appl. Phys. Lett.*, 1996, **69**, 1764.

36. J. C. Scott, J. H. Kaufman, P. J. Brock, R. DiPietro, J. Salem and J. A. Goitia, *J. Appl. Phys.*, 1996, **79**, 2745.

37. J. Cui, A. C. Wang, N. L. Edleman, J. Ni, P. Lee, N. R. Armstrong and T. J. Marks, *Adv. Mater.*, 2001, **13**, 1476.

38. A. K. Geim and K. S. Novoselov, *Nature Materials*, 2007, **6**, 183.

39. F. Zhang, M. Johansson, M. R. Andersson, J. C. Hummelen and O. Inganas, *Adv. Mater.*, 2002, **14**, 662.

40. S. S. Sun, *Organic Photovoltaics*, Taylor & Francis Group, Boca Raton, FL, 2005.

Chapter 3: The influence of molecular characteristics on PANI-PAAMPSA conductivity

Polyaniline (PANI) is considered to be an attractive conducting polymer for organic and polymer electronics due to its promising electrical and optical properties and environmental stability.[1-4] As mentioned in Chapter 1, the emeraldine base form of PANI (EB) is an insulator (Scheme 3.1 (a)). To obtain the conductive emeraldine salt form (ES) (Schemes 3.1 (b) and (c)), EB is proton doped by exposure to an acid. Typically, small-molecule acids, such as hydrochloric acid, are used to dope PANI.[5, 6] Such small-molecule acid doped PANI, however, has limited solubility in common solvents. While conductive, they cannot be processed from solutions or dispersions. PANI also exhibits a melting temperature that is above its degradation temperature, making melt-processible of PANI infeasible. Our route to obtain electrically conductive PANI that can be directly patterned from dispersions is the oxidative polymerization of aniline monomers on water-soluble polymer acid templates.[7-10] The polymer acid template serves two roles. In addition to doping PANI to yield the electrically conductive ES form, excess water-soluble pendant groups on the polymer acid template can impart water-dispersibility to the final material.[7-10] The resulting PANI is therefore not only electrically conductive, but can also be easily processed from an aqueous dispersion. In fact, much research has been carried out on PANI that is either chemically-,[8, 10, 11] electrochemically-,[12, 13] or enzymatically-[14, 15] synthesized on polymer-acid templates. This water dispersibility, however, comes at the expense of significantly

reduced conductivity of the final material, likely due to additional structural disorder that is introduced during template polymerization on polymer acids.[10, 16] The conductivities of polymer acid-templated PANI are thus generally lower (10^{-5} S/cm – 10^{-1} S/cm) than those of PANI that are doped with small-molecule acids (10 - 200 S/cm).[10, 16, 17] When such polymer acid-doped PANI is used as electrodes in electronic devices, such as organic thin-film transistors and organic solar cells, the bulk resistance of PANI limits current outputs in such devices.[2] It is thus imperative that we improve the electrical conductivity of polymer acid-doped PANI.

In this study, we used poly(2-acrylamido-2-methyl-1-propanesulfonic acid), or PAAMPSA, as the polymer acid template to dope PANI. PAAMPSA was chosen because both the monomer and the polymer are strong acids in aqueous solutions, so the pH of the aniline polymerization medium is maintained between 1 and 2.[18, 19] PANI synthesis at low pH levels ($\leq$ 3.0) is known to yield polymers with para-substituted aniline units.[15, 20] This linear structure of PANI has low defect densities and should thus result in high conductivity (10^{-1} -1 S/cm). When PANI is doped with a relatively weaker polymer acid than PAAMPSA, such as poly(vinyl phosphonic acid) (PVP), the final material was found to contain ortho or meta linkages. The structural defects can in turn result in lower conductivities (10^{-4} – 10^{-2} S/cm).[21] We also chose PAAMPSA as our polymer acid template because the amide groups in the repeating units of PAAMPSA (Scheme 3.1 (d)) can provide additional hydrogen bonding opportunities, which should further enhance the water dispersibility of PANI-PAAMPSA complexes.[1] To increase the conductivity of PANI-PAAMPSA, it is important to understand the factors that govern the electrical conductivity of the material. This chapter therefore examines the

influences of PAAMPSA molecular weight and aniline to acid composition on the conductivity of PANI-PAAMPSA.

THE INFLUENCE OF PAAMPSA MOLECULAR WEIGHT ON THE ELECTRICAL CONDUCTIVITY OF PANI-PAAMPSA

To determine the influence of PAAMPSA molecular weight on the electrical conductivity of PANI-PAAMPSA, we first synthesized PAAMPSA via conventional free-radical polymerization. We varied the molecular weights of PAAMPSA from 45 kg/mol to 724 kg/mol. We refer to the polymer as PAAMPSA-X where X refers to the poly(ethylene oxide)-, PEO-, equivalent number-average molecular weight of the polymer in kg/mol. We then oxidatively polymerized aniline on the PAAMPSA template at the 1:1:0.9 aniline : acid : oxidizing agent molar feed ratio. The resulting PANI-PAAMPSA is referred to as PANI-PAAMPSA-X with X being the PEO-equivalent number average molecular weight of the PAAMPSA in kg/mol. To obtain the non-conductive emeraldine base form of PANI, we deprotonated PANI-PAAMPSA through the addition of excess ammonium hydroxide. This dedoped PANI is referred to as PANI-X where X again denotes the PEO-equivalent number-average molecular weight of the initial PAAMPSA template in kg/mol. The synthesis procedure and molecular characteristics of polymers used were detailed in Chapter 2.

To examine the structure of PANI-PAAMPSA, we carried out ^{13}C solid-state NMR studies first on the polymer acid, and then on the doped and dedoped forms of PANI-PAAMPSA. The solid-state NMR experiments were performed in collaboration

with Jennifer L. Cross and Prof. Matthew P. Espe in the Chemistry Department at University of Akron. Figure 3.1 shows the ^{13}C solid-state NMR spectra of PAAMPSA-45 (solid line) and PAAMPSA-724 (dotted line). The peak assignments for PAAMPSA were made according to previous studies,[16, 22] and are included in Figure 3.1. Specifically, peak **a** (δ = 175 ppm) corresponds to the carbon in the acryl amide functionality; peak **b** (δ = 57 ppm) is due to the carbons in the methylene unit that is adjacent to the sulfonic acid group; peak **c** (δ = 54 ppm) is assigned to the methylene backbone carbon; peak **d** (δ = 42 ppm) represents the dimethylated carbon next to the amine; peak **e** (δ = 35 ppm) is associated with the methyne backbone carbon; peak **f** (δ = 28 ppm) corresponds to the six carbons in two methyl groups.

There is a subtle difference between the ^{13}C NMR spectrum of PAAMPSA-45 and that of PAAMPSA-724. Specifically, the line widths in the ^{13}C NMR spectrum of PAAMPSA-45 (solid line) are narrower than that of PAAMPSA-724 (dotted line). This decrease in line width indicates that PAAMPSA-45 is more "ordered" compared to PAAMPSA-724.[23] Given the sensitivity of NMR, the extent of order probed in these experiments reflect the polymer structure on a nanometer length scale. It does not reflect the extent of order over larger length scales. While both polymers are amorphous, our ^{13}C NMR indicates that PAAMPSA-45 has a more ordered local structure.

The ^{13}C solid-state NMR spectra of PANI-PAAMPSA-45 and that of PANI-45 are shown in Figures 3.2 (a) and (b), respectively. In addition to peaks attributable to the carbon environments of the polymer acid, a broad bump between 100 and 160 ppm is observed in the ^{13}C NMR spectrum of PANI-PAAMPSA-45 and is attributed to PANI

that is ionically associated with PAAMPSA. This broad bump is a result of the structural heterogeneities of doped PANI leading to different extents of delocalization of positive charges along the PANI backbone.[24, 25] To resolve the broad bump associated with PANI, we performed ^{13}C NMR on the dedoped form of PANI-PAAMPSA-45, or PANI-45 (Figure 3.2 (b)).

We examined the carbon environments of PANI-45 by performing ^{13}C NMR (Figure 3.2 (b)). We assigned the peaks in Figure 3.2 (b) according to previously published studies.[26] Specifically, peak **1** (δ = 158 ppm) is due to the carbon in the 1, 4 positions of the quinoid ring along the backbone. The other quinoid carbons appear at 136 ppm (peak **2**). The peak at 148 ppm (denoted **3** in Figure 3.2 (b)) and the peak at 142 ppm (denoted **4, 5** in Figure 3.2 (b)) are associated with the carbons in the para positions of the benzenoid rings along the PANI backbone. The other carbons on the benzenoid ring show up at slightly different chemical shifts depending on their proximity to the quinoid unit. The peak at 123 ppm (denoted **6, 7** in Figure 3.2 (b)) is assigned to benzenoid carbons that are directly attached to the quinoid rings (represented by **6** and **7** on the chemical structure). The benzenoid carbons that are one ring away from the quinoid unit appear at 114 ppm (peak **8**). The ^{13}C NMR spectrum is consistent with those published previously,[27, 28] and indicates that aniline was polymerized in a para-directed fashion in the presence of a PAAMPSA template, thereby resulting in linear PANI chains with low defect densities.[29]

The peaks between 10 and 70 ppm in Figure 3.2 (b) indicate the presence of residual PAAMPSA in PANI-45. To dedope PANI-PAAMPSA, excess ammonium hydroxide is added to dilute PANI-PAAMPSA aqueous dispersions. We added 10-, 20-

, 30-, 50-, and 80-fold molar excess of ammonium hydroxide to PANI-PAAMPSA-45, -83, -106, -255, and -724 dispersions, respectively. The dedoping process becomes increasingly inefficient with increasing PAAMPSA molecular weight due to mass transfer limitations of high molecular weight polymers. Figure 3.3 shows the ^{13}C NMR spectra of (a) PANI-724 and (b) PANI-45. The spectra appear to be largely similar, indicating the presence of linear, para-directed PANI and some residual PAAMPSA in both dedoped polymers. The two spectra, however, differ in the intensity of the PAAMPSA resonances; it appears that PANI-724 contains more residual PAAMPSA than PANI-45 despite the fact that more ammonium hydroxide was added to dedope PANI-PAAMPSA-724.

On the other hand, ^{15}N solid-state NMR provides interesting insights into the structure of PANI because ^{15}N chemical shifts in PANI are very sensitive to the distribution of the positive charges on the polymer backbone.[21, 29] In fact, the structure of PANI has been widely investigated using ^{15}N solid-state NMR.[21, 25, 29, 30] For example, Figure 3.4 shows the ^{15}N NMR spectrum of PANI that is enzymatically-synthesized on PVP.[29] Figure 3.5 shows the changes in chemical structure of PANI during its proton doping process. We assigned the peaks in Figure 3.4 according to the chemical structure of PANI shown in Figure 3.5.[26] Peak **1** at near 300 ppm in Figure 3.4 is broad and corresponds to residual unprotonated imine nitrogens (denoted **1** in Figure 3.5 (a)). Peak **2** (δ = 140 ppm) is associated with protonated imine nitrogens (denoted **2** in Figure 3.5 (b)) and peak **3** (δ = 81 ppm) is assigned to amine nitrogens (denoted **3** in Figure 3.5 (b)). The peak at 24.5 ppm is attributed to the presence of residual anilinium monomers.[31] The presence of unprotonated imine nitrogens suggests incomplete

protonation of PANI during its template polymerization on PVP. Given that the PANI is not fully doped, the low conductivity of this sample (~ 10^{-3} S/cm) is not surprising. Additionally, the presence of protonated imine nitrogens and amine nitrogens indicates that the positive charges are localized on the imine nitrogens along the PANI backbone, further contributing to the low conductivity of PANI-PVP. The chemical structure of PANI-PVP thus resembles that drawn in Figure 3.5 (b) where the charges are localized on the imine nitrogens in PANI backbone, rather than the one in Figure 3.5 (c). Such chemical structure where the cations are localized on individual imine nitrogens hinders efficient charge transport along the PANI backbone and thus results in lower conductivity to the material.

Figure 3.6 shows the ^{15}N NMR spectra of (a) PANI-PAAMPSA-724 and (b) PANI-PAAMPSA-45. The chemical structure of PANI during its doping process is shown in Figure 3.5; this chemical structure is used to assign the ^{15}N NMR peaks in Figure 3.6. Peak **1** (δ = 322 ppm) is attributed to residual unprotonated imine nitrogens in the ^{15}N NMR spectrum of PANI-PAAMPSA-724, as observed in that of PANI-PVP. The presence of these neutral imine nitrogens indicates that PANI-PAAMPSA-724 is also not completely doped as-synthesized. On the other hand, the ^{15}N NMR spectrum of PANI-PAAMPSA-45 does not exhibit any intensity in the range between 300 and 400 ppm, indicating that PANI-PAAMPSA-45 is completely doped as-synthesized.

In the ^{15}N NMR spectra of both PANI-PAAMPSA-724 and PANI-PAAMPSA-45, we observe a single peak at 115 ppm, midway between the chemical shifts for protonated imines (Figure 3.5 (b)-**2**) and neutral amines (Figure 3.5 (b)-**3**). This peak is assigned to the protonated amines whose charges are completely delocalized along the

PANI-PAAMPSA backbone (Figure 3.5 (c)-**4**).[21, 25, 29] Unlike the ^{15}N NMR spectrum of PANI-PVP (Figure 3.4), we only observe a single peak attributed to delocalized amine nitrogens in the ^{15}N NMR spectrum of PANI-PAAMPSA. Peaks associated with other nitrogen environments, including protonated imine nitrogens[25, 29] and uncharged amine nitrogens[21, 29] are not observed in the vicinity. The lack of these peaks indicates that only delocalized nitrogen species exist along both PANI-PAAMPSA-724 and -45 backbones (Figure 3.5 (c)-**4**). The extent of charge delocalization in PANI-PAAMPSA had not previously been observed in other polymer acid-templated PANI systems, and should result in the higher conductivities compared to systems like PANI-PVP.

In addition to the peaks associated with delocalized amine nitrogens, we observe a sharp and intense peak at 26 ppm in Figures 3.6 (a) and (b). Based on the chemical shift, we believe this peak arises from the presence of anilinium monomers that did not react during polymerization.[31] The assignment of this peak is further confirmed by the fact that it is suppressed when PANI-PAAMPSA is washed and precipitated repeatedly. For example, Figure 3.7 shows the ^{15}N NMR spectra of (a) three-times precipitated PANI-PAAMPSA-45 and (b) as-synthesized PANI-PAAMPSA-45. The peak at 26 ppm is suppressed greatly in the spectrum of three-times precipitated PANI-PAAMPSA-45 because most of anilinium monomers were removed during the multiple precipitations.

Figure 3.8 shows the ^{15}N NMR spectra of (a) PANI-724 and (b) PANI-45. Peak **1** at 320 ppm is associated with imine nitrogens (denoted **1** in Figure 3.5 (a)) and peak **5** at 73 ppm corresponds to amine nitrogens (denoted **5** in Figure 3.5 (a)).[31-33] There is no resonance at 26 ppm assigned to anilinium monomers in these spectra. The absence of

this peak indicates that unreacted anilinium monomers have been washed away during the deprotonation process. Careful examination of these ^{15}N NMR spectra also suggests the presence of residual PAAMPSA after deprotonation of PANI as observed in the ^{13}C NMR spectra of PANI-724 and PANI-45 (Figure 3.3). Figure 3.9 shows three fold magnified ^{15}N NMR spectra of (a) PANI-724 and (b) PANI-45 in the range between 80 and 200 ppm. A small peak at ~ 120 ppm is observed in both spectra, and this peak is assigned to the amide nitrogens associated with residual PAAMPSA after deprotonation of PANI. Consistent with the ^{13}C NMR spectra in Figure 3.3, the presence of this peak indicates that these PANI have not been completely deprotonated due to mass transfer limitations of high molecular weight polymers.

We have observed from ^{15}N NMR experiments that the molecular weight of PAAMPSA influences the structure of PANI-PAAMPSA. Specifically, PANI that is doped with PAAMPSA-724 is not completely doped, whereas PANI that is doped with PAAMPSA-45 is completely doped as-synthesized. It follows that the conductivity of PANI-PAAMPSA-45 should be higher than that of PANI-PAAMPSA-724.

To examine the electronic structure of PANI-PAAMPSA, we performed UV-vis-NIR spectroscopy on PANI-PAAMPSA samples. The UV-vis-NIR spectra of PANI-PAAMPSA are shown in Figure 3.10 (a). All the PANI-PAAMPSA samples exhibit absorptions that are characteristic of conductive PANI previously published.[34-36] The peak at 310 nm corresponds to the π-π^* transition of the benzenoid. The peak at 450 nm is attributed to the polaronic shoulder and the other absorption peak at approximately 800 nm corresponds to the polaron interband transition.[34-36] The presence of these absorption bands suggests the conductive form of PANI-PAAMPSA. The optical

spectrum of PANI-PAAMPSA-724 is consistent with that reported for PANI that adopts a "compact coil" structure, and is typically associated with materials having lower conductivities.[37] As we decrease the PAAMPSA molecular weight, however, the polaron interband transition broadens and red shifts, and the spectrum approaches that of an "expanded chain" structure.[37] The location of the polaron interband transition, λ_{max}, is quantified in Figure 3.10 (b) for clarity. In the "expanded chain" structure, charge transport should occur more efficiently compared to that in the "compact coil" structure. The conductivity of PANI-PAAMPSA should thus be higher in the "expanded chain" structure. The shift of λ_{max} to higher wavelengths with decreasing PAAMPSA molecular weight is therefore indicative of increasing conductivities.

Figure 3.11 shows the UV-vis-NIR spectrum of PANI-45. After deprotonation of PANI-PAAMPSA-45, the polaronic shoulder and polaron peak at 450 nm and 800 nm, respectively, completely disappear, while the emergence of a new absorption at 630 nm is observed due to the exciton transition of quinoid rings.[10, 17, 36] This observation is consistent with the UV-vis-NIR spectrum of emeraline base form of PANI, and indicates a para-directed, head-to-tail configuration of PANI when synthesized in the presence of PAAMPSA, as verified by the ^{13}C NMR studies on these materials (Figure 3.2).[10, 17, 36]

To examine the crystallinity of PANI-PAAMPSA, we acquired XRD on PANI that is doped with PAAMPSA having varying molecular weights, as shown in Figure 3.12. The peak at $2\theta = 26°$ is observed in all PANI-PAAMPSA samples. This peak is broader than other Bragg reflections and is associated with the ionic association between aniline and sulfonic acid groups.[16, 17] For PANI that is synthesized with the two higher molecular weights PAAMPSA (255 and 724 kg/mol), only the ionic association peak at

2θ = 26° is observed. For PANI that is synthesized with lower molecular weights PAAMPSA, other Bragg reflections are also observed. These peaks are associated with the crystallinity of PANI because PAAMPSA is amorphous (Figure 3.13). The number of Bragg reflections and the intensity of the reflections increase, indicating an increase in PANI crystallinity with decreasing PAAMPSA molecular weight.[6]

Because the crystallinity of PANI is low, we attempted to draw fibers in hopes to identify their crystal structure. Drawn fibers are generally more crystalline with large extents of orientation. There are thus forbidden reflections with drawn fibers, which can aid the determination of crystal structures and dimensions of PANI. We thus attempted to prepare PANI-PAAMPSA fibers by electrospinning.[38, 39] Figure 3.14 shows the electrospinning setup for the preparation of PANI-PAAMPSA fibers. The apparatus consists of a high voltage, low current transformer (Spellman CZE 1000R), a glass syringe with a hypodermic needle (20G1/2), a glass petri dish, and an aluminum (Al) foil that serves as a cathode. In the experimental setup, the hypodermic needle that is filled with an aqueous PANI-PAAMPSA dispersion is placed with its tip facing the petri dish. The positive end of the transformer is attached to the tip. The distance between the tip of the needle and the acetone surface is varied from 1 cm to 5 cm. The Al foil is placed under the petri dish containing acetone and is connected to electrical ground. Fibers can then be collected in the glass petri dish containing acetone. The potential difference between the tip and the counter electrode varies between 10 kV and 25 kV.

When we attempted to make PANI-PAAMPSA fibers at 10 kV using a 10 wt% PANI-PAAMPSA dispersion, the dispersion spread in acetone because the viscosity and surface tension of the dispersion were not high enough to maintain a stable droplet at the

end of the capillary tip. To make a stable drop at the end of the tip, we added > 5 wt% polyethylene oxide (PEO) into the 10 wt% PANI-PAAMPSA dispersion in hopes to increase viscosity. The PANI-PAAMPSA/PEO dispersion was markedly more viscous than PANI-PAAMPSA dispersion without PEO. Increasing the potential difference between the tip and counter electrode up to 25 kV resulted in a polymer dispersion drop, not a fiber, which precipitated into acetone. We also applied slight pressure on the syringe piston at 10 kV, but did not observe fiber formation at these conditions either. We then decreased the distance between the needle tip and the acetone surface from 5 cm to 1 cm; this method did not help to form fibers as well. Further increasing the applied potential up to 25 kV caused electrical sparks. As mentioned in Chapter 2, PANI-PAAMPSA forms electrostatically-stabilized sub-micron colloidal particles during polymerization due to strong ionic interactions between the sulfonic acid groups in PAAMPSA and aniline. Given the strong ionic interactions between PANI and PAAMPSA, such particles do not easily break up and their characteristics do not change with processing. In retrospect, fiber formation would first require the breaking up of these electrostatically stabilized particles, which is difficult given the strong ionic interactions. Identifying the crystal structure of PANI-PAAMPSA thus still remains challenging.

To examine the structure-conductivity relationships of PANI-PAAMPSA, we measured the bulk conductivity of PANI-PAAMPSA. For this experiment, we first prepared 5 wt% PANI-PAAMPSA dispersions in DI water; these dispersions were stirred for 10 days. The dispersions were then drop cast onto glass substrates with pre-defined gold electrodes. The thicknesses of the films range from 8 to 12 μm; the higher the

molecular weight of PAAMPSA that is used to dope PANI, the thicker the resulting PANI-PAAMPSA film. The electrical conductivities of these PANI-PAAMPSA films were measured using both the four-probe method and the transmission-line method at room temperature.[40, 41]

Figure 3.15 shows the electrical conductivity of PANI-PAAMPSA films as a function of the molecular weight of the corresponding PAAMPSA templates. As the molecular weight of PAAMPSA decreases from 724 to 45 kg/mol, the conductivity of PANI-PAAMPSA increases by approximately 3-fold (open circles); the highest conductivity we observed is 1.1 S/cm with PANI-PAAMPSA-45. The conductivities reported in Figure 3.15 represent averages from multiple measurements by both four-probe and transmission-line methods on films cast from different batches of dispersions and the error bars represent standard deviations from the average values. In all cases, the measured conductivities of PANI-PAAMPSA are significantly higher than those previously reported for PANI that were chemically synthesized on other polymer acids (10^{-5} - 10^{-2} S/cm),[10, 16, 17] and are slightly higher than those for PANI that were enzymatically synthesized on polymer acids (10^{-2} - 10^{-1} S/cm).[11, 14, 29] Given results from our solid-state NMR experiments, this enhanced conductivity of PANI-PAAMPSA compared to other polymer acid templated systems was somewhat expected. Specifically, our ^{13}C NMR experiments indicate a para-directed structure of PANI-PAAMPSA. This structure results in linear PANI chains with low defect densities and allows efficient charge transport along the PANI backbone. It is thus not surprising that PANI-PAAMPSA have higher conductivities (10^{-1} – 1 S/cm) compared to other PANI systems having high defect densities. For example, PANI that is enzymatically-

synthesized without a polymer acid template contains both ortho and meta linkages; crosslinking of PANI chains was also observed.[21] These structural defects act as electronic defects as they forbid the hopping of carriers, which is necessary for macroscopic conductivity.[21] Furthermore, ^{15}N NMR studies suggest that charge carriers are delocalized along the PANI-PAAMPSA backbone. This large extent of charge delocalization is not generally observed in other polymer acid-templated PANI systems. Instead, positive charges are typically localized on individual imine nitrogens in other polymer acid-doped PANI systems. With charges localized, these materials exhibit correspondingly lower electrical conductivities. We thus believe that the large extent of charge delocalization in PANI-PAAMPSA, not generally observed in other polymer acid templated PANI systems, is responsible for the high conductivity in our materials compared to other polymer acid-doped PANI systems.

The observed increase in the conductivity of PANI-PAAMPSA with decreasing PAAMPSA molecular weight is attributed to a more "open" structure of the polymer acid template at lower molecular weights. In the "open" conformation in water, the sulfonic acid groups are more accessible for doping,[37, 42] resulting in higher conductivities of PANI-PAAMPSA. The direct correlation between this electrical conductivity and polymer conformation is observed when comparing the electrical measurements to results from UV-vis-NIR spectroscopy. As the molecular weight of PAAMPSA decreases, we observed that the UV-vis-NIR spectrum of PANI-PAAMPSA approaches that of an "expanded chain" structure. When the polymer chains become more "expanded", the polaron band becomes more delocalized, so the conductivity increases. The shift of λ_{max} to higher wavelengths with decreasing PAAMPSA molecular weight therefore is

indicative of increasing the conductivity of PANI-PAAMPSA. We also observed a linear correlation between the extent of crystallinity and conductivity. An increase in the crystallinity of PANI-PAAMPSA was observed with decreasing PAAMPSA molecular weight, and this higher crystallinity is strongly correlated with a higher conductivity of the polymer. Additionally, our solid-state NMR experiments indicate the importance of local structural order of polymer acid template on the conductivity of PANI-PAAMPSA. An increase in the local order of PAAMPSA template (with decreasing PAAMPSA molecular weight) is directly correlated with an increase in the conductivity of PANI-PAAMPSA. Specifically, PANI that is doped with PAAMPSA of a small molecular weight is completely doped, and thus exhibits higher conductivity. This observation can be confirmed by the conductivity measurements of PANI-PAAMPSA films after exposure them to HCl vapor for additional doping. We exposed PANI-PAAMPSA films to HCl vapor for 30 min after the initial conductivity measurements.[15] We then remeasured the electrical conductivity of the films. Figure 3.16 shows the conductivity of PANI-PAAMPSA with varying PAAMPSA molecular weight before (○) and after (□) exposure to HCl vapor. The conductivities of PANI-PAAMPSA-724 and -255 increase slightly after exposure to HCl vapor, while the conductivities of the other samples remain largely unchanged. The observed increase in conductivity upon exposure to HCl vapor suggests that only PANI-PAAMPSA-724 and -255 were not completely doped as-synthesized. PANI that was synthesized with lower molecular weight PAAMPSA is completely doped as-synthesized; further exposure to acid does not improve the electrical conductivity.

In this study, we synthesized and characterized a series of water-dispersible PANI with PAAMPSA templates. Variation of the molecular weight of PAAMPSA allows for control over the resultant conductivity of PANI-PAAMPSA. Specifically, the conductivity of PANI-PAAMPSA increases as the molecular weight of PAAMPSA decreases. The increase in conductivity of PANI-PAAMPSA is directly correlated with increases in PANI crystallinity and conjugation length. Given that the crystallinity and conjugation length of PANI qualify the molecular order in PANI-PAAMPSA, we observed a linear correlation between molecular order and macroscopic charge transport in PANI-PAAMPSA.

THE INFLUENCE OF ANILINE TO ACID COMPOSITION ON THE ELECTRICAL CONDUCTIVITY OF PANI-PAAMPSA

We also investigated the influence of the composition of PANI-PAAMPSA, as probed by the aniline to acid molar ratio, on the electrical conductivity of the resulting material. For this study, we used PAAMPSA-45 to synthesize PANI at varying aniline to sulfonic acid group molar feed ratios of 1:0.5, 1:1, 1:1.5, 1:2, and 1:3. We refer to these polymers as PANI-PAAMPSA x:y where x:y is the aniline to sulfonic acid group molar ratio determined by x-ray photoelectron spectroscopy (XPS). Dedoped PANI-PAAMPSA x:y is denoted PANI x:y where x:y again denotes the aniline to sulfonic acid group molar ratio obtained by XPS.

To determine the structure of PANI-PAAMPSA in this series, we performed ^{13}C solid-state NMR on PANI-PAAMPSA samples. Figure 3.17 shows the ^{13}C NMR

spectra of PANI-PAAMPSA 1:0.72, 1:0.83, 1:1.26, and 1:1.91, as well as PAAMPSA-45. The ratios shown in Figure 3.17 are different from the prescribed molar feed ratios because a portion of unreacted aniline monomers is washed away during precipitation. The peaks for PAAMPSA-45 are assigned in Figure 3.17 (e) in accordance to the chemical structure.[16, 22] The peak assignments were detailed earlier in this chapter. In addition to the polymer acid peaks between 10 and 70 ppm, as well as that at 175 ppm, a broad bump due to charge delocalization along the PANI backbone[24, 25] appears between 100 and 160 ppm in the PANI-PAAMPSA spectra (Figure 3.17 (a)-(d)), and its intensity increases with decreasing PAAMPSA content. This observation indicates that PANI content increases in PANI-PAAMPSA samples as the PAAMPSA content decreases.

To resolve the peaks associated with PANI, we carried out ^{13}C NMR solid-state NMR on all the dedoped PANI-PAAMPSA samples. Figure 3.18 shows the ^{13}C NMR spectra on the dedoped form of PANI-PAAMPSA with varying aniline to acid molar ratios. The peaks in Figure 3.18 are assigned in accordance to the chemical structure of the base form of PANI. Like all the previous PANI-PAAMPSA samples analyzed, the chemical shifts shown in Figure 3.18 indicate that aniline is polymerized in a para-directed, head-to-tail fashion in the presence of PAAMPSA. This structure results in PANI that is linear and defect-free.[27, 28] Very similar carbon environments are observed in all the ^{13}C NMR spectra of PANI-PAAMPSA samples in this series. Despite changes in composition, all the PANI-PAAMPSA are structurally very similar.

To determine the nitrogen environments of PANI-PAAMPSA, we performed the ^{15}N solid-state NMR on PANI-PAAMPSA samples. Figure 3.19 contains the ^{15}N NMR spectra of PANI-PAAMPSA (a) 1:0.72, (b) 1:0.83, (c) 1:1.26, and (d) 1:1.91. In all the

^{15}N NMR spectra of PANI-PAAMPSA samples, we do not observe any peaks at ~ 320 ppm, which are associated with residual imine nitrogens (denoted **1** in Figure 3.5 (a)).[29, 31] This observation indicates that all the PANI-PAAMPSA samples in this series are completely doped as-synthesized. A single peak **4** is observed at 115 ppm in all the ^{15}N NMR spectra of PANI-PAAMPSA in this series (Figure 3.19). This peak is assigned to the protonated amines whose charges are delocalized along the PANI-PAAMPSA backbone (Figure 3.5 (c)-**4**).[21, 25, 29] We also observe a sharp and intense peak at 26 ppm in all the ^{15}N NMR spectra of PANI-PAAMPSA, and its intensity increases with increasing PAAMPSA content in PANI-PAAMPSA. This peak arises from residual anilinium monomers as mentioned above.[31] To examine the influence of such anilinium monomers on the conductivity of PANI-PAAMPSA, we remeasured the conductivity of PANI-PAAMPSA 1:0.83 after we removed the residual anilinium monomers by multiple precipitations. The conductivities were generally the same between the as-synthesized sample (1.09 S/cm) and the reprecipitated sample (1.01 S/cm). This observation indicates that the presence of anilinium monomers does not impact the conductivity of PANI-PAAMPSA. Our ^{15}N NMR experiments show that all the PANI-PAAMPSA samples in this series are fully doped as-synthesized and have large extents of charge delocalization along the backbone.

The XRD spectra of PANI-PAAMPSA with varying aniline to acid molar ratios are shown in Figure 3.20. The ionic association peak between aniline and sulfonic acid group is observed at $2\theta=26°$ in all the PANI-PAAMPSA samples.[43] The number of Bragg reflections and the intensity of the reflections appear to decrease, indicating a decrease in crystallinity with increasing PAAMPSA content in PANI-PAAMPSA.[6]

This observation is expected because PAAMPSA is amorphous; larger amount of amorphous polymer acid chains would make ordering of PANI chains difficult.

The UV-vis-NIR spectra of PANI-PAAMPSA samples are shown as a function of aniline to acid molar ratio in Figure 3.21 (a). The peaks corresponding to π-π^* transition of benzenoid, polaronic shoulder, and polaron interband transition[34-36] are observed in the spectra as previously described. As the PAAMPSA content increases in PANI-PAAMPSA, the polaron interband transition of PANI-PAAMPSA red shifts. The polaron interband transition blue shifts again with further increasing PAAMPSA content in PANI-PAAMPSA. The position of polaron interband transition peak (λ_{max}) is quantified in Figure 3.21 (b). The shift of λ_{max} to higher wavelengths typically indicates an increase in conjugation length of the material. As the content of sulfonic acid group increases, it is expected to increase the number of sites for doping PANI. The conjugation length of PANI therefore increases with increasing the amount of PAAMPSA. However, PAAMPSA is inherently insulating. Having excess PAAMPSA can thus hinder charge hopping and macroscopic conduction. Therefore, the conjugation length of PANI-PAAMPSA decreases with further increasing the PAAMPSA content.

To examine the structure-conductivity relationships of PANI-PAAMPSA as a function of aniline to acid ratios, we measured the electrical conductivities of PANI-PAAMPSA films in this series. The measured conductivities are shown in Figure 3.22 (open circles). As the sulfonic acid group content increases relative to that of aniline, the conductivity of PANI-PAAMPSA increases by approximately 6-fold. PANI-PAAMPSA at an aniline to sulfonic acid group ratio of 1:1.26 has the highest

conductivity of 2.6 S/cm in this series of polymer examined. Further increasing the PAAMPSA content, however, results in a decrease in the conductivity of PANI-PAAMPSA. This conductivity trend is directly correlated with the changes in conjugation lengths of PANI with compositions as observed in the UV-vis-NIR spectra (Figure 3.21 (b)). However, the structural changes of PANI-PAAMPSA with compositions observed from solid-state NMR and XRD studies are not correlated with the observed conductivity trend. These experiments indicate UV-vis-NIR to be a very sensitive measure of conductivity.

The ^{15}N NMR spectra of PANI-PAAMPSA also show that all the PANI-PAAMPSA films in this series are completely doped as-synthesized. This observation is corroborated with the conductivity measurements after exposure the PANI-PAAMPSA films to HCl. We exposed PANI-PAAMPSA films to HCl vapor for 30 min after the initial conductivity measurements,[15] and then remeasured the electrical conductivity of the films (open squares in Figure 3.22). The conductivities of all the PANI-PAAMPSA samples remain unchanged after exposure to HCl vapor; an indication that all the PANI-PAAMPSA samples are completely doped as-synthesized.[7, 43]

To identify the origin of the conductivity changes with compositions, we ideally would like to track the exact compositions of aniline that is associated with sulfonic acid groups that contribute to charge conduction. In the repeating unit of PANI EB, there are two amine nitrogens and two imine nitrogens (Scheme 3.1 (a)).[44, 45] During exposure to protonic acids, two acid groups are required per PANI repeat unit for complete doping (Scheme 3.1 (b)). The four nitrogens then share the two donated protons (Scheme 3.1 (c)). The optimal aniline to acid molar ratio of fully doped PANI-PAAMPSA should

thus be 1:0.5. In this series of PANI-PAAMPSA, the conductivity peaked at an aniline to acid molar ratio of 1:1.26. This molar ratio, however, accounts for all the aniline monomers and sulfonic acid groups present in the sample, whether they are ionically associated each other or not. Specifically, anilinium monomers, as well as extra sulfonic acid groups that are responsible for water dispersibility of the material are also present. To truly elucidate the influence of the aniline to acid molar ratio on conductivity, we would need to know the fractions of aniline and sulfonic acid groups that are ionically associated. We thus reprecipitated PANI-PAAMPSA into acetone to remove residual anilinium monomers from PANI-PAAMPSA. We observed a significant decrease in the intensity of the anilinium monomer peak in the ^{15}N NMR spectrum of PANI-PAAMPSA 1:0.83 after precipitation, indicating that much of the residual anilinium monomers have been removed (Figure 3.7). The molar ratio, as probed by XPS, increased from 1:0.83 to 1:1.23 after reprecipitation. We also measured the electrical conductivity of the reprecipitated PANI-PAAMPSA 1:0.83. Since residual aniline does not contribute towards the conductivity of PANI-PAAMPSA, the conductivity is unchanged after reprecipitation of the polymer (1.09 S/cm and 1.01 S/cm before and after reprecipitation, respectively). Even though we have effectively removed all the anilinium monomers, this procedure does not allow us to accurately account for the fractions of sulfonic acid groups that are ionically associated. This complication in determining the composition accurately has hindered our ability to quantitatively elucidate the influence of composition on the conductivity of PANI-PAAMPSA.

In this study, we observed that an optimum ratio of aniline to sulfonic acid groups exists for the maximum conductivity of PANI-PAAMPSA. The specific origin of this conductivity change with compositions remains unclear. The electrical conductivity, however, is strongly correlated with the electronic structure of the material; PANI-PAAMPSA with the highest conductivity contains the least electronic defects along the polymer backbone and has the longest conjugation length of PANI. The position of polaron peak maximum, λ_{max}, is thus a good indicator for the conductivity of PANI-PAAMPSA in this series.

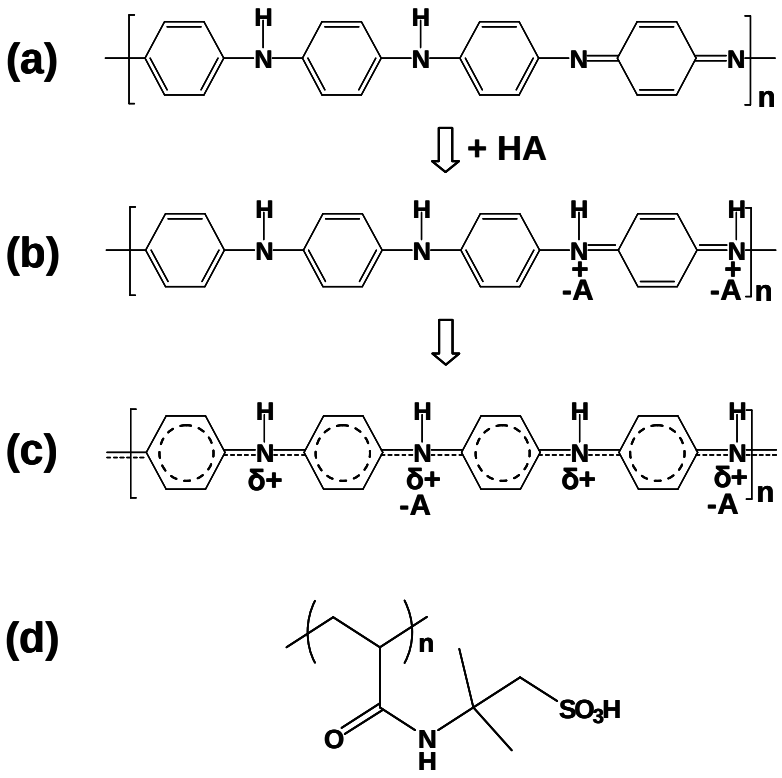

Scheme 3.1. Proton doping of (a) PANI emeradine base (EB). (b) PANI EB is protonated when exposed to an acid (HA). (c) Charge delocalization allows for charge transport along the PANI backbone.[44] (d) The chemical structure of PAAMPSA.

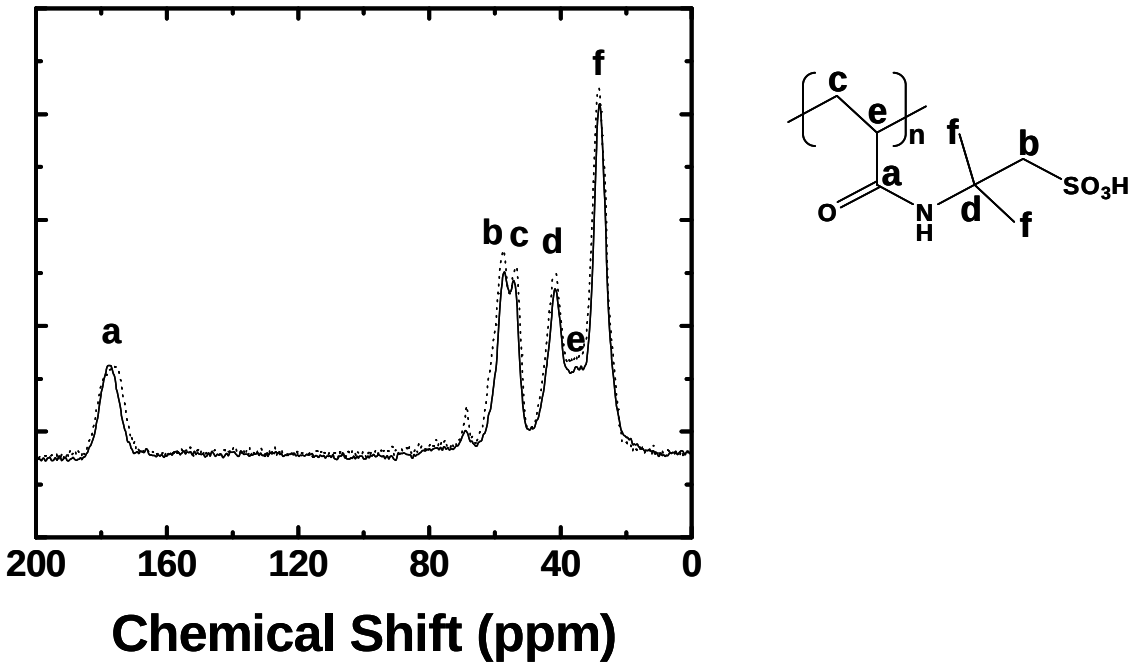

Figure 3.1. ^{13}C NMR spectra of PAAMPSA-45 (solid line) and PAAMPSA-724 (dotted line). The chemical shifts are labeled accordingly on the chemical structure of PAAMPSA that is included.

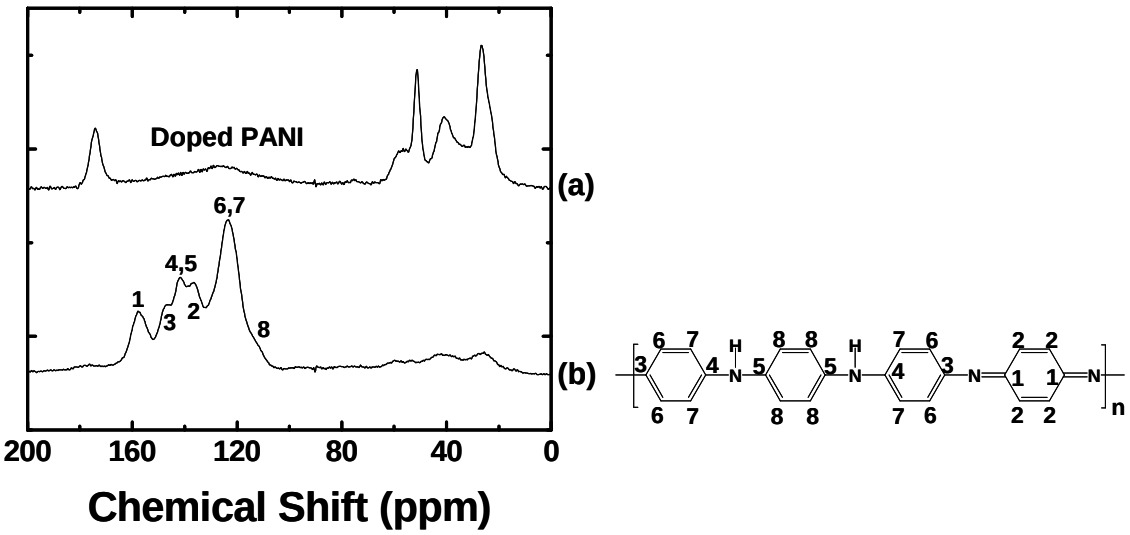

Figure 3.2. ^{13}C NMR spectra of (a) PANI-PAAMPSA-45 and (b) PANI-45. The chemical shifts of PANI-45 are labeled according to the chemical structure of the polymer that is included.

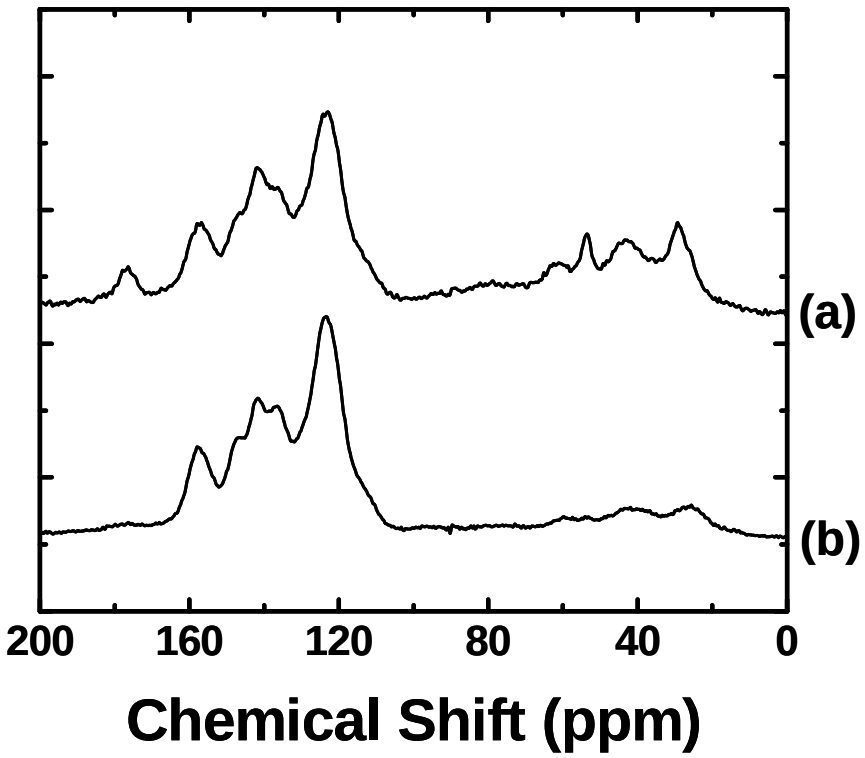

Figure 3.3. ^{13}C NMR spectra of (a) PANI-724 and (b) PANI-45. The intensity difference in the 10 – 70 ppm range is attributed to different amount of residual PAAMPSA after dedoping.

.

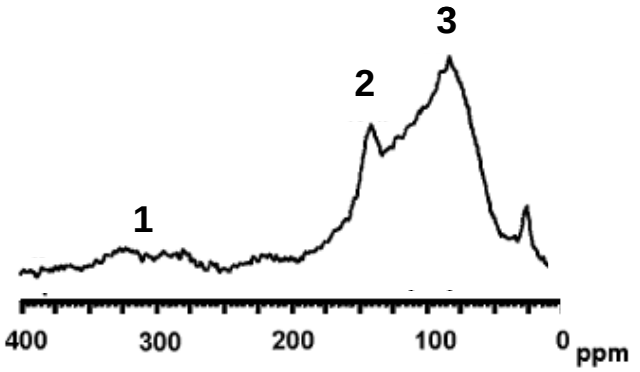

Figure 3.4. ^{15}N NMR spectrum of PANI-PVP. The chemical shifts are labeled according to the chemical structure as shown in Figure 3.5.[29]

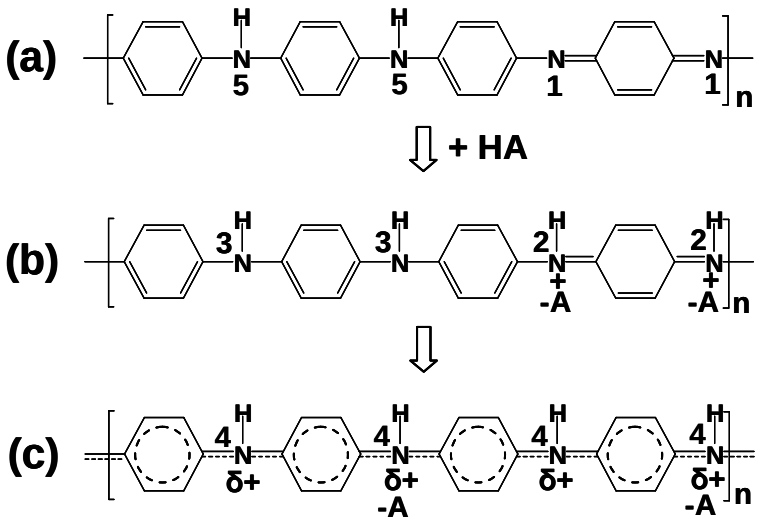

Figure 3.5. Chemical structure changes of PANI during its proton doping process. HA is an acid. The numbers are labeled according to the peak assignments of ^{15}N NMR spectra of PANI-PVP (Figure 3.4) and PANI-PAAMPSA (Figure 3.6, Figure 3.8, and Figure 3.19).

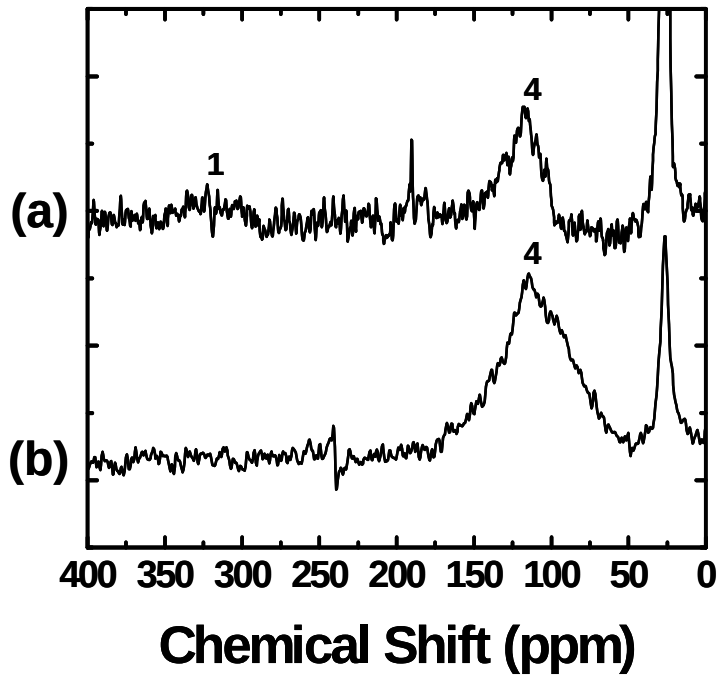

Figure 3.6. ^{15}N NMR spectra of (a) PANI-PAAMPSA-724 and (b) PANI-PAAMPSA-45. The chemical shifts are labeled according to the chemical structure as shown in Figure 3.5.

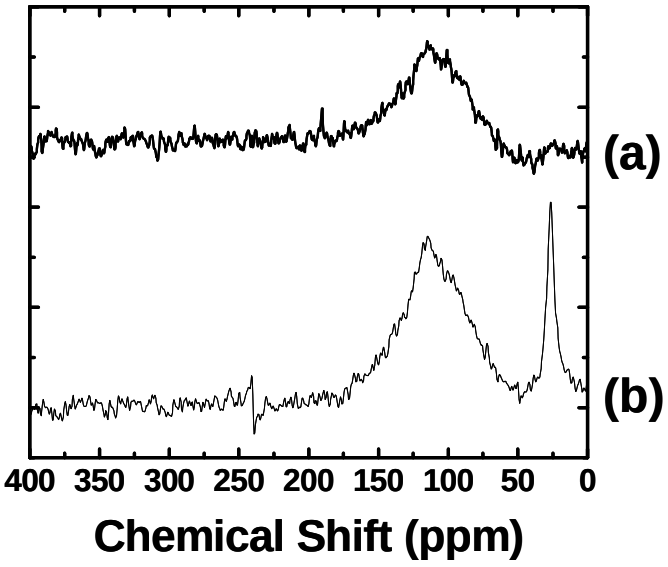

Figure 3.7. ^{15}N NMR spectra of (a) PANI-PAAMPSA-45 after three-times precipitation and (b) PANI-PAAMPSA-45.

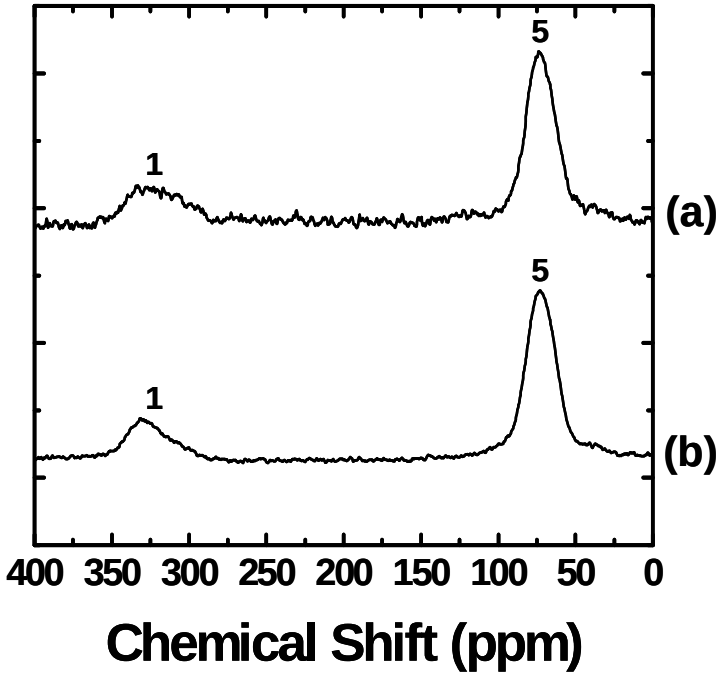

Figure 3.8. ^{15}N NMR spectra of (a) PANI-724 and (b) PANI-45. The chemical shifts are labeled according to the chemical structure of PANI shown in Figure 3.5.

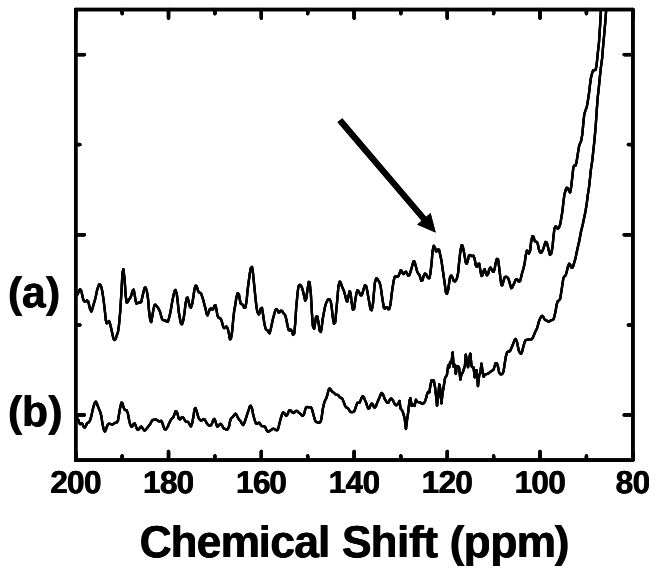

Figure 3.9. Magnified ^{15}N NMR spectra of (a) PANI-724 and (b) PANI-45 in the range between 80 and 200 ppm.

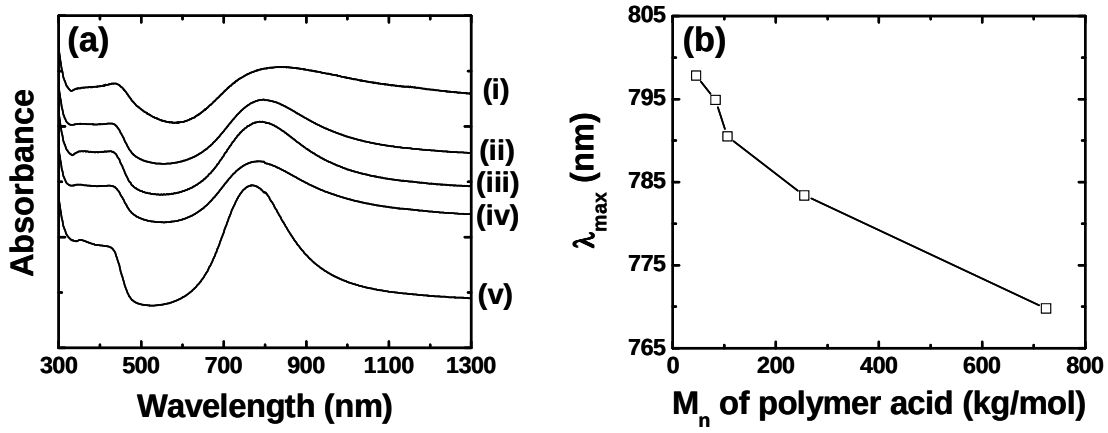

Figure 3.10. (a) UV-vis-NIR spectra of (i) PANI-PAAMPSA-45, (ii) -83, (iii) -106, (iv) -255, and (v) -724. The location of the polaron peak maximum, λ_{max}, of each spectrum is quantified in (b).

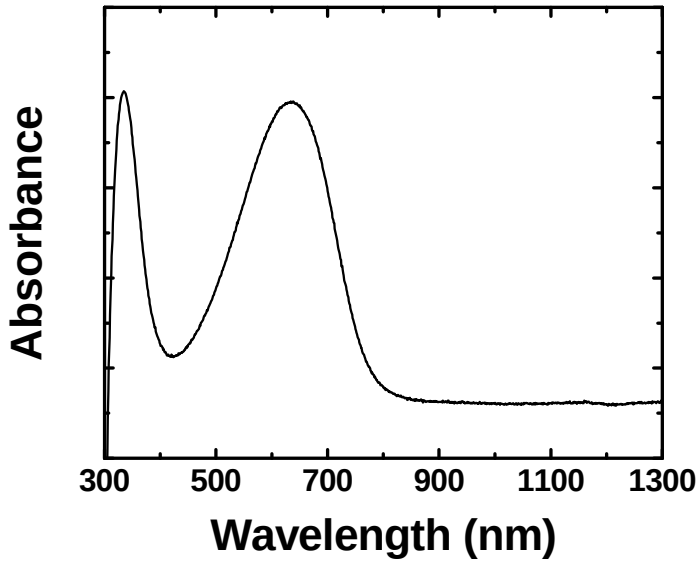

Figure 3.11. UV-vis-NIR spectrum of PANI-45.

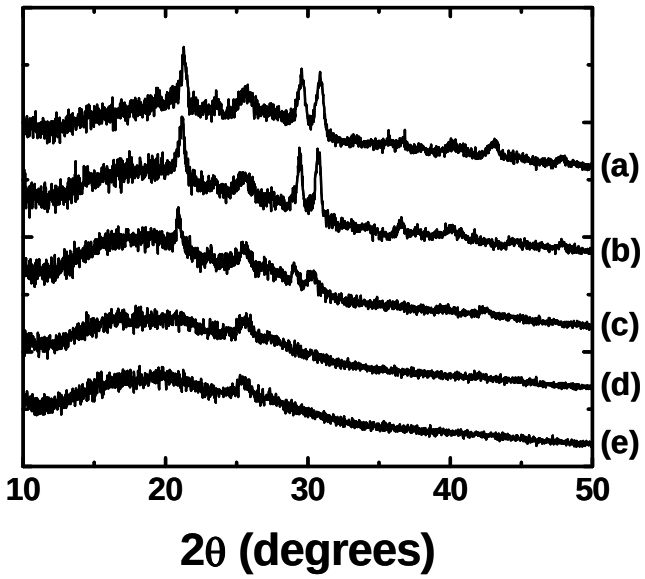

Figure 3.12. X-ray diffraction patterns of (a) PANI-PAAMPSA-45 (b) -83, (c) -106, (d) -255, and (e) -724.

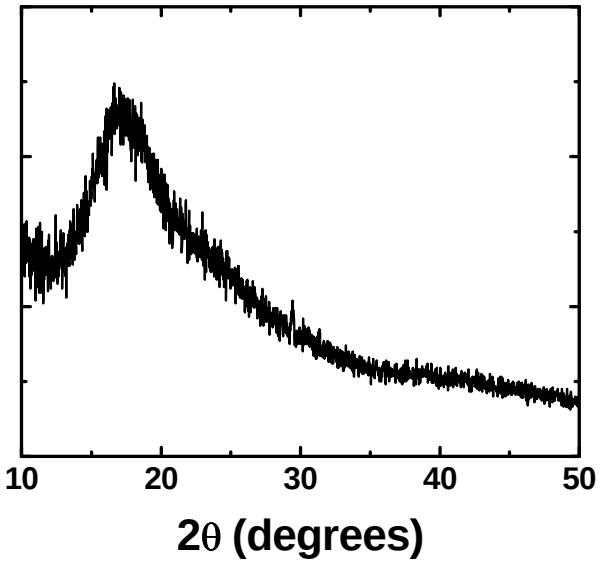

Figure 3.13. X-ray diffraction pattern of PAAMPSA-45.

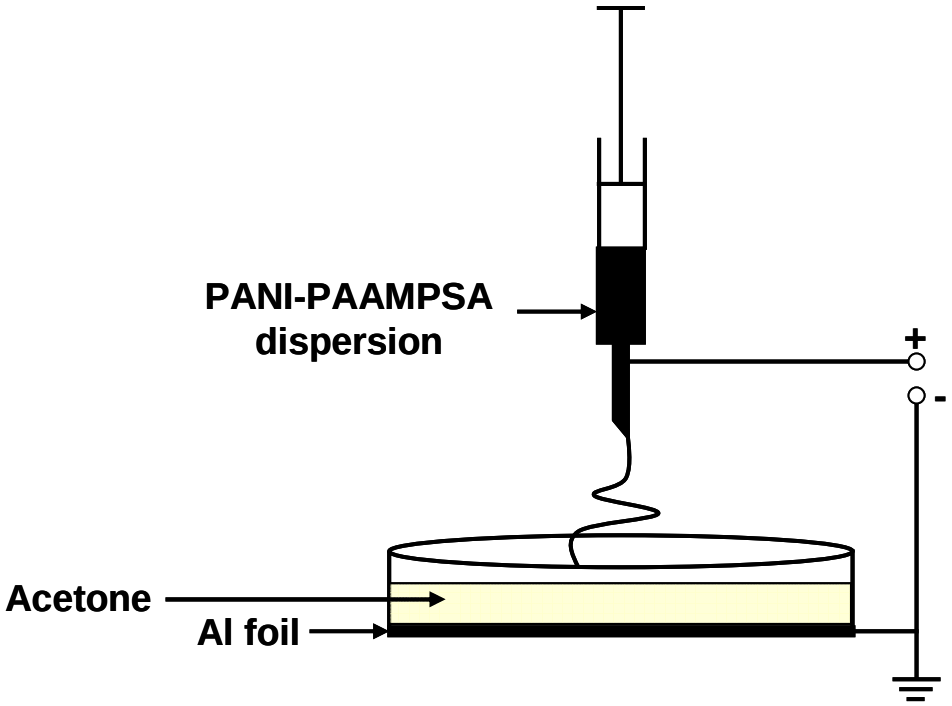

Figure 3.14. Electrospinning setup used to spin PANI-PAAMPSA fibers from an aqueous dispersion.

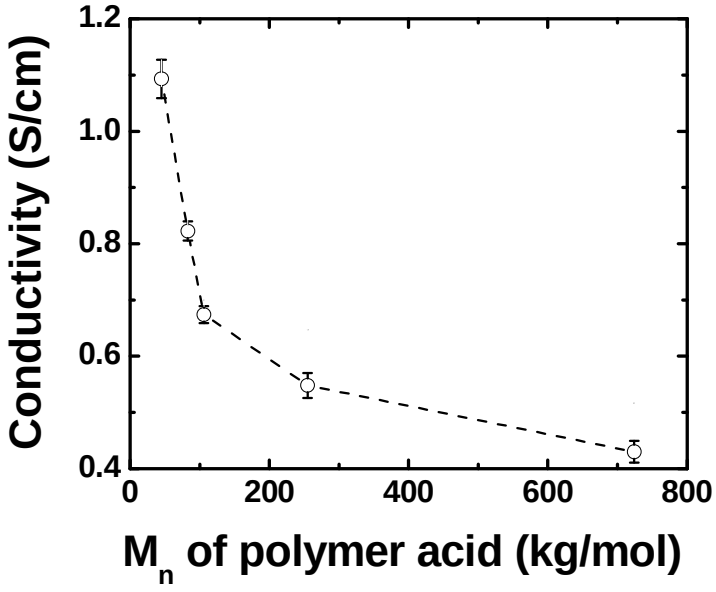

Figure 3.15. Bulk conductivity of PANI-PAAMPSA with varying PAAMPSA molecular weight.

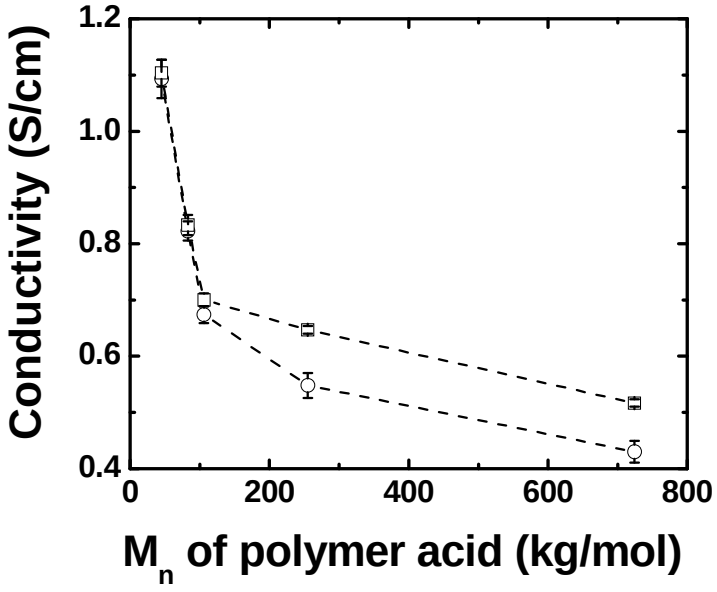

Figure 3.16. The bulk conductivity of PANI-PAAMPSA with varying PAAMPSA molecular weight before (○) and after (□) exposure to HCl vapor.

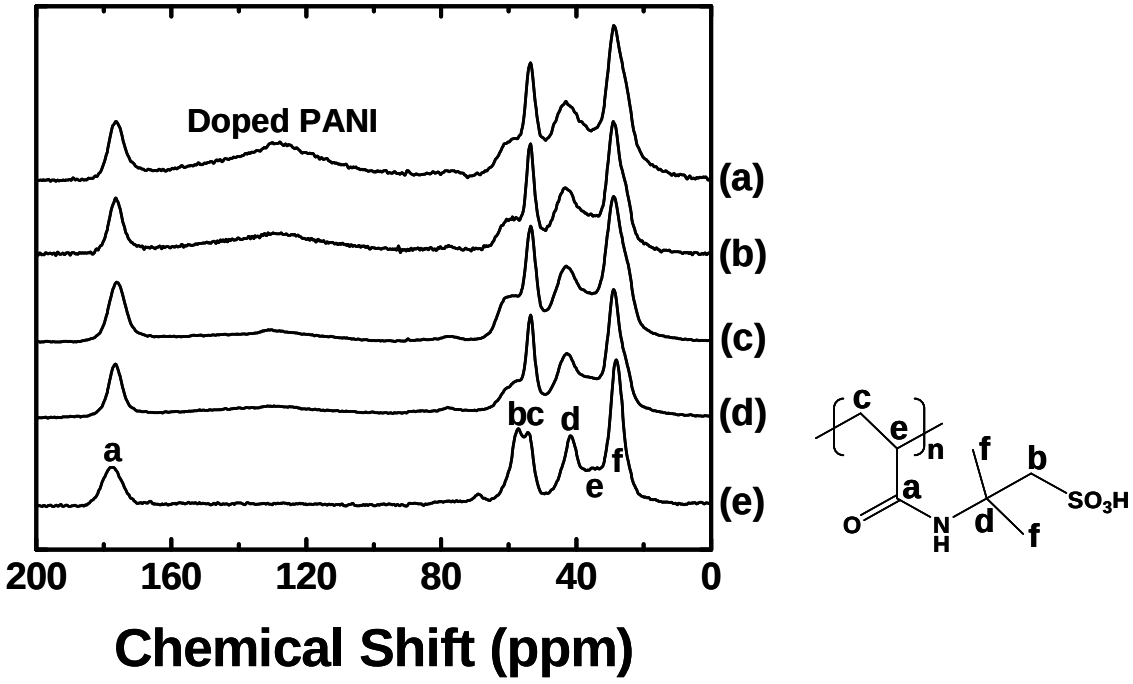

Figure 3.17. ^{13}C NMR spectra of (a) PANI-PAAMPSA 1:0.72, (b) 1:0.83, (c) 1:1.26, (d) 1:1.91, and (e) PAAMPSA-45. The chemical shifts of PAAMPSA-45 are labeled accordingly.

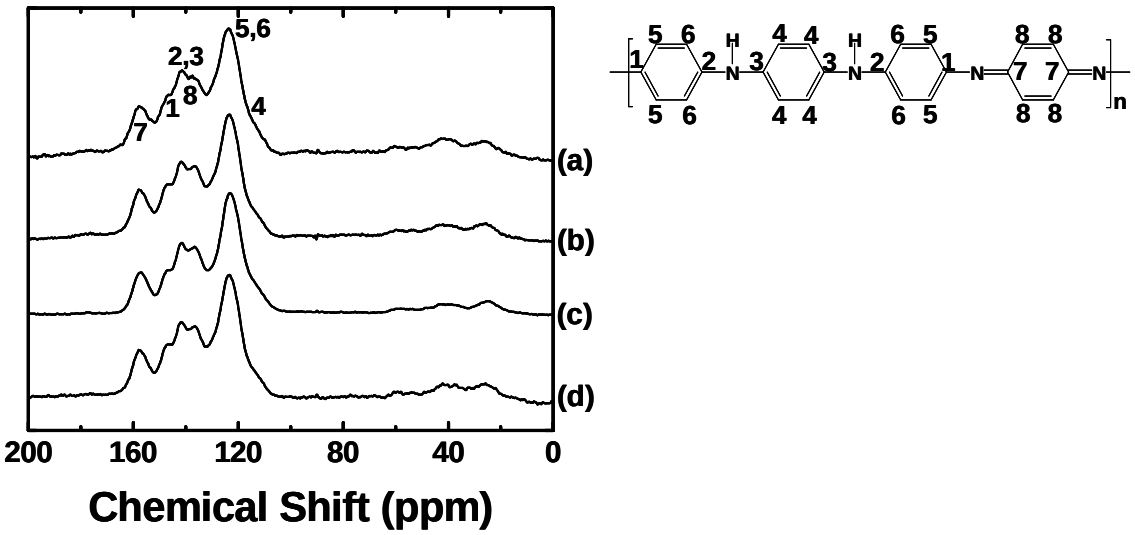

Figure 3.18. ^{13}C NMR spectra of (a) PANI-PAAMPSA 1:0.72, (b) 1:0.83, (c) 1:1.26, and (d) 1:1.91. The chemical shifts are labeled accordingly on the accompanying chemical structure.

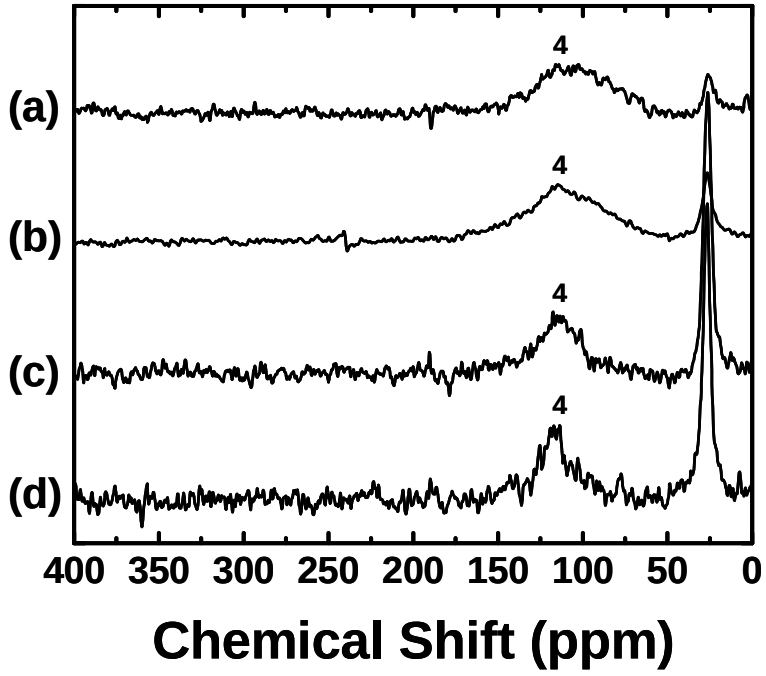

Figure 3.19. ^{15}N NMR spectra of (a) PANI-PAAMPSA 1:0.72, (b) 1:0.83, (c) 1:1.26, and (d) 1:1.91. The chemical shifts are labeled according to the chemical structure as shown in Figure 3.5.

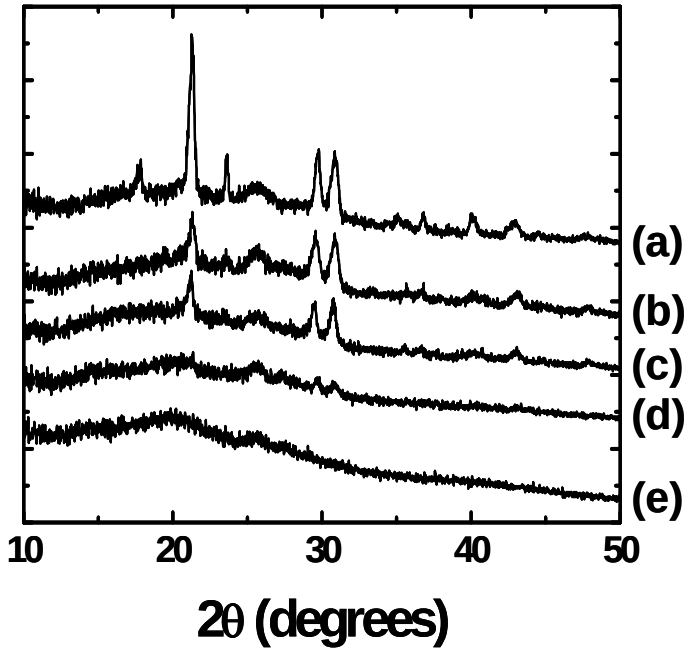

Figure 3.20. X-ray diffraction patterns of PANI-PAAMPSA (a) 1:0.72, (b) 1:0.83, (c) 1:1.05, (d) 1:1.26, and (e) 1:1.91.

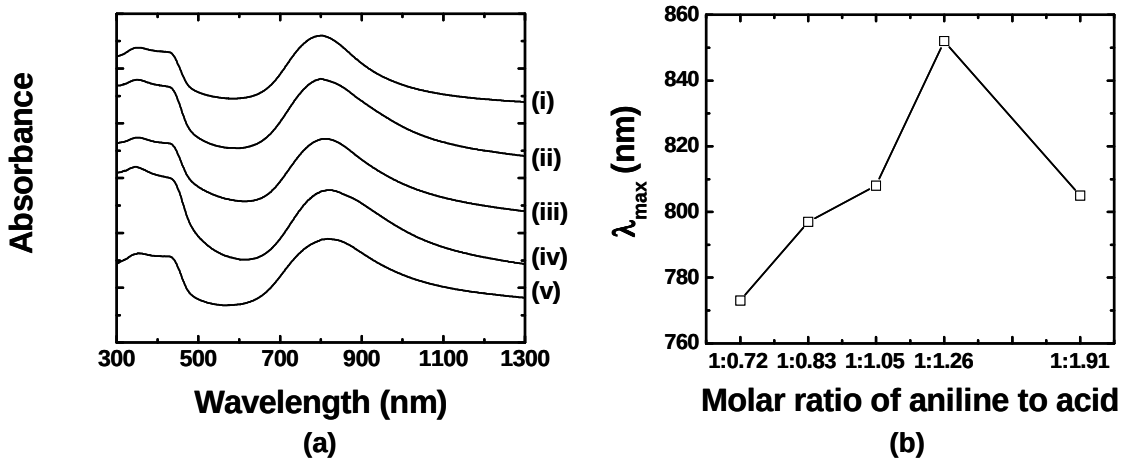

Figure 3.21. (a) UV-vis-NIR spectra of (i) PANI-PAAMPSA 1:0.72, (ii) 1:0.83, (iii) 1:1.05, (iv) 1:1.26, and (v) 1:1.91. The individual spectra have been shifted along the y axis for clarity. The location of peak maximum, λ_{max}, of each spectrum is quantified in (b).

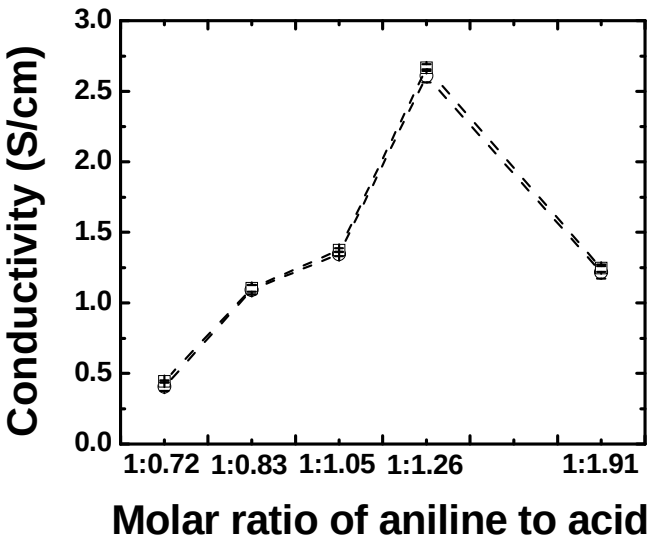

Figure 3.22. The bulk conductivity of PANI-PAAMPSA with varying aniline to acid molar ratios before (○) and after (□) exposure to HCl vapor.

REFERENCES

1. K. S. Lee, G. B. Blanchet, F. Gao and Y.-L. Loo, *Appl. Phys. Lett.*, 2005, **86**, 074102.
2. K. S. Lee, T. J. Smith, K. C. Dickey, J. E. Yoo, K. J. Stevenson and Y.-L. Loo, *Adv. Func. Mater.*, 2006, **16**, 2409.
3. A. G. MacDiarmid, *Synth. Met.*, 1997, **84**, 27.
4. V. Saxena and B. D. Malhotra, *Curr. Appl. Phys.*, 2003, **3**, 293.
5. A. P. Monkman and P. Adams, *Synth. Met.*, 1991, **41**, 891.
6. J. P. Pouget, M. E. Jozefowicz, A. J. Epstein, X. Tang and A. G. MacDiarmid, *Macromolecules*, 1991, **24**, 779.
7. W. Liu, A. L. Cholli, R. Nagarajan, J. Kumar, S. Tripathy, F. F. Bruno and L. Samuelson, *J. Am. Chem. Soc.*, 1999, **121**, 11345.
8. R. Nagarajan, S. Tripathy, J. Kumar, F. F. Bruno and L. Samuelson, *Macromolecules*, 2000, **33**, 9542.
9. M. Angelopoulos, N. Patel, J. M. Shaw, N. C.Labianca and S. A. Rishton, *J. Vac. Sci. Technol. B*, 1993, **11**, 2794.
10. S.-A. Chen and H.-T. Lee, *Macromolecules*, 1995, **28**, 2858.
11. B.-C. Ku, S.-H. Lee, W. Liu, J. Kumar, F. F. Bruno and L. A. Samuelson, *Mat. Res. Soc. Sym. Proc.*, 2002, **708**, BB10.12.1.
12. G. Li, M. Josowiez and J. Janata, *Electrochem. Solid-State Lett.*, 2002, **5**, D5.
13. P. N. Bartlett, P. R. Birkin, M. A. Ghanem and C.-S. Toh, *J. Mater. Chem.*, 2001, **11**, 849.

14. F. F. Bruno, R. Nagarajan, S. Roy, J. Kumar, S. Tripathy and L. Samuelson, *Mat. Res. Soc. Symp. Proc.*, 2001, **660**, JJ8.6.1.

15. W. Liu, J. Kumar, S. Tripathy, K. J. Senecal and L. Samuelson, *J. Am. Chem. Soc.*, 1999, **121**, 71.

16. H. S. Moon and J. K. Park, *J. Polym. Sci., Part A: Polym. Chem.*, 1998, **36**, 1431.

17. H. S. Moon and J. K. Park, *Synth. Met.*, 1998, **92**, 223.

18. S. Beuermann, M. Buback, P. Hesse, T. Junkers and I. Lacik, *Macromolecules*, 2006, **39**, 509.

19. S. R. Gooda and M. B. Huglin, *J. Polym. Sci., Part A: Polym. Chem.*, 1992, **30**, 1549.

20. L. A. Samuelson, A. Anagnostopoulos, K. S. Alva, J. Kumar and S. K. Tripathy, *Macromolecules*, 1998, **31**, 4376.

21. S. K. Sahoo, R. Nagarajan, S. Chakraborty, L. A. Samuelson, J. Kumar and A. L. Cholli, *J. Macromol. Sci., Part A: Pure Appl. Chem.*, 2002, **A39**, 1223.

22. A. Bozkurt, O. Ekinci and W. H. Meyer, *J. Appl. Polym. Sci.*, 2003, **90**, 3347.

23. W. L. Earl and D. L. VanderHart, *J. Mag. Res.*, 1982, **48**, 35.

24. S. Kaplan, E. M. Conwell, A. F. Richter and A. G. MacDiarmid, *Synth. Met.*, 1989, **29**, 235.

25. S. K. Sahoo, R. Nagarajan, L. Samuelson, J. Kumar, A. L. Cholli and S. K. Tripathy, *J. Macromol. Sci., Part A: Pure Appl. Chem.*, 2001, **A38**, 1315.

26. T. Hjertberg, W. R. Salaneck, I. Lundstrom, N. L. D. Somasiri and A. G. MacDiarmid, *J. Polym. Sci., Part C: Polym. Lett.*, 1985, **23**, 503.

27. S. Kababya, M. Appel, Y. Haba, G. I. Titelman and A. Schmidt, *Macromolecules*, 1999, **32**, 5357.

28. S. Kaplan, E. M. Conwell, A. F. Richter and A. G. MacDiarmid, *J. Am. Chem. Soc.*, 1988, **110**, 7647.

29. S. K. Sahoo, R. Nagarajan, S. Roy, L. A. Samuelson, J. Kumar and A. L. Cholli, *Macromolecules*, 2004, **37**, 4130.

30. S. K. Sahoo, D. W. Kim, J. Kumar, A. Blumstein and A. L. Cholli, *PMSE Preprints*, 2002, **87**, 394.

31. B. Wehrle, H.-H. Limbach, J. Mortensen and J. Heinze, *Angew. Chem. Int. Ed. Engl.*, 1989, **28**, 1741.

32. P. N. Adams, D. C. Apperley and A. P. Monkman, *Polymer*, 1993, **34**, 328.

33. A. F. Richter, A. Ray, K. V. Ramanathan, S. K. Manohar, G. T. Furst, S. J. Opella, A. G. MacDiarmid and A. J. Epstein, *Synth. Met.*, 1989, **29**, E243.

34. J. M. Ginder and A. J. Epstein, *Phys. Rev. B: Condens. Matter*, 1990, **41**, 10674.

35. P. M. McManus, R. J. Cushman and S. C. Yang, *J. Phys. Chem.*, 1987, **91**, 744.

36. S. Stafstrom, J. L. Bredas, A. J. Epstein, H. S. Woo, D. B. Tanner, W. S. Huang and A. G. MacDiarmid, *Phys. Rev. Lett.*, 1987, **59**, 1464.

37. A. G. MacDiarmid and A. J. Epstein, *Synth. Met.*, 1994, **65**, 103.

38. I. D. Norris, M. M. Shaker, F. K. Ko and A. G. MacDiarmid, *Synth. Met.*, 2000, **114**, 109.

39. N. J. Pinto, P. Carrion and J. X. Quinones, *Materials Science and Engineering*, 2004, **A366**, 1.

40. S. Luan and G. W. Neudeck, *J. Appl. Phys.*, 1992, **72**, 766.

41. J. Zaumseil, K. W. Baldwin and J. A. Rogers, *J. Appl. Phys.*, 2003, **93**, 6117.

42. A. G. MacDiarmid and A. J. Epstein, *Synth. Met.*, 1995, **69**, 85.

43. J. E. Yoo, J. L. Cross, T. L. Bucholz, K. S. Lee, M. P. Espe and Y.-L. Loo, *J. Mater. Chem.*, 2007, **17**, 1268.

44. A. J. Heeger, *Rev. Mod. Phys.*, 2001, **73**, 681.

45. A. J. Heeger, *Synth. Met.*, 2001, **125**, 23.

Chapter 4: The influence of PAAMPSA molecular weight distribution on the conductivity of PANI-PAAMPSA

The use of water soluble polymer acid templates to dope polyaniline (PANI) promotes water dispersibility, thereby solution processibility, to the resulting polymer acid-doped PANI. This water dispersibility, however, comes at the expense of reduced conductivity, likely due to additional structural disorder that is introduced during template polymerization.[1, 2] The conductivities of polymer acid templated PANI are thus generally low (10^{-5} - 10^{-2} S/cm).[1-6] Our first attempt to improve the conductivity of polymer acid-doped PANI involved the use of poly(2-acrylamido-2-methyl-1-propanesulfonic acid), or PAAMPSA, as a polymer acid template. As detailed in Chapter 3, we successfully improved the conductivity of PANI-PAAMPSA from 0.4 S/cm to 1.1 S/cm by decreasing the molecular weight of PAAMPSA. This initial observation implicated the importance of the polymer acid template on the conductivity of PANI, and suggests that further enhancement of conductivity is achievable through proper control of the molecular characteristics of polymer acid template. In this chapter, we detail how the molecular weight distribution of PAAMPSA impacts the structure and electrical conductivity of PANI-PAAMPSA.

For this study, we first synthesized PAAMPSA having a narrow molecular weight distribution via atom transfer radical polymerization (ATRP). We varied the molecular weights of these polymers from 30 kg/mol to 287 kg/mol. We refer to the resulting polymers as aPAAMPSA-X where X refers to the PEO-equivalent number average

molecular weight of the polymer in kg/mol. The polydispersity indices (PDIs) of these polymers range between 1.16 and 1.28, which are lower than those of PAAMPSA synthesized via conventional free-radical polymerization (CFRP) (PDI = 1.43 - 1.64). In fact, Figure 2.1 shows the GPC traces of (a) aPAAMPSA-30 (PDI = 1.16) and (b) PAAMPSA-45 (PDI = 1.43). While both traces are monomodal, the GPC trace of (a) aPAAMPSA-30 is significantly narrower than that of (b) PAAMPSA-45, indicating that aPAAMPSA-30 has a narrower molecular weight distribution compared to PAAMPSA-45. We then oxidatively polymerized aniline in the presence of aPAAMPSA at a 1:1:0.9 aniline : acid : oxidizing agent molar feed ratio, as same as the synthesis of PANI-PAAMPSA. The resulting PANI-aPAAMPSA is denoted as PANI-aPAAMPSA-X with X being the PEO-equivalent number-average molecular weight of the aPAAMPSA template in kg/mol. The detailed synthesis procedures and molecular characteristics of aPAAMPSA and PANI-aPAAMPSA were described in Chapter 2. PANI-aPAAMPSA were characterized and compared against PANI-PAAMPSA at comparable polymer acid molecular weight to examine the influence of PAAMPSA molecular weight distribution on the structure and conductivity of PANI-PAAMPSA.

Figure 4.1 plots the electrical conductivities of PANI-aPAAMPSA (solid circles) and those of PANI-PAAMPSA (open circles) as a function of the molecular weight of PAAMPSA (and aPAAMPSA). The PDIs of PAAMPSA (and aPAAMPSA) are labeled in brackets accordingly. The conductivity of PANI-aPAAMPSA increases as the molecular weight of aPAAMPSA decreases from 287 kg/mol to 30 kg/mol. This trend is consistent with that observed in PANI-PAAMPSA in Chapter 3. When we compare the electrical conductivities of PANI-PAAMPSA and PANI-aPAAMPSA at comparable

polymer acid molecular weights, we observe that the conductivity of PANI-aPAAMPSA is consistently twice to three times higher than that of PANI-PAAMPSA. As mentioned in Chapter 3, PANI that is doped with PAAMPSA of a high molecular weight is not completely doped because the large polymer acid chains are more compact in water so their sulfonic acid groups are less accessible for doping. The conductivity of the resulting PANI-PAAMPSA is thus generally lower than that of PANI that is doped with lower molecular weight PAAMPSA. Given this fact that a decrease in PAAMPSA molecular weight is correlated with increasing PANI-PAAMPSA conductivity, we speculate that narrow polymer acid molecular weight distributions reduce the population of excessively larger polymer acid chains, which are frequently associated with incomplete doping. This reduction of chain length distribution thus in turn enhances the inherent conductivity of the templated PANI.

To examine the nature of charge transport, we carried out temperature-dependent conductivity measurements on PANI-PAAMPSA and PANI-aPAAMPSA films in a cryostat between 81 K and 298 K. Figure 4.2 shows the temperature-dependent conductivities of (a) PANI-aPAAMPSA-30 and (b) PANI-PAAMPSA-45. As we reduce the cryostat temperature, the electrical conductivities of both samples decrease by more than two or three orders of magnitude. That the electrical conductivity deceases with decreasing temperature suggests semiconducting, rather than metallic, behavior in these polymers.[7] In a metal, conductivity should increase with decreasing temperature due to reduced electron scattering at low temperatures.[8] Further, the conductivity behavior in Figure 4.2 can be quantitatively described by an Arrhenius fit, suggesting that

charge transport in these polymers occurs via a thermally-activated hopping process.[9-13] Mathematically, this model is expressed as equation (4.1).[9-13]

$$\sigma(T) = \sigma_o \exp\left[-\left(\frac{T_o}{T}\right)^{1/2}\right] \qquad (4.1)$$

where σ is the conductivity, σ_o is the pre-exponential constant, T is temperature, and T_o resembles the activation energy for hopping and is quantified in Kelvin. Fitting the data to equation (4.1) results in T_o = 12,210 K for PANI-aPAAMPSA-30 and 20,610 K for PANI-PAAMPSA-45. T_o is smaller for PANI-aPAAMPSA-30 compared to PANI-PAAMPSA-45. This observation suggests that the barrier to hopping is reduced in PANI-aPAAMPSA-30 compared to PANI-PAAMPSA-45.

To verify that narrowing the molecular weight distribution of polymer acid template is indeed responsible for the conductivity enhancement in PANI-aPAAMPSA, we conducted a series of control experiments. First, we considered the differences in the polymerizations between PAAMPSA and aPAAMPSA. CFRP is straightforward, and does not require any additional reagents other than the initiator. ATRP is, however, more complicated than CFRP. Specifically, ATRP requires the use of a metal-ligand complex, typically composed of a copper salt and an aniline-containing ligand. The metal-ligand complex acts as a radical capping agent, which effectively reduces the instantaneous concentration of polymer radicals and thereby suppressing termination reactions. As a result, we can obtain the polymers with narrow molecular weight

distributions. Additionally, the use of the sodium salt form of AAMPSA, AAMPSA-Na, is required for ATRP because the sulfonic acid group in AAMPSA can protonate the coordinating amine ligand.[14] As such, we were concerned that residual metal ions, such as copper from the ATRP catalysts and sodium from the monomer, were responsible for the electrical conductivity enhancement we observed in PANI-aPAAMPSA. To quantify the presence of such metal impurities in aPAAMPSA, we carried out atomic absorbance spectroscopy on all the aPAAMPSA samples prior to PANI synthesis. In all the aPAAMPSA samples used, we only detected insignificant amounts of sodium (< 500 ppm in aPAAMPSA) and copper (< 50 ppm in aPAAMPSA) in the purified materials. These levels are near or at the detection limit of the instrument. Specifically, the minimum detectable sodium level is higher than that of copper because elemental sodium is pervasive in the atmosphere and is therefore difficult to exclude during atomic absorption spectroscopy experiments. In fact, atomic absorption spectroscopy experiments carried out on PAAMPSA-724, which was polymerized directly from AAMPSA via CFRP, exhibited a sodium level of 350 ppm despite not having been intentionally exposed to sodium. We thus attribute the detected sodium levels in aPAAMPSA to ambient contamination.

We also wanted to rule out the possibility of residual AAMPSA monomer doping of PANI as the origin of conductivity enhancement in PANI-aPAAMPSA. Indeed, previous reports have indicated that small molecule acid-doped PANI typically exhibits conductivities that are significantly higher than their polymer acid-doped counterparts.[15, 16] Further, our own experiments indicate that AAMPSA-doped PANI, though no longer solution processible, is more conductive (~ 10 S/cm) compared to PANI-PAAMPSA or

PANI-aPAAMPSA. To verify that residual AAMPSA had been completely removed prior to aniline polymerization, we conducted ^{1}H NMR on all PAAMPSA and aPAAMPSA samples. Figure 4.3 shows the ^{1}H NMR spectrum of AAMPSA. The different proton contributions have been labeled for clarity. Peak **a** (δ = 1.3 ppm) corresponds to the protons in the two methyl groups (six protons). Peak **b** (δ = 3.3 ppm) corresponds to the protons in the methylene unit adjacent to the sulfonic acid group (two protons). Peak **c** (δ = 5.5 - 5.7 ppm) is associated with the proton on the nonterminal carbon in the double bond (one proton) and peak **d** (δ = 5.9 - 6.3 ppm) is associated with the protons on the terminal carbon in the double bond (two protons). The ^{1}H NMR spectra of (a) aPAAMPSA-30 and (b) PAAMPSA-45 are also shown in Figure 4.4. The proton contributions have been labeled for clarity. Since peaks **a** and **b** are attributed to the protons in the side chains of repeat unit, they should be at the same chemical shifts (δ = 1.3 and 3.3 ppm, respectively) as the corresponding peaks in the ^{1}H NMR spectrum of AAMPSA monomer (**a** and **b**, respectively, in Figure 4.3). Peaks **c** and **d** in the ^{1}H NMR spectrum of AAMPSA monomer (δ = 5.5 - 5.7 and 5.9 - 6.3 ppm, respectively) should disappear after polymerization because these peaks are associated with the protons in the main chain of AAMPSA monomer where the polymerization occurs. Instead, the other peaks appear at 1.8 – 2.1 and 1.5 – 1.8 ppm after polymerization (denoted **c** and **d** in the ^{1}H NMR spectra of (a) PAAMPSA and (b) aPAAMPSA in Figure 4.4). These peaks represent the methyne and methylene backbone protons, respectively. The rest of peaks are associated with protons in solvents. The most pronounced peak at 4.7 ppm is from water; this peak is observed in the spectra of both PAAMPSA-45 and aPAAMPSA-30. The peaks at 1.7 and 3.6 ppm, as well as those in 2.7 – 2.9 ppm are only observed in

the spectrum of aPAAMPSA-30. These peaks are associated with residual solvents from the ATRP reaction. Specifically, the peaks at 1.7 and 3.6 ppm are due to the presence of residual THF; the peaks at 2.7 – 2.9 ppm are due to the presence of residual DMF. Of particular interest are the protons associated with the double bond of AAMPSA that appear between 5.5 and 6.3 ppm (paeks **c** and **d** in Figure 4.3). These peaks are not observed in the ^{1}H NMR spectra of aPAAMPSA-30 and PAAMPSA-45 (Figure 4.4 (a) and (b)), indicating the complete removal of residual AAMPSA (or AAMPSA-Na) upon polymerization and purification. Given the results above, we are confident that the observed higher conductivities of PANI-aPAAMPSA do in fact originate from the narrower molecular weight distributions of aPAAMPSA.

To further substantiate our claim, we carried out an additional control experiment that further probes the molecular weight distribution of polymer acid as the origin for conductivity differences between PANI-PAAMPSA and PANI-aPAAMPSA. For this experiment, we synthesized aPAAMPSA with a broad molecular weight distribution via ATRP. To make this polymer, we intentionally leaked air into the polymerization medium during the ATRP reaction, so the resulting polymer has a broad molecular weight distribution. This polymer, aPAAMPSA-226, has a PDI of 1.62. PANI-aPAAMPSA-226 exhibits the conductivity of 0.58 ± 0.02 S/cm; this conductivity is shown as a solid triangle in Figure 4.5. For comparison, Figure 4.5 also includes all the conductivities of PANI-aPAAMPSA (solid circles) and those of PANI-PAAMPSA (open circles) studied for this study as a function of the molecular weight of polymer acid template. The PDIs of PAAMPSA (and aPAAMPSA) are labeled in brackets accordingly as well. The conductivity of PANI-aPAAMPSA-226 is approximately half

that of PANI-aPAAMPSA-287 (1.07 ± 0.03 S/cm), a PANI specimen that was synthesized on aPAAMPSA having nominally comparable molecular weight as aPAAMPSA-226 but with a narrower molecular weight distribution (PDI = 1.28). On the other hand, the conductivity of PANI-aPAAMPSA-226 is comparable with that of PANI-PAAMPSA-255, a PANI specimen that was template synthesized on a CFRP-derived PAAMPSA having comparable molecular weight and molecular weight distribution (PDI = 1.64) with aPAAMPSA-226. This comparison implicates a strong correlation between conductivity and molecular weight distribution.

Additionally, we blended three aPAAMPSAs of narrow molecular weight distributions: aPAAMPSA-22 (PDI = 1.11), aPAAMPSA-40 (PDI = 1.24), and aPAAMPSA-64 (PDI = 1.19) at a mass ratio of 1:2:2 to create an aPAAMPSA with a broad molecular weight distribution. The resulting polymer has a PEO-equivalent number-average molecular weight of 45 kg/mol and a PDI of 1.40. This polymer is referred to as aPAAMPSA-<45> in this study. We template polymerized aniline on this polymer acid template, and the resulting PANI-PAAMPSA-<45> exhibits an electrical conductivity of 1.25 ± 0.03 S/cm (solid square in Figure 4.5). This conductivity is again approximately half that of PANI-aPAAMPSA-30 (2.39 ± 0.03 S/cm) but is comparable with that of PANI-PAAMPSA-45 (1.09 ± 0.03 S/cm). The PDIs of aPAAMPSA-30 and PAAMPSA-45 are 1.16 and 1.43, respectively. The combination of our control experiments indeed indicates the influence of molecular weight distribution of the polymer acid template on the conductivity of PANI-PAAMPSA (or PANI-aPAAMPSA).

The conductivity enhancement due to a narrowing of the molecular weight distribution of the polymer acid is accompanied by structural differences between PANI-

PAAMPSA and PANI-aPAAMPSA, which were probed by UV-vis-NIR spectroscopy. Figure 4.6 shows the UV-vis-NIR spectra of PANI-aPAAMPSA with varying aPAAMPSA molecular weights. All the PANI-aPAAMPSA samples exhibit absorptions that are characteristic of conductive PANI previously published.[17-19] Specifically, the peak at 310 nm corresponds to the π-π^* transition of the benzenoid and the peak at 450 nm is attributed to the polaronic shoulder.[17-19] The other absorption peak at approximately 800 nm corresponds to the polaron interband transition.[17-19] The polaron interband transition of PANI-aPAAMPSA broadens and red shifts as the molecular weight of aPAAMPSA decreases, similar with the trend observed in the PANI-PAAMPSA with decreasing PAAMPSA molecular weight (as observed in Chapter 3).

On the other hand, Figure 4.7 compares (a) the UV-vis-NIR spectrum of PANI-aPAAMPSA-30 to (b) that of PANI-PAAMPSA-45. Both spectra exhibit absorptions that are characteristic of conductive PANI.[6] The polaron interband transition (approximately at 800 nm) of PANI-aPAAMPSA-30, however, is red shifted compared to that of PANI-PAAMPSA-45. A red shift in the polaron interband transition generally implies an increase in the PANI conjugation length,[6, 17-19] suggesting that charges are delocalized over larger length scales in PANI-aPAAMPSA-30 compared to PANI-PAAMPSA-45. For completeness, we have plotted the peak position of the polaron interband transition, λ_{max}, in Figure 4.8 for all the samples we have examined in this study. We observe a strong correlation between the conductivity and the λ_{max} recorded for all of our samples. Specifically, λ_{max} increases linearly with increasing the conductivity of PANI-PAAMPSA (and PANI-aPAAMPSA). We have also plotted the

λ_{max}s of PANI-aPAAMPSA-226 (solid triangle) and PANI-aPAAMPSA-<45> (solid square). Their λ_{max}s match the linear fit of λ_{max} versus conductivity for PANI-PAAMPSA (and PANI-aPAAMPSA) samples. The linear correlations between the conductivities and λ_{max}s of PANI-PAAMPSA (and PANI-aPAAMPSA) indeed suggest that it is the size distribution of PAAMPSA (and aPAAMPSA) that influences the conductivity of PANI-PAAMPSA (and PANI-aPAAMPSA).

X-ray diffraction (XRD) experiments carried out on PANI-aPAAMPSA and PANI-PAAMPSA also reveal significant structural differences. Figure 4.9 shows the XRD spectra of PANI-aPAAMPSA with varying aPAAMPSA molecular weights. The peak at $2\theta = 26°$ is associated with the ionic association between aniline and sulfonic acid groups in aPAAMPSA.[2, 3] The other Bragg reflections correspond to the crystallinity of PANI. aPAAMPSA is amorphous and only contributes to the amorphous bump in the XRD spectrum of PANI-aPAAMPSA. The XRD spectrum of aPAAMPSA-30 is shown in Figure 4.10. When the molecular weight of aPAAMPSA decreases, the number of Bragg reflections and the intensity of the reflections gradually increase, indicating an increase in the crystallinity of PANI with decreasing aPAAMPSA molecular weight.[6, 20] This trend is similar to what was observed in PANI-PAAMPSA as a function of PAAMPSA molecular weight in Chapter 3. On the other hand, Figure 4.11 (a) contains the XRD spectra of PANI-aPAAMPSA-30, PANI-PAAMPSA-45, as well as PANI-aPAAMPSA-<45> and PANI-AAMPSA, the monomer acid doped counterpart. Figures 4.11 (b) and (c) provide magnified views of the XRD spectra in the ranges of $18^o \leq 2\theta \leq 23^o$ and $27^o \leq 2\theta \leq 33^o$, respectively. While the XRD spectra of PANI-PAAMPSA-45

and PANI-aPAAMPSA-<45> are similar (Figure 4.11 (b)), the Bragg reflection at 2θ = 21.2^{o} in the XRD traces of PANI-PAAMPSA-45 and PANI-aPAAMPSA-<45> is shifted to smaller 2θ = 20.6^{o} in the XRD traces of PANI-aPAAMPSA-30 and PANI-AAMPSA. Furthermore, we observe two weak Bragg reflections in Figure 4.11 (c) for PANI-PAAMPSA-45 and PANI-aPAAMPSA-<45>, but three Bragg reflections for PANI-aPAAMPSA-30 and PANI-AAMPSA. The combination of these observations implies that PANI-aPAAMPSA-30 adopts a crystal structure that is different from that of PANI-PAAMPSA-45 or PANI-aPAAMPSA-<45>, but one that is similar to PANI-AAMPSA. Given PANI is the only crystallizable species in the polymer complexes and that the polymer complexes are chemically identical, we are surprised to see differences in the crystal structures of PANI-PAAMPSA and PANI-aPAAMPSA. We believe that the different crystal structure of PANI is responsible for the higher conductivity of PANI-aPAAMPSA. To identify the crystal structure of PANI, we attempted to draw fibers by electro-spinning[21, 22] because the crystallinity of PANI is low in our materials. The drawn samples will be more oriented and thus have a higher crystallinity. There should also be forbidden reflections with drawn fibers, which will aid the determination of crystal structures and dimensions of PANI. XRD can be then carried out on these drawn fibers for crystal lattice determination. As detailed in Chapter 3, PANI-PAAMPSA (and PANI-aPAAMPSA) fibers, however, were not successfully drawn. PANI-PAAMPSA (and PANI-aPAAMPSA) forms electrostatically-stabilized sub-micron colloidal particles during the polymerization by strong ionic interactions between sulfonic acid groups in PAAMPSA and aniline. Given the strong ionic interactions between PANI and

PAAMPSA, such particles do not easily break apart and their characteristics cannot be easily changed with processing. With these strongly bound PANI-PAAMPSA particles, it is difficult to form PANI-PAAMPSA fibers. Identifying the crystal structure of PANI-PAAMPSA and that of PANI-aPAAMPSA remains challenging.

In conclusion, narrowing the molecular weight distribution of the polymer acid that is subsequently used to template synthesize PANI strongly influences the structure and conductivity of resulting PANI-PAAMPSA complexes. The use of aPAAMPSA of comparable molecular weight but narrower molecular weight distribution results in the PANI that adopts a different crystal structure, is more crystalline, and has longer conjugation lengths. Given the fact that PANI-PAAMPSA (and PANI-aPAAMPSA) forms electrostatically-stabilized colloidal particles, the crystallinity or conjugation length of PANI qualifies the molecular order within the particles. Since PANI chains are ionically associated with PAAMPSA (or aPAAMPSA) chains in the particles, the molecular order within the particles indicates how the PANI chains are aligned and therefore how efficient charge transport occurs within the particles. The increases in PANI crystallinity and conjugation length therefore provide an indirect measure of efficient intra-particle charge transport. Therefore, a two- to three-fold higher conductivity of PANI-aPAAMPSA compared to PANI-PAAMPSA is attributed to the fact that more efficient intra-particle charge transport occurs along the PANI-aPAAMPSA backbones. This chapter thus implicates the importance of the molecular characteristics of polymer acid template in efficient intra-particle charge transport of PANI-PAAMPSA (or PANI-aPAAMPSA) samples and further in the high electrical conductivity of the materials. Such studies should enable the development of PANI that

is not only easily processible from solution, but also sufficiently conductive for electronic applications in organic and polymer electronics.

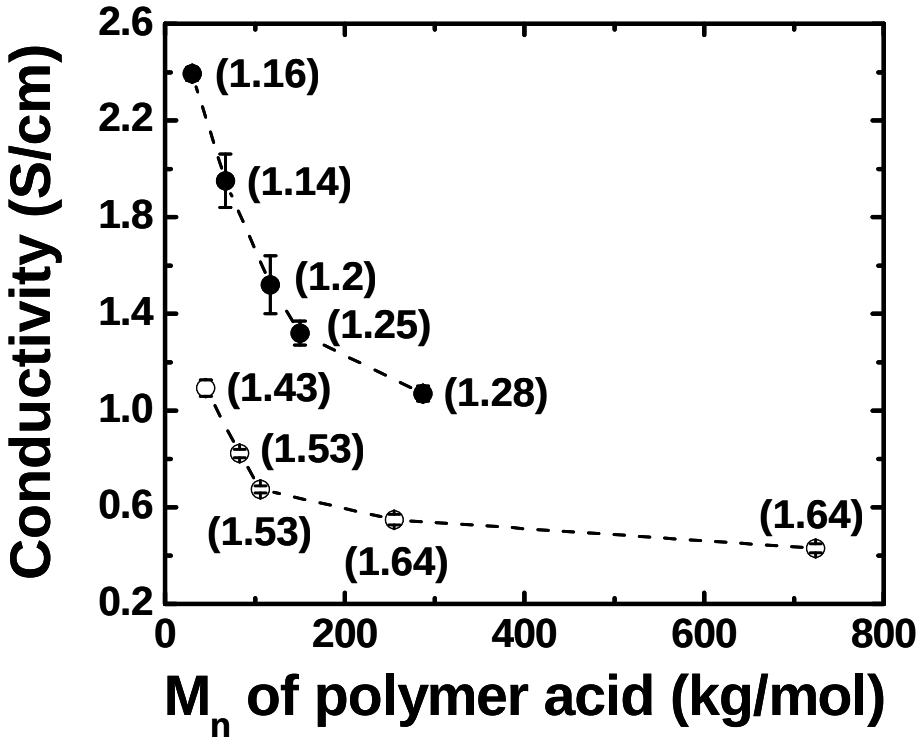

Figure 4.1. The conductivities of PANI-aPAAMPSA (●) and PANI-PAAMPSA (○) with varying PAAMPSA (or aPAAMPSA) molecular weights. The PDIs of PAAMPSA (and aPAAMPSA) are labeled in brackets accordingly.

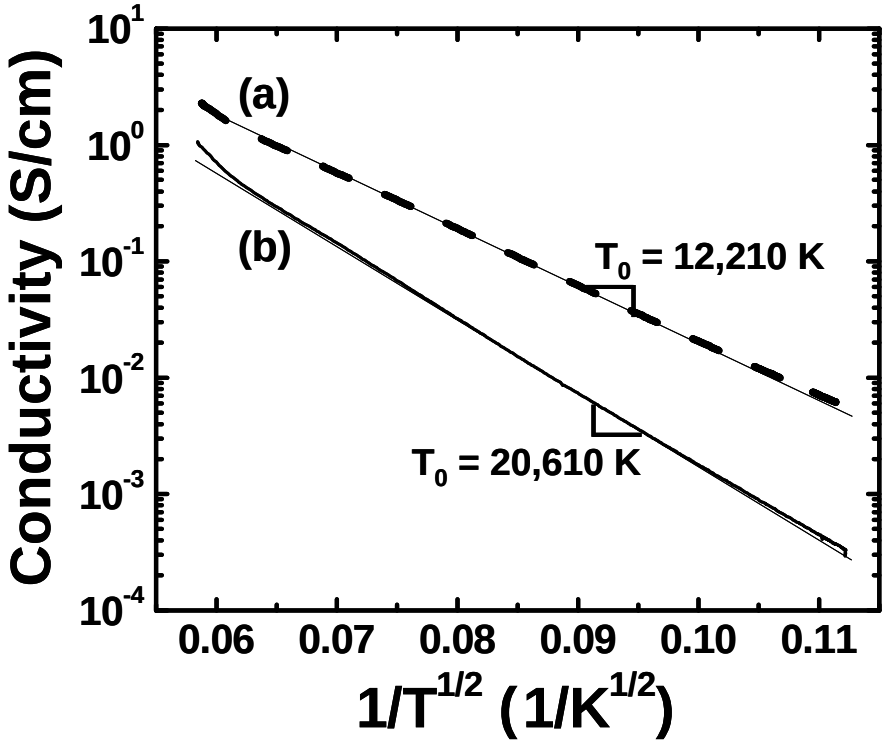

Figure 4.2. Temperature-dependent conductivity of (a) PANI-aPAAMPSA-30 and (b) PANI-PAAMPSA-45. T_o suggests the activation energy for hopping.

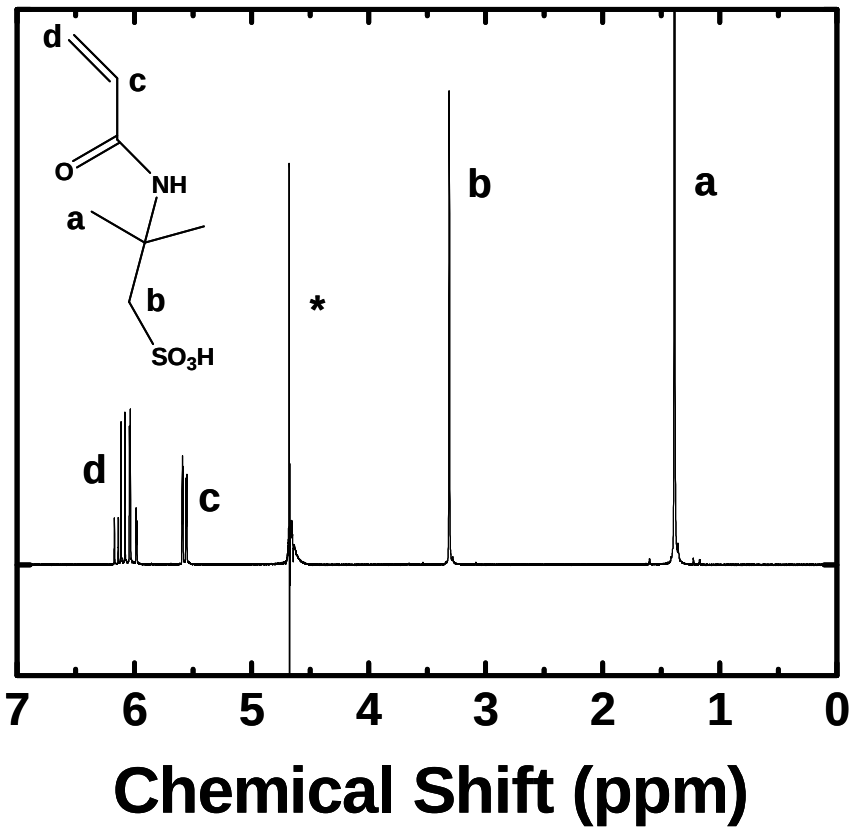

Figure 4.3. ^{1}H NMR spectrum of AAMPSA in deuterium oxide. The peaks have been labeled accordingly. * indicates the water peak.

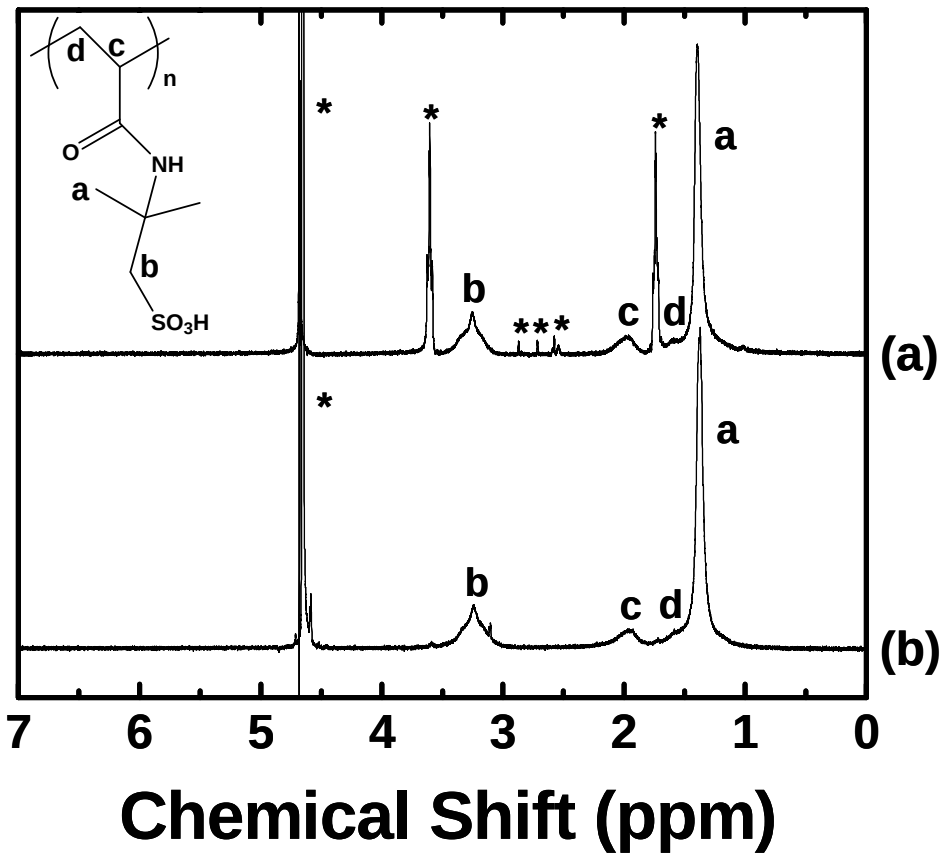

Figure 4.4. ^{1}H NMR spectra of (a) aPAAMPSA-30 and (b) PAAMPSA-45 in deuterium oxide. The peaks have been labeled accordingly. * indicates solvent peaks. The peak at 4.7 ppm is from water. In (a), the peaks at 1.7 and 3.6 ppm are from the residual THF and peaks in 2.7 - 2.9 ppm are from residual DMF.

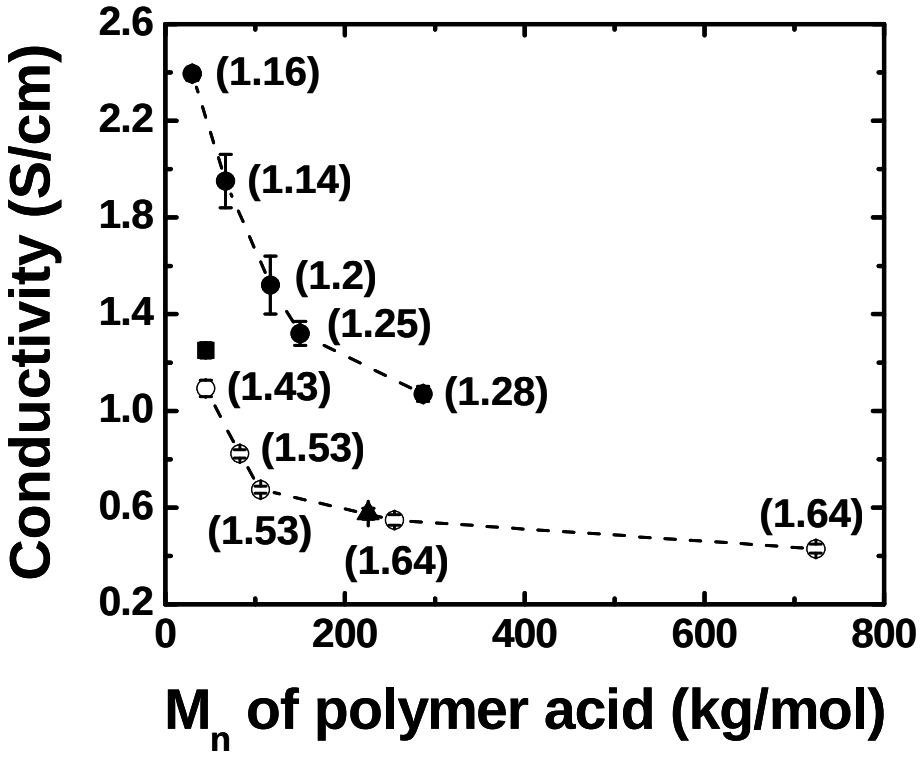

Figure 4.5. The conductivities of PANI-aPAAMPSA (●) and PANI-PAAMPSA (○) with varying PAAMPSA (or aPAAMPSA) molecular weights. The PDIs of PAAMPSA (and aPAAMPSA) are labeled in brackets accordingly. The conductivities of PANI-aPAAMPSA-<45> (PDI = 1.40, ■) and PANI-aPAAMPSA-226 (PDI = 1.62, ▲) are also included.

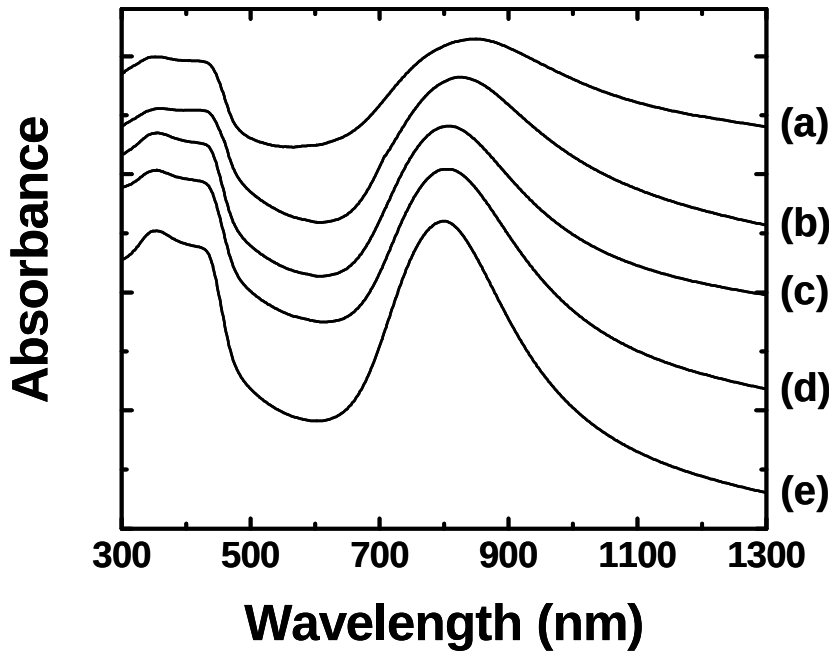

Figure 4.6. The UV-vis-NIR spectra of (a) PANI-aPAAMPSA-30, (b) -67, (c) -117, (d) -150, and (e) -287. The individual spectra have been shifted along the y axis for clarity.

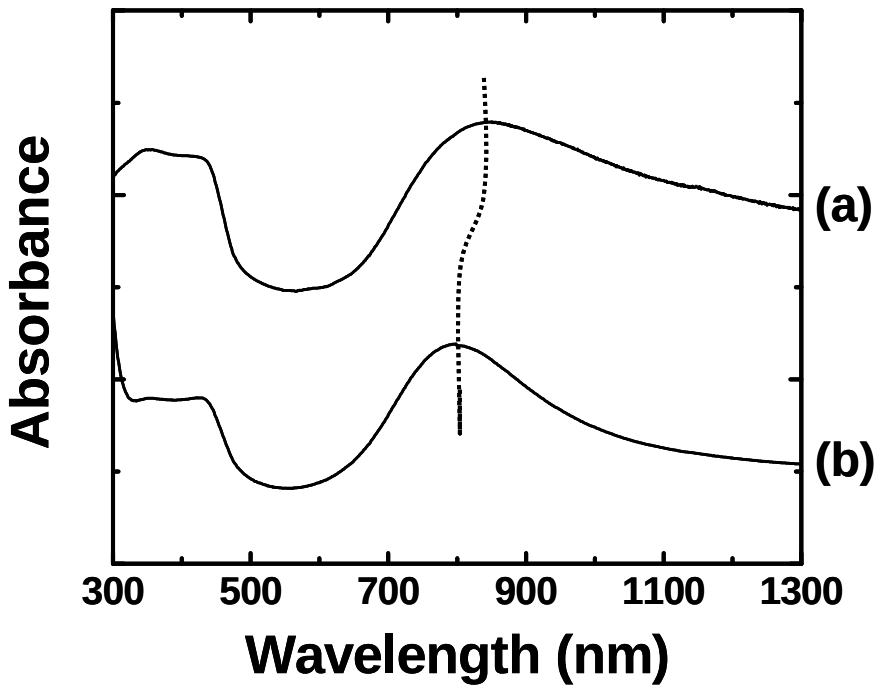

Figure 4.7. The UV-vis-NIR spectra of (a) PANI-aPAAMPSA-30 and PANI-PAAMPSA-45.

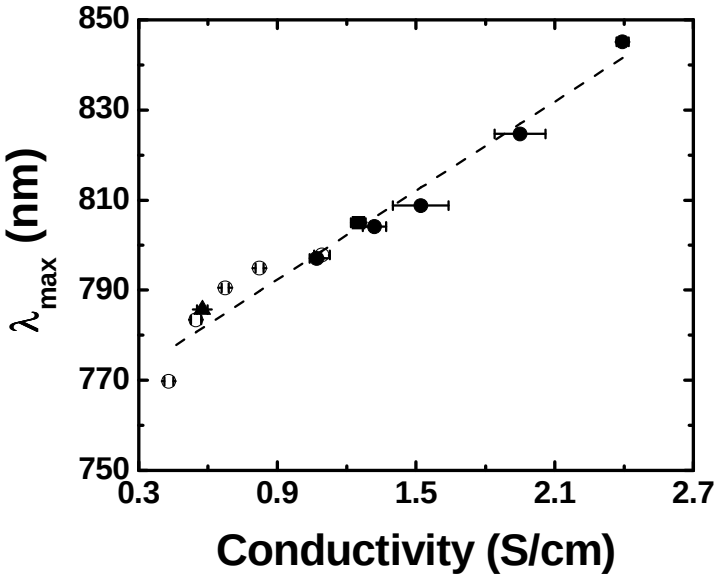

Figure 4.8. The position of the polaron peak, λ_{max}, extracted from the UV-vis-NIR spectra of PANI-aPAAMPSA (●) and PANI-PAAMPSA (○) as a function of the conductivity of the materials. λ_{max} of PANI-aPAAMPSA-<45> (■) and PANI-aPAAMPSA-226 (▲) are also included.

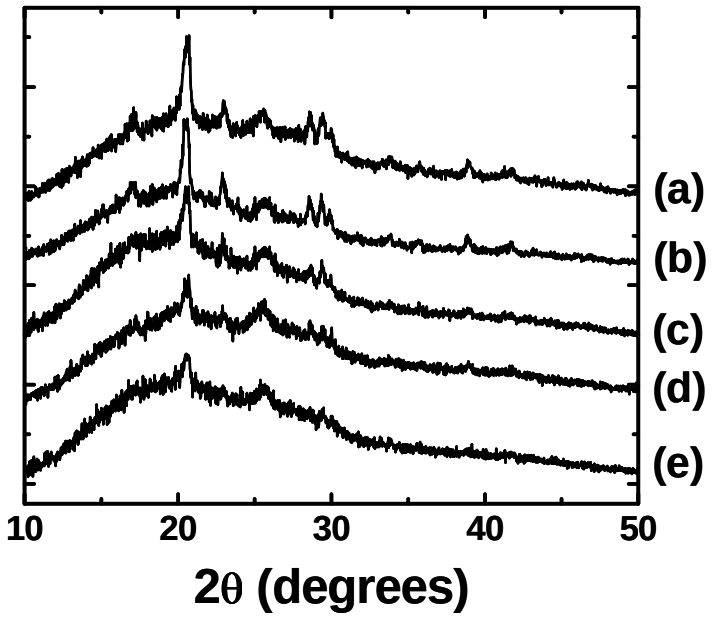

Figure 4.9. XRD spectra of (a) PANI-aPAAMPSA-30, (b) -67, (c) -117, (d) -150, and (e) -287. The individual spectra have been shifted along the y axis for clarity.

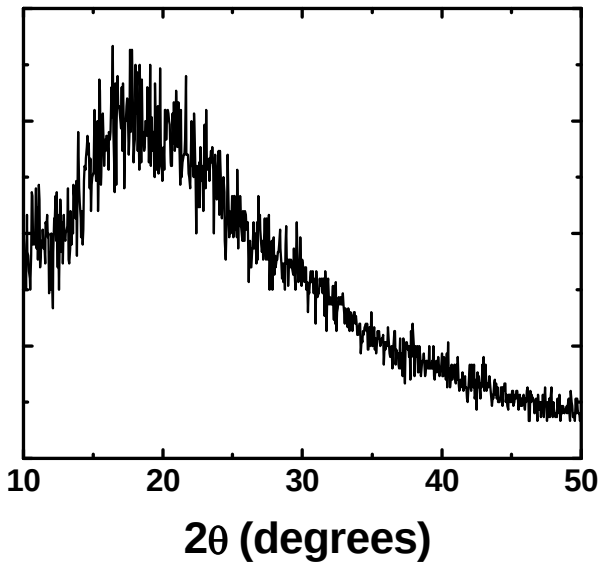

Figure 4.10. XRD spectrum of aPAAMPSA-30.

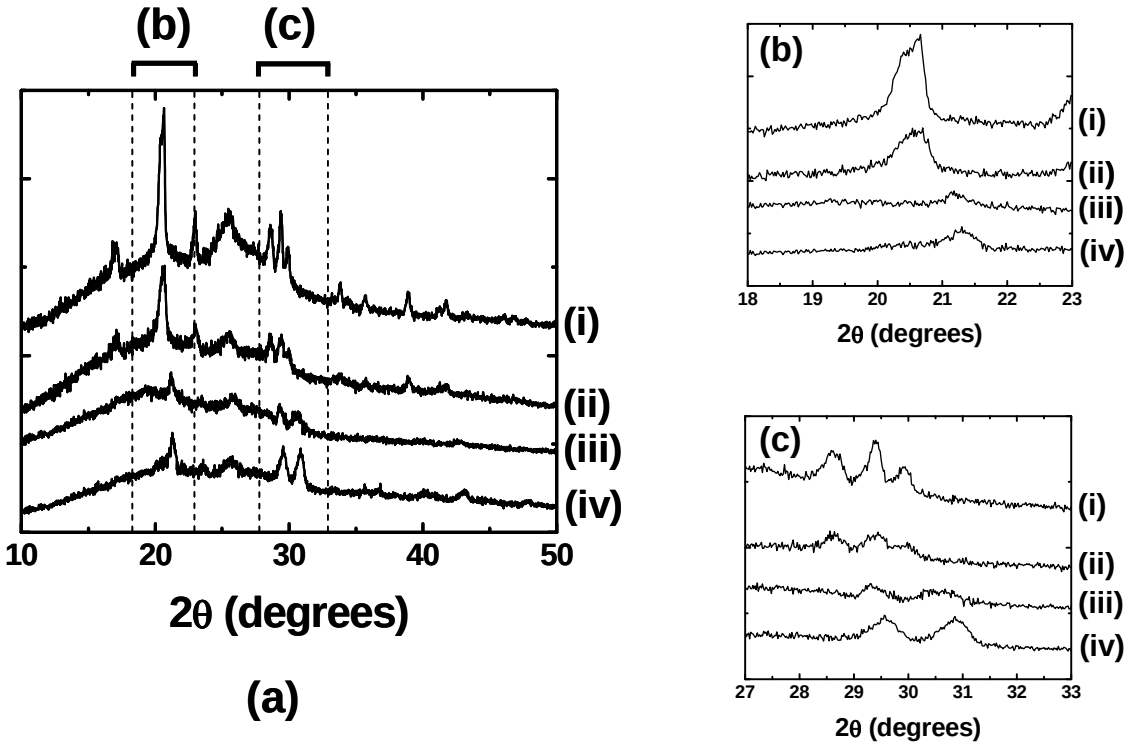

Figure 4.11. (a) XRD spectra of (i) PANI-AAMPSA, (ii) PANI-aPAAMPSA-30 and (iii) -<45>, and (iv) PANI-PAAMPSA-45. The XRD spectra are magnified in (b) from $18^o < 2\theta < 23^o$ and in (c) from $27^o < 2\theta < 33^o$ for comparison.

REFERENCES

1. S.-A. Chen and H.-T. Lee, *Macromolecules*, 1995, **28**, 2858.
2. H. S. Moon and J. K. Park, *J. Polym. Sci., Part A: Polym. Chem.*, 1998, **36**, 1431.
3. H. S. Moon and J. K. Park, *Synth. Met.*, 1998, **92**, 223.
4. Y. Cao, J. Qiu and P. Smith, *Synth. Met.*, 1995, **69**, 187.
5. A. G. MacDiarmid, *Synth. Met.*, 2002, **125**, 11.
6. J. E. Yoo, J. L. Cross, T. L. Bucholz, K. S. Lee, M. P. Espe and Y.-L. Loo, *J. Mater. Chem.*, 2007, **17**, 1268.
7. S. M. Sze, *Semiconductor devices: Physics and Technology*, John Wiley & Sons, Inc., New York, 2002.
8. B. G. Streetman and S. K. Banerjee, *Solid State Electronic Devices*, Prentice Hall, Saddle River, 2006.
9. K. Lee, S. Cho, S. H. Park, A. J. Heeger, C.-W. Lee and S.-H. Lee, *Nature*, 2006, **441**, 65.
10. R. Murugesan and E. Subramanian, *Bull. Mater. Sci.*, 2003, **26**, 529.
11. T. A. Skotheim and J. Reynolds, *Conjugated polymers: theory, synthesis, properties, and characterization (Handbook of conducting polymers)* CRC Press, Boca Raton, 2007.
12. G. Horowitz, *Adv. Mater.*, 1998, **10**, 365.
13. J. Y. Kim, J. H. Jung, D. E. Lee and J. Joo, *Synth. Met.*, 2002, **126**, 311.
14. S. Perrier, S. P. Armes, X. S. Wang, F. Malet and D. M. Haddleton, *J. Poly. Sci., Poly. Chem.*, 2001, **39**, 1696.
15. A. G. MacDiarmid and A. J. Epstein, *Synth. Met.*, 1994, **65**, 103.

16. S. M. Ahmed, *Eur. Polym. J.*, 2002, **38**, 1151.

17. J. M. Ginder and A. J. Epstein, *Phys. Rev. B: Condens. Matter*, 1990, **41**, 10674.

18. P. M. McManus, R. J. Cushman and S. C. Yang, *J. Phys. Chem.*, 1987, **91**, 744.

19. S. Stafstrom, J. L. Bredas, A. J. Epstein, H. S. Woo, D. B. Tanner, W. S. Huang and A. G. MacDiarmid, *Phys. Rev. Lett.*, 1987, **59**, 1464.

20. J. P. Pouget, M. E. Jozefowicz, A. J. Epstein, X. Tang and A. G. MacDiarmid, *Macromolecules*, 1991, **24**, 779.

21. B. Ding, E. Kimura, T. Sato, S. Fujita and S. Shiratori, *Polymer*, 2004, **45**, 1895.

22. A. J. Heeger, *Synth. Met.*, 2001, **125**, 23.

Chapter 5: PANI-PAAMPSA conductivity enhancement due to its particle connectivity

Water-dispersible, polymer acid-doped polyaniline (PANI) is widely used in organic electronics, chemical sensors, conductive coatings, etc.[1, 2] Despite their wide spread use, the conductivity of such polymer acid-doped PANI is highly variable depending on the synthesis and processing procedures.[3-5] Accordingly, a great deal of work has been performed on controlling the conductivity of polymer acid doped-PANI by changing the functional groups of the polymer acid templates and the synthetic parameters, or by exposing the conducting polymers to a solvent or organic compound.[5-7] Despite numerous studies on the electrical conductivity of PANI, the origin of conductivity in these systems remains poorly understood. Given the promise of organic electronics and the potential wide incorporation of conducting polymers in these devices, it is important that we understand the factors that govern the conductivity of these materials.

We detailed the strong processing-structure-conductivity relationships of PANI that is doped with a polymer acid of poly(2-acrylamido-2-methyl-1-propanesulfonic acid), or PAAMPSA, in Chapters 3 and 4. Specifically, controlling the molecular characteristics of PAAMPSA template, such as its molecular weight and molecular weight distribution, strongly influence both the structure and the conductivity of PANI-PAAMPSA. For example, we observed strong correlations between the crystallinity of PANI and the conductivity of PANI-PAAMPSA. As mentioned in Chapter 2, PANI-

PAAMPSA forms electrostatically-stabilized particles during polymerization by strong ionic interactions between the sulfonic acid groups of PAAMPSA and aniline. Given that PANI-PAAMPSA forms such particles, we infer that the crystallinity qualifies the molecular order within these particles and therefore provides an indirect measure of intra-particle charge transport. In order for macroscopic conduction to occur across the bulk PANI-PAAMPSA films, however, inter-particle charge transport should be also considered. In this chapter, we elucidate how the molecular characteristics of polymer acid template influence inter-particle charge transport in PANI-PAAMPSA films. We will thus examine the structural characteristics of the same PANI-PAAMPSA studied in Chapters 3 and 4 on a larger length scale. As a reminder, two series of PAAMPSA were prepared as a function of molecular weight. One series was synthesized via conventional free-radical polymerization (CFRP) so their molecular weight distributions are broad (PDI = 1.43 – 1.64). The other series was synthesized via atom transfer radical polymerization (ATRP) so their molecular weight distributions are relatively narrow (PDI = 1.14 – 1.28) compared to those of CFRP-derived PAAMPSA. The ATRP-derived PAAMPSAs are referred to as aPAAMPSA. Full characterization of PAAMPSA and aPAAMPSA are provided in Table 2.1 of Chapter 2. We denote PANI that was doped with CFRP-derived PAAMPSA as PANI-PAAMPSA-X, where X is the poly(ethylene oxide)-equivalent number-average molecular weight of PAAMPSA in kg/mol. The other series of PANI is referred to as PANI-aPAAMPSA-X.

To synthesize PANI-PAAMPSA (and PANI-aPAAMPSA), PAAMPSA (and aPAAMPSA) is first dissolved in water. Aniline is then added and oxidatively polymerized along the PAAMPSA (and aPAAMPSA) backbone. The sulfonic acid

groups in PAAMPSA (and aPAAMPSA) are responsible for doping PANI. Extra sulfonic acid groups can render water-dispersibility to the PANI-PAAMPSA (and PANI-aPAAMPSA) complexes. As increasingly more sulfonic acid groups participate in the doping of PANI during the course of polymerization, PAAMPSA (or aPAAMPSA) becomes less hydrophilic, and PANI-PAAMPSA (and PANI-aPAAMPSA) forms electrostatically-stabilized colloidal particles, the size of which is arrested during polymerization by strong ionic interactions between the sulfonic acid groups of PAAMPSA (and aPAAMPSA) and the PANI backbone.[8] As such, the particles characteristics do not change even when PANI-PAAMPSA is purified, dried, and then resuspended in water for further processing. Such particles can be imaged by transmission electron microscopy (TEM). Figure 5.1 shows the representative TEM micrographs of (a) PANI-PAAMPSA-724, (b) PANI-PAAMPSA-45, and (c) PANI-aPAAMPSA-30. All the samples were drop cast from 0.0001 wt% PANI-PAAMPSA (and PANI-aPAAMPSA) in 0.1 M NaCl aqueous solution. Detailed discussion about this sample preparation will be described later in this chapter. The PANI-PAAMPSA particles are clearly observed in the TEM micrographs.

Figure 5.2 shows the atomic force micrograph (AFM) micrographs of (a) PANI-PAAMPSA-724, (b) PANI-PAAMPSA-45, and (c) PANI-aPAAMPSA-30. The films were drop cast from 5 wt% aqueous polymer dispersions. The micrograph of PANI-PAAMPSA-724 (PDI of PAAMPSA-724 = 1.64) is highly irregular and reveals large particles of approximately a micron in size (Figure 5.2 (a)). The root mean square (rms) roughness of this film is 60.3 nm. Similarly-cast PANI-PAAMPSA-724 films exhibit a conductivity of 0.43 ± 0.02 S/cm. In contrast, the micrograph of PANI-PAAMPSA-45

(PDI of PAAMPSA-45 = 1.43) appears smoother (Figure 5.2 (b)). Smaller particles are observed and the rms roughness of this film is 41.5 nm. The conductivity of PANI-PAAMPSA-45 films is 1.09 ± 0.03 S/cm. The micrograph of PANI-aPAAMPSA-30 (PDI of aPAAMPSA-30 = 1.16) is shown in Figure 5.2 (c). The particles in PANI-aPAAMPSA-30 film appear to be comparable in size with that in PANI-PAAMPSA 45 and the rms roughness of the film is 36.4 nm. PANI-aPAAMPSA-30 films exhibit the conductivity of 2.39 ± 0.03 S/cm. Since PANI-PAAMPSA (and PANI-aPAAMPSA) forms electrostatically stabilized particles, macroscopic conduction should be governed by point contacts between particles in the solid-state. This chapter explores inter-particle charge transport in PANI-PAAMPSA (and PANI-aPAAMPSA) by quantifying the packing of PANI-PAAMPSA (and PANI-aPAAMPSA) particles.

To establish that the macroscopic charge transport is governed by how PANI-PAAMPSA (and PANI-aPAAMPSA) particles pack in the solid state, we quantified the size and size distribution of PANI-PAAMPSA (and PANI-aPAAMPSA) particles by dynamic light scattering (DLS) on dilute aqueous dispersions. All our DLS experiments were carried out on 0.0001 wt% PANI-PAAMPSA (and PANI-aPAAMPSA) in 0.1 M NaCl aqueous solution. These polymer and salt concentrations were selected after a series of control experiments. Specifically, we added NaCl to the dispersions to screen interparticle electrostatic interactions and eliminate particle aggregation.[9] The control experiments were detailed in Chapter 2. Figure 5.3 contains the number-weighted DLS intensity distribution of (a) PANI-PAAMPSA-724, (b) PANI-PAAMPSA-45, and (c) PANI-aPAAMPSA-30. The mean hydrodynamic particle diameters (D_h) extracted from these distributions are 1230 ± 25, 543 ± 9, and 560 ± 11 nm, respectively. The standard

deviation was determined from the variation in the DLS number-average intensity distribution during the seven DLS runs per sample. To confirm that these mean hydrodynamic diameters are truly representative of the size of isolated individual particles, we compared these values against those obtained via TEM. TEM samples were prepared by drop casting the same dilute aqueous dispersions used in DLS experiments on copper grids. The particles observed in Figures 5.1 (a) - (c) are spherical and their sizes are consistent with those extracted from DLS. Our experiments indicate that PANI-PAAMPSA (and PANI-aPAAMPSA) particle size increases with increasing molecular weight of PAAMPSA (and aPAAMPSA).

The size distribution of the PANI-PAAMPSA (and PANI-aPAAMPSA) particles was also characterized by quantifying the full width of the DLS number-average intensity distribution at half its maximum intensity (FWHM). The FWHM of the intensity distribution of PANI-PAAMPSA-724, PANI-PAAMPSA-45, and PANI-aPAAMPSA-30 are 926 ± 69, 636 ± 12, and 374 ± 4 nm, respectively. The size distribution of PANI-PAAMPSA (and PANI-aPAAMPSA) particles scales with the molecular weight distribution of the polymer acid. Table 5.1 lists the particle size and size distribution of all the PANI-PAAMPSA (and PANI-aPAAMPSA) examined in our study. A total of twelve PANI-PAAMPSA (and PANI-aPAAMPSA) samples were synthesized on polymer acid templates having varying molecular weight and molecular weight distribution. Additionally, we examined the particle characteristics of two control specimens to further probe the influences of molecular weight distribution of polymer acid on the size distribution of the PANI-PAAMPSA (and PANI-aPAAMPSA) particles. PANI-aPAAMPSA-226 refers PANI that was template synthesized with aPAAMPSA-

226 having a broad molecular weight distribution (PDI = 1.62). PANI-aPAAMPSA-<45> refers to PANI that was template synthesized on a blend of aPAAMPSA having varying molecular weights.[10] The average molecular weight of this aPAAMPSA blend is 45 kg/mol with a PDI of 1.40. The correlation between the molecular characteristics of PAAMPSA (or aPAAMPSA) and the size and size distribution of PANI-PAAMPSA (or PANI-aPAAMPSA) particles are more clearly illustrated in Figures 5.4 and 5.5. Figure 5.4 shows the mean hydrodynamic diameter of PANI-PAAMPSA (and PANI-aPAAMPSA) particles as a function of PAAMPSA (and aPAAMSPA) molecular weight. The particle size of PANI-PAAMPSA (and PANI-aPAAMPSA) increases with increasing molecular weight of PAAMPSA (and aPAAMPSA). Figure 5.5 shows the size distribution of PANI-PAAMPSA (and PANI-aPAAMPSA) particles as a function of the PDI of PAAMPSA (and aPAAMPSA). It is clearly observed that the size distribution of the particles increases with increasing the molecular weight distribution of PAAMPSA, so with increasing PAAMPSA (and aPAAMPSA) PDI.

Accordingly, the relationship between the molecular characteristics of PAAMPSA and the size and size distribution of PANI-PAAMPSA particles implicates a correlation between the characteristics of the particles and the macroscopic conductivities of PANI-PAAMPSA; smaller particles and those of narrower size distribution lead to higher conductivities when PANI-PAAMPSA is drop cast as films.

The mechanism by which macroscopic conduction occurs in PANI-PAAMPSA should be associated with the way in which the particles pack in the cast film. To address how PANI-PAAMPSA particles pack in drop cast films, the macroscopic volume

fraction of the PANI-PAAMPSA (and PANI-aPAAMPSA) particles is quantified from DLS results using Equation (5.1).

$$\phi_i = \frac{4\pi}{3}\rho_i \int_0^\infty (r)^3 f_i(r) dr \qquad (5.1)$$

In this equation, $f_i(r)$ is the normalized number-average particle size distribution that is obtained from DLS experiments for polymer i and ρ_i is the number density of particles. Given that PANI-PAAMPSA (and PANI-aPAAMPSA) particles are spherical and individually isolated (see the TEM images of the materials in Figure 5.1), we assumed that our materials can be adequately modeled with hard sphere interparticle interactions. Assuming hard spheres with radius r, the macroscopic packing fraction, ϕ_i, can be estimated. Alternatively, if ϕ_i is known, we can estimate the number density of particles in the solid film by Equation (5.1).

To determine the macroscopic packing fraction of PANI-PAAMPSA (and PANI-aPAAMPSA) particles, we performed molecular simulations of film formation of PANI-PAAMPSA in collaboration with William P. Krekelberg and Prof. Thomas M. Truskett in Chemical Engineering at the University of Texas at Austin. We accounted for the packing of approximately 2000 particles in the film by considering them as hard spheres having the size and size distribution that were experimentally determined by DLS. The concentration of this hard sphere system was simulated using the Lubachevsky-Stillinger algorithm.[11] In this method, event-driven molecular dynamics for the particles is carried out in a periodically-replicated simulation cells.[12] The simulation cell volume is kept

constant while the radius of the *j*th particle $r_j(t)$ is allowed to grow linearly with time *t* according to the Equation (5.2).

$$r_j(t) = r_j(0) + \Gamma \frac{r_j(0)}{\langle r_j(0) \rangle} \sqrt{\frac{k_B T}{m}} t \qquad (5.2)$$

where $\langle r_j(0) \rangle$ is the average initial particle radius, Γ is a dimensionless growth rate, T is the temperature, k_B is the Boltzmann constant, and m is the particle mass. We simulated $\Gamma = 0.05,\ 0.005,\ 0.001$ and 0.0001. This range of Γ covers a very wide range of effective concentration rates known to produce amorphous packing of the hard spheres. In fact, the AFM images of PANI-PAAMPSA samples show that the packing of particles is random in the solid state (Figure 5.2). When the packing does not accommodate further particle growth, relative to the cell dimension, the system is considered "jammed".[12] To determine the macroscopic packing fraction of this jammed system, we quantified the small changes in sphere size, Δd, from one collision to the next using Equation (5.3).

$$\Delta d = \frac{1}{N_c} \sum_{k=2}^{N_c} \frac{r^{\max}(t_k) - r^{\max}(t_{k-1})}{r^{\max}(t_k)} \qquad (5.3)$$

where $r^{\max}(t_k)$ and $r^{\max}(t_{k-1})$ are the radii of the largest sphere at the k^{th} and $(k\text{-}1)^{\text{th}}$ collision, and N_c is the number of collisions used to calculate Δd. For this

experiment, we used $N_c = 10^4$ and consider the system jammed when $\Delta d \leq 5 \times 10^{-9}$. To obtain a particle size distribution for the simulation at each state point, we scaled the experimental intensities such that the total number of particles was approximately 2000. The Lubachevksy-Stillinger compressions were initialized from the equilibrated hard sphere fluid configurations at a packing fraction of $\phi = 0.3$. For each particle size distribution and growth rate, Γ, 30 independent randomly jammed configurations were created. The average jammed packing fractions of these systems are presented in Table 5.2. The resulting packing fractions only vary by a few percent over a wide range of particle size distributions and effective concentration rates. Specifically, the macroscopic packing fraction is 0.649 ± 0.007 for all the PANI-PAAMPSA (and PANI-aPAAMPSA) having varying PAAMPSA molecular characteristics. Given the DLS intensity distributions and assuming a constant macroscopic packing fraction across all samples, we are thus able to estimate particle density for individual PANI-PAAMPSA and PANI-aPAAMPSA samples.

To examine the correlation between the packing density and the macroscopic electrical conductivity of PANI-PAAMPSA (and PANI-aPAAMPSA), we plotted the conductivity of PANI-PAAMPSA as a function of particle density in Figure 5.6. The conductivity of PANI-PAAMPSA (and PANI-aPAAMPSA) scales linearly with particle density, which is reducible from the molecular characteristics of PAAMPSA. This observation is consistent with the assumption that conduction pathways are governed by contacts between particles in the solid-state.

To examine the concentration profile of PANI-PAAMPSA (and PANI-aPAAMPSA) films, we carried out depth profile measurements on the films using x-ray photoelectron spectroscopy (XPS). An argon ion beam was used to sputter the films for 5-10 minute intervals and XPS measurements were conducted after each interval to probe the changes in the chemical composition with film depth. Figures 5.7 (a) and (b) contain representative high-resolution XPS spectra of PANI-PAAMPSA-724 in the nitrogen and sulfur regions, respectively, with increasing film depth. The nitrogen spectrum was deconvoluted into three components. The peak at 399.2 eV is attributed to the amide groups in PAAMPSA, and the one centered at 400.4 eV is attributed to the protonated nitrogens associated with polarons and bipolarons in PANI-PAAMPSA (denoted N_1^+). The peak located at 401.3 eV is attributed to the protonated nitrogens that are ionically associated with the sulfonic acid groups in PAAMPSA (denoted N_2^+).[13, 14] The integrated peak intensity is proportional to the concentration of the individual species. The detailed procedures of spectrum deconvolution were described in Chapter 2. The concentration of protonated nitrogens relative to that of amide nitrogens is high in the surface scan (Figure 5.7 (a)-(i)). Its relative concentration then decreases deeper into the PANI-PAAMPSA film. This trend is quantified in Figure 5.7 (c) where the relative concentration of N_2^+, normalized to that on the surface, is plotted as a function of film depth. The concentration of N_2^+ decreases rapidly with film depth, and it levels off at approximately 300 nm below the surface. A similar analysis was carried out with the sulfur region of the XPS spectra. The sulfur XPS spectra were deconvoluted into two sets of doublets. A pair of peaks are located at 167.5 and 168.7 eV, and another set of peaks are located at 168.3 and 169.5 eV.[15, 16] The doublet at lower binding energy

corresponds to the sulfurs in the ionized sulfonic acid groups of PAAMPSA ($-SO_3^-$), and that at higher binding energy corresponds to the sulfurs in the sulfonic acid groups of PAAMPSA ($-SO_3H$) that do not participate in the protonation of PANI.[15, 16] With increasing film depth, the concentration of the ionized sulfonic acid decreases compared to that of the neutral sulfonic acid. This trend is also quantified in Figure 5.7 (c) where the relative concentration of ionized sulfonic acid, normalized by the surface concentration, is plotted with the film depth. Similar to the relative concentration of the protonated nitrogens, that of the ionized sulfonic acid decreases rapidly with the film depth. This decrease slows down as we sputter into the film. We noticed a subtle difference between the decay in the relative concentration of N_2^+ and that of ionized sulfur. The relative concentration of N_2^+ plateaus 300 nm below the film surface whereas that of ionized sulfonic acid continues to decrease. We believe this difference is due to slight damage of the film by ion sputtering during depth profiling experiments, causing the apparent relative concentration of ionized sulfur to continue to decrease.[17] Indeed, an additional doublet at 163.5 and 164.7 eV is observed in the sulfur XPS spectra in Figure 5.7 (b). This doublet is attributed to elemental sulfur or thiol moieties (-SH).[17] The constant bombardment of argon ions can lead to oxygen loss within the sulfonic acid groups of PAAMPSA, which leaves behind the elemental sulfur or thiols. Such ion beam damage was previously reported in PEDOT-PSS film conducted sputtering and depth profile experiments.[17] Despite the slight film damage, however, the XPS depth profiling experiments indeed suggest that the concentrations of the ionized species of PANI (protonated nitrogens) and PAAMPSA (ionized sulfonic acid groups) are preferentially enhanced on the surface of the particles. This observation is in contrast

with what is known for commercially-available conducting polymer, poly(ethylene dioxythiophene) that is doped with poly(styrenesulfonic acid), or PEDOT-PSS. In PEDOT-PSS, a thin overlayer of insulating PSS is frequently observed.[18, 19] This insulating PSS overlayer hampers macroscopic conduction, and it can also change the work function of the PEDOT-PSS with exposure to humidity.[20] In contrast, the conductive portions are preferentially segregated to the surface of the PANI-PAAMPSA (and PANI-aPAAMPSA).

To further examine the surface mediated conduction in PANI-PAAMPSA (and PANI-aPAAMPSA) films, we estimated the particle surface area per unit volume of the cast film (A_i/V) based on Equation (5.4).

$$A_i / V = 4\pi\rho_i \int_0^\infty r^2 f_i(r) dr \qquad (5.4)$$

Again, we used the same packing fraction of 0.64 to calculate A_i/V. The electrical conductivity of PANI-PAAMPSA (and PANI-aPAAMPSA) is plotted as a function of A_i/V in Figure 5.8. The conductivity increases superlinearly with A_i/V, suggesting that charge transport occurs at the surface of the particles. If macroscopic conduction occurs through the bulk of the particles (i.e., if the particles are chemically homogeneous), the conductivity would be constant with increasing A_i/V since the macroscopic volume fractions are comparable for all the samples. In fact, the contacts between particles would provide resistance along the conduction paths, and since their number generally increases with A_i/V, the conductivity may decrease with A_i/V for the

films consisting of chemically homogeneous particles. Since the conductivity of PANI-PAAMPSA (and PANI-aPAAMPSA) increases with A_i/V, we hypothesize that charge transport occurs at the surface of the particles in PANI-PAAMPSA (and PANI-aPAAMPSA) films.

The electrical conductivities of PANI-PAAMPSA (and PANI-aPAAMPSA) are strongly dependent on the details of the synthesis parameters. Specifically, we observed strong correlations between the molecular characteristics of PAAMPSA and the electrical conductivity of PANI-PAAMPSA (and PANI-aPAAMPSA) in Chapters 3 and 4. The conductivity of PANI-PAAMPSA (and PANI-aPAAMPSA) increases with decreasing PAAMPSA (and aPAAMPSA) molecular weight, and it further increases with narrowing molecular weight distribution of PAAMPSA. We also observed the strong correlations between the crystallinity and the conductivity of PANI-PAAMPSA (and PANI-aPAAMPSA) samples; the conductivity of PANI-PAAMPSA (and PANI-aPAAMPSA) increases with increasing the crystallinity of PANI. Given that the synthesis of PANI-PAAMPSA (and PANI-aPAAMPSA) results in the formation of electrostatically-stabilized colloidal particles, this crystallinity only qualifies the molecular order within these particles and therefore provides an indirect measure of intra-particle charge transport. In order for macroscopic conduction to occur across the PANI-PAAMPSA (and PANI-aPAAMPSA) films, however, inter-particle charge transport should be also considered in addition to the intra-particle charge transport. This chapter demonstrated that a higher particle density per unit film results in the improved inter-particle charge transport, leading to the higher conductivity of the film. The combination of this

observation with the crystallinity-conductivity correlations strongly suggests that both inter- and intra-particle conduction are important for macroscopic conduction across the PANI-PAAMPSA (and PANI-aPAAMPSA) film. We also demonstrated in this chapter that surface mediated conduction occurs in PANI-PAAMPSA (and PANI-aPAAMPSA) film, in contrast with PEDOT-PSS film.

Table 5.1. Physical characteristics of PANI-PAAMPSA (or PANI-aPAAMPSA).

Nomenclature	D_h of PANI-PAAMPSA or PANI-aPAAMPSA[(b)] (nm)	FWHM[(a)] of PANI-PAAMPSA or PANI-aPAAMPSA[(b)] (nm)
PANI-PAAMPSA-45	543 ± 9	636 ± 12
PANI-PAAMPSA-83	699 ± 17	671 ± 15
PANI-PAAMPSA-106	774 ± 16	703 ± 3
PANI-PAAMPSA-255	908 ± 18	788 ± 13
PANI-PAAMPSA-724	1232 ± 25	926 ± 69
PANI-aPAAMPSA-30	560 ± 11	374 ± 5
PANI-aPAAMPSA-67	626 ± 13	373 ± 4
PANI-aPAAMPSA-117	739 ± 15	394 ± 9
PANI-aPAAMPSA-150	782 ± 18	414 ± 9
PANI-aPAAMPSA-287	820 ± 16	430 ± 15
PANI-aPAAMPSA-226	827 ± 17	636 ± 32
PANI-aPAAMPSA-<45>	586 ± 11	551 ± 23

(a) The full width of the size distribution of particle acquired by DLS at half its maximum intensity. (b) Standard deviation determined from 5-7 independent runs to account for run-to-run variations.

Table 5.2. Final particle packing fractions for each system and particle growth rate.

Nomenclature	ϕ_i			
	$\Gamma = 0.05$	$\Gamma = 0.005$	$\Gamma = 0.001$	$\Gamma = 0.0001$
PANI-PAAMPSA-45	0.662	0.684	0.689	0.692
PANI-PAAMPSA-83	0.656	0.674	0.679	0.683
PANI-PAAMPSA-106	0.654	0.673	0.677	0.681
PANI-PAAMPSA-255	0.653	0.671	0.675	0.679
PANI-PAAMPSA-724	0.649	0.666	0.669	0.673
PANI-aPAAMPSA-30	0.647	0.663	0.667	0.670
PANI-aPAAMPSA-67	0.645	0.662	0.665	0.669
PANI-aPAAMPSA-117	0.643	0.658	0.662	0.665
PANI-aPAAMPSA-150	0.643	0.658	0.662	0.665
PANI-aPAAMPSA-287	0.642	0.658	0.662	0.665

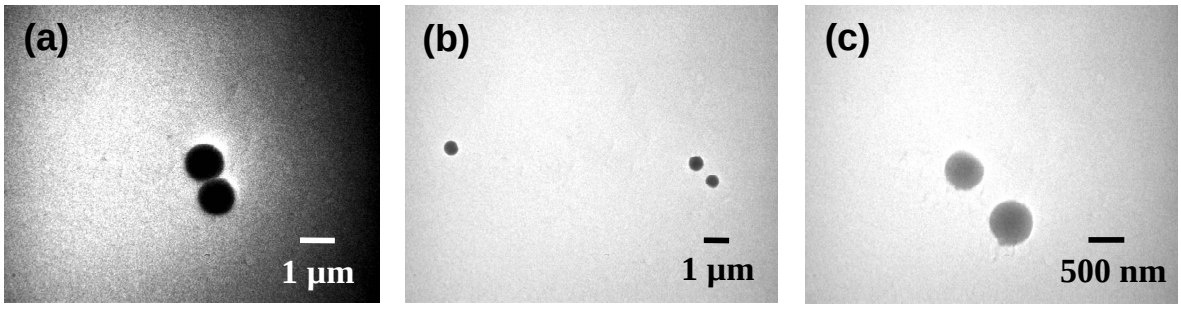

Figure 5.1. TEM images of (a) PANI-PAAMPSA-724, (b) PANI-PAAMPSA-45, and (c) PANI-aPAAMPSA-30.

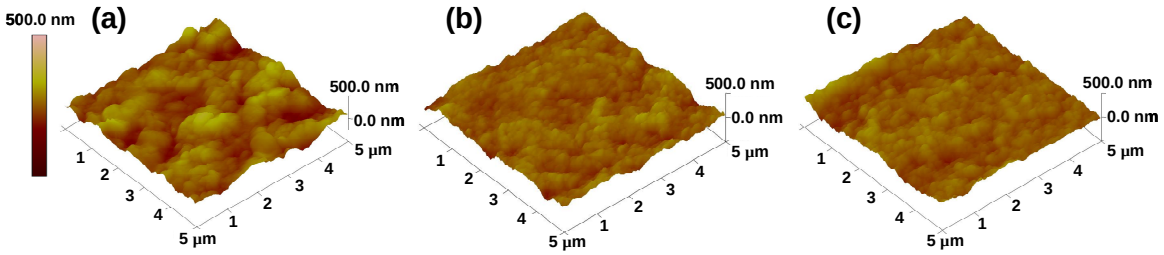

Figure 5.2. AFM images of (a) PANI-PAAMPSA-724 (rms roughness of ≈ 60.3 nm), (b) PANI-PAAMPSA-45 (rms roughness of ≈ 41.5 nm), and (c) PANI-aPAAMPSA-30 (rms roughness of ≈ 36.4 nm).

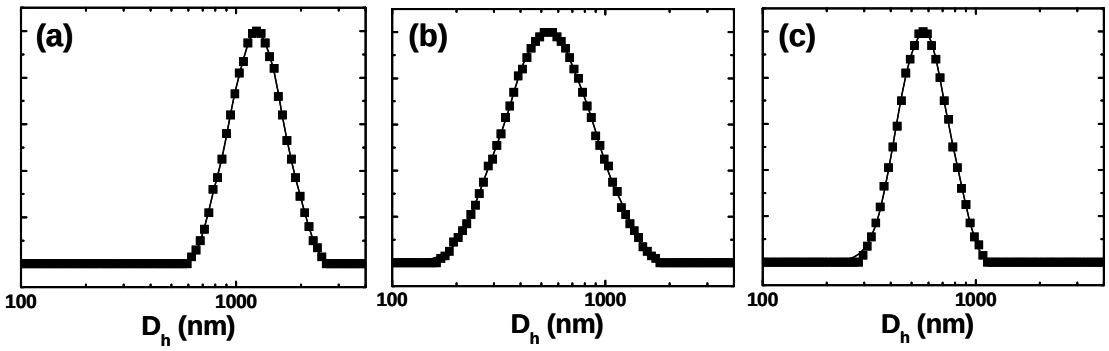

Figure 5.3. Number-weighted intensity distributions of (a) PANI-PAAMPSA-724, (b) PANI-PAAMPSA-45, and (c) PANI-aPAAMPSA-30 measured by DLS at 25 °C in 0.1 M NaCl (0.0001 wt% polymer).

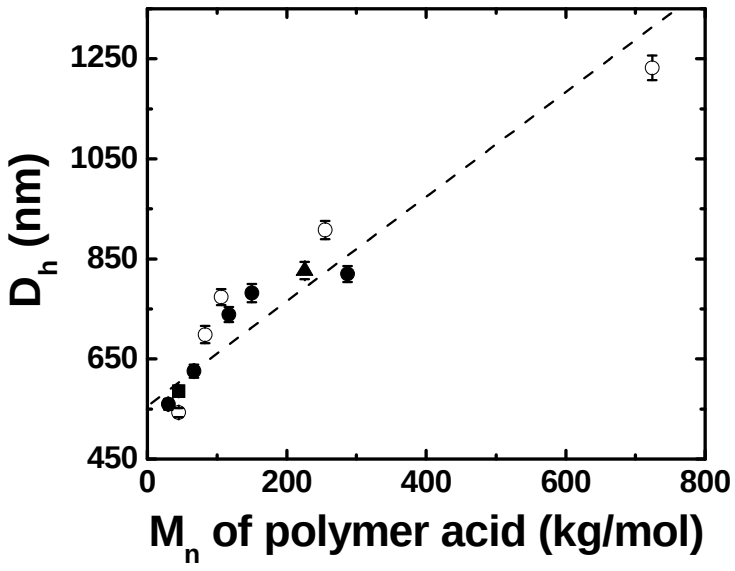

Figure 5.4. The mean hydrodynamic diameters of PANI-PAAMPSA (○) and PANI-aPAAMPSA (●) as a function of the molecular weight of polymer acid template. A fit (dash line) to the data is included each. The mean hydrodynamic diameters of PANI-aPAAMPSA-<45> (■) and PANI-aPAAMPSA-226 (▲) are also included.

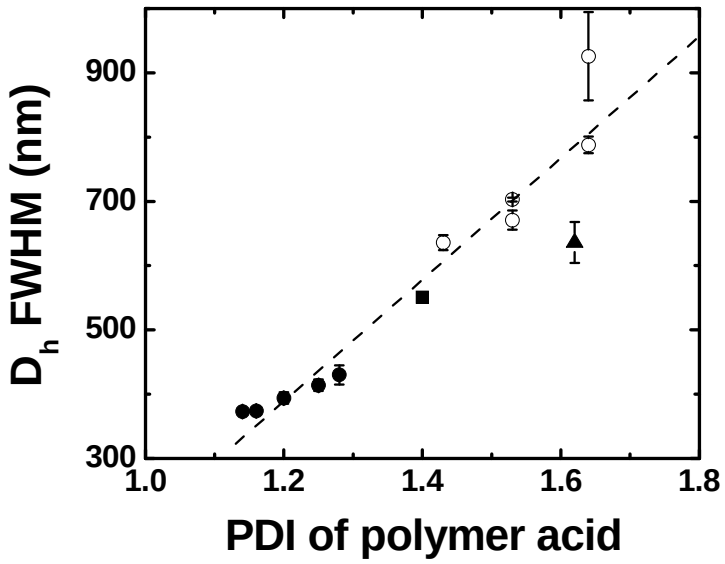

Figure 5.5. The particle size distributions, determined by the full width of the DLS intensity distribution at half its maximum intensity (FWHM), of PANI-PAAMPSA (○) and PANI-aPAAMPSA (●) as a function of the molecular weight distribution (quantified by PDI) of polymer acid template. A fit (dash line) to the data is included each. The particle size distributions of PANI-aPAAMPSA-<45> (■) and PANI-aPAAMPSA-226 (▲) are also included.

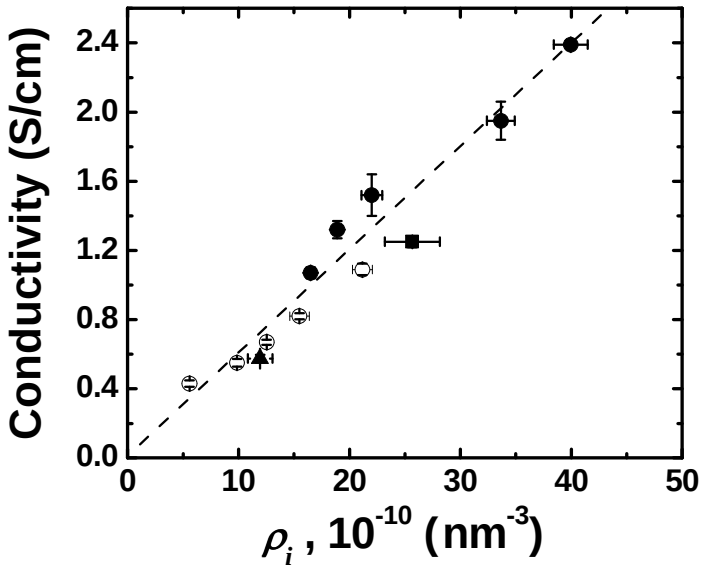

Figure 5.6. The conductivities of PANI-PAAMPSA (○) and PANI-aPAAMPSA (●) as a function of particle number density, ρ_i. ρ_i is calculated based on the assumption of ϕ_i=0.64 for all polymers examined. A fit (dash line) to the data is included each. The electrical conductivities of PANI-aPAAMPSA-<45> (■) and PANI-aPAAMPSA-226 (▲) are also included.

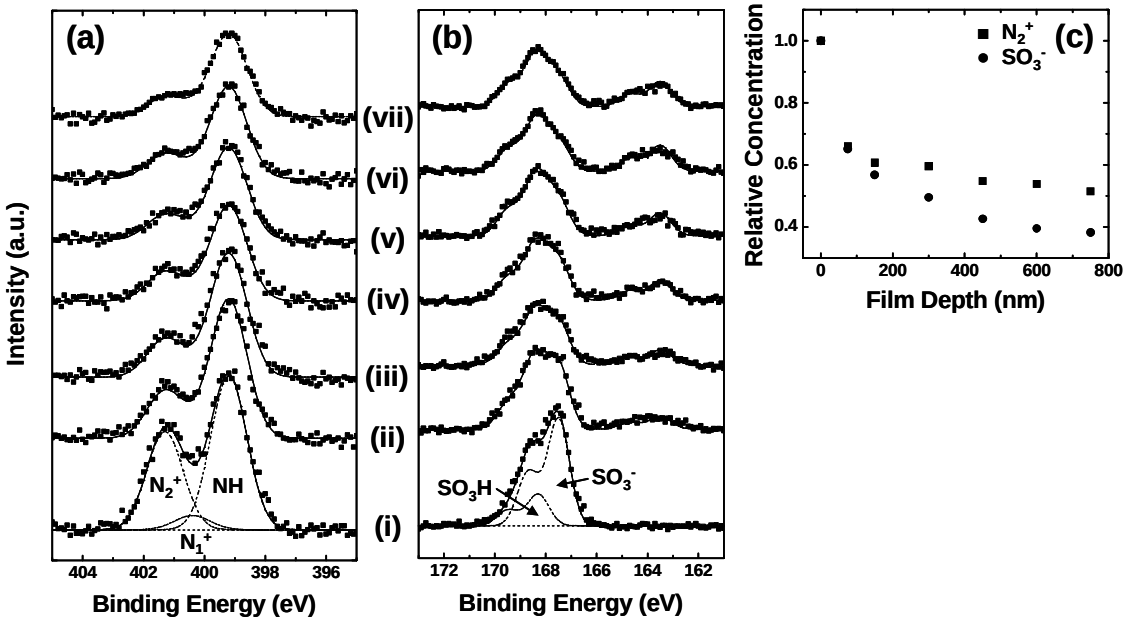

Figure 5.7. XPS spectra of the (a) nitrogen and (b) sulfur regions for (i) as-cast PANI-PAAMPSA-724 (with peak deconvolution) and the same film upon sputtering for (ii) 75 nm, (iii) 150 nm, (iv) 300 nm, (v) 450 nm, (vi) 600 nm, and (vii) 750 nm. The overall fit is shown with a solid line in each spectrum. The relative concentrations of protonated nitrogen (N_2^+, ■) and ionized sulfur ($-SO_3^-$, ●), normalized by the surface concentrations of the respective elements before sputtering, are shown in (c).

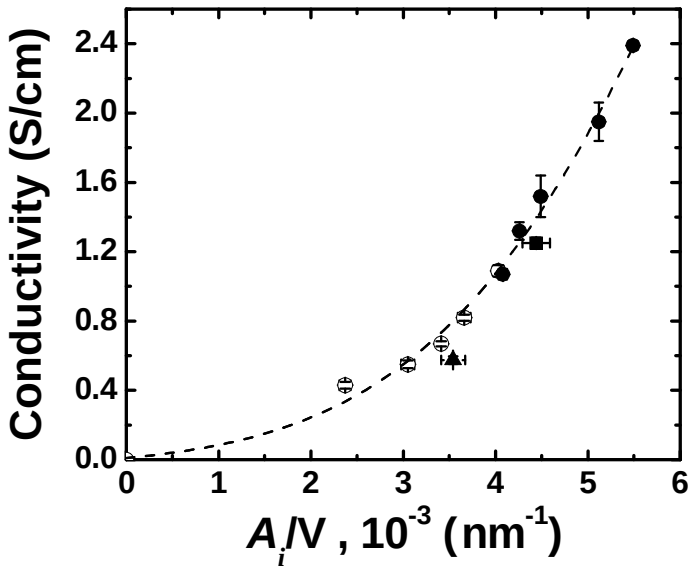

Figure 5.8. The conductivities of PANI-PAAMPSA (○) and PANI-aPAAMPSA (●) as a function of particle surface area per unit cast film, A_i/V. A_i/V is calculated based on the assumption of ϕ_i=0.64 for all polymers examined. A fit (dash line) to the data is included each. The electrical conductivities of PANI-aPAAMPSA-<45> (■) and PANI-aPAAMPSA-226 (▲) are also included.

REFERENCES

1. K. S. Lee, G. B. Blanchet, F. Gao and Y.-L. Loo, *Appl. Phys. Lett.*, 2005, **86**, 074102.
2. K. S. Lee, T. J. Smith, K. C. Dickey, J. E. Yoo, K. J. Stevenson and Y.-L. Loo, *Adv. Func. Mater.*, 2006, **16**, 2409.
3. S.-A. Chen and H.-T. Lee, *Macromolecules*, 1995, **28**, 2858.
4. A. G. MacDiarmid and A. J. Epstein, *Synth. Met.*, 1995, **69**, 85.
5. H. S. Moon and J. K. Park, *J. Polym. Sci., Part A: Polym. Chem.*, 1998, **36**, 1431.
6. S. K. M. Jo¨nsson, J. Birgerson, X. Crispin, G. Greczynski, W. Osikowicz, A. W. D. v. d. Gonc, W. R. Salaneck and M. Fahlmana, *Synth. Met.*, 2003, **139**, 1.
7. J. Ouyang, Q. Xu, C.-W. Chu, Y. Yang, G. Li and J. Shinar, *Polymer*, 2004, **45**, 8443.
8. L. Sun, S. C. Yang and J.-M. Liu, *Polym. Prepr.*, 1992, **33**, 379.
9. M. Sedlak, *Langmuir*, 1999, **15**, 4045.
10. J. E. Yoo, T. L. Bucholz, S. Jung and Y.-L. Loo, *J. Mater. Chem.*, 2008, **18**, 3129.
11. B. D. Lubachevsky and F. H. Stillinger, *J. Stat. Phys*, 1990, **60**, 561.
12. D. C. Rapaport, *The Art of Molecular Dynamics Simulation*, Cambridge University Press, Cambridge, 2004.
13. E. T. Kang, K. G. Neoh and K. L. Tan, *Prog. Polym. Sci.*, 1998, **23**, 277.
14. J. Yue and A. J. Epstein, *Macromolecules*, 1991, **24**, 4441.
15. J. Y. Kim, J. H. Jung, D. E. Lee and J. Joo, *Synth. Met.*, 2002, **126**, 311.
16. K. Z. Xing, M. Fahlman, X. W. Chen, O. Inganaes and W. R. Salaneck, *Synth. Met.*, 1997, **89**, 161.

17. X. Crispin, S. Marciniak, W. Osikowicz, G. Zotti, A. W. D. V. D. Gon, F. Louwet, M. Fahlman, L. Groenendaal, F. D. Schryver and W. R. Salaneck, *J. Polym. Sci., Part B: Polym. Phys.*, 2003, **41**, 2561.

18. J. Hwang, F. Amy and A. Kahn, *Org. Electron.*, 2006, **7**, 387.

19. K. Z. Xing, M. Fahlman, X. W. Chen, O. Inganas and W. R. Salaneck, *Synth. Met.*, 1997, **89**, 161.

20. N. Koch, A. Vollmer and A. Elschner, *Appl. Phys. Lett.*, 2007, **90**, 043512.

21. S. Torquato, T. M. Truskett and P. G. Debenedetti, *Phys. Rev. Lett.*, 2000, **84**, 2064.

22. T. M. Truskett, S. Torquato and P. G. Debenedetti, *Phys. Rev. E*, 2000, **62**, 993.

Chapter 6: Highly conductive polymer films through post-processing dichloroacetic acid annealing and their applications in organic solar cells

We have characterized water-dispersible polyaniline (PANI) that is template synthesized with poly(2-acrylamido-2-methyl-1-propane sulfonic acid), or PAAMPSA, in the previous chapters. Specifically, we demonstrated that the conductivity of PANI-PAAMPSA is governed by how conductive PANI-PAAMPSA particles pack when drop cast as films. PANI-PAAMPSA forms particles during the course of polymerization and their structures are arrested by strong ionic interactions between PANI and PAAMPSA. The size and size distribution of such particles – which dictate the final packing in the solid state – are controlled by adjusting the molecular weight and the molecular weight distribution of PAAMPSA at the onset of polymerization.

Dr. Kwang Seok Lee, a former graduate student in our group, used such PANI-PAAMPSA drop cast films as electrodes in organic thin-film transistors (OTFTs).[1] The performance of such thin-film transistors was limited by the bulk resistance of PANI-PAAMPSA electrodes. Current crowding was observed at high gate voltages. To improve device performance, PANI-PAAMPSA having dramatically improved conductivities was used to replace the original PANI-PAAMPSA. We improved the electrical conductivity of PANI-PAAMPSA by post-processing solvent annealing; the resulting material was two orders of magnitude more conductive than the original PANI-PAAMPSA. The concept of post-processing solvent annealing is comparable to

"secondary doping" of PANI that is doped with small molecule acids. During secondary doping, a solvent is introduced to induce structural rearrangement of PANI.[2, 3] Specifically, PANI undergoes a "compact coil" to "extended chain" conformational change, which results in an increase in the electrical conductivity.[2, 3] For example, the conductivity of PANI doped with camphor sulfonic acid (CSA) increases significantly when exposed to specific solvents.[2, 3] The conductivity of PANI-CSA is 0.2 S/cm. When this PANI-CSA film is exposed in m-cresol, its conductivity increases up to 300 S/cm.[2, 3] The conductivity improvement originates from a change in the PANI-CSA conformation from a compact coil to an extended chain conformation.[2, 3] The extended chain conformation increases charge delocalization along the PANI backbone, thereby enabling more efficient charge transport.

Our previous experiments, however, indicated that treating PANI-PAAMPSA with m-cresol does not improve the conductivity of the polymer. While secondary doping with a fluorinated alcohol also increases the conductivity of PANI-CSA,[4, 5] fluorinated alcohols do not alter the conductivity of PANI-PAAMPSA. This phenomenon indicates that secondary doping of PANI is specific to the particular solvent used.

Dr. Kwang Seok Lee discovered that dichloroacetic acid (DCA) can induce structural changes in PANI-PAAMPSA, thereby improving its conductivity.[6] DCA has been reported to be a good solvent for PANI-CSA[7] and PANI that is doped with 2-acrylamido-2-methyl-1-propane sulfonic acid (AAMPSA; the monomer of PAAMPSA).[8, 9] Although preliminary results indicated structural rearrangement of PANI-PAAMPSA after DCA treatment, the origin of conductivity enhancement was not clearly understood.

In this chapter, we detail the role of DCA during the structural rearrangement of PANI-PAAMPSA and we further elucidate the origin of PANI-PAAMPSA conductivity improvement by DCA treatment. More importantly, we show that this DCA treatment is also applicable to other polymer acid-doped conducting polymers for their conductivity improvements. To assess the effect of the improved conductivity, we incorporated DCA-treated conducting polymers into organic solar cells (OSCs) as anodes. For comparison, untreated conducting polymers were also incorporated as anodes in reference OSCs of the same dimensions and geometry.

For this study, we first spin coated PANI-PAAMPSA films on Si/SiO_2 substrates at 1000 rpm from a 5 wt% aqueous dispersion. The PANI-PAAMPSA films were baked at 90 °C for 3 minutes to remove residual water. We then gently agitated the films in pre-heated DCA (Acros Organics, 99+%) at 90 ºC. Subsequently, PANI-PAAMPSA films were baked at 145 ºC for 30 minutes. After DCA treatment, we exposed the films to $< 10^{-7}$ Torr vacuum for more than 3 hours to remove residual DCA prior to any characterization. The electrical conductivities of DCA-treated PANI-PAAMPSA films were then measured using the four-point probe technique previously described in Chapter 2. We also measured the conductivities of PANI-PAAMPSA films prior to DCA treatment for reference. Figure 6.1 shows the representative current-voltage (I-V) characteristics of (a) untreated and (b) DCA-treated PANI-PAAMPSA films. The current is on the order of 10^{-1} mA when a voltage of 10 V is applied on the as-cast PANI-PAAMPSA film (Figure 6.1 (a)). After DCA treatment, the current levels increased by more than two orders of magnitude at the same applied voltage (Figure 6.1 (b)), and the thicknesses decreased by approximately 20 percent. Normalizing the

slopes by the lengths and the cross-sectional areas of the films reveals an average conductivity of 47.79 ± 10.52 S/cm for DCA-treated PANI-PAAMPSA films and an average conductivity of 0.43 ± 0.02 S/cm for as-cast PANI-PAAMPSA films. Table 6.1 summarizes the conductivities of the following conducting polymers studied in this chapter before and after DCA treatment: PANI-PAAMPSA, PANI doped with a poly(styrene sulfonic acid), or PANI-PSS, and poly(ethylene dioxythiophene) doped with a PSS, or PEDOT-PSS. The conductivities were measured from the multiple samples from different batches of dispersions for each sample, and also from the multiple films separately exposed to DCA. The variations in the measurements were used to determine the standard deviations on the conductivity.

We characterized the electronic structures of PANI-PAAMPSA films before and after DCA treatment using UV-vis-NIR spectroscopy (Figure 6.2). Figure 6.2 (a) shows the UV-vis-NIR spectrum of untreated PANI-PAAMPSA. The peak at 310 nm corresponds to the π-π^* transition of the benzenoid. The peak at 450 nm is attributed to the polaronic shoulder and the peak at approximately 800 nm corresponds to the polaron interband transition.[10-12] This optical spectrum is consistent with previously-reported spectra of PANI having conductivities in the range of 0.01 – 1 S/cm, and is interpreted as PANI having a compact coil conformation.[2, 3] Figure 6.2 (b) reveals the UV-vis-NIR spectrum of DCA-treated PANI-PAAMPSA. This spectrum is drastically different from that of untreated PANI-PAAMPSA. Specifically, the absorption at ~ 800 nm red shifts; a broad absorption now appears over 1000 nm. This broad absorption is often referred to as the “free charge carrier tail”, and suggests that the polymer has an extended chain conformation.[2, 3] Such changes in UV-vis-NIR spectrum suggests that the chain

conformation of PANI-PAAMPSA has changed from a compact coil conformation to an extended chain conformation upon DCA exposure. As mentioned earlier, the extended chain conformation is generally associated with conductive polymers having significantly improved charge transport.[2, 3] As such, one would expect the conductivity of DCA-treated PANI-PAAMPSA to be significantly higher than that of the untreated system.

We also examined the morphology of PANI-PAAMPSA films before and after DCA treatment using atomic force microscopy (AFM); representative micrographs are shown in Figures 6.3 (a) and (b), respectively. Figure 6.3 (a) reveals high surface roughness (a root mean square (rms) roughness of 60.3 nm in the 5×5 μm scan window); the film composes of sub-micron particles. We observed a drastically different morphology after DCA treatment. Figure 6.3 (b) shows a featureless film with a rms roughness of 4.3 nm; sub-micron particles are eliminated after DCA treatment so conduction is no longer limited by the particle-particle contacts provided points of resistance.

Given that DCA treatment can relax PANI-PAAMPSA particles, the introduction of DCA must influence the ionic interactions between the sulfonic acid groups of PAAMPSA and aniline. To determine the role of DCA during structural rearrangement of PANI-PAAMPSA, we measured the ionization constant (pK_a) of DCA and PAAMPSA. We carried out the pK_a measurements at 70 ºC. DCA treatment of PANI-PAAMPSA was carried out at 90 ºC. We were, however, not able to make the pK_a measurements at 90 ºC because water evaporation can change the concentration of DCA in water during measurements. As such, the pK_a measurements were all carried out at 70 ºC. For this experiment, we titrated acid solutions (10^{-5} M of DCA and 10^{-7} M

of PAAMPSA) using a 10^{-1} M sodium hydroxide (NaOH) solution. The pH values were tracked as a function of the amount of NaOH solution we added to the acid solution. The pK_a was determined by reading the pH at the half point to neutralization.[13] Figure 6.4 shows the titration curves of DCA at 10^{-5} M (■) and 10^{-3} M (●) aqueous solutions. The same pK_a values are observed within error at both concentrations. Specifically, the pK_a for DCA was measured to be 0.70 for 10^{-5} M and 0.72 for 10^{-3} M solution. This observation indicates that the pK_a is independent of acid concentration. Figure 6.5 shows the titration curve of PAAMPSA (■) at 10^{-7} M aqueous solution. The titration curve of DCA (●) at 10^{-5} M solution is also included in Figure 6.5 for comparison. The pK_as of PAAMPSA and DCA are 2.29 and 0.70, respectively. We also measured the pK_a of PAAMPSA (■) and DCA (●) at room temperature (Figure 6.6); the pK_a of PAAMPSA and DCA is 2.41 and 1.21, respectively. The pK_a values of DCA at room temperature agree with the values published in the literature.[14] These observations strongly indicate that DCA is a stronger acid than PAAMPSA. This finding is surprising given that sulfonic acids are generally known to be stronger than acetic acids. Simultaneously, we also compared the pK_a of AAMPSA with that of DCA to examine the effects of molecular architecture (polymer versus monomer). Figure 6.7 shows the titration curves of AAMPSA (■) and DCA (●) at room temperature. Both acids were prepared at the same concentration of 10^{-5} M. The pK_a of AAMPSA and DCA is 0.52 and 1.21, respectively. These pK_a values agree with previously reported values for the respective acids.[14] The pK_a of AAMPSA is indeed lower than that of DCA at the same conditions. It therefore appears that the increase in pK_a of PAAMPSA compared to that of AAMPSA is due to molecular architecture differences. This difference is attributed

to electrostatic interactions between the acid groups in a polymer acid. In PAAMPSA, each repeat unit contains an acid group. Electrostatic interactions thus make it more difficult to ionize neighboring acid groups given the spatial proximity. As a result, the pK_a of a polymer acid is typically higher than its respective monomer.[15] These pK_a measurements indicate that the pK_a of DCA is lower than that of PAAMPSA. Since DCA is a stronger acid than PAAMPSA, DCA can effectively disrupt the ionic interactions between the sulfonic acid groups in PAAMPSA and aniline, allowing PAAMPSA and PANI to structurally relax, thereby eliminating the particle nature of PANI-PAAMPSA that was originally arrested during polymerization. We then remove DCA from the PANI-PAAMPSA film by placing the film under high vacuum. X-ray photoelectron spectroscopy (XPS) experiments corroborate our hypothesis and indicate that the strong ionic associations between PANI and PAAMPSA are moderated after DCA treatment.[6] We do not observe the presence of chlorine in XPS, a strong indication that DCA was completely removed after treatment. Such DCA-treated PANI-PAAMPSA adopts an extended chain structure and consequently exhibits higher conductivities.

To evaluate the versatility of this post-processing DCA treatment, we attempted to improve the conductivities of other polymer acid-doped conducting polymer films, including those of PANI-PSS and PEDOT-PSS. To synthesize PANI-PSS, we started by ion exchanging commercially-available PSS-Na (Alfa Aesar; M_w = 500 kg/mol) to its acidic form. Once the PSS-Na was converted to its acidic form, PANI-PSS was synthesized with the same procedures that we employed to synthesize PANI-PAAMPSA. The synthesis procedures of PANI-PAAMPSA were detailed in Chapter 2. After

synthesis and purification of PANI-PSS, its 5 wt% aqueous dispersions were prepared for further characterization. The DCA treatment of PANI-PSS was carried out with the same procedures mentioned above for that of PANI-PAAMPSA, except for the annealing temperature. After we soaked the PANI-PSS films in pre-heated DCA at 90 ºC, PANI-PSS films were baked at 90 ºC, as opposed to 145 ºC for PANI-PAAMPSA, for 30 minutes because the glass transition temperature (Tg) of PSS is lower than that of PAAMPSA (≈ 108 ºC as opposed to ≈ 175 ºC).[16, 17] This baking step effectively drives away residual DCA. We also exposed these DCA-treated PANI-PSS films to < 10^{-7} Torr vacuum for more than 3 hours to remove any last remaining DCA prior to characterization. DCA is also a good solvent for PSS and its pK_a is lower than that of PSS. Figure 6.8 shows the titration curves of PSS (■) and DCA (●) prepared at 10^{-7} M and 10^{-5} M, respectively. These pK_a measurements were performed at 70 °C. The pK_as of PSS and DCA are 1.95 and 0.70, respectively. Since the pK_a of DCA is lower than that of PSS, it is expected that DCA can also moderate the ionic interactions between PANI and PSS, just as it did in PANI-PAAMPSA.

Figure 6.9 shows the nitrogen and sulfur XPS spectra of untreated and DCA-treated PANI-PSS films. The detailed experimental procedures for these experiments and the subsequent data fitting were described in Chapter 2. Figures 6.9 (a) and (b) show the XPS nitrogen spectra of untreated and DCA-treated PANI-PSS films, respectively. The nitrogen spectrum was deconvoluted into three components.[18] A peak is located at 399.2 eV, corresponding to the neutral amine and imine sites of PANI.[18] The peak at 400.4 eV is assigned to the protonated nitrogens (N_1^+) of PANI that are associated with polarons and bipolarons in PANI-PSS.[18] The third peak is

located at 401.3 eV, and it is attributed to the protonated nitrogens (N_2^+) of PANI that are ionically associated with the sulfonic acid groups of PSS.[18] A FWHM of 1.4 eV is maintained during the fitting of all three peaks. The concentration of protonated nitrogens (N_2^+) is high in untreated PANI-PSS film relative to neutral nitrogens (Figure 6.9 (a)), which indicates that a large portion of nitrogens in PANI is strongly associated with negatively charged sulfonic acid groups in PSS. After DCA treatment, the relative concentration of the protonated nitrogens (N_2^+) changes (Figure 6.9 (b)). Figures 6.9 (c) and (d) show the XPS sulfur spectra of untreated and DCA-treated PANI-PSS films, respectively. The sulfur spectrum was deconvoluted into two doublets.[19] A doublet with peaks located at 167.5 and 168.7 eV is assigned to the ionized sulfonic acid groups ($-SO_3^-$) of PSS that are associated with the protonated nitrogens of PANI.[19] Another doublet with peaks located at 168.3 and 169.5 eV corresponds to the unionized sulfonic acid groups ($-SO_3H$) of PSS.[19] The FWHM of the individual peaks of the doublets is kept to 1.0 eV during peak fitting. Consistent with observations in the nitrogen spectra, we observe that the concentration of ionized sulfonic acid groups ($-SO_3^-$) changes after DCA treatment relative to that of unionized sulfonic acid groups ($-SO_3H$). These observations in nitrogen and sulfur spectra strongly suggest that the strong ionic interactions between PANI and PSS are moderated with DCA treatment. This moderation of ionic interactions between PANI and PSS occurs because DCA is a stronger acid than PSS so DCA can interrupt the associations between PANI and PSS. On the other hand, chlorine was not detected in any of the XPS spectrum of DCA-treated PANI-PSS film, which indicates that there is no residual DCA in the film. This

observation suggests that the conductivity enhancement is not due to DCA doping of PANI. Rather, DCA merely induces structural rearrangement of PANI-PSS.

To examine how the introduction of DCA induces changes in the electronic structure of PANI-PSS, we collected the UV-vis-NIR spectra of untreated and DCA-treated PANI-PSS films, shown in Figures 6.10 (a) and (b), respectively. The UV-vis-NIR spectrum of untreated PANI-PSS film is consistent with that of untreated PANI-PAAMPSA. The peak at 310 nm is associated with the π-π^* transition of the benzenoid; the peak at 450 nm is attributed to a polaronic shoulder; a polaron peak at approximately 800 nm is observed.[10-12] These peaks are signatures of the emeraldine salt form of PANI. After DCA treatment, the polaron peak is largely suppressed and a broad absorption appears in the near-IR region, which suggests that the chain conformation of PANI-PSS has changed from a compact coil to an extended chain conformation.[3] This observation is consistent with changes in the UV-vis-NIR spectra of PANI-PAAMPSA before and after DCA treatment. It is therefore expected that the conductivity of DCA-treated PANI-PSS is significantly higher than that of untreated PANI-PSS because charge delocalization is greatly enhanced in the extended chain conformation of DCA-treated PANI.[2, 3]

We also observed the morphologies of PANI-PSS films before and after DCA treatment. Figure 6.11 shows the AFM micrographs of (a) untreated and (b) DCA-treated PANI-PSS films. Similar with PANI-PAAMPSA films, PANI-PSS film becomes much smoother after DCA treatment. The rms roughness of untreated PANI-PSS film is 13.7 nm in the 5×5 μm scan window, and that of DCA-treated PANI-PSS film is 2.9 nm. This featureless and smooth morphology of PANI-PSS film after DCA

treatment would provide more efficient charge transport across the film because the macroscopic conduction is no longer limited to inter-particle point contacts after DCA treatment. This mechanism for conductivity improvement is similar to the one for PANI-PAAMPSA.

The observed structural rearrangement of PANI-PSS after DCA treatment should increase the electrical conductivity of PANI-PSS when the polymer is exposed to DCA. The conductivity measurements were performed using four-point probe measurements. Figure 6.12 (a) shows representative I-V characteristics of untreated PANI-PSS film. After DCA treatment on the same film, the I-V characteristics were also observed (Figure 6.12 (b)). The current is on the order of 10^{-1} mA at 10 V bias in the untreated PANI-PSS film (Figure 6.12 (a)). After DCA treatment, the current increases by more than two orders of magnitude at the same applied voltage (Figure 6.12 (b)) on the same film. Accordingly, the conductivity increases from 0.20 ± 0.02 S/cm in untreated PANI-PSS films to 58.77 ± 9.21 S/cm in DCA-treated PANI-PSS films. This conductivity improvement is accompanied by drastic changes in the molecular structures of PANI-PSS after DCA treatment, as observed in PANI-PAAMPSA films. DCA is a stronger acid than either PAAMPSA or PSS, so it is capable of moderating the ionic interactions between PANI and PAAMPSA (or PSS). This moderation of interactions between PANI and PAAMPSA (or PSS) allows PANI-PAAMPSA (or PANI-PSS) to adopt an extended chain conformation that enables more efficient charge transport.

In fact, the structural rearrangement – thereby the conductivity improvement – of polymer acid-doped PANI, including PANI-PAAMPSA and PANI-PSS, should be occurred with any reagent that is a good plasticizer for polymer acids and has a lower pK_a

than those of the polymer acids. For example, exposure to trichloroacetic acid (TCA) also improves the conductivity of PANI-PAAMPSA; TCA-treated PANI-PAAMPSA exhibits a conductivity of 40.76 ± 6.35 S/cm. This conductivity improvement is also attributed by structural rearrangement of PANI-PAAMPSA because TCA is a good plasticizer for PAAMPSA and its pK_a (0.89 at 25 °C) is lower than that of PAAMPSA (2.41 at 25 °C). While the pK_a of hydrochloric acid (HCl; pK_a = -7 at 25 °C) is lower than that of PAAMPSA, the conductivity of HCl-treated PANI-PAAMPSA is only slightly increased to 2.35 ± 0.12 S/cm. Since HCl is not a plasticizer or a good solvent for PAAMPSA, exposing PANI-PAAMPSA to HCl only serves to dope the originally undoped sites in the polymer. No structural rearrangement of PANI-PAAMPSA accompanies this process. Indeed, the UV-vis-NIR spectrum of PANI-PAAMPSA remains comparable before and after HCl exposure; only a slight red shift of the polaron peak position is observed (Figure 6.13). The spectrum does not show a free carrier tail after HCl treatment. The absence of free-carrier tail implies that PANI-PAAMPSA remains in the "compact coil" structure after HCl treatment. On the other hand, we do not observe any conductivity improvement when PANI-PAAMPSA is exposed to dimethylsulfoxide (DMSO), because the solvent is not acidic (pK_a = 35 at 25 °C). Collectively, these results imply that both conditions that the solvent should be a good plasticizer for the polymer acid dopant and the solvent must have a lower pK_a compared to the dopant are very critical for the structural rearrangement of polymer acid-doped PANI.

We also assessed whether this same DCA treatment can improve the conductivity of a commercially-available polymer acid-doped conducting polymer, PEDOT-PSS. For this experiment, we used a PEDOT-PSS dispersion as-received from Baytron P. The DCA treatment of PEDOT-PSS was carried out under the same conditions for that of PANI-PSS. We exposed the DCA-treated PEDOT-PSS film to $< 10^{-7}$ Torr vacuum for more than 3 hours to remove residual DCA prior to any characterization. We then measured the conductivities of PEDOT-PSS before and after DCA treatment using four-point probe measurements. Figure 6.14 shows the I-V characteristics of (a) untreated and (b) DCA-treated PEDOT-PSS films. The current of untreated PEDOT-PSS film is on the order of 10^{-1} mA at a 10 V bias (Figure 6.14 (a)). The current of PEDOT-PSS film, however, improves significantly after DCA treatment compared to those of PANI-PAAMPSA and PANI-PSS films; the current of the same film after DCA treatment increases by more than three orders of magnitude given the same applied voltage (Figure 6.14 (b)). This improvement translates to a conductivity of 0.50 ± 0.05 and 616 ± 85.4 S/cm for untreated and DCA-treated PEDOT-PSS films, respectively. In fact, the conductivity of DCA-treated PEDOT-PSS film is the highest amongst any polymer acid-doped conducting polymers previously reported.[20]

To examine the origin of this improvement in conductivity in PEDOT-PSS by DCA treatment, we studied the changes in the electronic structure of PEDOT-PSS after DCA treatment. Figure 6.15 shows the UV-vis-NIR spectra of (a) untreated and (b) DCA-treated PEDOT-PSS films. In the UV-vis-NIR spectrum of as-cast PEDOT-PSS film, a peak at 280 nm related to the π-π^* transition and a broad band at approximately 800 nm associated with polaron interband transition are observed. The polaron rides on

an increasing background suggesting that untreated PEDOT-PSS has an extended chain conformation. This observation is in drastic contrast with the structure of untreated PANI-PAAMPSA and PANI-PSS.[3] The spectrum in Figure 6.15 (a) is consistent with the UV-vis-NIR spectrum of PEDOT-PSS previously reported.[20, 21] After DCA treatment, the UV-vis-NIR spectrum of PEDOT-PSS only showed modest changes. We observe slightly stronger absorption in the near-IR region in the UV-vis-NIR spectrum of DCA-treated PEDOT-PSS. Despite such small changes in the electronic structure of PEDOT-PSS, the conductivity of PEDOT-PSS increases significantly after DCA treatment. To investigate the origin of the highly improved conductivity of PEDOT-PSS film after DCA treatment, we examined the macroscopic changes in the morphology of PEDOT-PSS before and after DCA treatment.

Figure 6.16 shows the AFM micrographs of (a) untreated and (b) DCA-treated PEDOT-PSS films. The untreated PEDOT-PSS film is very smooth (Figure 6.16 (a)) with an rms roughness of 0.9 nm over the 5×5 μm scan window. After DCA treatment, the morphology of the film changes significantly (Figure 6.16 (b)); the film becomes much rougher. The rms roughness of DCA-treated PEDOT-PSS film increases up to 2.6 nm in the same scan window. Typically, the surface of PEDOT-PSS film is dominated by an insulating layer of PSS.[22, 23] This structure is different from that of PANI-PAAMPSA. In PANI-PAAMPSA, the conducting layer of the polymer is preferentially enhanced on the surface of the film as observed in Chapter 5. Because PSS is segregated to the surface of PEDOT-PSS film and it is the counter ion, DCA likely dissolves away excess PSS overlayer during DCA treatment, thereby enhancing the

conductivity of PEDOT-PSS along the surface.[20] The removal of the insulating PSS overlayer can dramatically increase the lateral conductivity of the material.[20]

The chemical environments of untreated and DCA-treated PEDOT-PSS films were investigated using XPS. The detailed experimental procedures for these experiments were described in Chapter 2. Figures 6.17 (a) and (b) shows the XPS sulfur spectra of untreated and DCA-treated PEDOT-PSS films, respectively. The sulfur spectra were each deconvoluted into three doublets.[24] During data fitting, a FWHM of 1.2 eV is maintained for the individual peaks within each doublet. A doublet consisting of peaks at 164.5 and 165.6 eV corresponds to the protonated thiophene units in PEDOT.[24] The positive charges in PEDOT is not localized on one monomer unit, but is delocalized over several adjacent rings, resulting in a spread in values of the binding energies.[23, 24] This broad distribution of binding energies results in an asymmetric tail on the higher energy side of the PEDOT sulfur signal.[24] When PEDOT-PSS (Baytron P) is spun on a substrate, it has been reported that the film contains sodium residues from the oxidizing agent ($Na_2S_2O_8$) used during the polymerization of PEDOT.[25, 26] Sodium ions are in turn associated with the ionized sulfonic acids in PSS. In the case of sulfonic acids in PSS, the signal is thus fitted with two doublets corresponding to $SO_3^-H^+$, as well as $SO_3^-Na^+$.[24] The peaks associated with these sulfonic acids are only separated by 0.4 eV, and hence they overlap strongly.[24] The lower binding energy component with a doublet at 168.4 and 169.6 eV corresponds to $SO_3^-Na^+$, whereas the high binding energy component with a doublet at 168.8 and 170.0 eV is associated with $SO_3^-H^+$.[24] After DCA treatment, the concentration of the sulfurs in PEDOT increases relative to those of total sulfurs in PSS (Figure 6.17 (b)), compared to those in untreated PEDOT-PSS film

(Figure 6.17 (a)). This observation suggests that the relative concentration of PEDOT increases on the surface of PEDOT-PSS film after DCA treatment. The oxygen spectra of untreated and DCA-treated PEDOT-PSS films are shown in Figures 6.17 (c) and (d), respectively. The oxygen spectra were deconvoluted with three different chemical environments.[24] The highest binding energy peak at 533.7 eV corresponds to the oxygens in the dioxyethylene bridge of PEDOT.[24] The oxygens in $SO_3^-H^+$ contain two components, whose peaks are located at 532.4 and 533.5 eV, respectively.[24] The lower binding energy peak at 532.4 eV originates from oxygens that are double bonded to the sulfurs in the sulfonic acid groups of $SO_3^-H^+$, whereas the higher binding energy peak corresponds to the hydroxyl-oxygens.[24] The intensity ratio is 2:1, in agreement with the chemical composition in $SO_3^-H^+$. The peak at 531.9 eV is associated with the oxygens in $SO_3^-Na^+$.[24] Consistent with the observations in the sulfur spectra, we observe the higher concentration of PEDOT oxygens after DCA treatment, indicating that the relative concentration of PEDOT increases after DCA treatment. The combination of the observations of sulfur and oxygen spectra suggests that the PSS layer is removed from the surface of PEDOT-PSS film with DCA treatment. This enhancement of the conducting PEDOT-PSS domains on the surface of the film after DCA treatment can remarkably increase the conductivity of PEDOT-PSS by more than three orders of magnitude. We did not detect chlorine in DCA-treated PEDOT-PSS films, which indicates that DCA has been completely removed from PEDOT-PSS films after treatment. We have established indirectly that the mechanism of conductivity improvement for PEDOT-PSS by DCA treatment is different from that of PANI-PAAMPSA (or PANI-PSS). We speculate that this difference likely arises from the fact

that the doping mechanism is different for PANI and PEDOT. It follows that the roles the polymer acids play in each case is different. While PANI is doped via protonation by PAAMPSA (or PSS), PEDOT is oxidatively doped in the presence of PSS. Since PSS in PEDOT-PSS is only a counter ion, the pK_a of the solvent used for conductivity improvement is not important for improving the conductivity of PEDOT-PSS. Rather, the solvent should be a good solvent for PSS so that the insulating PSS overlayer in PEDOT-PSS film can be dissolved away during solvent annealing. DCA is a good solvent for PSS and thus the conductivity of PEDOT-PSS is enhanced significantly after DCA treatment.

To examine the versatility of DCA-treated conducting polymers, we applied the materials in organic solar cells (OSCs). A solar cell is a device that converts solar energy into electrical energy. In particular, OSCs have attracted interest because they promise to be light weight, mechanically flexible counterparts to inorganic solar cells that can be made out of solution-processible materials.[27] Indium tin oxide (ITO) is widely used as the anode in OSCs because of its low resistance and high optical transparency.[28] Although the ITO anode provides many advantages in OSCs, its brittleness limits the flexibility of the devices when the devices are fabricated on plastic substrates. Moreover, the high material and production costs of ITO limit the development of solution processible and low-cost OSCs. As such, several candidates, such as carbon nanotube films[29] and conducting polymers,[30] have been reported as replacement candidates for ITO. We also used conducting polymers, such as PANI-PAAMPSA and PEDOT-PSS, to replace ITO in OSCs. To investigate how the enhanced conductivity of

DCA-treated conducting polymers affects the performance of OSCs, we fabricated OSCs with DCA-treated conducting polymers as well.

To fabricate these OSCs, we used a blend of poly(3-hexylthiophene), P3HT, and [6,6]-phenyl-C61-butyric acid methyl ester (PCBM) as the photoactive layer. P3HT was the electron donor and PCBM was the electron acceptor. Aluminum was used as the cathode. The active area was kept as 0.0625 cm^2 for all the devices. These devices were all fabricated and tested in air. The procedures of device fabrication and characterization were detailed in Chapter 2.

When conducting polymers are used as anodes in OSCs, however, conducting polymers are not optically transparent and thus they also absorb light, unlikely ITO anode. Light absorption at the anode would decrease the light intensity that the photoactive layer could absorb, eventually resulting in the lower device performance. Figure 6.18 (a) shows the UV-vis-NIR spectrum of P3HT. P3HT is responsible for light absorption in the photoactive layer of P3HT and PCBM; PCBM does not absorb light significantly. P3HT absorbs light in the range between 400 and 600 nm (Figure 6.18 (a)). Figure 6.18 contains the UV-vis-NIR spectra of the following conducting polymers we used as anodes in this study: (b) untreated and (c) DCA-treated PANI-PAAMPSA and (d) untreated and (e) DCA-treated PEDOT-PSS. The range of light absorption in these conducting polymers is generally different from that of light absorption in P3HT. As such, the incorporation of these materials as anodes should not influence the light absorption of photoactive layer.

Figure 6.19 shows the current density-voltage (J-V) characteristics of the OSCs with untreated and DCA-treated PANI-PAAMPSA anodes, as well as of those with ITO

anode, under illumination (100 mW/cm^2). The OSCs with ITO anodes were also fabricated with same dimensions and geometry for comparison. The details of device characteristics of these OSCs are summarized in Table 6.2. The devices with ITO anodes exhibit a short circuit current density (J_{sc}) of 7.87 ± 0.18 mA/cm^2, an open circuit voltage (V_{oc}) of 0.60 ± 0.01 V, a fill factor (FF) of 0.49 ± 0.01, and an efficiency of 2.31 ± 0.15 %. These device statistics were acquired from 63 devices in air. The device performance is comparable with those of previously reported devices fabricated with the same structure using the same materials.[31]

The J-V characteristics of a representative device with untreated PANI-PAAMPSA anode are also shown in Figure 6.19 (solid line). Of 49 devices tested, the average short circuit current density was 1.95 ± 0.08 mA/cm^2 and the open circuit voltage was 0.52 ± 0.01 V, resulting in a fill factor of 0.38 ± 0.01 and a device efficiency of 0.39 ± 0.05 %. The device efficiency is lower than that of the devices with ITO anodes because the short circuit current density and open circuit voltage were both lower. The lower short circuit current density is attributed to the significantly lower conductivity of PANI-PAAMPSA compared to ITO (0.4 S/cm versus 10^3 S/cm). The open circuit voltage depends on the energy levels of the photoactive layer and the work functions of the electrodes.[32] The work function of aluminum is 4.2 eV,[33] that of PANI-PAAMPSA is ~ 4.8 eV,[6] and that of ITO is ~ 5.0 eV.[33] The difference in the work functions of anodes and cathodes is smaller in devices with PANI-PAAMPSA anodes compared to those with ITO anodes. This decreased difference in work function is consistent with the observation that devices with PANI-PAAMPSA anodes exhibit a lower open circuit

voltage compared to of devices with ITO anodes. Accordingly, the devices with PANI-PAAMPSA anodes exhibit lower fill factor and efficiency.

Figure 6.19 also contains the J-V characteristics of a representative device with DCA-treated PANI-PAAMPSA anode (dash-dotted line). The device with DCA-treated PANI-PAAMPSA anode exhibits improved short circuit current density, while maintaining the same open circuit voltage, when compared to that with the device with untreated PANI-PAAMPSA anode (solid line). The device characteristics are quantified in Table 6.2 and these values were averaged from 59 devices. An efficiency of 0.97 ± 0.18 % is observed in these devices with a short circuit current density of 4.95 ± 0.16 mA/cm^2, an open circuit voltage of 0.51 ± 0.02 V, and a fill factor of 0.38 ± 0.02. That the open circuit voltage remains unchanged between the devices with untreated and DCA-treated PANI-PAAMPSA anodes suggests that the change in energy level between the devices is negligible. Instead, the higher conductivity of DCA-treated PANI-PAAMPSA anode results in higher short circuit current density in the devices. Additionally, the higher conductivity of DCA-treated PANI-PAAMPSA anode also influences the series and shunt resistances in the devices. The series resistance was quantified by the inverse slop of the J-V curve at high voltages (0.8 V < V < 1.0 V) and the shunt resistance was quantified by the inverse slop of J-V curve between -0.1 V and 0.1 V. The resistances were determined during illumination. The series resistances of the devices with untreated and DCA-treated PANI-PAAMPSA anodes are 5.32 ± 1.72 Ω cm^2 and 3.93 ± 1.41 Ω cm^2, respectively, and the shunt resistances of those devices are 840.34 ± 112.35 Ω cm^2 and 1503.5 ± 256.34 Ω cm^2, respectively. As expected in Figure 6.19 by the inverse slope of J-V characteristics at the specific voltages, the higher

conductivity of DCA-treated PANI-PAAMPSA anode results in lower series resistances and higher shunt resistances in the devices. As mentioned in Chapter 2, the series resistance is attributed by all the resistance contributions in the devices from bulk transport, interface transfer, to transport through the electrodes. Among these variations, only the conductivity of anode is different between the devices with untreated and DCA-treated PANI-PAAMPSA anodes. The highly conductive DCA-treated PANI-PAAMPSA anodes thus directly result in lower series resistances in the devices. The higher shunt resistances in the devices with DCA-treated PANI-PAAMPSA anodes reduce leakage current in the devices. The efficiency of devices with DCA-treated PANI-PAAMPSA anodes, however, remains lower than those of devices with ITO anodes. These observations are due to the lower conductivity of DCA-treated PANI-PAAMPSA anode compared to ITO and smaller difference in work function of anodes and cathodes in the devices with DCA-treated PANI-PAAMPSA anodes.

As mentioned earlier, we dramatically improved the conductivity of PEDOT-PSS up to 616.29 ± 85.4 S/cm by DCA treatment, and this conductivity is the highest among the polymer acid template synthesized conducting polymers. To examine the versatility of this highly conductive DCA-treated PEDOT-PSS film, we also used this material as anodes in OSCs. The dimensions and geometry of these devices are the same as those of the devices with untreated and DCA-treated PANI-PAAMPSA anodes. Figure 6.20 shows the J-V characteristics of a representative device with untreated (solid line) and DCA-treated (dash-dotted line) PEDOT-PSS anodes. The same J-V characteristics of the device with ITO anode in Figure 6.19 is also included in Figure 6.20 (dash line) for reference. The detailed device characteristics of these devices are included in Table 6.2.

These device characteristics were acquired from total 57 and 63 devices with untreated and DCA-treated PEDOT-PSS anodes, respectively. Consistent with the devices with untreated and DCA-treated PANI-PAAMPSA anodes, the device performance is improved significantly in devices with DCA-treated PEDOT-PSS anodes compared to those of devices with untreated PEDOT-PSS anodes. The short circuit current density is improved by two and a half fold because of the higher conductivity of DCA-treated PEDOT-PSS anodes. The open circuit voltage, however, is maintained because DCA treating the PEDOT-PSS anode does not influence the energy level of devices. Moreover, lower series resistances and higher shunt resistances are observed in the devices with DCA-treated PEDOT-PSS anodes. These observations result in higher fill factor and thus higher efficiency in devices with DCA-treated PEDOT-PSS anodes compared to those of devices with untreated PEDOT-PSS anodes. Specifically, the devices with untreated PEDOT-PSS anodes exhibit a short circuit current density of 4.59 ± 0.11 mA/cm^2, an open circuit voltage of 0.55 ± 0.01 V, a fill factor of 0.38 ± 0.02, and an efficiency of 0.97 ± 0.14 %. Devices with DCA-treated PEDOT-PSS anodes exhibit a short circuit current density of 7.36 ± 0.14 mA/cm^2, an open circuit voltage of 0.55 ± 0.01 V, a fill factor of 0.52 ± 0.01, and an efficiency of 2.12 ± 0.16 %. The performance of devices with DCA-treated PEDOT-PSS anodes is now comparable with that of devices with ITO anodes (Figure 6.20; dash line), suggesting an opportunity to replace ITO with conducting polymers.

In this chapter, we have improved the conductivity of PANI-PAAMPSA by more than two orders of magnitude using a simple post-processing DCA treatment. The conductivity improvement is accompanied by drastic changes in the molecular structures

of PANI-PAAMPSA. Because DCA is a good plasticizer for PAAMPSA and its pK_a (1.21 at room temperature) is lower than that of PAAMPSA (2.41 at room temperature), DCA can effectively disrupt the strong ionic interactions between PANI and PAAMPSA. This moderation of ionic interactions allows PANI-PAAMPSA to relax from the particle nature that was arrested during polymerization. PANI-PAAMPSA is thus able to rearrange from a compact coil to an extended chain conformation. This extended chain conformation enables more efficient charge transport, thereby improving the conductivity of PANI-PAAMPSA. This DCA treatment is not only specific for PANI-PAAMPSA, it generally applies to polymer acid-doped conducting polymer systems, such as commercially-available PEDOT-PSS. In fact, we improved the conductivity of PEDOT-PSS by more than three orders of magnitude through DCA treatment. The higher conductivity improvement of PEDOT-PSS compared to PANI-PAAMPSA is attributed to their different mechanism in conductivity enhancement via DCA treatment. The role of DCA is different in each polymer because the polymer acid plays differently in each case because of their different doping mechanism. The use of DCA-treated conducting polymer anodes can improve the performance of OSCs. Specifically, short circuit current density increases by approximately two and a half fold and thus the device efficiency is improved by the same amount. Moreover, when DCA-treated PEDOT-PSS films are used as anodes in OSCs, their device performance is comparable with that of the devices with ITO anodes. This result indicates that it is feasible to use more easily processible conducting polymers instead of ITO for fabricating OSCs, with the potential to obtain lower cost and more mechanically flexible devices.

Table 6.1. Conductivities of conducting polymers before and after DCA treatment. The conductivities of PANI that is doped with poly(styrene sulfonic acid), or PANI-PSS, and poly(ethylene dioxythiophene) that is doped with PSS, or PEDOT-PSS are also studied.

	Conductivity (S/cm)	
	Before treatment	**After treatment**
PANI-PAAMPSA	0.43 ± 0.02	47.79 ± 10.52
PANI-PSS	0.20 ± 0.02	58.77 ± 9.21
PEDOT-PSS	0.50 ± 0.05	616.29 ± 85.4

Table 6.2. The device characteristics of OSCs with different anodes. The performances of the OSCs with ITO anodes are also included. The parameters were determined under AM 1.5, 100 mW/cm^2 illumination.

Anode	J_{sc} (mA/cm^2)	V_{oc} (V)	Fill factor (FF)	Efficiency (%)	Series resistance (Ω cm^2)	Shunt resistance (Ω cm^2)
PANI-PAAMPSA	1.95 ± 0.08	0.52 ± 0.01	0.38 ± 0.01	0.39 ± 0.05	5.32 ± 1.72	840.34 ± 112.35
DCA-treated PANI-PAAMPSA	4.95 ± 0.16	0.51 ± 0.02	0.38 ± 0.02	0.97 ± 0.18	3.93 ± 1.41	1503.5 ± 256.34
PEDOT-PSS	4.59 ± 0.11	0.55 ± 0.01	0.38 ± 0.02	0.97 ± 0.14	8.58 ± 2.51	552.49 ± 100.21
DCA-treated PEDOT-PSS	7.36 ± 0.14	0.55 ± 0.01	0.52 ± 0.01	2.12 ± 0.16	2.49 ± 0.87	1786.7 ± 214.85
ITO	7.87 ± 0.18	0.60 ± 0.01	0.49 ± 0.01	2.31 ± 0.15	3.64 ± 1.56	1689.5 ± 278.38

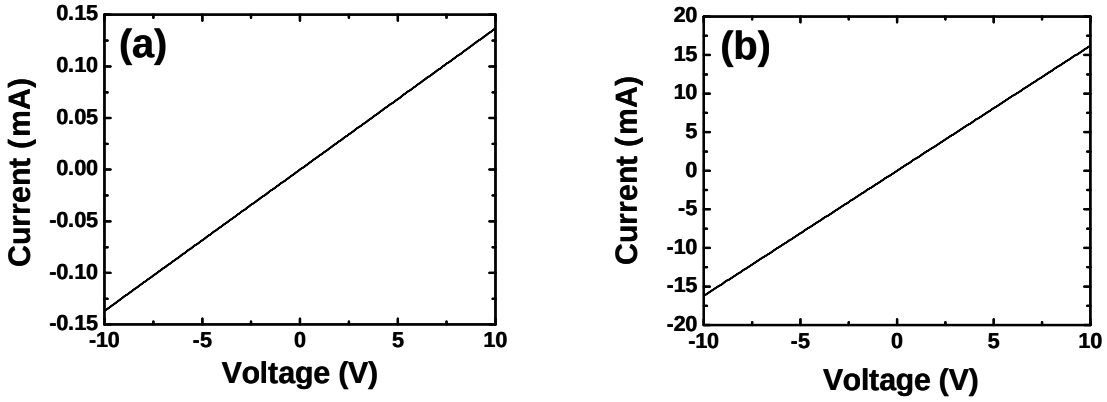

Figure 6.1. I-V characteristics of (a) untreated and (b) DCA-treated PANI-PAAMPSA obtained during four-point probe measurements.

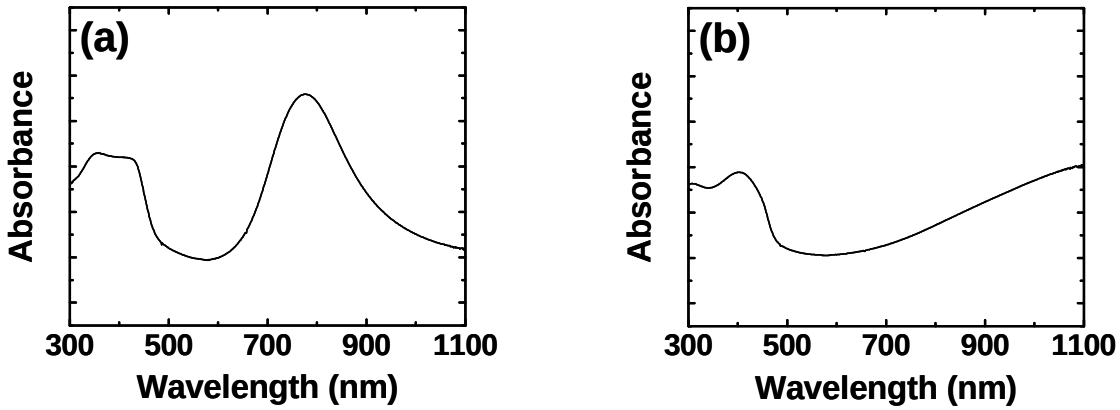

Figure 6.2. UV-vis-NIR spectra of (a) untreated and (b) DCA-treated PANI-PAAMPSA.

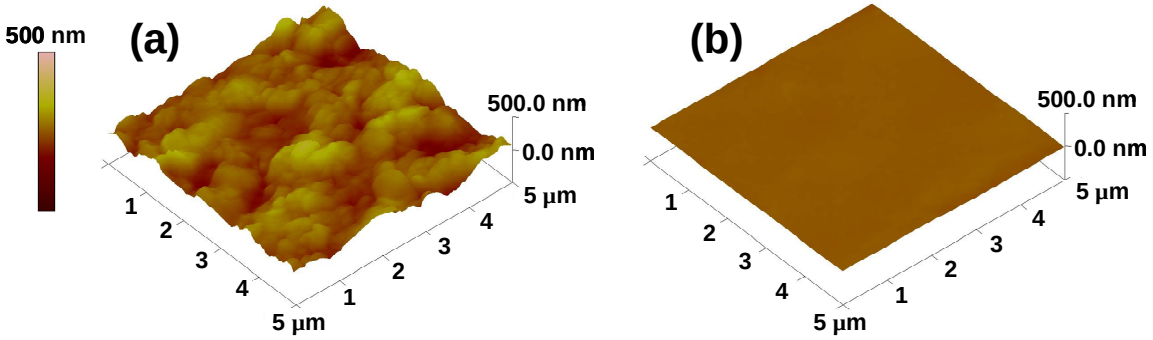

Figure 6.3. AFM images of (a) untreated and (b) DCA-treated PANI-PAAMPSA determined at the same height scales.

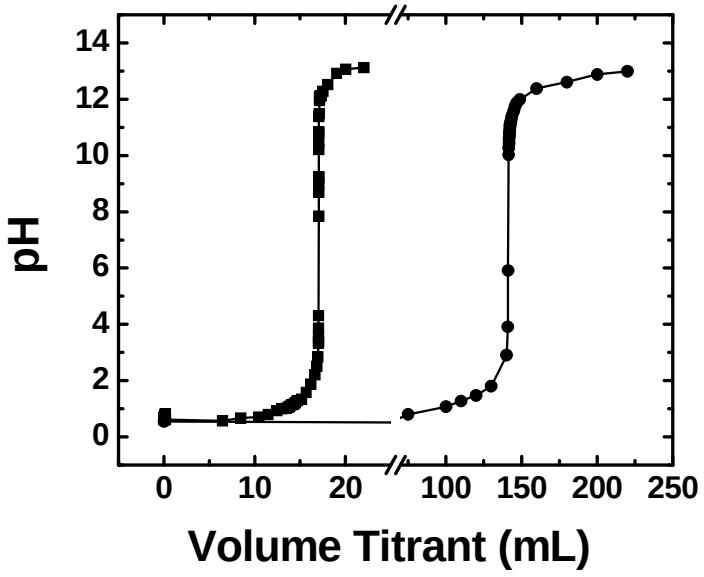

Figure 6.4. Titration curves of DCA at 10^{-5} M (■) and 10^{-3} M (●). Titration was carried out at 70 ºC.

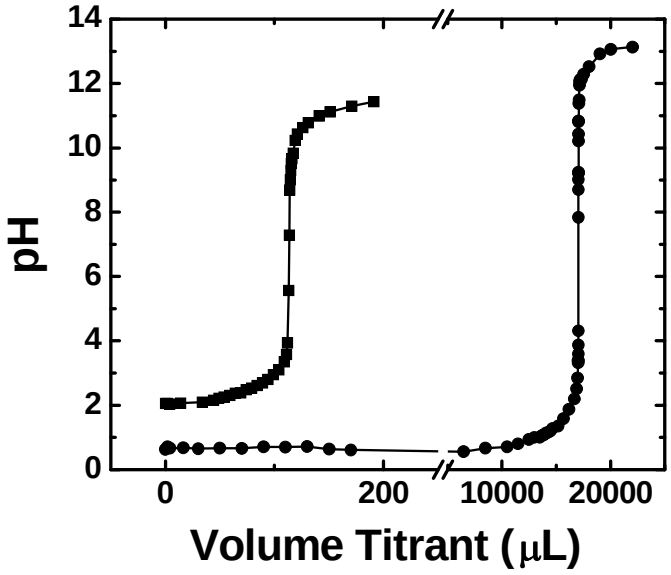

Figure 6.5. Titration curves of PAAMPSA (■) and DCA (●) at 10^{-7} M and 10^{-5} M, respectively. Titration was carried out at 70 ºC.

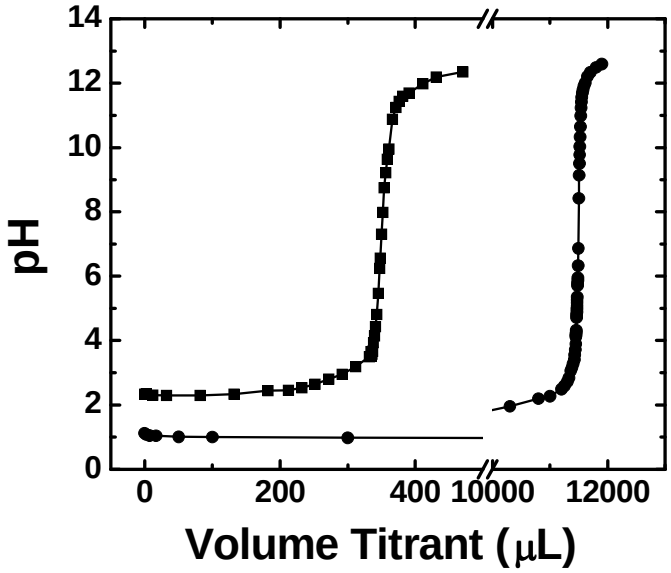

Figure 6.6. Titration curves of PAAMPSA (■) and DCA (●) at 10^{-7} M and 10^{-5} M, respectively. Titration was carried out at room temperature.

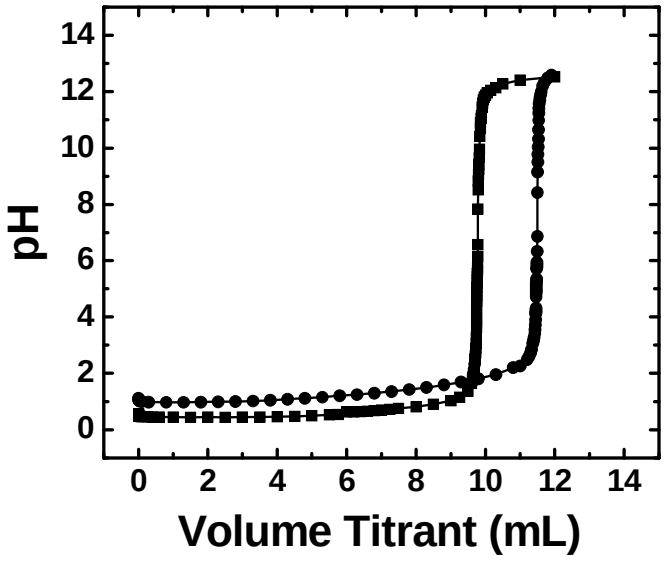

Figure 6.7. Titration curves of AAMPSA (■) and DCA (●) at room temperature. The same concentration of 10^{-5} M was used for both acid solutions.

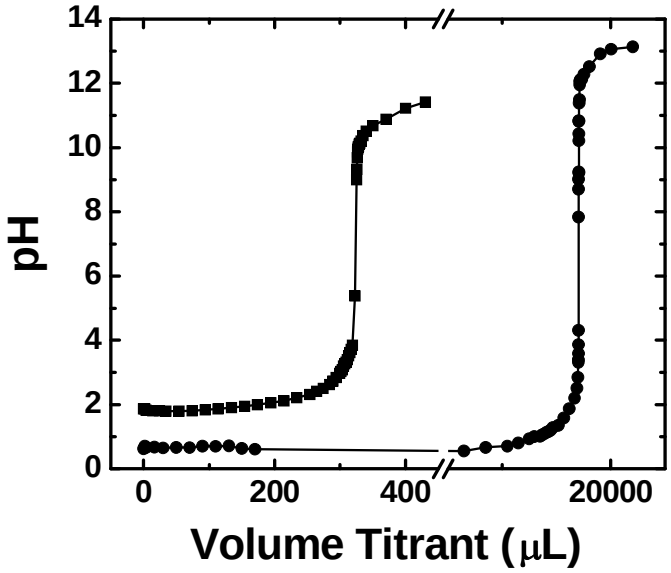

Figure 6.8. Titration curves of PSS (■) and DCA (●) at 10^{-7} M and 10^{-5} M, respectively. Titration was carried out at 70 ºC.

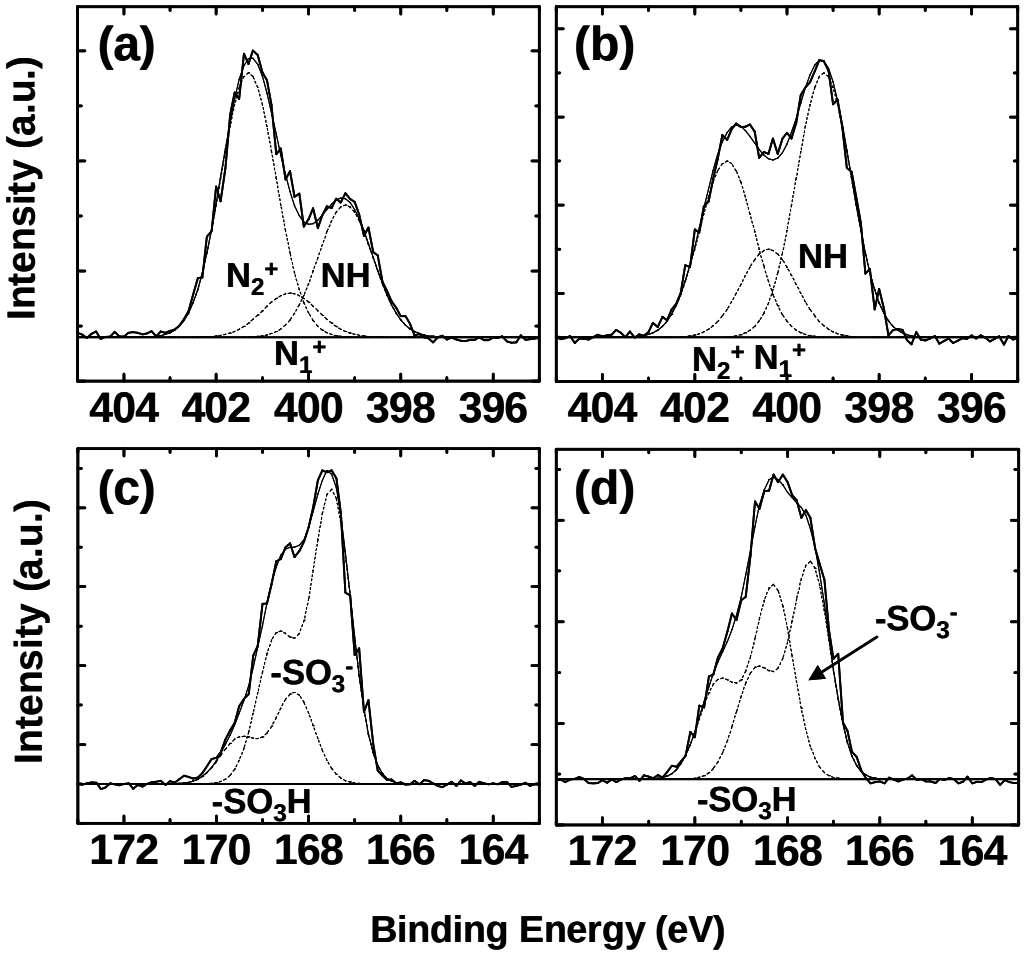

Figure 6.9. XPS nitrogen spectra of (a) untreated and (b) DCA-treated PANI-PSS, and sulfur spectra of (c) untreated and (d) DCA-treated PANI-PSS, respectively.

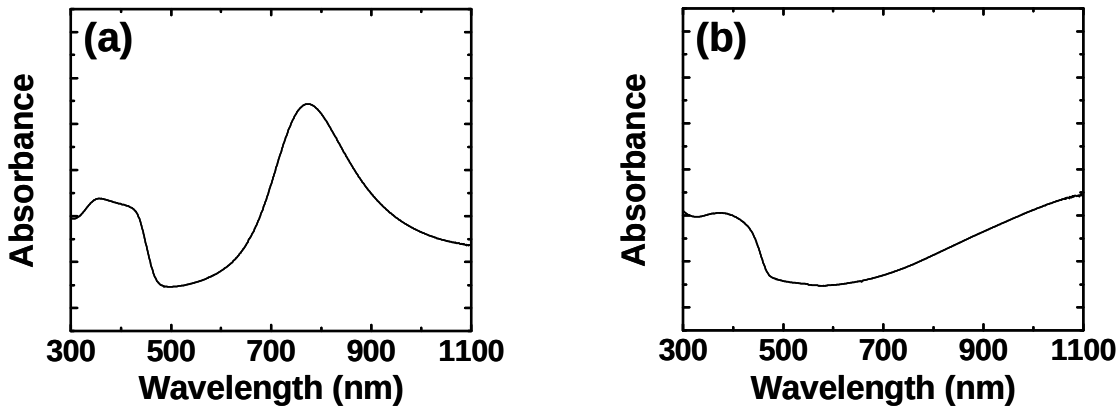

Figure 6.10. UV-vis-NIR spectra of (a) untreated and (b) DCA-treated PANI-PSS.

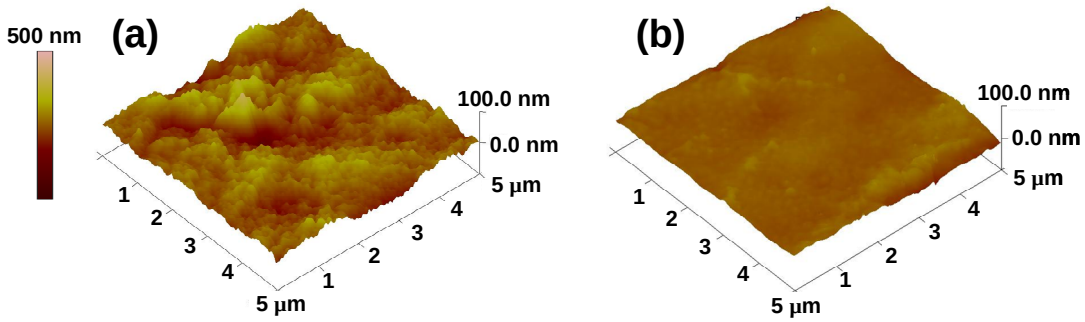

Figure 6.11. AFM images of (a) untreated and (b) DCA-treated PANI-PSS.

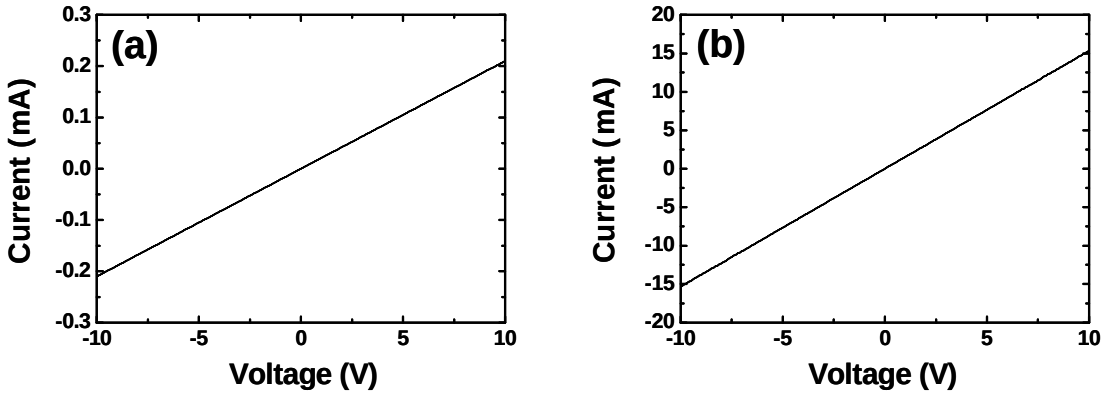

Figure 6.12. I-V characteristics of (a) untreated and (b) DCA-treated PANI-PSS.

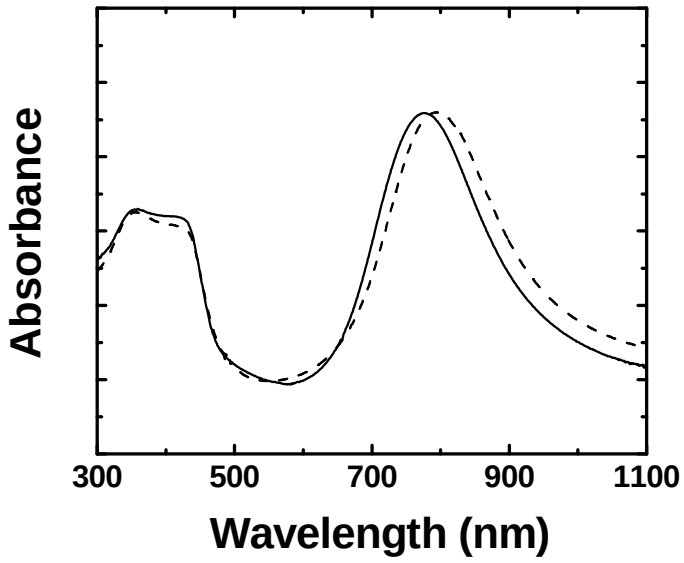

Figure 6.13. UV-vis-NIR spectra of untreated (solid line) and HCl-treated (dash line) PANI-PAAMPSA.

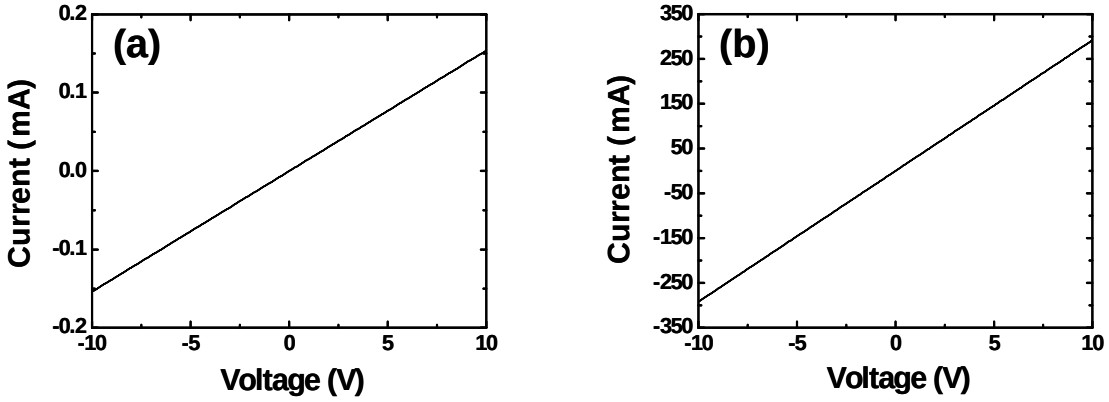

Figure 6.14. I-V characteristics of (a) untreated and (b) DCA-treated PEDOT-PSS.

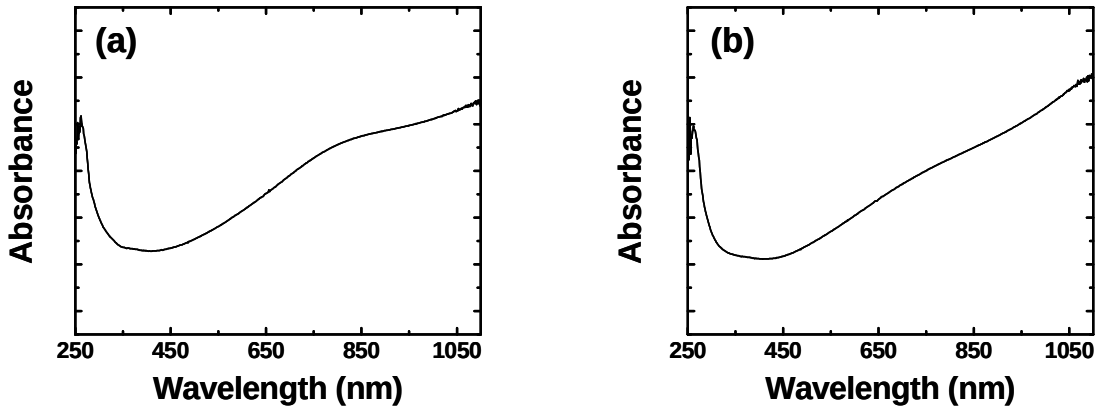

Figure 6.15. UV-vis-NIR spectra of (a) untreated and (b) DCA-treated PEDOT-PSS.

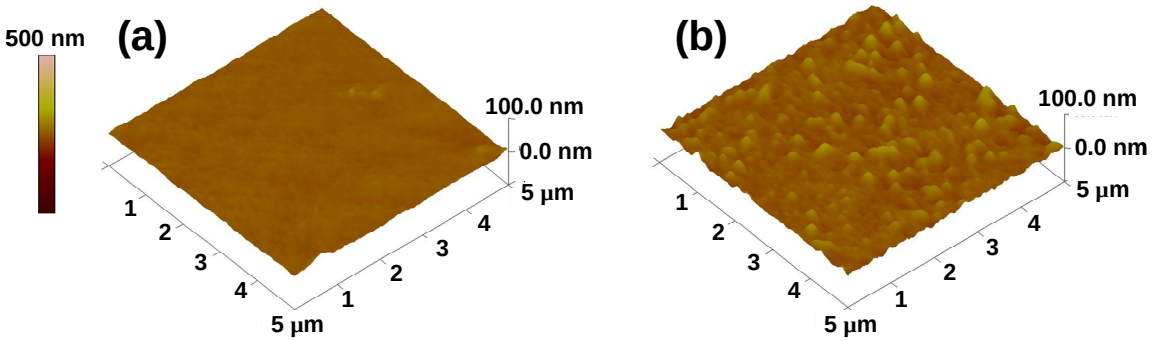

Figure 6.16. AFM images of (a) untreated and (b) DCA-treated PEDOT-PSS.

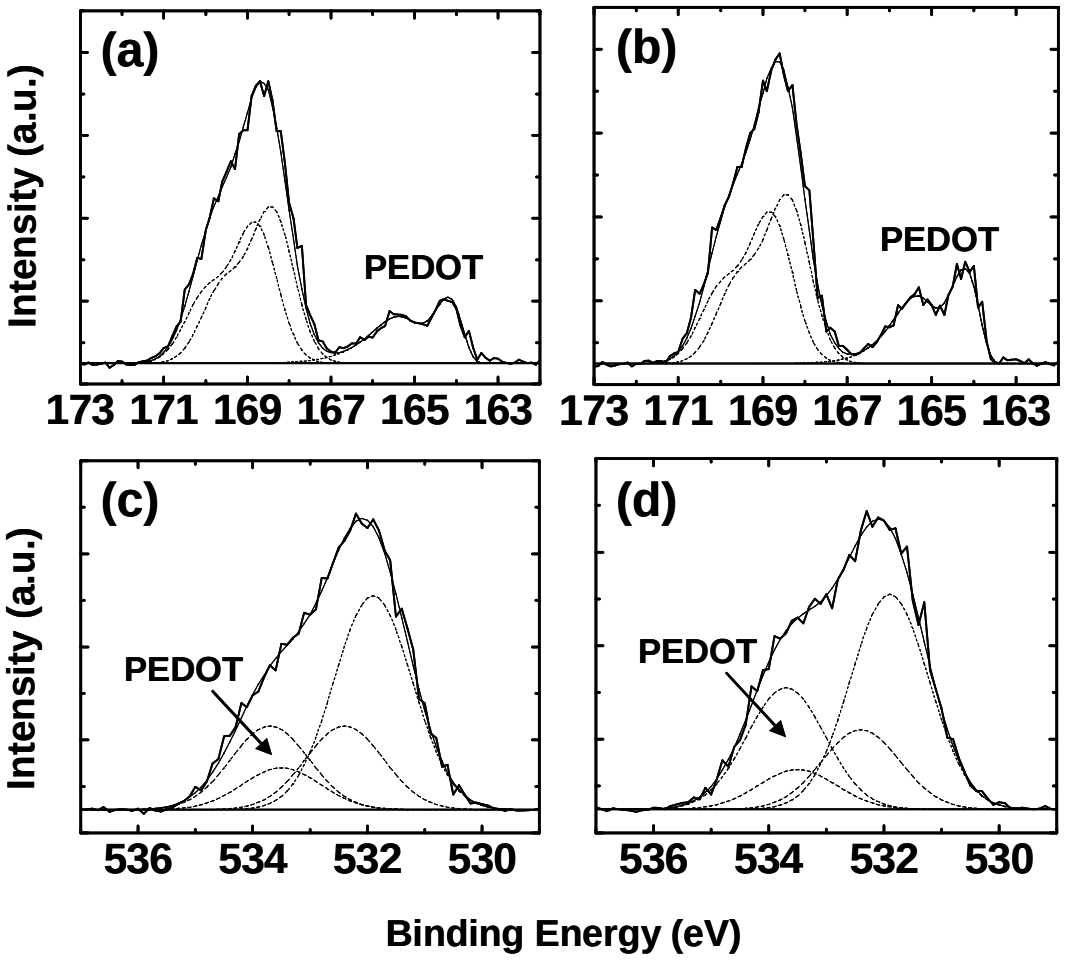

Figure 6.17. XPS sulfur spectra of (a) untreated and (b) DCA-treated PEDOT-PSS, and oxygen spectra of (c) untreated and (d) DCA-treated PEDOT-PSS, respectively.

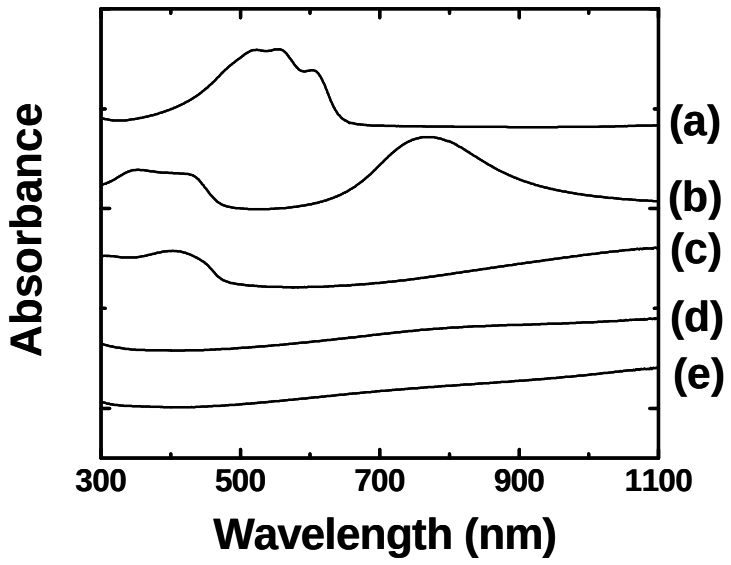

Figure 6.18. UV-vis-NIR spectra of (a) P3HT, (b) untreated and (c) DCA-treated PANI-PAAMPSA, and (c) untreated and (d) DCA-treated PEDOT-PSS.

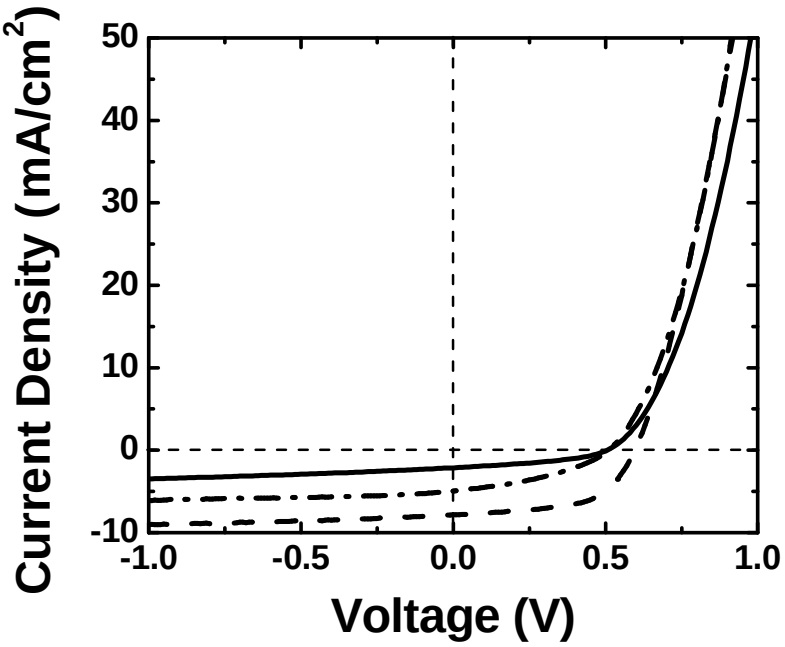

Figure 6.19. J-V characteristics of OSCs with untreated (solid line) and DCA-treated (dash-dotted line) PANI-PAAMPSA anodes under illumination (100 mA/cm^2). The J-V characteristics of an OSC with ITO anode are also included (dash line).

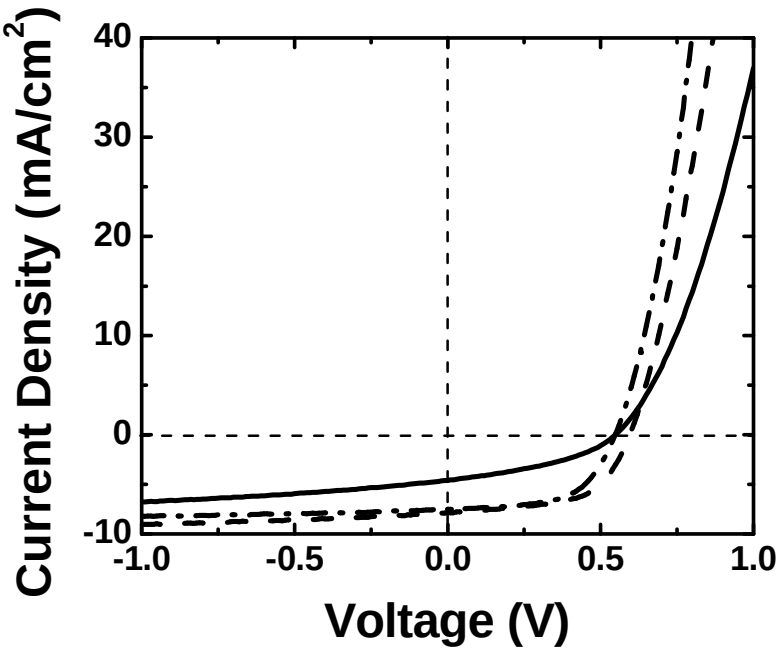

Figure 6.20. J-V characteristics of OSCs with untreated (solid line) and DCA-treated (dash-dotted line) PEDOT-PSS anodes under illumination (100 mA/cm^2). The J-V characteristics of an OSC with ITO anode are also included (dash line).

REFERENCES

1. K. S. Lee, T. J. Smith, K. C. Dickey, J. E. Yoo, K. J. Stevenson and Y.-L. Loo, *Adv. Func. Mater.*, 2006, **16**, 2409.
2. A. G. MacDiarmid and A. J. Epstein, *Synth. Met.*, 1994, **65**, 103.
3. A. G. MacDiarmid and A. J. Epstein, *Synth. Met.*, 1995, **69**, 85.
4. P. Rannou, A. Gawlicka, D. Berner, A. Pron, M. Nechtschein and D. Djurado, *Macromolecules*, 1998, **31**, 3007.
5. A. R. Hopkins, P. G. Rasmussen, R. A. Basheer, B. K. Annis, G. D. Wignall and W. A. Hamilton, *Synth. Met.*, 1998, **97**, 47.
6. K. S. Lee, in *Chemical Engineering*, The University of Texas at Austin, Austin, 2007, pp. 85.
7. Y. Cao, J. Qiu and P. Smith, *Synth. Met.*, 1995, **69**, 187.
8. D. L. Yang, P. N. Adams, L. Brown and B. R. Mattes, *Synth. Met.*, 2006, **156**, 1225.
9. M. F. Hundley, P. N. Adams and B. R. Mattes, *Synth. Met.*, 2002, **129**, 291.
10. J. M. Ginder and A. J. Epstein, *Phys. Rev. B: Condens. Matter*, 1990, **41**, 10674.
11. P. M. McManus, R. J. Cushman and S. C. Yang, *J. Phys. Chem.*, 1987, **91**, 744.
12. S. Stafstrom, J. L. Bredas, A. J. Epstein, H. S. Woo, D. B. Tanner, W. S. Huang and A. G. MacDiarmid, *Phys. Rev. Lett.*, 1987, **59**, 1464.
13. C. Bailey, Acid-base chemistry titration, http://www.calpoly.edu/~cbailey/125LabExperiments/Titration/Titration.html.
14. D. R. Lide, *CRC Handbook of Chemistry and Physics*, CRC Press, Boca Raton (FL), 2006.

15. S. Lifson, B. Kaufman and H. Lifson, *The Journal of Chemical Physics*, 1957, **27**, 1356.

16. A. Bozkurt, *Turk J Chem*, 2005, **29**, 117.

17. J. T. Sejdic and A. Easteal, *J. Appl. Polym. Sci.*, 2000, **75**, 619.

18. J. Yue and A. J. Epstein, *Macromolecules*, 1991, **24**, 4441.

19. J. Y. Kim, J. H. Jung, D. E. Lee and J. Joo, *Synth. Met.*, 2002, **126**, 311.

20. J. Ouyang, Q. Xu, C.-W. Chu, Y. Yang, G. Li and J. Shinar, *Polymer*, 2004, **45**, 8443.

21. J. Ouyang, C.-W. Chu, F.-C. Chen, Q. Xu and Y. Yang, *Adv. Func. Mater.*, 2005, **15**, 203.

22. X. Crispin, S. Marciniak, W. Osikowicz, G. Zotti, A. W. D. V. D. Gon, F. Louwet, M. Fahlman, L. Groenendaal, F. D. Schryver and W. R. Salaneck, *J. Polym. Sci., Part B: Polym. Phys.*, 2003, **41**, 2561.

23. G. Greczynski, T. Kugler and W. R. Salaneck, *Thin Solid Films*, 1999, **354**, 129.

24. G. Greczynski, T. Kugler, M. Keil, W. Osikowicz, M. Fahlman and W. R. Salaneck, *J. Electron Spectrosc. Relat. Phenom.*, 2001, **121**, 1.

25. J. Hwang, F. Amy and A. Kahn, *Org. Electron.*, 2006, **7**, 387.

26. L. Groenendaal, F. Jonas, D. Freitag, H. Pielartzik and J. R. Reynolds, *Adv. Mater.*, 2000, **7**, 481.

27. R. H. Friend, R. W. Gymer, A. B. Holmes, J. H. Burroughes, R. N. Marks, C. Taliani, D. D. C. Bradley, D. A. D. Santos, J. L. Bredas, M. Logdlund and W. R. Salaneck, *Nature*, 1999, **397**, 121.

28. H. Hoppe and N. S. Sariciftci, *J. Mater. Res.*, 2004, **19**, 1924.

29. M. W. Rowell, M. A. Topinka, M. D. McGehee, H.-J. Prall, G. Dennler, N. S. Sariciftci, L. Hu and G. Gruner, *Appl. Phys. Lett.*, 2006, **88**, 233506.

30. Y.-S. Hsiao, W.-T. Whang, C.-P. Chen and Y.-C. Chen, *J. Mater. Chem.*, 2008, **18**, 5948.

31. E. Kymakis, N. Kornilios and E. Koudoumas, *J. Phys. D: Appl. Phys.*, 2008, **41**, 165110.

32. G. G. Malliaras, J. R. Salem, P. J. Brock and J. C. Scott, *J. Appl. Phys.*, 1998, **84**, 1538.

33. J. S. Kim, B. Lagel, E. Moons, N. Johansson, I. D. Baikie, W. R. Salaneck, R. H. Friend and F. Cacialli, *Synth. Met.*, 2000, **111**, 315.

Chapter 7: Conclusions and Future work

CONCLUSIONS

Polyaniline (PANI) is an attractive conducting polymer for organic and polymer electronics[1-3] because of its promising electrical and optical properties, as well as environmental stability.[4, 5] Frequently, PANI is doped with small molecule acids to achieve high electrical conductivities. The resulting PANI is highly conductive (~ 200 S/cm), but is limited in solubility in common solvents.[6, 7] The material is thus generally not solution-processible. PANI also exhibits a melting temperature that is above its degradation temperature, making melt-processing of PANI infeasible. To overcome this technical barrier, we have chosen to work with PANI that is doped with a polymer acid, rather than a small molecule acid. The polymer acid used in our study is poly(2-acrylamido-2-methyl-1-propanesulfonic acid), or PAAMPSA. The polymer acid serves two roles: in addition to doping PANI to produce the electrically conductive form, excess sulfonic acid groups impart water dispersibility to the final material.[8] The resulting PANI is therefore not only electrically conductive, but also easily processible from aqueous dispersions. This water dispersibility, however, comes at the expense of reduced conductivity. In fact, the conductivities of polymer acid-doped PANI have generally been low (10^{-5} – 10^{-1} S/cm),[9, 10] and these low conductivities have in turn limited the utility of these materials in organic electronics. Given the promise of broad applications of conducting polymers in organic electronics, this thesis focuses on

understanding the processing-structure-property relationships of PANI-PAAMPSA with hopes to improve the electrical conductivity of polymer acid-doped PANI systems.

We improved the electrical conductivity of PANI-PAAMPSA from 0.4 S/cm to 2.5 S/cm by controlling the molecular weight and molecular weight distribution of PAAMPSA. The conductivity of PANI-PAAMPSA increases as the molecular weight of PAAMPSA decreases. Additionally, PANI that is doped with PAAMPSA having a narrower molecular weight distribution is two to three times as conductive as PANI that is doped with PAAMPSA of comparable molecular weight but having a broader molecular weight distribution. Strong correlations between the electrical conductivity and the structure of PANI-PAAMPSA are observed; conductivity increases with increasing crystallinity and conjugation length of PANI. The crystallinity and conjugation length of PANI qualify the molecular order in PANI-PAAMPSA; increases in molecular order enhance charge transport in PANI-PAAMPSA films.

PANI-PAAMPSA forms electrostatically stabilized sub-micron particles during aniline polymerization due to strong ionic interactions between the sulfonic acid groups of PAAMPSA and the aniline. The connectivity of these particles is therefore important for macroscopic conduction in the PANI-PAAMPSA films. In fact, we discovered that the size and size distribution of PANI-PAAMPA particles are strongly influenced by the molecular weight and molecular weight distribution of PAAMPSA. Specifically, templating aniline polymerization with a higher molecular weight PAAMPSA results in bigger PANI-PAAMPSA particles; templating aniline polymerization with a broader molecular weight distribution PAAMPSA results in particles with a larger size distribution. Since conduction in PANI-PAAMPSA films is governed by how these

particles pack in the solid state, the macroscopic conductivity of PANI-PAAMPSA films is found to scale by a single parameter, i.e., particle density, reducible from the molecular weight and molecular weight distribution of PAAMPSA. Specifically, higher particle density enhances inter-particle charge transport, leading to higher conductivity of the cast PANI-PAAMPSA film. We also found the PANI-PAAMPSA particles to be chemically inhomogeneous. Specifically, the conductive portions of the polymer complex preferentially segregate to the surface of particles. Conduction in these materials is therefore surface mediated. This surface mediated charge transport is in contrast with that in commercially-available conducting polymer, poly(ethylene dioxythiophene) that is doped with poly(styrene sulfonic acid), or PEDOT-PSS. In PEDOT-PSS, insulating PSS preferentially segregates to the surface.

We further improved the conductivity of PANI-PAAMPSA by more than two orders of magnitude via post-processing solvent annealing with DCA. Since DCA is a good plasticizer for PAAMPSA and its pK_a is lower than that of PAAMPSA (pK_as of DCA and PAAMPSA are 1.21 and 2.41, respectively, at room temperature), it can effectively disrupt the strong ionic interactions between PANI and PAAMPSA, thereby relaxing the electrostatically stabilized particles that were arrested during polymerization. PANI-PAAMPSA chains are thus allowed to rearrange from a compact coil to an extended chain conformation that enables more efficient charge transport. DCA-treated PANI-PAAMPSA exhibits an average conductivity of 48 S/cm. The DCA treatment is not only specific to PANI-PAAMPSA. Exposing PEDOT-PSS to DCA results in conductivities approaching 600 S/cm; this conductivity is the highest reported amongst any other polymer acid-doped conducting polymer systems. The mechanism of

conductivity improvement in PEDOT-PSS by DCA treatment, however, is different from that of PANI-PAAMPSA. While PANI is doped via protonation by PAAMPSA, PEDOT is oxidatively doped in the presence of PSS to attain it conductive form. PSS thus only serves as a counter ion in PEDOT-PSS. As such, the pK_a of the plasticizer used to induce structural rearrangement is not important in PEDOT-PSS. Indeed, the conductivity of PEDOT-PSS has reportedly been improved via exposure to ethylene glycol, dimethyl sulfoxide, and sorbitol;[11, 12] all of which are good solvents for PSS but are not acidic.

We also assessed the functionality of PANI-PAAMPSA as anodes in organic solar cells (OSCs). PANI-PAAMPSA effectively performs as anodes in OSCs that contain a blend of poly(3-hexylthiophene), P3HT, and [6,6]-phenyl-C61-butyric acid methyl ester (PCBM) as the active layer. Specifically, the OSCs with PANI-PAAMPSA anodes exhibit an average short circuit current density of 1.95 mA/cm^2, open circuit voltage of 0.52 V, fill factor of 0.38, and efficiency of 0.39 %. Conductivity improvement of PANI-PAAMPSA via DCA treatment can directly influence the device performance in OSCs. The use of DCA-treated PANI-PAAMPSA as anodes increases device performance (i.e., short circuit current density and thereby efficiency) of OSCs by approximately two and a half fold. Specifically, the OSCs with DCA-treated PANI-PAAMPSA anodes exhibit short circuit current density and efficiency as high as 4.95 mA/cm^2 and 0.97 %, respectively.

The electrical and optical properties of conducting polymers have led to many proposed applications, such as sensors,[13, 14] conductive coatings,[15, 16] organic electronics,[17, 18] etc. However, conducting polymers have been only used in special

fields that do not require high power outputs due to their inherently low conductivities compared to metals. We have explored the factors that govern the electrical conductivity of conducting polymers. Our understanding of the processing-structure-property relationships of conducting polymers should help pave the way for future device developments.

FUTURE WORK

Improving the conductivity of PANI-PAAMPSA

We have improved the electrical conductivity of PANI-PAAMPSA by manipulating the structure of the material. In particular, we dramatically improved the conductivity of PANI-PAAMPSA by post-processing solvent annealing with DCA; its average conductivity is 48 S/cm. The conductivity is the highest among reported polymer acid-doped PANI systems. It is, however, still several orders of magnitude lower than those of inorganic materials that are widely used in organic electronic devices. For example, the conductivity of indium tin oxide (ITO), a material that is widely used as anodes in OSCs, is on the order of 10^3 S/cm.[19] While we have successfully incorporated DCA-treated PANI-PAAMPSA as anodes in OSCs, their performance is still not as high as those of devices with ITO anodes. However, we observed comparable efficiency in devices with ITO anodes and in those with DCA-treated PEDOT-PSS anodes. The average conductivity of DCA-treated PEDOT-PSS is 600 S/cm. This observation suggests that we still need to improve the conductivity of PANI-PAAMPSA by an order of magnitude to truly replace ITO.

Exposing the PANI-PAAMPSA film to DCA allows for tremendous structural rearrangement; we no longer observed PANI-PAAMPSA particles that were arrested during polymerization. This structural rearrangement eliminates inter-particle charge transport, and the bulk conductivity of PANI-PAAMPSA improves dramatically as a consequence. The crystallinity of PANI-PAAMPSA, however, is still low and not dramatically different before and after DCA treatment. Given that conductivity is correlated with the crystallinity of PANI, work should be carried out to improve the crystallinity of these films. To increase crystallinity, we can preferentially orient the films, for example, by stretching. In fact, the conductivity of PANI that is doped with camphor sulfonic acid (CSA) has been shown to improve from 0.2 S/cm to 1000 S/cm when the film is exposed to m-cresol and stretched uniaxially.[20-22] The enhanced conductivity is comparable with that of ITO. If we can further improve the conductivity of PANI-PAAMPSA up to these levels by first exposing the film to DCA and then preferentially orienting it, PANI-PAAMPSA should be very attractive replacements for metals as electrodes in many electronic devices, such as organic solar cells and organic light-emitting diodes. When the devices are all composed of organic materials for the active layer as well as the electrodes, we can develop large area, flexible, and low-cost electronic devices without any loss of device performance from easily processible PANI dispersion.

Understanding the anisotropic conductivity of conducting polymers

As described in Chapter 6, PANI-PAAMPSA is a promising material as the anode in OSCs. PANI-PAAMPSA can also be used as the hole transport layer (HTL) between

the anode and the photoactive layer in OSCs, as shown in Figure 7.1.[23-25] PANI-PAAMPSA HTLs can provide a conductive pathway for holes to migrate from the photoactive layer into the anode, thereby improving hole extraction to the external anode.[23]

We observed in Chapter 6 that the OSCs with DCA-treated PANI-PAAMPSA anodes exhibit improved device performance compared to those with untreated PANI-PAAMPSA anodes. Given the fact that macroscopic conduction may occur directionally in the devices, in-plane charge transport of PANI-PAAMPSA should be important when the material is used as the anode in OSCs. The highly improved conductivity of DCA-treated PANI-PAAMPSA, therefore, would be responsible for improving the device performance. When PANI was incorporated as the HTL in OSCs (ITO was used as anodes in these devices), however, our preliminary experiments showed poor device performance in OSCs with DCA-treated PANI-PAAMPSA HTLs compared to those with untreated PANI-PAAMPSA HTLs. As the HTL, charges need to be carried across the HTL, so vertical charge transport across the thickness of the film dominates. We therefore suspect that macroscopic conduction in and through PANI-PAAMPSA films is anisotropic. It appears that the in-plain conductivity of PANI-PAAMPSA increases, but the through-plain conductivity of PANI-PAAMPSA decreases after DCA treatment.

To confirm this hypothesis, we can first carry out depth profiling experiments using x-ray photoelectron spectroscopy (XPS) to determine the compositions of DCA-treated PANI-PAAMPSA film as a function of depth. Conductive atomic force microscopy (AFM) also should help us examine the current changes in surface of the

films after DCA treatment with the changes in their morphology. These results should be compared against those of untreated PANI-PAAMPSA films.

The conductive AFM experiments should also provide us with additional evidence that the insulating PSS overlayer in PEDOT-PSS film is removed after DCA treatment, resulting in significantly improved lateral conductivity of the material, as already observed in Chapter 6 by XPS.

The understanding of these chemically inhomogeneous structures of conducting polymers and their influences on the conductivity of the materials films presents opportunities to predict which applications the materials can be used for *a priori*.

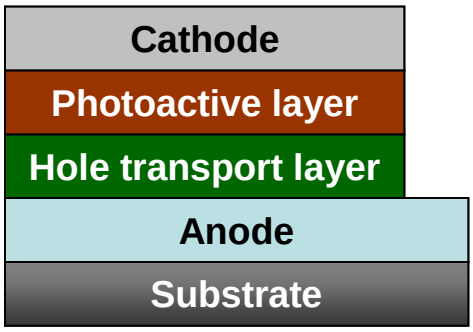

Figure 7.1. Cross-section representation of an OSC including the hole transport layer.

REFERENCES

1. E. M. Genies, P. Hany and C. Santier, *J. Appl. Electrochem.*, 1988, **18**, 751.
2. B. P. Jelle and G. Hagen, *J. Electrochem. Soc.*, 1993, **140**, 3560.
3. V. Saxena and B. D. Malhotra, *Curr. Appl. Phys.*, 2003, **3**, 293.
4. D. Chinn, J. DuBow, J. Li, J. Janata and M. Josowicz, *Chem. Mater.*, 1995, **7**, 1510.
5. D. Chinn, J. DuBow, M. Liess, M. Josowicz and J. Janata, *Chem. Mater.*, 1995, **7**, 1504.
6. S.-A. Chen and H.-T. Lee, *Macromolecules*, 1995, **28**, 2858.
7. H. S. Moon and J. K. Park, *J. Polym. Sci., Part A: Polym. Chem.*, 1998, **36**, 1431.
8. M. Angelopoulos, N. Patel, J. M. Shaw, N. C. Labianca and S. A. Rishton, *J. Vac. Sci. Technol., B: Microelectron. Nanometer Struct.*, 1993, **11**, 2794.
9. Y. Cao, J. Qiu and P. Smith, *Synth. Met.*, 1995, **69**, 187.
10. A. G. MacDiarmid, *Synth. Met.*, 2002, **125**, 11.
11. J. Y. Kim, J. H. Jung, D. E. Lee and J. Joo, *Synth. Met.*, 2002, **126**, 311.
12. J. Ouyang, Q. Xu, C.-W. Chu, Y. Yang, G. Li and J. Shinar, *Polymer*, 2004, **45**, 8443.
13. P. N. Bartlett and P. R. Birkin, *Synth. Met.*, 1993, **61**, 15.
14. N. Mano, J. E. Yoo, J. Tarver, Y.-L. Loo and A. Heller, *J. Am. Chem. Soc.*, 2007, **129**, 7006.
15. Y. Niu, *Polym. Compos.*, 2006, **27**, 627.
16. D. R. Smith, M. A. Moy, A. R. Dolan and T. D. Wood, *Analyst*, 2006, **131**, 547.

17. K. S. Lee, T. J. Smith, K. C. Dickey, J. E. Yoo, K. J. Stevenson and Y.-L. Loo, *Adv. Func. Mater.*, 2006, **16**, 2409.

18. M. S. Lee, H. S. Kang, H. S. Kang, J. Joo, A. J. Epstein and J. Y. Lee, *Thin Solid Films*, 2005, **477**, 169.

19. J. Ouyang, C.-W. Chu, F.-C. Chen, Q. Xu and Y. Yang, *Adv. Func. Mater.*, 2005, **15**, 203.

20. A. G. MacDiarmid and A. J. Epstein, *Synth. Met.*, 1994, **65**, 103.

21. A. G. MacDiarmid and A. J. Epstein, *Synth. Met.*, 1995, **69**, 85.

22. H.-S. Xu, Z. Y. Cheng, Q. M. Zhang, P.-C. Wang and A. G. MacDiarmid, *Synth. Met.*, 2000, **108**, 133.

23. K. Pichler, *Philosophical Transactions of the Royal Society of London, Series A: Mathematical and Phisical Sciences*, 1997, **335**, 829.

24. A. Reale, T. M. Brown, A. Di Carlo, F. Giannini, F. Brunrtti, E. Leonardi, M. Lucci, M. L. Terranova, S. Orlanducci, E. Tamburri, F. Toschi and V. Sessa, *Proceedings of SPIE*, 2006, **6334**, 63340Y.

25. M. W. Rowell, M. A. Topinka, M. D. McGehee, H.-J. Prall, G. Dennler, N. S. Sariciftci, L. Hu and G. Gruner, *Appl. Phys. Lett.*, 2006, **88**, 233506.

Bibliography

1. A. J. Heeger, *Rev. Mod. Phys.*, 2001, **73**, 681.
2. A. G. MacDiarmid, *Rev. Mod. Phys.*, 2001, **73**, 701.
3. H. Shirakawa, *Rev. Mod. Phys.*, 2001, **73**, 713.
4. C. K. Chiang, C. R. Fincher, Jr., Y. W. Park, A. J. Heeger, H. Shirakawa, E. J. Louis, S. C. Gau and A. G. MacDiarmid, *Phys. Rev. Lett.*, 1977, **39**, 1098.
5. Electrical conductivity, **http://en.wikipedia.org/wiki/Electrical_conductivity**.
6. C. K. Chiang, Y. W. Park and A. J. Heeger, *J. Chem. Phys*, 1978, **69**, 5098.
7. A. J. Epstein and Y. Yang, *MRS Bull.*, 1997, **22**, 13.
8. T. A. Skotheim, R. L. Elsenbaumer and J. R. Reynolds, *Handbook of conducting polymers*, Marcel Dekker, New York, 1998.
9. M. Leclerc and K. Faid, *Adv. Mater.*, 1997, **9**, 1087.
10. R. D. McCullough, *Adv. Mater.*, 1998, **10**, 93.
11. L. B. Groenendaal, F. Jonas, D. Freitag, H. Pielartzik and J. R. Reynolds, *Adv. Mater.*, 2000, **12**, 481.
12. E.-C. Chang, M.-Y. Hua and S.-A. Chen, *J. Polym. Res.*, 1998, **5**, 249.
13. M. Angelopoulos, N. Patel, J. M. Shaw, N. C. Labianca and S. A. Rishton, *J. Vac. Sci. Technol., B: Microelectron. Nanometer Struct.*, 1993, **11**, 2794.
14. Bayer AG, Eur. Patent, 440957, 1991.
15. J. Janata and M. Josowicz, *Nature*, 2003, **2**, 19.
16. P. Zarras, N. Anderson, C. Webber, D. J. Irvin, J. A. Irvin, A. Guenthner and J. D. Stenger-Smith, *Radiat. Phys. Chem.*, 2003, **68**, 387.

17. Engadget, *The Sony Drive XEL-1 OLED TV: 1,000,000:1 contrast starting December 1st, October 1 2007, retrieved on October 1 2007*.

18. H. Hoppe and N. S. Sariciftci, *J. Mater. Res.*, 2004, **19**, 1924.

19. G. Horowitz, *Organic Field-Effect Transistors*, CRC Press, New York, 2007.

20. M.-K. Song, W. I. Jung and R. H. -W., *Mol. Crys. Liq. Crys.* 1998, **316**, 337.

21. J.-S. Huh, H. R. Hwang, J. G. Roh, D. D. Lee and J.-O. Lim, *Mat. Res. Soc. Symp. Proc.*, 2002, **698**, EE 3.2.1.

22. J.-C. Lassegues and D. Rodriguez, *Proc. SPIE*, 1992, **1728**, 241.

23. M. Gerard, A. Chaubey and B. D. Malhotra, *Biosens. Bioelectron.*, 2002, **17**, 345.

24. Y. M. Lee, S. Y. Ha, Y. K. Lee, D. H. Suh and S. Y. Hong, *Ind. Eng. Chem. Res.*, 1999, **38**, 1917.

25. *Principles of electronic materials and devices*, McGraw-Hill, Boston, 2006.

26. A. G. MacDiarmid and A. J. Epstein, *Faraday Discuss. Chem. Soc.*, 1989, **88**, 317.

27. H. Letheby, *J. Am. Chem. Soc.*, 1862, **15**, 161.

28. R. d. Surville, M. Jozefowicz, L. T. Yu, J. Perichon and R. Buvet, *Electrochem. Acta*, 1968, **13**, 1451.

29. J. C. Chiang and A. G. MacDiarmid, *Synth. Met.*, 1986, **13**, 193.

30. A. G. MacDiarmid, *Angew. Chem. Int. Ed. Engl.*, 2001, **40**, 2581.

31. P. McManus, S. C. Yang and R. J. Cushman, *J. Chem. Soc. Commun.*, 1985, **1**, 1556.

32. G. Wnek, *Synth. Met.*, 1986, **15**, 213.

33. A. G. MacDiarmid and A. J. Epstein, *Synth. Met.*, 1994, **65**, 103.

34. A. G. MacDiarmid and A. J. Epstein, *Synth. Met.*, 1995, **69**, 85.

35. Y. Min, Y. Xia, A. G. MacDiarmid and A. J. Epstein, *Synth. Met.*, 1995, **69**, 159.

36. A. J. Heeger, *Angew. Chem., Int. Ed.*, 2001, **40**, 2591.

37. Y. Cao, P. Smith and A. J. Heeger, *Synth. Met.*, 1992, **48**, 91.

38. L. Sun, S. C. Yang and J.-M. Liu, *Polym. Prepr.*, 1992, **33**, 379.

39. B.-C. Ku, S.-H. Lee, W. Liu, J. Kumar, F. F. Bruno and L. A. Samuelson, *Mat. Res. Soc. Sym. Proc.*, 2002, **708**, BB10.12.1.

40. S.-A. Chen and H.-T. Lee, *Macromolecules*, 1995, **28**, 2858.

41. R. Nagarajan, S. Tripathy, J. Kumar, F. F. Bruno and L. Samuelson, *Macromolecules*, 2000, **33**, 9542.

42. G. Li, M. Josowiez and J. Janata, *Electrochem. Solid-State Lett.*, 2002, **5**, D5.

43. P. N. Bartlett, P. R. Birkin, M. A. Ghanem and C.-S. Toh, *J. Mater. Chem.*, 2001, **11**, 849.

44. F. F. Bruno, R. Nagarajan, S. Roy, J. Kumar, S. Tripathy and L. Samuelson, *Mat. Res. Soc. Symp. Proc.*, 2001, **660**, JJ8.6.1.

45. W. Liu, J. Kumar, S. Tripathy, K. J. Senecal and L. Samuelson, *J. Am. Chem. Soc.*, 1999, **121**, 71.

46. K. Shannon and J. E. Fernandez, *J. Chem. Soc. Chem. Commun.*, 1994, **1**, 643.

47. J. E. Yoo, J. L. Cross, T. L. Bucholz, K. S. Lee, M. P. Espe and Y.-L. Loo, *J. Mater. Chem.*, 2007, **17**, 1268.

48. J. H. Hwang and S. C. Yang, *Synth. Met.*, 1989, **29**, E271.

49. K. Miyatake, J.-S. Cho, S. Takeoka and E. Tsuchida, *Macromol. Chem. Phys.* , 1999, **200**, 2597.

50. S. K. Sahoo, R. Nagarajan, S. Chakraborty, L. A. Samuelson, J. Kumar and A. L. Cholli, *J. Macromol. Sci., Part A: Pure Appl. Chem.*, 2002, **A39**, 1223.

51. S. K. Sahoo, R. Nagarajan, L. Samuelson, J. Kumar, A. L. Cholli and S. K. Tripathy, *J. Macromol. Sci., Part A: Pure Appl. Chem.*, 2001, **A38**, 1315.

52. D. R. Smith, M. A. Moy, A. R. Dolan and T. D. Wood, *Analyst*, 2006, **131**, 547.

53. J. E. Yoo, T. L. Bucholz, S. Jung and Y.-L. Loo, *J. Mater. Chem.*, 2008, **18**, 3129.

54. K. S. Lee, G. B. Blanchet, F. Gao and Y.-L. Loo, *Appl. Phys. Lett.*, 2005, **86**, 074102.

55. K. S. Lee, T. J. Smith, K. C. Dickey, J. E. Yoo, K. J. Stevenson and Y.-L. Loo, *Adv. Func. Mater.*, 2006, **16**, 2409.

56. S. Beuermann, M. Buback, P. Hesse, T. Junkers and I. Lacik, *Macromolecules*, 2006, **39**, 509.

57. S. R. Gooda and M. B. Huglin, *J. Polym. Sci., Part A: Polym. Chem.*, 1992, **30**, 1549.

58. L. A. Samuelson, A. Anagnostopoulos, K. S. Alva, J. Kumar and S. K. Tripathy, *Macromolecules*, 1998, **31**, 4376.

59. H. S. Moon and J. K. Park, *J. Polym. Sci., Part A: Polym. Chem.*, 1998, **36**, 1431.

60. H. S. Moon and J. K. Park, *Synth. Met.*, 1998, **92**, 223.

61. S. K. Sahoo, R. Nagarajan, S. Roy, L. A. Samuelson, J. Kumar and A. L. Cholli, *Macromolecules*, 2004, **37**, 4130.

62. T. Akai, T. Abe, T. Shimomura and K. Ito, *Jpn. J. Appl. Phys.*, 2001, **40**, L1327.

63. P. N. Bartlett and P. R. Birkin, *Synth. Met.*, 1993, **61**, 15.

64. R. V. Belosludov, A. A. Farajian, Y. Kikuchi, H. Mizuseki and Y. Kawazoe, *Comput. Mater. Sci.*, 2006, **36**, 130.

65. Y. Niu, *Polym. Compos.*, 2006, **27**, 627.

66. R. J. Young and P. A. Lovell, *Introduction to Polymers*, Chapman & Hall, London, 1991.

67. S. Perrier, S. P. Armes, X. S. Wang, F. Malet and D. M. Haddleton, *J. Poly. Sci., Poly. Chem.*, 2001, **39**, 1696.

68. V. M, H. A and W. P, *J. Appl. Polym. Sci.*, 1991, **42**, 629.

69. M. Angelopoulos, N. Patel, J. M. Shaw, N. C.Labianca and S. A. Rishton, *J. Vac. Sci. Technol. B*, 1993, **11**, 2794.

70. L. Sun, H. Liu, R. Clark and S. C. Yang, *Synth. Met.*, 1997, **84**, 67.

71. W. Reusch, NMR spectroscopy, http://www.cem.msu.edu/~reusch/VirtualText/Spectrpy/nmr/nmr1.htm, Accessed October 22, 2006.

72. H. Meng, D. F. Perepichka, M. Bendikov, F. Wudl, G. Z. Pan, W. Yu, W. Dong and S. Brown, *J. Am. Chem. Soc.*, 2003, **125**, 15151.

73. S. Kaplan, E. M. Conwell, A. F. Richter and A. G. MacDiarmid, *J. Am. Chem. Soc.*, 1988, **110**, 7647.

74. S. Kaplan, E. M. Conwell, A. F. Richter and A. G. MacDiarmid, *Synth. Met.*, 1989, **29**, 235.

75. S. Kababya, M. Appel, Y. Haba, G. I. Titelman and A. Schmidt, *Macromolecules*, 1999, **32**, 5357.

76. H. S. Chan, H. S. Munro, C. Davies and E. T. Kang, *Synth. Met.*, 1988, **22**, 365.

77. P. Snauwaert, R. Lazzaroni, J. Riga and J. J. Verbist, *Synth. Met.*, 1987, **16**, 245.

78. D. A. Shirley, *Phys. Rev. B*, 1972, **5**, 4709.

79. E. T. Kang, K. G. Neoh and K. L. Tan, *Prog. Polym. Sci.*, 1998, **23**, 277.

80. J. Yue and A. J. Epstein, *Macromolecules*, 1991, **24**, 4441.

81. J. Y. Kim, J. H. Jung, D. E. Lee and J. Joo, *Synth. Met.*, 2002, **126**, 311.

82. G. Greczynski, T. Kugler and W. R. Salaneck, *Thin Solid Films*, 1999, **354**, 129.

83. K. Z. Xing, M. Fahlman, X. W. Chen, O. Inganaes and W. R. Salaneck, *Synth. Met.*, 1997, **89**, 161.

84. X-ray Diffraction (XRD), http://www.physics.pdx.edu/~pmoeck/phy381/Topic5a-XRD.pdf.

85. J. M. Ginder and A. J. Epstein, *Phys. Rev. B: Condens. Matter*, 1990, **41**, 10674.

86. P. M. McManus, R. J. Cushman and S. C. Yang, *J. Phys. Chem.*, 1987, **91**, 744.

87. S. Stafstrom, J. L. Bredas, A. J. Epstein, H. S. Woo, D. B. Tanner, W. S. Huang and A. G. MacDiarmid, *Phys. Rev. Lett.*, 1987, **59**, 1464.

88. K. S. Schmitz, *An Introduction to Dynamic Light Scattering by Macromolecules*, Academic Press, New York, 1990.

89. M. Sedlak, *Langmuir*, 1999, **15**, 4045.

90. S. Luan and G. W. Neudeck, *J. Appl. Phys.*, 1992, **72**, 766.

91. J. Zaumseil, K. W. Baldwin and J. A. Rogers, *J. Appl. Phys.*, 2003, **93**, 6117.

92. J. P. Travers and M. Nechtschein, *Synth. Met.*, 1987, **21**, 135.

93. V. Bulovic and S. R. Forrest, *Chem. Phys. Lett.*, 1995, **238**, 88.

94. G. Yu, J. Gao, J. C. Hummelen, F. Wudl and A. J. Heeger, *Science*, 1995, **270**, 1789.

95. M. W. Rowell, M. A. Topinka, M. D. McGehee, H.-J. Prall, G. Dennler, N. S. Sariciftci, L. Hu and G. Gruner, *Appl. Phys. Lett.*, 2006, **88**, 233506.

96. A. R. Schlatmann, D. W. Floet, A. Hillberer, F. Garten, P.J.M.Smulders, T. M. Klapwijk and G. Hadziioannou, *Appl. Phys. Lett.*, 1996, **69**, 1764.

97. J. C. Scott, J. H. Kaufman, P. J. Brock, R. DiPietro, J. Salem and J. A. Goitia, *J. Appl. Phys.*, 1996, **79**, 2745.

98. J. Cui, A. C. Wang, N. L. Edleman, J. Ni, P. Lee, N. R. Armstrong and T. J. Marks, *Adv. Mater.*, 2001, **13**, 1476.

99. A. K. Geim and K. S. Novoselov, *Nature Mat.*, 2007, **6**, 183.

100. F. Zhang, M. Johansson, M. R. Andersson, J. C. Hummelen and O. Inganas, *Adv. Mater.*, 2002, **14**, 662.

101. S. S. Sun, *Organic Photovoltaics*, Taylor & Francis Group, Boca Raton, FL, 2005.

102. A. G. MacDiarmid, *Synth. Met.*, 1997, **84**, 27.

103. V. Saxena and B. D. Malhotra, *Curr. Appl. Phys.*, 2003, **3**, 293.

104. A. P. Monkman and P. Adams, *Synth. Met.*, 1991, **41**, 891.

105. J. P. Pouget, M. E. Jozefowicz, A. J. Epstein, X. Tang and A. G. MacDiarmid, *Macromolecules*, 1991, **24**, 779.

106. W. Liu, A. L. Cholli, R. Nagarajan, J. Kumar, S. Tripathy, F. F. Bruno and L. Samuelson, *J. Am. Chem. Soc.*, 1999, **121**, 11345.

107. A. Bozkurt, O. Ekinci and W. H. Meyer, *J. Appl. Polym. Sci.*, 2003, **90**, 3347.

108. W. L. Earl and D. L. VanderHart, *J. Mag. Res.*, 1982, **48**, 35.

109. T. Hjertberg, W. R. Salaneck, I. Lundstrom, N. L. D. Somasiri and A. G. MacDiarmid, *J. Polym. Sci., Part C: Polym. Lett.*, 1985, **23**, 503.

110. S. K. Sahoo, D. W. Kim, J. Kumar, A. Blumstein and A. L. Cholli, *PMSE Preprints*, 2002, **87**, 394.

111. B. Wehrle, H.-H. Limbach, J. Mortensen and J. Heinze, *Angew. Chem. Int. Ed. Engl.*, 1989, **28**, 1741.

112. P. N. Adams, D. C. Apperley and A. P. Monkman, *Polymer*, 1993, **34**, 328.

113. A. F. Richter, A. Ray, K. V. Ramanathan, S. K. Manohar, G. T. Furst, S. J. Opella, A. G. MacDiarmid and A. J. Epstein, *Synth. Met.*, 1989, **29**, E243.

114. I. D. Norris, M. M. Shaker, F. K. Ko and A. G. MacDiarmid, *Synth. Met.*, 2000, **114**, 109.

115. N. J. Pinto, P. Carrion and J. X. Quinones, *Mater. Sci. Eng.*, 2004, **A366**, 1.

116. A. J. Heeger, *Synth. Met.*, 2001, **125**, 23.

117. Y. Cao, J. Qiu and P. Smith, *Synth. Met.*, 1995, **69**, 187.

118. A. G. MacDiarmid, *Synth. Met.*, 2002, **125**, 11.

119. S. M. Sze, *Semiconductor devices: Physics and Technology*, John Wiley & Sons, Inc., New York, 2002.

120. B. G. Streetman and S. K. Banerjee, *Solid State Electronic Devices*, Prentice Hall, Saddle River, 2006.

121. K. Lee, S. Cho, S. H. Park, A. J. Heeger, C.-W. Lee and S.-H. Lee, *Nature*, 2006, **441**, 65.

122. R. Murugesan and E. Subramanian, *Bull. Mater. Sci.*, 2003, **26**, 529.

123. T. A. Skotheim and J. Reynolds, *Conjugated polymers: theory, synthesis, properties, and characterization (Handbook of conducting polymers)* CRC Press, Boca Raton, 2007.

124. G. Horowitz, *Adv. Mater*., 1998, **10**, 365.

125. S. M. Ahmed, *Eur. Polym. J.*, 2002, **38**, 1151.

126. B. Ding, E. Kimura, T. Sato, S. Fujita and S. Shiratori, *Polymer*, 2004, **45**, 1895.

127. S. K. M. Jo¨nsson, J. Birgerson, X. Crispin, G. Greczynski, W. Osikowicz, A. W. D. v. d. Gonc, W. R. Salaneck and M. Fahlmana, *Synth. Met.*, 2003, **139**, 1.

128. J. Ouyang, Q. Xu, C.-W. Chu, Y. Yang, G. Li and J. Shinar, *Polymer*, 2004, **45**, 8443.

129. B. D. Lubachevsky and F. H. Stillinger, *J. Stat. Phys*, 1990, **60**, 561.

130. D. C. Rapaport, *The Art of Molecular Dynamics Simulation*, Cambridge University Press, Cambridge, 2004.

131. X. Crispin, S. Marciniak, W. Osikowicz, G. Zotti, A. W. D. V. D. Gon, F. Louwet, M. Fahlman, L. Groenendaal, F. D. Schryver and W. R. Salaneck, *J. Polym. Sci., Part B: Polym. Phys.*, 2003, **41**, 2561.

132. J. Hwang, F. Amy and A. Kahn, *Org. Electron.*, 2006, **7**, 387.

133. K. Z. Xing, M. Fahlman, X. W. Chen, O. Inganas and W. R. Salaneck, *Synth. Met.*, 1997, **89**, 161.

134. N. Koch, A. Vollmer and A. Elschner, *Appl. Phys. Lett.*, 2007, **90**, 043512.

135. P. Rannou, A. Gawlicka, D. Berner, A. Pron, M. Nechtschein and D. Djurado, *Macromolecules*, 1998, **31**, 3007.

136. A. R. Hopkins, P. G. Rasmussen, R. A. Basheer, B. K. Annis, G. D. Wignall and W. A. Hamilton, *Synth. Met.*, 1998, **97**, 47.

137. K. S. Lee, in *Chemical Engineering*, The University of Texas at Austin, Austin, 2007, pp. 85.

138. D. L. Yang, P. N. Adams, L. Brown and B. R. Mattes, *Synth. Met.*, 2006, **156**, 1225.

139. M. F. Hundley, P. N. Adams and B. R. Mattes, *Synth. Met.*, 2002, **129**, 291.

140. C. Bailey, Acid-base chemistry titration, http://www.calpoly.edu/~cbailey/125LabExperiments/Titration/Titration.html.

141. D. R. Lide, *CRC Handbook of Chemistry and Physics*, CRC Press, Boca Raton (FL), 2006.

142. S. Lifson, B. Kaufman and H. Lifson, *J. Chem. Phys.*, 1957, **27**, 1356.

143. A. Bozkurt, *Turk J Chem.*, 2005, **29**, 117.

144. J. T. Sejdic and A. Easteal, *J. Appl. Polym. Sci.*, 2000, **75**, 619.

145. J. Ouyang, C.-W. Chu, F.-C. Chen, Q. Xu and Y. Yang, *Adv. Func. Mater.*, 2005, **15**, 203.

146. G. Greczynski, T. Kugler, M. Keil, W. Osikowicz, M. Fahlman and W. R. Salaneck, *J. Electron Spectrosc. Relat. Phenom.*, 2001, **121**, 1.

147. L. Groenendaal, F. Jonas, D. Freitag, H. Pielartzik and J. R. Reynolds, *Adv. Mater.*, 2000, **7**, 481.

148. R. H. Friend, R. W. Gymer, A. B. Holmes, J. H. Burroughes, R. N. Marks, C. Taliani, D. D. C. Bradley, D. A. D. Santos, J. L. Bredas, M. Logdlund and W. R. Salaneck, *Nature*, 1999, **397**, 121.

149. Y.-S. Hsiao, W.-T. Whang, C.-P. Chen and Y.-C. Chen, *J. Mater. Chem.*, 2008, **18**, 5948.

150. E. Kymakis, N. Kornilios and E. Koudoumas, *J. Phys. D: Appl. Phys.*, 2008, **41**, 165110.

151. G. G. Malliaras, J. R. Salem, P. J. Brock and J. C. Scott, *J. Appl. Phys.*, 1998, **84**, 1538.

152. J. S. Kim, B. Lagel, E. Moons, N. Johansson, I. D. Baikie, W. R. Salaneck, R. H. Friend and F. Cacialli, *Synth. Met.*, 2000, **111**, 315.

153. E. M. Genies, P. Hany and C. Santier, *J. Appl. Electrochem.*, 1988, **18**, 751.

154. B. P. Jelle and G. Hagen, *J. Electrochem. Soc.*, 1993, **140**, 3560.

155. D. Chinn, J. DuBow, J. Li, J. Janata and M. Josowicz, *Chem. Mater.*, 1995, **7**, 1510.

156. D. Chinn, J. DuBow, M. Liess, M. Josowicz and J. Janata, *Chem. Mater.*, 1995, **7**, 1504.

157. N. Mano, J. E. Yoo, J. Tarver, Y.-L. Loo and A. Heller, *J. Am. Chem. Soc.*, 2007, **129**, 7006.

158. M. S. Lee, H. S. Kang, H. S. Kang, J. Joo, A. J. Epstein and J. Y. Lee, *Thin Solid Films*, 2005, **477**, 169.

159. H.-S. Xu, Z. Y. Cheng, Q. M. Zhang, P.-C. Wang and A. G. MacDiarmid, *Synth. Met.*, 2000, **108**, 133.

160. K. Pichler, *Philosophical Transactions of the Royal Society of London, Series A: Mathematical and Phisical Sciences*, 1997, **335**, 829.

161. A. Reale, T. M. Brown, A. Di Carlo, F. Giannini, F. Brunrtti, E. Leonardi, M. Lucci, M. L. Terranova, S. Orlanducci, E. Tamburri, F. Toschi and V. Sessa, *Proceedings of SPIE*, 2006, **6334**, 63340Y.

Vita

Joung Eun Yoo graduated from Suhmoon Girls' High School in 1998 in Seoul, Korea. In 2002, Joung Eun graduated Summa cum Laude in class from Chung-Ang University with a Bachelor of Science in Chemical Engineering. Upon graduation, Joung Eun continued at Chung-Ang University as a graduate student where she researched the miscibility of polymer blends under the supervision of Professor Chang-Keun Kim. She was awarded a Master of Science degree in Chemical Engineering in 2004. The same year, Joung Eun entered the Ph.D. program in Chemical Engineering at the University of Texas at Austin where she researched the understanding the processing-structure-property relationships of water-dispersible, conductive polyaniline under the supervision of Professor Yueh-Lin Loo. Upon completion of her doctorate degree, Joung Eun will begin work as a Post Doctoral Fellow with Professor Bernard Kippelen in Electrical and Computer Engineering at Georgia Institute of Technology, Georgia.

Permanent address: 201-704 Hyundai Apt. Gueui 3dong Gwangjin-gu, Seoul, Republic of Korea

This manuscript was typed by Joung Eun Yoo.